CONTROL OF A PLANAR CABLE-ACTUATED PARALLEL MANIPULATOR WITH REALISTIC CABLES

A THESIS SUBMITTED TO
THE GRADUATE SCHOOL OF NATURAL AND APPLIED SCIENCES
OF
MIDDLE EAST TECHNICAL UNIVERSITY

BY

ONUR DÜZGÖREN

IN PARTIAL FULFILLMENT OF THE REQUIREMENTS
FOR
THE DEGREE OF MASTER OF SCIENCE
IN
MECHANICAL ENGINEERING

JULY 2018

Approval of the thesis:

CONTROL OF A PLANAR CABLE-ACTUATED PARALLEL MANIPULATOR WITH REALISTIC CABLES

submitted by **ONUR DÜZGÖREN** in partial fulfillment of the requirements for the degree of **Master of Science in Mechanical Engineering Department, Middle East Technical University** by**,**

Prof. Dr. Halil KALIPÇILAR _____
Dean, Graduate School of **Natural and Applied Sciences**

Prof. Dr. Mehmet Ali Sahir ARIKAN _____
Head of Department, **Mechanical Engineering**

Prof. Dr. Mustafa Kemal ÖZGÖREN _____
Supervisor, **Mechanical Engineering Dept., METU**

Examining Committee Members:

Assoc. Prof. Dr. Ender Ciğeroğlu _____
Mechanical Engineering Dept., METU

Prof. Dr. Mustafa Kemal ÖZGÖREN _____
Mechanical Engineering Dept., METU

Prof. Dr. Eres SÖYLEMEZ _____
Mechanical Engineering Dept., METU

Assist. Prof. Dr. Ali Emre TURGUT _____
Mechanical Engineering Dept., METU

Prof. Dr. Sıtkı Kemal İDER _____
Mechanical Engineering Dept., Çankaya University

Date: 06/07/2018

I hereby declare that all the information in this document has been obtained and presented in accordance with academic rules and ethical conduct. I also declare that, as required by these rules and conduct, I have fully cited and referenced all material and results that are not original to this work.

Name, Last name : Onur DÜZGÖREN

Signature :

ABSTRACT

CONTROL OF A PLANAR CABLE-ACTUATED PARALLEL MANIPULATOR WITH REALISTIC CABLES

Düzgören, Onur
M.Sc., Department of Mechanical Engineering
Supervisor: Prof. Dr. Mustafa Kemal Özgören

July 2018, 216 Pages

The cable-actuated parallel manipulators comprise a new class of robotic systems which utilize length-controlled unilateral force elements like cables or wires to move and orient an object. They provide several benefits over conventional parallel robots, such as larger workspace, simpler structure, and higher payload/manipulator weight ratio. However, the cables can only be pulled but not pushed. Besides, they may sag due to their own weight. Therefore, the cable-actuated manipulators pose challenges in modeling and control. In this thesis, a planar cable-actuated manipulator is studied. It consists of a payload and two cables with nonnegligible masses. Each cable is divided into a finite number point masses connected by massless rigid segments. The appropriate number of segments required for a realistic modeling is one of the issues studied in this thesis. After the modeling stage, an inverse-dynamics controller is developed in order to make the payload track a desired trajectory. This controller needs the angles of the cable segments, which are not feasible to measure. Therefore, two methods are proposed to estimate them. The first method is based on a lower order model of the cables with a smaller number of segments. The second method is based on the assumption that the cables remain in pseudo-static equilibrium. Moreover, the tension in each cable segment is

monitored during the motion and the input forces are readjusted online to prevent slackness in any of the segments. For this purpose, an optimization algorithm is developed in order to determine the control forces with a compromise between the segment tensions and the tracking error. The performance of the controller is demonstrated and assessed through several simulations carried out by choosing the reference motions as square wave, deployment, and circular motions.

Keywords: Cable-Actuated Parallel Manipulator, Cable Robot Control, Tension Monitoring and Control, Lumped-Mass Cable Model, Lower-Order Dynamic Approximate Modeling

ÖZ

KABLOLARI GERÇEKÇİ OLAN DÜZLEMSEL KABLO EYLETİMLİ BİR PARALEL MANİPÜLATÖRÜN KONTROLÜ

Düzgören, Onur
Yüksek Lisans, Makine Mühendisliği Bölümü
Tez Yöneticisi: Prof. Dr. Mustafa Kemal Özgören

Temmuz 2018, 216 Sayfa

Kablo eyletimli paralel manipülatörler, bir cismi hareket ettirmek ve yönlendirmek için kablo ya da tel gibi uzunlukları kontrol edilebilen tek yönlü kuvvet elemanlarını kullanan robotik sistemlerin yeni bir sınıfıdır. Geleneksel bir paralel manipülatöre göre daha geniş çalışma alanı, daha basit yapı ve daha yüksek faydalı yük/manipülatör ağırlığı oranı gibi birçok avantaj sağlamaktadırlar. Fakat kablolar sadece çekilebilir ama itilemezler. Bunun yanında, kendi ağırlıkları nedeniyle sarkma yapabilirler. Bu nedenle, kablo eyletimli manipülatörler modelleme ve kontrol konularında yeni zorluklar yaratmaktadır. Bu tezde düzlemsel bir kablo eyletimli paralel manipülatör üzerinde çalışılmıştır. Bu manipülatör bir faydalı yük ve kütleleri ihmal edilmeyen iki kablodan oluşmaktadır. Her bir kablo, kütlesiz parçalarla birbirine bağlı belli sayıda nokta kütlelere ayrıştırılmıştır. Gerçekçi bir modelleme için gereken parça sayısı bu tezde çalışılan konulardan biridir. Modelleme aşamasından sonra, faydalı yüke istenen yörüngeyi takip ettirebilmek için bir ters-dinamik kontrolcüsü geliştirilmiştir. Bu kontrolcü, ölçümü uygulanabilir olmayan kablo parça açılarına ihtiyaç duymaktadır. Dolayısıyla, bu açıları kestirmek için iki yöntem ileri sürülmüştür. İlk yöntem, daha düşük sayıda parça içeren kabloların oluşturduğu düşük mertebeli bir modele dayanmaktadır.

İkincisi ise kabloların sanki-statik dengede kaldıkları varsayımını temel almıştır. Bunun yanı sıra her bir kablo parçasında oluşan gerilmeler hareket esnasında gözlemlenmekte ve gevşeklik durumunda girdi kuvvetleri yeniden çevrimiçi olarak düzenlenmektedir. Bu amaçla, kontrol kuvvetlerini takip hatası ve parça gerilmeleri arasındaki uzlaşma ile belirleyecek bir optimizasyon algoritması geliştirilmiştir. Kontrolcü performansı, kare dalga, tedrici yer değiştirme hareketi ve dairesel hareket referans komutları ile yapılan simülasyonlar yardımıyla gösterilmiş ve değerlendirilmiştir.

Anahtar Kelimeler: Kablo Eyletimli Paralel Manipülatör, Kablolu Robot Kontrolü, Gerilme Denetimi ve Kontrolü, Toplanmış Kütleli Kablo Modeli, Düşük Mertebeli Yaklaşık Dinamik Modelleme

To My Family and Fiancée, Kardelen Aktaş

ACKNOWLEDGEMENTS

With great pleasure, I would like to thank my advisor Prof. Dr. Mustafa Kemal Özgören for his valuable guidance, advice, criticism and encouragements throughout the research.

My heartiest thanks to my mother Mrs. Hacer Düzgören, my father Mr. Kemal Düzgören and my sister Miss. Buse Düzgören for their endless support during this study and throughout my life. Without them, this work would not be completed.

I wish my deepest gratitude to my fiancée Kardelen Aktaş without whose love, understanding, patience and encouragements throughout, this thesis wouldn't be possible.

I sincerely thank my managers Dr. Burcu Dönmez and Dr. Murat Şahin, in Mechatronics Design Department of Roketsan Missile Ind. for their generous support. I am highly indebted to my colleagues Mr. Ali Emrah Yarar, Mr. Melih Metin Pekkaptan and Mr. Ata Dönmez for their friendship, advice and selfless help during various stages of this study.

TABLE OF CONTENTS

LIST OF TABLES

TABLES

LIST OF FIGURES

FIGURES

LIST OF SYMBOLS

r_1	: Length of the 1st Cable Segment
$r_{1,h}$	: Length of the 1st Cable Segment for Higher-Order Model
$r_{1,l}$	: Length of the 1st Cable Segment for Lower-Order Model
r_2	: Length of the 2nd Cable Segment
$r_{2,h}$	: Length of the 2nd Cable Segment for Higher-Order Model
$r_{2,l}$	: Length of the 2nd Cable Segment for Lower-Order Model
l	: Length of Rigid Cable Segment
θ_i	: Angle of the ith Cable Segment
$\theta_{i,h}$	: Angle of the ith Cable Segment for Higher-Order Model
$\theta_{i,l}$	: Angle of the ith Cable Segment for Lower-Order Model
$\theta_{i,e}$	: Estimated Angle of the ith Cable Segment
F_1	: Force applied to the 1st Cable Segment
F_2	: Force applied to the 2nd Cable Segment
e_i	: Tangential Unit Vector of ith Cable Segment
n_i	: Normal Unit Vector of ith Cable Segment
T_i	: Tension of ith Cable Segment
T_{limit}	: Limiting Tension Value for a Cable Segment
q_i	: ith Generalized Coordinate
N_{total}	: Total Number of Segments in the Cable Robot
$N_{total,h}$	: Total Number of Segments for Higher-Order Model of the Cable Robot
$N_{total,l}$	: Total Number of Segments for Lower-Order Model of the Cable Robot
m	: Degree of Freedom of the Cable Robot
n	: Number of Generalized Coordinates
λ_i	: ith Lagrange Multiplier
m_{ee}	: Mass of End-Effector

g : Gravitational Acceleration

N_1 : Number of Segments in the Right-Cable

$N_{1,h}$: Number of Segments in the Right-Cable of Higher-Order Model

$N_{1,l}$: Number of Segments in the Right-Cable of Lower-Order Model

N_2 : Number of Segments in the Left-Cable

$N_{2,h}$: Number of Segments in the Left-Cable of Higher-Order Model

$N_{2,l}$: Number of Segments in the Left-Cable of Lower-Order Model

Q_k : Generalized Force associated with q_k

Q_k' : Generalized Constraint Force associated with q_k

φ : Constraint Equation

$\widehat{M}$: Mass Matrix

$\widehat{K}$: Stiffness Matrix

$\widehat{N}$: Coriolis and Centrifugal Force Coefficient Matrix

$\bar{g}$: Gravity Force Vector

$\omega_{highest}$: Highest Frequency encountered in Fourier Expansion

ω_i : ith Natural Frequency of Single Cable

x_{Tip} : x-Coordinate of Tip Point of Single Cable

$\bar{q}^*$: Desired Generalized Coordinate Vector

$\bar{p}^*$: Desired x and y Coordinates Vector of End-effector

$\bar{e}$: Position Error Vector

$\widehat{K}_d$: Derivative Gain Matrix

$\widehat{K}_p$: Proportional Gain Matrix

$\hat{J}$: Jacobian Matrix

$\bar{a}^*$: Desired Node Acceleration Vector

$\bar{a}'$: Available Node Acceleration Vector

f_i : Objective Function for ith Node

CHAPTER 1

INTRODUCTION

It is a need for human to move an object from one point to another for decades. In early days of mankind, this requirement was met with some primitive methods; however, with rapid industrialization, it becomes inevitable to find out new mechanical systems which provide convenience in terms of their labor force independence. Moreover, this transportation demand hasn't been limited to only moving an object. Depending on the complexity of process, there may be requirement for high accuracy, high speed or energy efficiency of rigid body motion. Because of these demands, new mechanical systems, called *robots*, received high importance and many researchers and engineers focused on wide range of robotic fields. At first stage of robotics, *serial manipulators (robots)* drew researchers' attention. This type of manipulators can be simply defined as successive group of links which are combined with joints and do not form a closed kinematic loop, some examples of which are illustrated in Figure 1.1 and Figure 1.2. The tip of this open kinematic chain is called *end-effector* and it may be easily equipped with proper devices like gripper, painter, welder, etc. depending on the defined operation.

Figure 1.1: A Serial Manipulator Developed by ABB™ [1]

Figure 1.2: A SCARA Serial Manipulator Developed by Mitsubishi™ [2]

In today's industrial world, serial manipulators form the big percentage of use. However, due to some insufficiencies that can be mainly listed as low load/inertia ratio, relatively lower positioning accuracy, repeatability and stiffness; they are not appropriate for every operation. Therefore, *parallel manipulators (robots)* emerged as a new mechanical construction to eliminate these lacking features of serial manipulators.

1.1 Parallel Manipulators (Robots)

Unlike serial manipulators, parallel manipulators (robots) contain closed loop kinematic chains which are combined at end-effector; therefore, they share the payload imposed on the end-effector, which is a superior characteristic. Thus one can automatically conclude that parallel manipulators have higher load/inertia ratio compared to the serial ones. Furthermore, due to its mechanical structure that is built by more than one independent closed kinematic loop, they present better stiffness performance which directly enhances positioning accuracy. Another aspect that provides better positioning accuracy is less accommodation of joint errors to end-effector since parallel manipulator has fewer joints in one leg of robot compared to a serial manipulator. As a simple illustration, serial manipulator can be imagined as single human arm, while parallel manipulator is two human arms joined at hands. Intuitively, it is easier to lift or move an object with total force applied by using two arms with respect to single arm. On the other hand, it becomes

more difficult to reach a far point with combined arms, meaning that limited workspace is one of the main drawbacks of parallel manipulators.

Advantages of parallel manipulator make them more attractive and people began to deal with its theory. One of the first parallel manipulators constructions appears in a patent filed in 1928 by J.E.Gwinnett which is planned to be used in movie theater (Figure 1.3) [3].

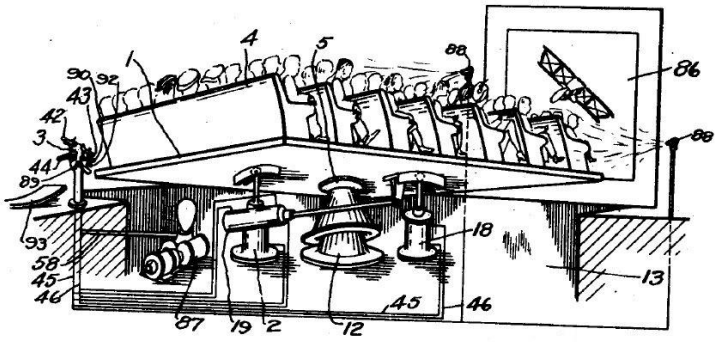

Figure 1.3: Parallel Manipulator Construction Described by J.E. Gwinnet in a US Patent of 1928 [3]

Some other early famous designs are the Gough Platform (Figure 1.4) proposed by Gough and Whitehall in 1947 as a test machine of tires and the Stewart Platform (Figure 1.5) published by D.Stewart in 1965 to be used as flight simulator.

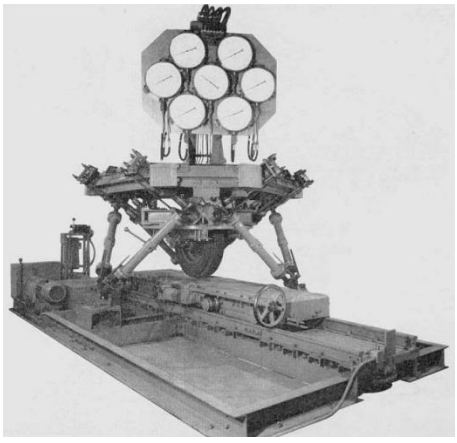

Figure 1.4: Gough Platform [4]

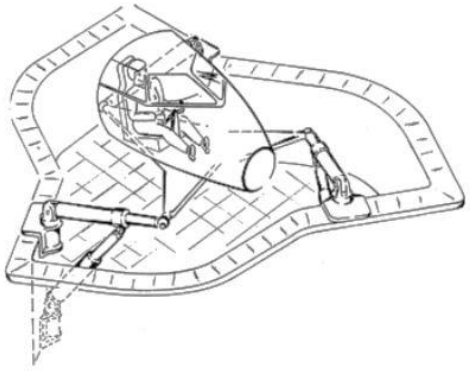

Figure 1.5: Stewart Platform, 1965 [5]

In today's industry, parallel manipulators are used for various applications requiring especially highly dynamic movements, high positioning accuracy, and carrying high loads. Nevertheless, there exist some applications which require motion of end-effector in large workspaces or simple robot construction for low cost. In these cases, a rigid link parallel manipulator lacks meeting desired characteristics. Because of that a new area of robotics emerged as cable-based parallel manipulators (robots).

1.2 Cable-Actuated Parallel Manipulators (Robots)

Cable-actuated parallel manipulators, which are also named cable-based robots, cable-driven robots or wire robots in literature, are the new types of robots formed by a moving platform, i.e. end-effector, a fixed body and cables. These cables are used to connect end-effector and fixed body instead of placing rigid links for the same purpose. By changing active lengths of these cables, position and orientation of end-effector can be arranged. Cables are generally rolled on a pulley which is rotated by an electric motor so that cable length changes.

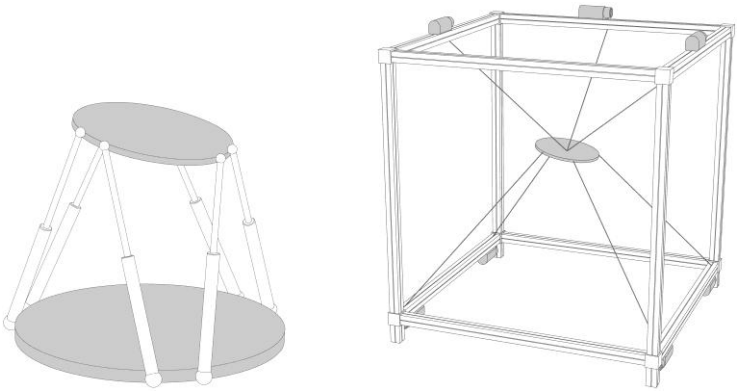

Figure 1.6: Rigid Link and Cable-Based Parallel Manipulators [6]

Cable-based parallel manipulators can be classified in two main types as fully constrained or under constrained systems in terms of degree of freedom of end-effector and number of cables used to move it. For fully constrained robot, number of cables contained in system needs to be (n+1) with proper cable arrangement if end-effector has n degrees of freedom [7]. If there exist more than (n+1) cables, then the manipulator becomes over constrained. If it is less, then it is defined as under constrained manipulator meaning that gravity, which is uncontrollable, plays an auxiliary role to determine the exact pose of end-effector. In fully constrained parallel manipulators, all parameters that are effective to find out end-effector position and orientation can be arranged as desired by changing cable lengths.

The terms “under constrained” and “fully constrained” for cable robots are also explained clearly on a simple planar application in research of Gorman, Jablokow and Cannon [8]. As they stated, the number of cables used in a robot is based on the type of application. An under constrained cable robot might have the ability of manipulating all degrees of freedom of a payload by using gravity. For instance, cable configuration (a) in Figure 1.7 is sufficient to control position of an object with the help of gravity. However, in case of additional rotation control of the same object, these three degrees of freedom are not possible to be controlled independently using only two cables like in the case of (b) of Figure 1.7. A three-cable configuration shown in (c) of Figure 1.7, is just enough to control the position of the object on plane without depending on the existence of gravity. Nevertheless,

it still lacks capability of independent control of position and orientation. That's why a 4th cable is required to control three degrees of freedom as indicated in (d), Figure 1.7. Similar to the previous one, in this configuration gravity has no deterministic influence on the pose of the object.

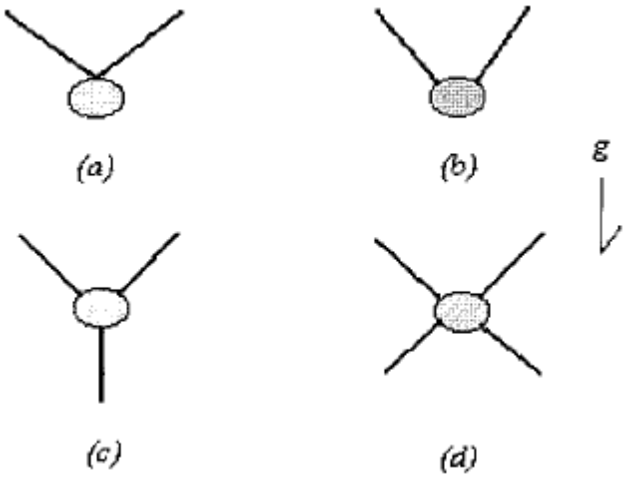

Figure 1.7: Under Constrained (a), (b) and Fully Constrained (c), (d) Planar Cable Configurations [8]

1.2.1 Under Constrained Cable-Actuated Parallel Manipulators (Robots)

Although fully constrained cable-based parallel manipulators are deterministic and provides ease of positioning and orienting the end-effector in a fully controllable manner, they might be inappropriate for some applications where it is undesirable to have cables passing through workspace or below end-effector height level. Then in these applications, using an under constrained cable robot becomes more feasible since it has no cables connecting end-effector to the base of the fixed body.

There are some good, creative designs to eliminate the cables connected to the base of fixed body and obtain fully constrained cable robot at the same time, one of which can be seen in the study of Kawamura S. as *Falcon 7* (Figure 1.8). However, this kind of structure adds complexity to the system compared to simple mechanical structure of under constrained cable robots. For this reason, it is logical to consider

under constrained cable robots as a first design option if its capabilities are sufficient to meet system requirements.

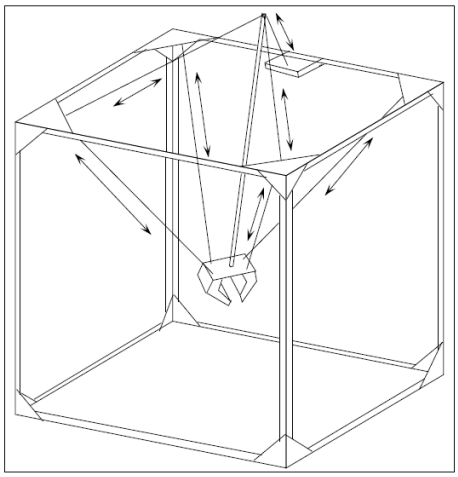

Figure 1.8: Fully Constrained Cable Based Parallel Manipulator Design of Kawamura S. [9]

1.3 Advantages of Cable-Actuated Parallel Manipulators (Robots)

Some of the main advantages of the cable-actuated robots, which make them the point of interest in field of robotics in recent years, are listed as follows:

- Larger workspace: Cables are simply defined as the links of the cable robot. However, they differ from traditional rigid links since their lengths can be easily changed as long as there exists enough cable wrapped around the pulleys. This property provides the opportunity of reaching points far from the pulleys, which means very large workspaces.
- High load/inertia ratio and few moving parts: Cables are the only motion transmitting elements of cable-based parallel manipulators. Since they have relatively low inertia compared to rigid links and great axial stiffness, advantage of high load/inertia of the robot emerges. In addition, actuators of cable robot do not have to be moved unlike traditional robots, which prevents increase in the inertia. On the other hand, in traditional manipulators, construction constitutes several links having greater mass than

cable, connected with joints at which actuators are located and all have to move to accomplish defined task.

- High speed: The advantage of high load/inertia ratio automatically brings the capability of moving at high speeds.
- Simple mechanical structure: For a cable-based robot, it is sufficient to have only cables and pulleys to build it up and complete its function with enough performance.
- Low cost: Property of having simple structure reduces its cost because the number of components contained within the robot is relatively low and they are more affordable compared to the functional parts of rigid link parallel manipulators.
- Ease of disassembly/reassembly: Simple structure also gives the benefit of easily disassembling and reassembling in case of maintenance, repair or need of reconstruction caused by a change in the intended use. This is because the only parts that must be concerned are again cables and pulleys.
- Ease of transportation: Cable robots are easy to be transported to another workspace due to their advantages of simple structure and ease of disassembling. Furthermore, this transportation process is easier since cables are relatively low in both mass and volume.
- Reconfigurability: Depending on the aimed task or workspace, a cable manipulator can be reconfigured by rearranging the locations of pulleys or their heights from the base. Ease of disassemble/reassemble helps it out and reconfiguration is not a big trouble for cable robots.

1.4 Applications of Cable-Actuated Parallel Manipulators (Robots)

Favorable characteristics of cable-actuated manipulators make them attractive to be used in variety of applications, which are mainly listed as payload handling, operations in hazardous areas, operations performed in large workspaces with heavy objects, medical applications, etc.

The first cable robot got into use is the NIST Robocrane [10]. This cable robot is designed to be utilized in the applications of lifting and maneuvering heavy loads. In one of the applications of NIST RoboCrane, it is used to carry a platform which is equipped with a robot to weld ships as shown in Figure 1.11 [11]. Furthermore, a small soft material machining prototype of RoboCrane is also built by NIST, an image of which is presented in Figure 1.12 [12].

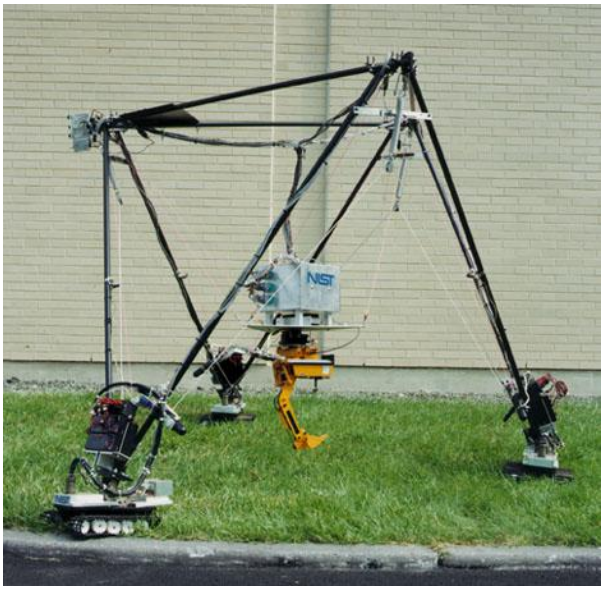

Figure 1.9: NIST RoboCrane Mobile 2 m Prototype [13]

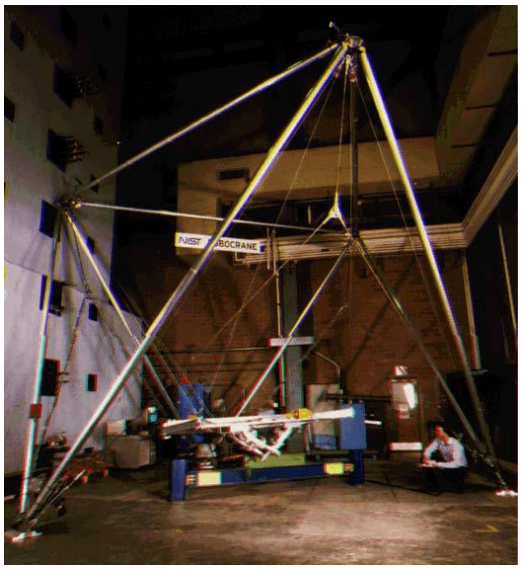

Figure 1.10: 6 meter RoboCrane Prototype [14]

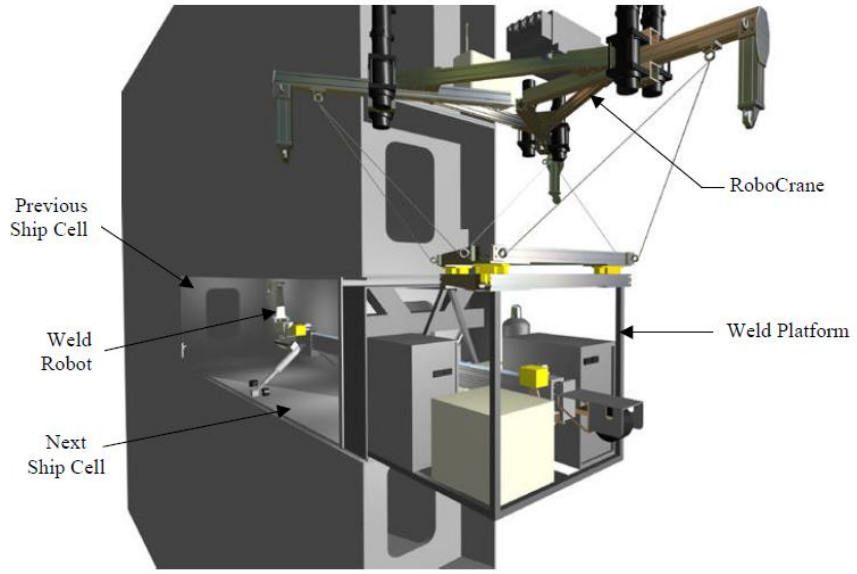

Figure 1.11: The NIST RoboCrane used in Ship Welding Application [11]

Figure 1.12: RoboCrane Prototype for Machining Soft Material [12]

Wire robots are made use of object handling operations especially in large workspaces. One of the designs developed by Fraunhofer IPA is displayed in Figure 1.13. This fully constrained cable-driven robot is proposed to handle objects with mass of up to 40 kg.

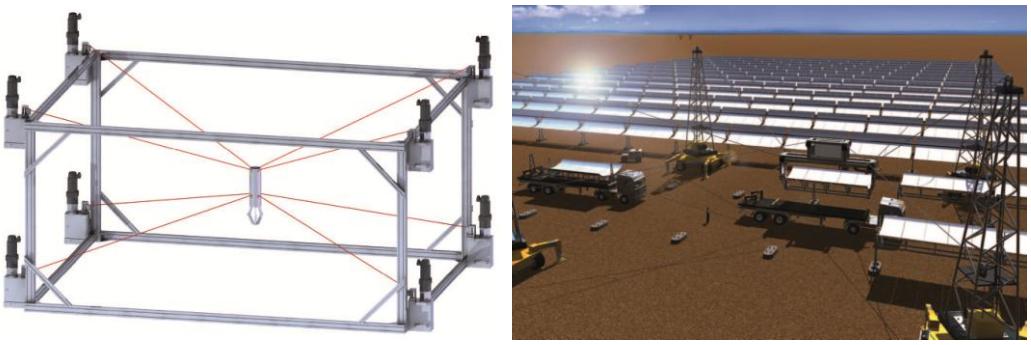

Figure 1.13: A Fully Constrained Cable Robot for Object Handling [15]

As already stated, cable robots have vital importance in medical applications, where they are utilized for rehabilitation. On the Figure 1.14 and Figure 1.15, there can be observed several applications with this purpose of use.

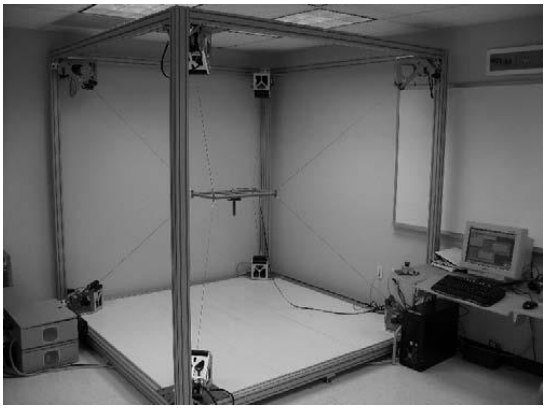

Figure 1.14: A Cable Robot for Upper Limb Neurorehabilitation [16]

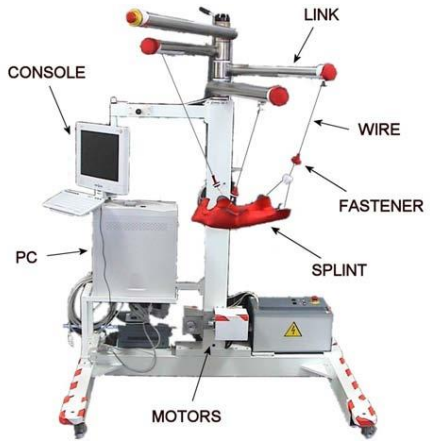

Figure 1.15: Cable Robot with 3 Wires used for Upper Limb Neurorehabilitation, named NeReBot [17]

Cable-actuated robots are very suitable for large radio telescope applications since they serve large workspaces. One of the famous applications of this type is the FAST project of China, where feed cabin of the telescope is actuated by cables [18]. The LAR (Large Adaptive Reflector) is another concept for giant radio telescopes which again contains cables, called *tethers*, for actuation.

Figure 1.16: The Five-Hundred-Meter Aperture Spherical Radio Telescope (FAST) Project [18]

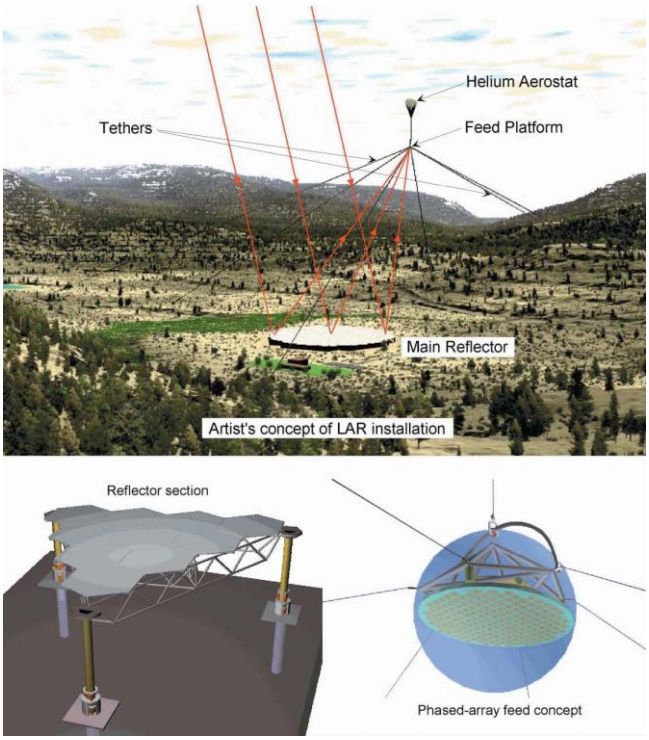

Figure 1.17: The Large Adaptive Reflector, *LAR* [19]

Another famous application of cable robot is the SkyCam™ (stabilized camera system) that is used in sports arenas. In this system, it is employed an underconstrained cable manipulator to move the platform carrying a camera.

Figure 1.18: A Skycam™ [20]

Cable-actuated parallel manipulators become point of interest in the field of hazardous operations in remote areas. For this reason, there exist several designs proposed in the literature one of which is illustrated on the below Figure 1.19.

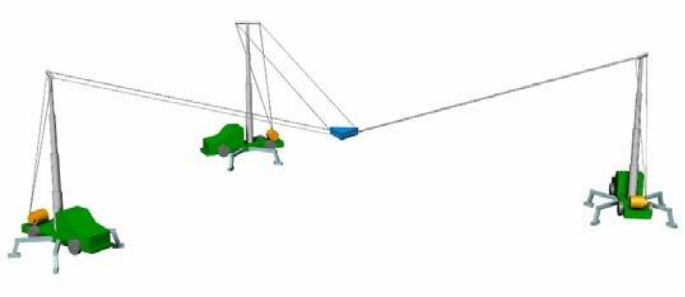

Figure 1.19: A Rapidly Deployable Cable Robot for Rescue Operations [21]

There are also some applications of cable robots, where they are employed to move patients in hospital environment, a conceptual design of which is presented in Figure 1.20 [22].

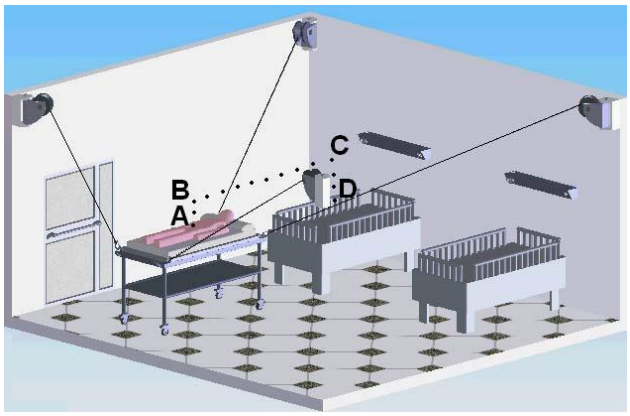

Figure 1.20: Application of Cable Robot in Hospital Environment [22]

As a remote environment and outdoor application, a cable robot is used for algae harvesting operation, details of which are presented in study [23].

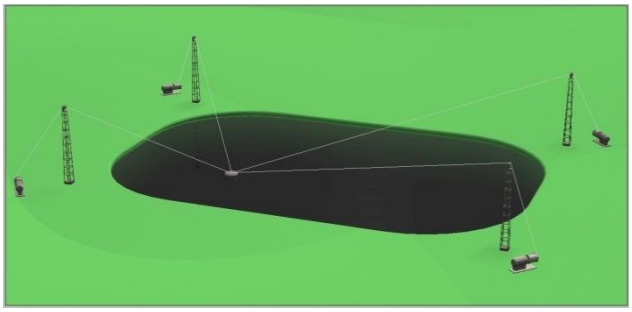

Figure 1.21: CAD Model a Cable Robot for Algea Harvesting [23]

There exist also some conceptual designs of cable robot for agricultural applications some of which are displayed in Figure 1.22 .

Figure 1.22: Agricultural Applications of Cable Robots [24]

By taking advantage of reconfigurability and large workspace of cable robots, they can be used in airplane maintenance application like the design proposed in the study of Nguyen and Gouttefarde [25].

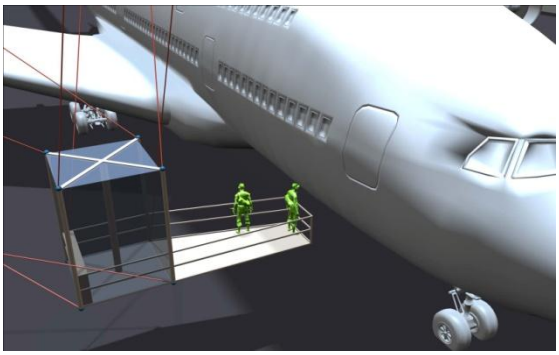

Figure 1.23: A Cable Robot used in Airplane Maintenance Application [25]

A cable robot with 8 cables is employed in a low-speed wind tunnel as suspension system for an aircraft model, shown in Figure 1.24. Another wind tunnel implementation of cable robot is presented in the research of Lafourcade, et al. [26].

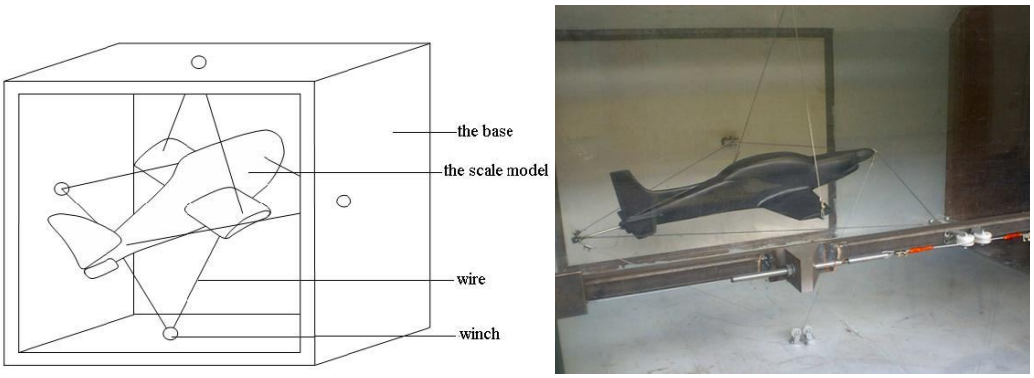

Figure 1.24: A Cable Robot with 8 Cables used in Low-Speed Wind Tunnel [27]

In study of Bosscher, et al. [28], a fully constrained cable manipulator is proposed to be used in contour crafting system for construction application. In this respect, a mobile platform that is used for contour crafting is driven by cable robot like presented in Figure 1.25.

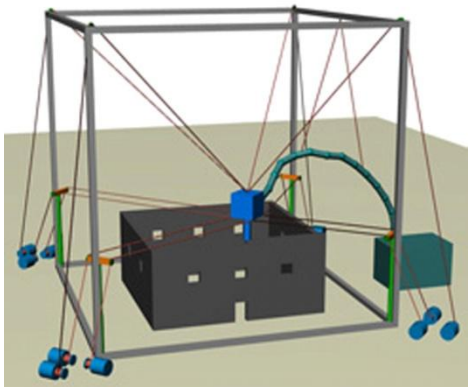

Figure 1.25: Contour Crafting Platform Driven by a Cable-Actuated Parallel Manipulator [28]

1.5 Challenges of Cable-Actuated Parallel Manipulators (Robots)

Although cable-actuated robots serve several advantages and they take part in many application areas of industry, there exist some challenges to be addressed. Challenges related to modeling and control topics are mainly classified into the following subtitles.

- Modeling of Cable Robots with Realistic Cables: It is critical to include mass and the sagging effect of the cables in modeling of cable robots to reflect the real behavior of the manipulator. Therefore, it is one of the obstacles to develop a comprehensive dynamic model which contains inertial effects of the cables. In addition, cables have relatively low stiffness compared to rigid links and that's why they induce vibration to the system.
- Controller Design: A cable-actuated robot is a nonlinear system which comprises wires with variable lengths and a payload hanged at the connection of them. Hence it has vital importance to propose an appropriate controller which has capability of positioning and orienting the payload with high accuracy and compensation of system nonlinearities.
- Tension Constraints of Cables: Due to unilateral constraint imposed by the cables, there emerges an additional requirement for controller: In order not to lose control of the cables, controller of the manipulator is designed such that it never gives rise to negative tension on the cables.

1.6 Literature Review

Many studies and researches are carried out about the challenges of the cable manipulators mentioned on Section 1.5 all around the world. In this section, it is aimed to present main strategies proposed in literature about these problematic subjects.

In their study [29], Korayem et al. developed a 6-DOF under constrained cable robot called *ICASBOT*. In this research, cable is modeled as combination of two linkages with a prismatic joint. However, its mass and sagging effect is not included within the model but a symbolic 2 grams of mass assigned for the cables due to the requirement of used software. A PD controller is designed in order to control pose of the end-effector, which is visually sensed with the help of two cameras. In research [30], another 6-DOF cable driven robot with 8 cables is studied by Lamauru et al., where control strategy is based on optimization of tension distribution with the help of redundancy. According to the approach presented in this study, PID controller generates the regarding cable tensions by using the error in cable lengths and these tensions are rearranged to be able to obtain optimal tension distribution. Desired cable lengths are derived from inverse kinematics of corresponding planned path. Elasticity of cables are studied in [31] by modeling them as axial linear springs on a redundantly driven cable robot by Khosravi and Taghirad. Controller algorithm is applied in cable length space and PD controller is designed so that it ensures positive cable tensions. In their article [32], Du et al. proposed a model by including dynamic behavior of cables with their slowly changing lengths. In this approach, bending and torsion stiffness of cables are assumed to be negligible. Cables are divided into nodes so that dynamic model contains first two or three vibration modes; however, there is not proposed a certain approach to clarify this issue completely. In addition, they used planar two-cable robot, which is very similar to the one considered in this thesis, to investigate the fidelity of their discrete model. To do that, they modeled this planar robot, one end of which is fixed, in ADAMS software for comparison. It is applied a sinusoidal movement to the free end of cable robot and a point mass is hanged to represent a

payload. Corresponding responses showed that proposed modeling technique matches up with the ADAMS model. In study [33], a dynamic model is developed by Lambert and Nohan in order to simulate a three-tethered aerostat positioning system. According to the proposed approach, each cable (*tether*) is discretized into viscoelastic elements which are connected at the point-loaded nodes, which represent the distributed cable mass. For controller strategy, a PID and an optimal LQG controller are designed with the help of linearized dynamic model. Moreover, a feedforward controller term is also added to these techniques in order to eliminate motion disturbances. In research of Lytle et al. [34], two-level controller is utilized at first level of which cable lengths are controlled by using the measured rotation of motors as feedback. At second level, trajectory planning stage takes place so that smooth trajectories between target points are obtained. For this level of controller, inverse kinematics is used to convert desired positions into cable lengths to be meaningful for first level controller. Zi et al. modeled 50-m scaled version of cable robot used in radio telescope with actuator dynamics [35]. Moreover, sagging effect of cables are contained within the model by formulating them as parabolic curves to be able to calculate cable lengths more accurately which will directly affect the positioning accuracy of the cable robot. These parabolic shapes of cables are obtained by using the force appeared on it at static equilibrium by assuming that cable robot moves very slowly. However, masses of the cables are ignored in derivation of equations of motion. In order to reduce effects of disturbances sourced from wind and improve tracking ability of the manipulator, a fuzzy controller with PI control is employed. In another research [36], where dynamics of 50-m scaled model of radio telescope is studied again but in this study lumped mass model is utilized for cable modeling by distributing the cable mass into nodes of discretization. According to study [37], Afshari and Meghdari derived the equations of motion of RoboCrane using constraint Lagrange method, where a triangular platform is modeled with 4 point masses and cable masses are assumed to be negligible. In addition, geometry of the cables is modeled as straight lines. It is defined a new, time-efficient Jacobian matrix which reduces the computation time in both determination of workspace and solution of dynamics equations. In study [38], trajectory control problem of under constrained cable robots is addressed by

Yamamoto et al. . It is employed an inverse dynamics calculation for feedback linearization to control the hanged object carried by the manipulator. In dynamics modeling, cables are assumed to be massless straight lines. In the study [39] conducted by Oh and Agrawal, a controller which is based on feedback linearization with reference governor, is developed for under constrained cable robot without violating the tension constraints imposed by unilateral cables. In this strategy, the reference governor rearranges the desired final position in case of possible constraint violation. In other words, it satisfies the tension constraint in exchange for some loss in desired position of end-effector. In derivation of dynamic equations of motion, cables are regarded as massless and straight line elements. A 3D cable robot with 5 cables is modeled including the actuator dynamics, based on the formulation of Lagrange's principle by Filipovic et al. [40]. Cables are specified as un-stretchable, rigid elements with zero mass in this model. In study [41] , Babaghasabha et al. developed an adaptive robust sliding mode controller for fully constrained cable manipulator by also ensuring positive cable tensions during motion. In modeling of cable robot, cables are considered as rigid and massless. Conversely, in study of [42], dynamics model of fully constrained cable robot is expressed including the inertial effects of the cables by Wei et al. . Sagging effects of log-span cables are taken into account considering the catenary model and corresponding cable lengths are found out with length of a catenoid under the action of gravity, i.e. its own weight. Resulting cable length is dicretized into N parts with time varying lengths. Actuator dynamics is also included in the model of cable robot. It is proposed a modified-PD feedforward controller and stability is analysed with the help of stability theory of Lyapunov. As a different type of cable robot, in their research [43], K.Agrawal, et.al. analyzed a two-stage planar cable manipulator, which is proposed to be used in marine applications. Due to operation environment, disturbance induced on the stationary frame of the manipulator needs to be considered. A robust controller is developed to eliminate negative effects of the disturbance and also provide positive tension values on the cables. The controller takes advantage of redundant degree of freedom of the system to accomplish this task. In the dynamic model developed within this study, inertial and sagging effects of wires are neglected. In study [44], an over-constrained cable-based parallel

manipulator is point of interest and its dynamic model is built by including the axial flexibility of the cables (modeled as linear spring) with utilization of the singular perturbation theory. However, sagging effect of them is neglected. To be able to control this axially elastic cable system, a composite controller is proposed where an already developed inverse dynamics controller for rigid body system is combined with a PD controller to control the fast dynamics. German et al. studied a 3-cable under constrained robot and they developed a sliding mode controller in order to provide stability of the robot for the case of different masses of moved objects [8]. In modeling stage, cables are regarded as straight lines with zero masses. Moreover, the manipulated object is taken as point mass since it is aimed to control only Cartesian coordinates. In another research of cable robots [45], Bedoustani et al. derived equations of motion based on Lagrange dynamics by considering the change in the mass of the cables during motion. Nevertheless, sagging effect of them is neglected and modeled as rigid elements. In order to prevent possible slackness of cables, redundancy of the robot is used and tension distribution is optimized such that all cables maintain their positive tensions. In study [46], lumped-mass modeling technique is utilized and cable mass is uniformly distributed to the nodes of the discretized cable by Caverly and Forbes. Axial flexibility of each segment is included within the model by modeling them as linear springs. However, sagging effect is neglected and geometry of cables is considered as straight line.

1.7 Research Focus and Contributions

After completion of literature review, it is noticed that there are some open issues to be studied about the challenges explained in Section 1.5. For this reason, critical points related with these challenges are worked out in this thesis, details of which are described on the following lines. All the developed methods and strategies are implemented on a planar cable-actuated parallel manipulator with two cables and a point mass end effector, which is a type of under constrained cable robot.

- Modeling of Cable Robots with Realistic Cables: In this thesis, dynamic model of cable robot is built up by including both cable mass and its sagging effect. In this respect, lumped mass modeling approach is utilized by dividing a continuous cable into N number of segments and cable mass is uniformly distributed to the nodes formed at segment connections. Furthermore, these segments are combined with revolute joint so that sagging effect is reflected in the model. An approximate approach is also developed to determine the required number of divisions to model a cable in a realistic manner.
- Controller Design: After building a comprehensive dynamic model, an inverse dynamics controller is proposed in task space to control x and y coordinates of end-effector accurately. This control scheme helps out to linearize the nonlinearities in equations of motion and also decouples them. This characteristic of inverse dynamics controller gives an opportunity of using linear conventional controllers. A PD controller is used in this thesis for this purpose. Moreover, two main approaches are presented to estimate segment angles which are necessary for inverse dynamics controller. The first one of these approaches is lower-order model approach, which uses a coarse cable robot model with lower number of segments on the cables. Second one is the pseudo-static approach with the assumption of cables at static equilibrium. Effect of measurement of end-effector pose and 1^{st} segment angles are also analyzed through variety of simulations.
- Tension Constraints of Cables: In order to keep all cable segments under tension, an optimization algorithm is proposed. This algorithm prevents negative tension at any cable segment by the exchange for some loss in the desired motion. The significant feature of the optimization operation is that it minimizes this loss and gives the closest motion to the desired one under the present conditions.

1.8 Thesis Organization

The thesis consists of 5 chapters.

- Chapter 2: Steps of mathematical modeling are explained in detail with all assumptions and simplifications. Kinematics, static equilibrium equations and constraint Lagrange equations of planar cable robot are derived in this context. Then, analysis of natural frequencies of a single cable and how it is used for segment number determination are described in depth. Lastly, the algorithm to build equations of motion for any possible combination of segment numbers is presented.
- Chapter 3: This chapter starts with brief background information about inverse dynamics controller. Then, details of designed controller are presented. Angle estimation methods are also served with illustrative block diagrams in this chapter. In the last part of the chapter, literature survey of measurement methods that can be employed in a cable robot is provided.
- Chapter 4: Controller strategy is tested through several simulation scenarios and conditions in this chapter. These simulations are repeated to include all possible combinations of angle estimation methods with inverse dynamics controller. Effects of measurement of different system variables are analyzed and evaluated through simulations.
- Chapter 5: Summary of completed work up to this chapter is given at the beginning. Then, results of simulations are evaluated and possible future works are suggested.

CHAPTER 2

MATHEMATICAL MODEL

In this study, each cable of two-cable planar parallel robot is discretized into *N* parts, which are called *cable segments* at the rest of the thesis and cable mass is uniformly distributed on to the nodes of segment intersections as point masses. All nodes are connected to each other with rigid segment links with the help of a frictionless revolute joint. Therefore, cable is modeled as axially rigid since transverse motion is more dominant than axial motion. In other words, axial deformation is assumed to be negligible.

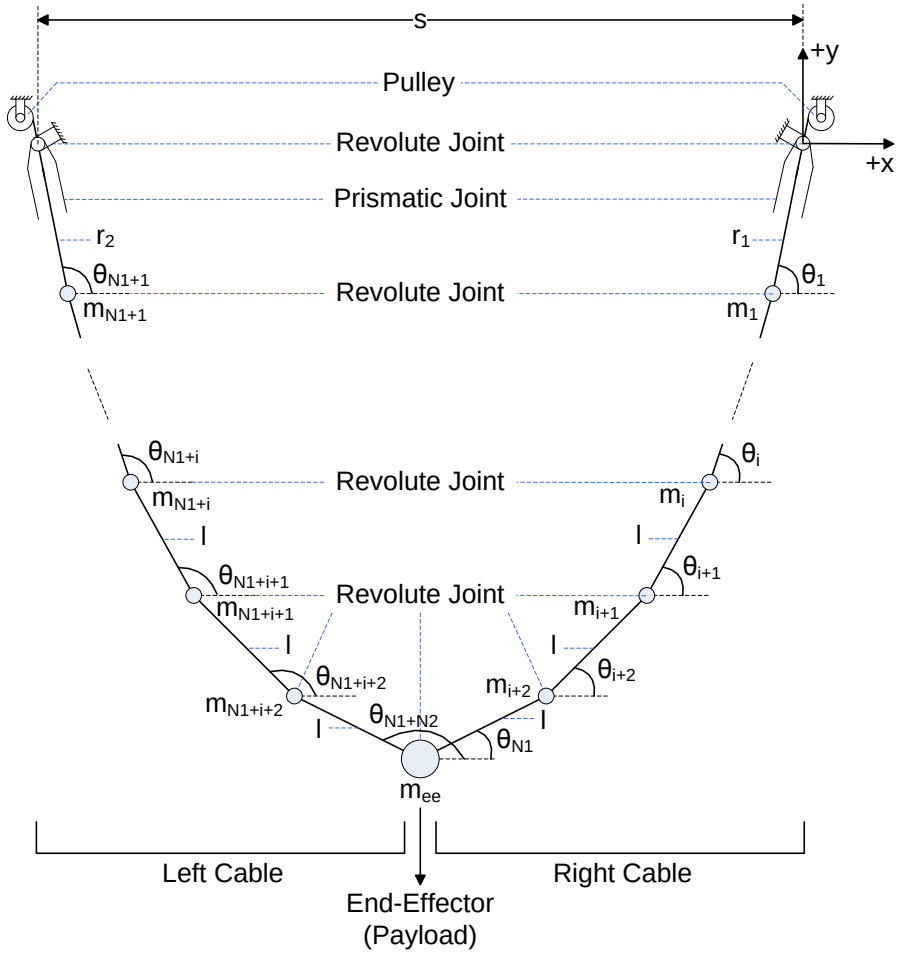

Figure 2.1: Discrete Model of Two-Cable Planar Parallel Cable Robot

In the discrete model, first cable segments which are the closest to actuators and pulleys have variable lengths that are represented by $\bar{r} = [r_1, r_2]^T$. On the other hand, all other segment lengths starting from the 2nd segment to the last one connected to end-effector are modeled as constant length links and this length is symbolized by l. Due to variable lengths of 1st segments (r_1 and r_2), there exist prismatic joints in order to enable translational motion. Moreover, prismatic joints are connected with frictionless revolute joints on to the ground so that rotations of 1st segments are also allowed with respect to ground. Constant length between these two revolute joints is indicated with s. In addition, angles of cable segments making with the horizontal axis are defined by $\bar{\theta} = [\theta_1, \theta_2, \dots, \theta_N]^T$. In this technique, it is important to note that there are no actual revolute or prismatic joints existing in the real manipulator. They constitute discretized cable model with rigid segment links appear between them and provides opportunity of including cable dynamics in the cable robot model.

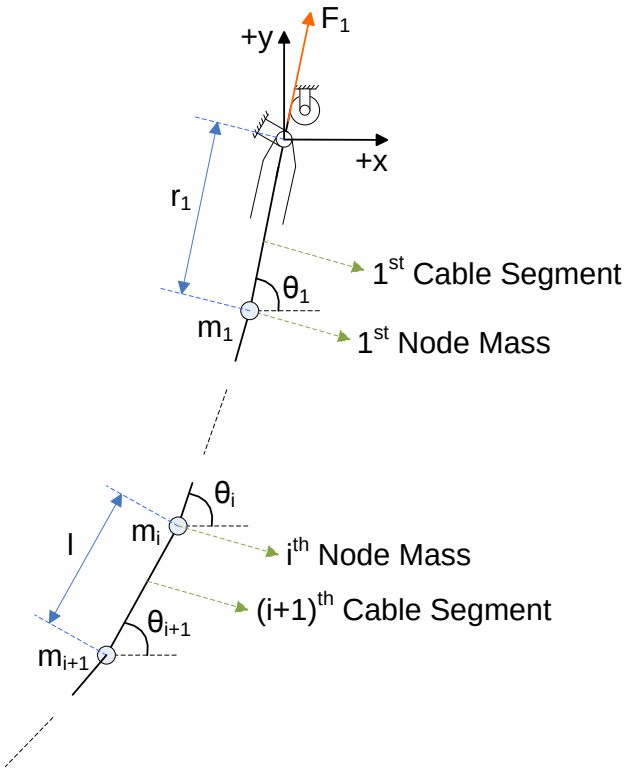

Figure 2.2: A Closer Look to Discrete Cable Model

As Figure 2.2 shows, pulling force vector of 1st cable segments is $\bar{F} = [F_1, F_2]^T$ and direction of pulling forces F_1 and F_2 are collinear with 1st segment lengths r_1 and r_2, respectively.

Kinematics, static equilibrium, and dynamics of two-cable planar parallel cable robot are analyzed with prescribed system parameters as follows:

2.1 Degree of Freedom of the System

$$m = Dim * L - \sum_{i}^{L} j_i * n_{c,i} \tag{2-1}$$

where

Dim: motion dimension of the system, which is 3 since cable parallel robot is planar

L: number of mobile links

$\sum_i^L j_i * n_{c,i}$: total number of constrained degrees of freedom by joints

Resulting from the need of discretizing each cable with different number of segments, cable on the right side is assumed to be divided into N_1 number of segments, while the one on the left side has N_2 segments. Total number of segments including in whole planar cable parallel robot is represented with N_{total}.

Number of joints, j:

$$\begin{aligned} j &= (N_1 + N_2 + 1\ Revolute\ Joints) + (2\ Prismatic\ Joints) \\ &= (N_{total} + 3\ )\ 1DOF\ Joints \end{aligned} \tag{2-2}$$

Number of mobile links, L:

$$\begin{aligned} L &= (N_1 + N_2\ Cable\ Segments) + (2\ Prismatic\ Bodies) \\ &= (N_{total} + 2\ ) \end{aligned} \tag{2-3}$$

Number of loops, n_L:

$$n_L = j - L = (N_{total} + 3\ ) - (N_{total} + 2\ ) = 1 \tag{2-4}$$

Degree of freedom, m:

$$\begin{aligned} m = Dim * L - \sum_{i}^{L} j_i * n_{c,i} &= 3 * (N_{total} + 2\ ) - 2 * (N_{total} + 3\ ) \\ &= N_{total} \end{aligned} \tag{2-5}$$

Number of joint variables, n_{jv}:

$$n_{jv} = 2n_L + m = 2 + N_{total} \tag{2-6}$$

$N_{total} + 2$ number of joint variables are formed of two 1st segment variable lengths ($\bar{r} = [r_1, r_2]^T$) and N_{total} number of segment angles ($\bar{\theta} = [\theta_1, \theta_2, \dots, \theta_{Ntotal}]^T$).

2.2 Kinematic Analysis

Cartesian positions of cable nodes are expressed with the help of unit vector notation illustrated below.

2.2.1 Unit Vectors

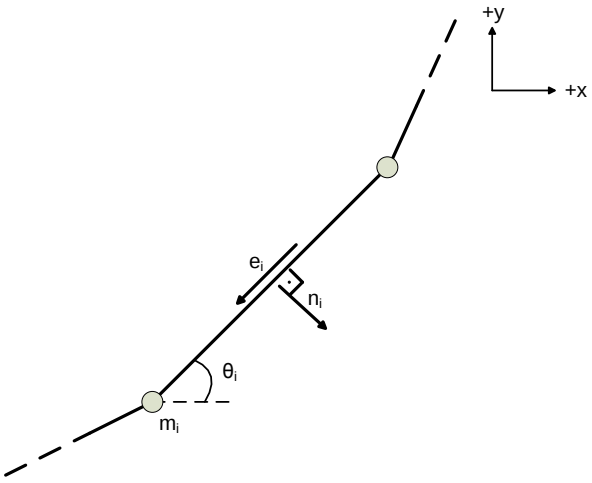

Figure 2.3: Unit Vectors

Tangential unit vector notation: $$e_i = [-\cos\theta_i \quad -\sin\theta_i] \tag{2-7}$$

Normal unit vector notation: $$n_i = [\sin\theta_i \quad -\cos\theta_i] \tag{2-8}$$

1st time derivative of unit vectors:

$$\dot{e}_i = [\dot{\theta}_i \sin\theta_i \quad -\dot{\theta}_i \cos\theta_i] = \dot{\theta}_i[\sin\theta_i \quad -\cos\theta_i] = \dot{\theta}_i n_i \tag{2-9}$$

$$\dot{n}_i = [\dot{\theta}_i \cos\theta_i \quad \dot{\theta}_i \sin\theta_i] = \dot{\theta}_i[\cos\theta_i \quad \sin\theta_i] = -\dot{\theta}_i e_i \tag{2-10}$$

2nd time derivative of unit vectors:

$$\begin{aligned}\ddot{e}_i &= \left[\ddot{\theta}_i \sin\theta_i + \dot{\theta}_i^{\,2} \cos\theta_i \quad -\ddot{\theta}_i \cos\theta_i + \dot{\theta}_i^{\,2} \sin\theta_i\right] \\ &= \ddot{\theta}_i[\sin\theta_i \quad -\cos\theta_i] + \dot{\theta}_i[\dot{\theta}_i \cos\theta_i \quad \dot{\theta}_i \sin\theta_i] \\ &= \ddot{\theta}_i n_i + \dot{\theta}_i \dot{n}_i\end{aligned} \tag{2-11}$$

$$\begin{aligned}\ddot{n}_i &= \left[\ddot{\theta}_i \cos\theta_i - \dot{\theta}_i^{\,2} \sin\theta_i \quad \ddot{\theta}_i \sin\theta_i + \dot{\theta}_i^{\,2} \cos\theta_i\right] \\ &= \ddot{\theta}_i[\cos\theta_i \quad \sin\theta_i] - \dot{\theta}_i[\dot{\theta}_i \sin\theta_i \quad -\dot{\theta}_i \cos\theta_i] \\ &= -\ddot{\theta}_i e_i - \dot{\theta}_i \dot{e}_i\end{aligned} \tag{2-12}$$

2.2.2 Position Equations

Position equations of segment nodes on the right cable are formed with the help of unit vectors derived on previous section:

1st right-node:

$p_{1x,r} = -r_1 \cos\theta_1$ and $p_{1y,r} = -r_1 \sin\theta_1$:

$$p_{1,r} = [-r_1 \cos\theta_1 \quad -r_1 \sin\theta_1] = r_1 e_1 \tag{2-13}$$

2nd right-node:

$p_{2x,r} = -r_1 \cos\theta_1 - l\cos\theta_2$ and $p_{2y,r} = -r_1 \sin\theta_1 - l\sin\theta_2$:

$$p_{2,r} = [-r_1 \cos\theta_1 - l\cos\theta_2 \quad -r_1 \sin\theta_1 - l\sin\theta_2] = r_1 e_1 + l e_2 \qquad (2\text{-}14)$$

….

….

N_1^{th} right-node:

$$p_{N1,r} = r_1 e_1 + \sum_{j=2}^{N1} l e_j \qquad (2\text{-}15)$$

In a similar way, position vectors of segment nodes on the left cable are generated:

1st left-node:

$p_{1x,l} = -s - r_2 \cos\theta_{N1+1}$ and $p_{1y,l} = -r_2 \sin\theta_{N1+1}$:

$$p_{1,l} = [-r_2 \cos\theta_{N1+1} \quad -r_2 \sin\theta_{N1+}] = r_2 e_{N1+1} \qquad (2\text{-}16)$$

2nd left-node:

$p_{2x,l} = -r_2 \cos\theta_{N1+1} - l\cos\theta_{N1+2}$ and $p_{2y,l} = -r_2 \sin\theta_{N1+1} - l\sin\theta_{N1+2}$:

$$\begin{aligned} p_{2,l} &= [-r_2 \cos\theta_{N1+1} - l\cos\theta_{N1+2} \quad -r_2 \sin\theta_{N1+1} - l\sin\theta_{N1+2}] \\ &= r_2 e_{N1+1} + l e_{N1+2} \end{aligned} \qquad (2\text{-}17)$$

….

….

N_2^{th} left-node:

$$p_{N2,l} = [-s \quad 0] + r_2 e_{N1+1} + \sum_{j=2}^{N2} l e_{N1+j} \qquad (2\text{-}18)$$

2.2.3 Velocity Equations

Velocity equations of segment nodes on the right cable are formed with the help of velocity level unit vectors:

1st right-node:

$\dot{p}_{1x,r} = -\dot{r_1}\cos\theta_1 + r_1\dot{\theta_1}\sin\theta_1$ and $\dot{p}_{1y,r} = -\dot{r_1}\sin\theta_1 - r_1\dot{\theta_1}\cos\theta_1$:

$$\begin{aligned}\dot{p}_{1,r} &= [-\dot{r_1}\,cos\,\theta_1 + r_1\dot{\theta_1}\,sin\,\theta_1 \quad -\dot{r_1}\,sin\,\theta_1 - r_1\dot{\theta_1}\,cos\,\theta_1] \\ &= \dot{r_1}e_1 + r_1\dot{e_1}\end{aligned} \tag{2-19}$$

2nd right-node:

$\dot{p}_{2x,r} = -\dot{r_1}\cos\theta_1 + r_1\dot{\theta_1}\sin\theta_1 + l\dot{\theta_2}\sin\theta_2$ and $\dot{p}_{2y,r} = -\dot{r_1}\sin\theta_1 - r_1\dot{\theta_1}\cos\theta_1 - l\dot{\theta_2}\cos\theta_2$:

$$\begin{aligned}\dot{p}_{2,r} &= [-\dot{r_1}\,c\,\theta_1 + r_1\dot{\theta_1}\,s\,\theta_1 + l\dot{\theta_2}\,s\,\theta_2 \quad -\dot{r_1}\,s\,\theta_1 - r_1\dot{\theta_1}\,c\,\theta_1 - l\dot{\theta_2}\,c\,\theta_2] \\ &= \dot{r_1}e_1 + r_1\dot{e_1} + l\dot{e_2}\end{aligned} \tag{2-20}$$

In formulation of $\dot{p}_{2,r}$, "c" and "s" represent "cos" and "sin" respectively.

….

….

N_1th right-node:

$$\dot{p}_{N1,r} = \dot{r_1}e_1 + r_1\dot{e_1} + \sum_{j=2}^{N1} l\dot{e_j} \tag{2-21}$$

In a similar way, position vectors of segment nodes on the left cable are generated:

1st left-node:

$\dot{p}_{1x,l} = -\dot{r_2}\,cos\,\theta_{N1+1} + r_2\dot{\theta}_{N1+1}\,sin\,\theta_{N1+1}$ and

$\dot{p}_{1y,l} = -\dot{r_2}\,sin\,\theta_{N1+1} - r_2\dot{\theta}_{N1+1}\,cos\,\theta_{N1+1}$:

$$\begin{aligned}&\dot{p}_{1,l}\\&= [-\dot{r_2}\, c\, \theta_{N1+1} + r_2\dot{\theta}_{N1+1}\, s\, \theta_{N1+1} \quad -\dot{r_2}\, s\, \theta_{N1+1} - r_2\dot{\theta}_{N1+1}\, c\, \theta_{N1+1}]\\&= \dot{r_2}e_{N1+1} + r_2\dot{e}_{N1+1}\end{aligned} \tag{2-22}$$

In formulation of $\dot{p}_{1,l}$, "c" and "s" represent "cos" and "sin" respectively.

2nd left-node:

$\dot{p}_{2x,l} = -\dot{r_2}\, cos\, \theta_{N1+1} + r_2\dot{\theta}_{N1+1}\, sin\, \theta_{N1+1} + l\dot{\theta}_{N1+2}\, sin\, \theta_{N1+2}$ and

$\dot{p}_{2y,l} = -\dot{r_2}\, sin\, \theta_{N1+1} - r_2\dot{\theta}_{N1+1}\, cos\, \theta_{N1+1} - l\dot{\theta}_{N1+2}\, cos\, \theta_{N1+2}$:

$$\dot{p}_{2,l} = [\dot{p}_{2x,l} \quad \dot{p}_{2y,l}] = \dot{r_2}e_{N1+1} + r_2\dot{e}_{N1+1} + l\dot{e}_{N1+2} \tag{2-23}$$

….

….

N_2th left-node:

$$\dot{p}_{N2,l} = \dot{r_2}e_{N1+1} + r_2\dot{e}_{N1+1} + \sum_{j=2}^{N2} l\dot{e}_{N1+j} \tag{2-24}$$

2.3 Static Equilibrium Analysis

In this section, static equilibrium equations of two-cable planar parallel cable robot are derived in order to solve system parameters at static equilibrium. For this purpose, force balance equations are written thanks to the free body diagram of segment nodes. Static equilibrium solution provides cable segment tensions, which are represented by T_i, and corresponding cable segment angles, θ_i.

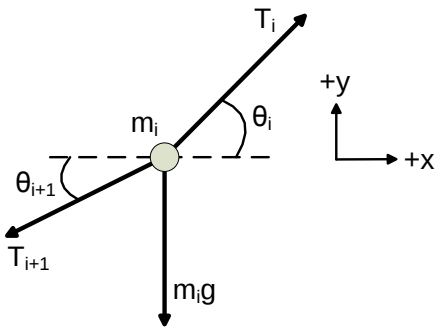

Figure 2.4: Free Body Diagram for Right-Cable Node Masses

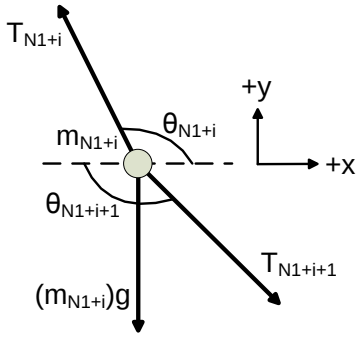

Figure 2.5: Free Body Diagram for Left-Cable Node Masses

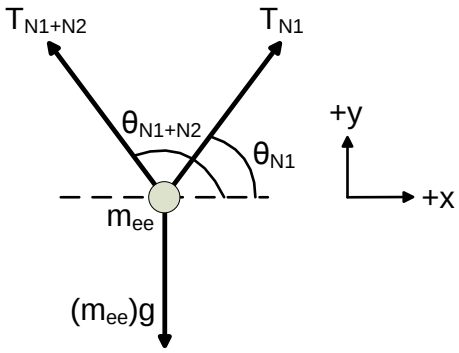

Figure 2.6: Free Body Diagram for End-Effector (Payload) Node Mass

Force equilibrium for right cable:

Force equilibrium along x-axis:

$$F_{x,r,i} = 0 \rightarrow T_i \cos\theta_i - T_{i+1} \cos\theta_{i+1} = 0 \tag{2-25}$$

Force equilibrium along y-axis:

$$F_{y,r,i} = 0 \rightarrow T_i \sin\theta_i - T_{i+1} sin\,\theta_{i+1} - m_i g = 0 \quad (2\text{-}26)$$

where $i = 1,2, \dots , N_1$

Force equilibrium for left cable:

Force equilibrium along x-axis:

$$F_{x,l,i} = 0 \rightarrow -T_i cos(\pi - \theta_i) + T_{i+1} cos(\pi - \theta_{i+1}) = 0 \quad (2\text{-}27)$$

Force equilibrium along y-axis:

$$F_{y,l,i} = 0 \rightarrow T_i \sin(\pi - \theta_i) - T_{i+1} sin(\pi - \theta_{i+1}) - m_i g = 0 \quad (2\text{-}28)$$

where $i = (N_1 + 1), (N_1 + 2), \dots , (N_1 + N_2)$

Force equilibrium for end-effector node:

Force equilibrium along x-axis:

$$F_{x,ee} = 0 \rightarrow T_{N1} cos\,\theta_{N1} + T_{N1+N2} cos(\pi - \theta_{N1+N2}) = 0 \quad (2\text{-}29)$$

Force equilibrium along y-axis:

$$F_{y,ee} = 0 \rightarrow T_{N1} \sin\theta_{N1} - T_{N1+N2} sin(\pi - \theta_{N1+N2}) - m_{N1} g = 0 \quad (2\text{-}30)$$

There exist total of $2 * (N_1 + N_2 - 1)$ number of algebraic equations. These equations contain also $2 * (N_1 + N_2 - 1)$ number of unknowns, which are composed of $N_1 + N_2 - 1$ number of cable tensions and $N_1 + N_2 - 1$ number of cable segment angles. Consequently, this set of equations for static equilibrium can be solved with unique solution for given $\bar{r} = [r_1, r_2]^T$.

2.4 Dynamics

In this section, explicit equations of motion are obtained by utilizing Lagrange dynamics because it provides ease of system modeling by serving the advantages listed on the next section.

2.4.1 Advantages of Lagrange Dynamics

Lagrangian formulation provides significant advantages in dynamic modeling studies some of which are listed below.

- It provides ease of working with scalars like kinetic and potential energy (K and U) compared to dealing with vectors [47].
- There is no need to draw free body diagram because it is always dealt with scalars.
- Deriving accelerations is not required.
- It is not required to consider all forces within the system. In other words, forces that make no work are not taken into account if they are not point of interest.
- Lagrangian expression (L) can be written by using the any possible coordinates. Then, there is no obstacle to differ these coordinates with more appropriate ones to describe the system symmetry in more descriptive way [47].
- Constrained problems can be more easily formulated with the help of Lagrange equations [47].

2.4.2 Lagrange Equations without Constraints

It has vital importance to formulate dynamics of a system in order to simulate it and additionally to design a controller for it [48]. Therefore, it is critical to understand the basic derivation theory of Lagrange equations to be able to build following sections of the thesis on a strong base.

Derivation of Lagrange equations requires formulation of Lagrangian, "L" by subtracting potential energy of the system from its kinetic energy. These equations can be derived by utilizing virtual displacement approach or Hamilton's principle of least action [48].

$$L = K - U \quad \text{where} \quad K\text{: Kinetic Energy and} \quad U\text{: Potential Energy}$$

In order to identify system, generalized coordinates are defined such that number of them is equal to the degree of freedom of the system in case of unconstrained problem.

$$G = \{q_1, q_2, \dots, q_m\} \text{ where } m\text{: Degree of Freedom}$$

$$\bar{q} = [q_1 \quad q_2 \quad \cdots \quad q_m]^T \text{ : vector of generalized coordinates}$$

Kinetic and potential energy functions are formed based on generalized coordinates and their derivatives.

Kinetic Energy Function: $K = K(\bar{q}, \dot{\bar{q}}) = \frac{1}{2}\sum_{i=1}^{N} m_i {V_i}^2 + \frac{1}{2}\sum_{i=1}^{N} \vec{\omega}_i . \check{J}_i . \vec{\omega}_i$ where N:number of moving bodies

Translational velocities: $\vec{V}_i = \vec{V}_{i/F(0)}$; ${V_i}^2 = \vec{V}_i . \vec{V}_i = \overline{V_i}^T \, \overline{V_i}$

Rotational velocities: $\vec{\omega}_i = \vec{\omega}_{i/F(0)}$; $\vec{\omega}_i . \check{J}_i . \vec{\omega}_i = \overline{\omega_i}^T \, \widehat{J_i} \, \overline{\omega_i}$

All velocities must be expressed in terms of $\bar{q}$ and $\dot{\bar{q}}$.

Potential Energy Function: $U = U(\bar{q}) = U_g + U_{spr}$

where U_g: potential energy due to gravity; $U_g = \sum_{i=1}^{L} m_i g h_i$ where h_i: elevation of body i from a suitable datum.

U_{spr} : potential energy stored in elastic members; $U_{spr} = \sum_{i=1}^{L} \frac{1}{2} k_i (\Delta s_i)^2 + \sum_{j=1}^{R} \frac{1}{2} k_j (\Delta \theta_i)^2$ where L: number of linear elastic members and R: number of rotational elastic members

Dissipation Energy Function: $D = D(\bar{q}, \dot{\bar{q}}) = \underbrace{\frac{1}{2}\sum_{k=1}^{M} c_k (\Delta V_k)^2}_{linear\ friction} + \underbrace{\frac{1}{2}\sum_{r=1}^{M'} c_r (\Delta \omega_r)^2}_{rotational\ friction}$:

Rayleigh's dissipation function for viscous friction.

ΔV_k and $\Delta \omega_r$ must be expressed in terms of $\bar{q}$ and $\dot{\bar{q}}$.

Generalized force vector are generated by writing the virtual work expression. This derivations enables to obtain forces that are not included within potential energy (U) and dissipation functions (D).

Virtual Work: $\delta W = \sum_{k=1}^{n} Q_k \delta q_k = \sum_{i=1}^{N} \overrightarrow{F_i}.\delta\vec{z}_i + \sum_{j=1}^{M} \overrightarrow{M_j}.\delta\vec{\gamma}_i$

where $\overrightarrow{F_i}$: a force applied at a point P_i of the system

$\delta\vec{z}_i$: virtual linear displacement of P_i (must be expressed in terms of $\delta q_1, \dots, \delta q_n$)

$\overrightarrow{M_i}$: a moment applied at a body B_j

$\delta\vec{\gamma}_i$: virtual angular displacement of B_j (must be expressed in terms of $\delta q_1, \dots, \delta q_n$)

At first step, instead of forming Lagrangian expression "L", more explicit form of Euler-Lagrange equations is preferred to be able to interpret effect of each scalar function on the system more easily. Hence generalized momenta are formulized as follows:

$$P_k = \frac{\partial K}{\partial \dot{q}_k}$$

As a result, explicit Lagrange equations without constraint are stated in the below form:

$$\dot{P}_k - \frac{\partial K}{\partial q_k} + \frac{\partial D}{\partial \dot{q}_k} + \frac{\partial U}{\partial q_k} = Q_k \;\Rightarrow\; \frac{d}{dt}\left(\frac{\partial K}{\partial \dot{q}_k}\right) - \frac{\partial K}{\partial q_k} + \frac{\partial D}{\partial \dot{q}_k} + \frac{\partial U}{\partial q_k} = Q_k$$

Same formulation can also be presented in a form including Lagrangian expression "L":

$$\frac{d}{dt}\left(\frac{\partial L}{\partial \dot{q}_k}\right) - \frac{\partial L}{\partial q_k} + \frac{\partial D}{\partial \dot{q}_k} = Q_k$$

As indicated before, two-cable planar parallel cable robot has N_{total} degrees of freedom in general case. Generalized coordinate vector is created by cable segment angles and variable 1st segment lengths of cable, i.e. $\bar{q} = [\bar{\theta} \quad \bar{r}]^T$. Note that system

has N_{total} number of segment angles and two of 1st segment lengths meaning that the number of generalized coordinates is $N_{total} + 2$. This implies that there should exist two constraint equations in case of 1st segment pulling forces F_1 and F_2 are specified so that complete set of motion equations are generated.

2.4.3 Lagrange Equations with Constraints

m: DOF of the system

n: number of the generalized coordinates ($n > m$)

Therefore, n generalized coordinates are interrelated with $g = n - m$ independent constraint equations.

Motivations:

1) In cases of dry friction where normal reaction forces are required. Normal reactions appear as constraint forces.
2) In cases in which we are interested in some of the reaction forces and moments. Again, they appear as constraint forces.
3) Number of equations increase but they get simpler.
    - Reduction in the chance of making mistakes.
    - Physical interpretations become easier.
4) In the cases of "nonholonomic" constraints, it is inevitable to live with them during the deviation phase.

Constraint Equations:

They are generally expressed in the velocity level:

$$\sum_{k=1}^{n} \psi_{jk}\, \dot{q}_k + \psi_{j0} = 0 \qquad for\ j = 1,2, \dots, g$$

It is clear that the generalized force of constraint, Q', do not perform any work, meaning:

$$\delta W' = \sum_{k=1}^{n} Q'_k \, \delta q_k = 0$$

As it can be seen, this work expression includes,δq_k, i.e. virtual displacements. It is a need to somehow relate this virtual work, $\delta W'$, with constraint equations, but position level constraint equations do not include any δq_k. Therefore they must be expressed in velocity level in order to obtain δq_k inside of them, which is indicated below:

Virtual Variation Form of the Constraint Equations:

$$\sum_{k=1}^{n} \psi_{jk} \, \delta q_k = 0 \qquad for\ j = 1,2, \dots, g$$

Introduce "g" number of coefficients: $\lambda_1, \lambda_2, \dots, \lambda_g$

In order to relate this virtual variation and generalized constraint force, "λ"s can be used as coefficients and virtual variation equation can be rewritten as follows:

$$\sum_{j=1}^{g} \lambda_g \left[\sum_{k=1}^{n} \psi_{jk} \, \delta q_k \right] = 0 \ \xrightarrow{yields} \ \sum_{k=1}^{n} \left[\sum_{j=1}^{g} \psi_{jk} \, \lambda_j \right] \delta q_k = 0$$

Definition:

$Q'_k = \sum_{j=1}^{g} \psi_{jk} \, \lambda_j$: Generalized constraint force associated with q_k

$$\delta W' = \sum_{k=1}^{n} Q'_k \, \delta q_k = 0$$

Interpretation: As long as the constraints are satisfied, the virtual work done ($\delta W'$) by the constraint forces vanishes ($\delta W' = 0$).

Lagrange Multipliers: $\lambda_1, \lambda_2, \dots, \lambda_g$

Lagrange Equations with Constraints:

$$\dot{P}_k - \frac{\partial K}{\partial q_k} + \frac{\partial D}{\partial \dot{q}_k} + \frac{\partial U}{\partial q_k} = Q_k + Q'_k \qquad for\ k = 1,2,\dots,n$$

$$\sum_{k=1}^{n} \psi_{jk}\, \dot{q}_k + \psi_{j0} = 0 \qquad for\ j = 1,2,\dots,g$$

Note: $\dot{P}_k = \frac{d}{dt}\left(\frac{\partial L}{\partial \dot{q}_k}\right)$ and $\frac{\partial L}{\partial q_k} = \frac{\partial K}{\partial q_k} - \frac{\partial U}{\partial q_k}$ $where\ L = K - U$

Therefore, Lagrange equation can also be written as

$$\frac{d}{dt}\left(\frac{\partial L}{\partial \dot{q}_k}\right) - \frac{\partial L}{\partial q_k} + \frac{\partial D}{\partial \dot{q}_k} = Q_k \qquad for\ k = 1,2,\dots,n$$

Total Number of Equations: n (Lagrange Equations) + g (Constraint Equations)

Total Number of Unknowns: $q_1, q_2, \dots, q_n$; $\lambda_1, \lambda_2, \dots, \lambda_g$ ($n + g$ unknowns)

During derivation phase, $q_1, q_2, \dots, q_n$ must be treated as if they are all independent when expressing K, U, D, and δW. The constraint equations take the care of relationships, which are appended to the Lagrange equations. In other words, in expressing K, U, D, and δW it is assumed that all the constraints are removed (i.e., mathematical free body diagram drawing).

2.4.4 Construction of Constraint Lagrange Equations for Two-Cable Planar Parallel Cable Robot

1) Generalized coordinate vector: $\bar{q}^T = [\bar{\theta}^T, \bar{r}^T]$. While $\bar{\theta}$ represents the vector of cable segment angles, $\bar{r}$ is the vector of variable lengths of 1st segments of each cable.

2) Form kinetic and potential energy terms (K, U) for Lagrangian expression ($L = K - U$):

Kinetic Energy: $K = K(\bar{q}, \dot{\bar{q}}) = K\left(\bar{\theta}, \dot{\bar{\theta}}, \bar{r}, \dot{\bar{r}}\right) = \sum_{i=1}^{n} \frac{1}{2} m_i {v_i}^T v_i$ where $v_i = \begin{bmatrix} \dot{x}_i \\ \dot{y}_i \end{bmatrix}$,

$(\dot{x}_i, \dot{y}_i)$: x and y velocity components of i[th] node mass

There does not take place any kinetic energy formed by rotational speed of a component contained in the system since all node masses are assumed to be point masses and rigid links between them are assumed to be massless.

Potential Energy: $U = U(\bar{q}) = U(\bar{\theta}, \bar{r}) = \sum_{i=1}^{n} m_i g y_i$

Lagrangian:

$$L = K - U = \sum_{i=1}^{n} \frac{1}{2} m_i {v_i}^T v_i - \sum_{i=1}^{n} m_i g y_i = \sum_{i=1}^{n} \left[\frac{1}{2} m_i {v_i}^T v_i - m_i g y_i \right]$$

3) Find out the related components of the ordinary Lagrange equations (meaning Lagrange equations without constraint) requiring some partial and time derivatives:

$$\frac{d}{dt}\left(\frac{\partial L}{\partial \dot{q}_k}\right) - \frac{\partial L}{\partial q_k} + \frac{\partial D}{\partial \dot{q}_k} = Q_k \qquad for\ k = 1,2,\dots,n$$

It is assumed that all joints within the system are frictionless and bodies included are not exposed to any dissipation effect. Therefore, $\frac{\partial D}{\partial \dot{q}_k}$ expression vanishes to zero and Lagrange equations take the following simpler form:

$$\frac{d}{dt}\left(\frac{\partial L}{\partial \dot{q}_k}\right) - \frac{\partial L}{\partial q_k} = Q_k \qquad for\ k = 1,2,\dots,n$$

4) Write generalized force vector, Q_k:

$$\sum_{k=1}^{n} Q_k \delta q_k = \sum_{i=1}^{N} \vec{F_i}.\delta \vec{z_i} + \sum_{j=1}^{M} \overrightarrow{M_j}.\delta \vec{\gamma}_i$$

There is not applied any moment on the system; therefore, $\sum_{j=1}^{M} \overrightarrow{M_j}.\delta \vec{\gamma}_i$ term drops out and generalized force depends on only forces:

$$\sum_{k=1}^{n} Q_k \delta q_k = \sum_{i=1}^{N} \vec{F_i}.\delta\vec{z}_i = F_1\delta r_1 + F_2\delta r_2$$

Then, generalized force vector becomes:

$$\bar{Q} = \underbrace{[0 \quad 0 \quad \ldots \quad 0 \quad F_1 \quad F_2]^T}_{(Ntotal+2)\ number\ of\ elements} \tag{2-31}$$

F_1 and F_2 are the specified forces applied along r_1 and r_2 respectively.

5) Write position level constraint equations, i.e. loop-closure equations, by equating the x and y components of end-effector position by approaching from right and left cable sides of the planar robot:

$\bar{p} = \begin{bmatrix} x \\ y \end{bmatrix} = f_1(\bar{\theta}_{right}, r_1) = f_1(\bar{\theta}_{left}, r_2)$ where $\bar{p}$ is the x and y coordinate vector of end-effector.

where $\bar{\theta}_{right}$ is the vector of segment angles and r_1 is the length of 1st cable segment, both of which belong to the cable on right side. Similarly, $\bar{\theta}_{left}$ is the vector of segment angles and r_2 is the length of 1st cable segment, both of which belong to the cable on left side.

Constraint is holonomic type since it can be expressed in position level. Therefore, it can be written in the following simplified form:

$\varphi(\bar{q}) = \varphi(\bar{\theta}, \bar{r})$ where $\bar{q}$ is the vector of generalized coordinates.

6) Write velocity equations by differentiating the position level equations:

$$\frac{d[\varphi(\bar{q})]}{dt} = \frac{d[\varphi(\bar{\theta}, \bar{r})]}{dt} = \widehat{\emptyset}(\bar{q})\dot{\bar{q}} = \widehat{\emptyset}(\bar{\theta}, \bar{r}) \begin{bmatrix} \dot{\bar{\theta}} \\ \dot{\bar{r}} \end{bmatrix} \tag{2-32}$$

7) Find out the coefficients of the 1st derivative of the generalized coordinates (i.e. coefficients of $\dot{q_k}$) from velocity equations. These coefficients will be the ψ_{jk} of the virtual variation form of the velocity level equations. When these coefficients (ψ_{jk}) are multiplied with Lagrange multipliers (λ_j), generalized constraint force associated with q_k is obtained ($Q'_k = \sum_{j=1}^{g} \psi_{jk}\, \lambda_j$).

8) Form generalized constraint force vector: $Q'_k = \sum_{j=1}^{g} \emptyset_{jk}\, \lambda_j$

9) Write acceleration equations by differentiating the velocity level equations:

$$\frac{d\left[\hat{\emptyset}(\bar{q})\dot{\bar{q}}\right]}{dt} = \dot{\hat{\emptyset}}(\bar{q})\dot{q} + \hat{\emptyset}(\bar{q})\ddot{\bar{q}} \tag{2-33}$$

10) Write acceleration level kinematic relation in the following form in order to obtain $\ddot{\bar{r}}$ in terms of $\ddot{\bar{\theta}}$:

$$\ddot{\bar{r}} = \hat{R}\ddot{\bar{\theta}} + \bar{m} \tag{2-34}$$

11) Form the Lagrange equations with constraints:

$$\frac{d}{dt}\left(\frac{\partial L}{\partial \dot{q_k}}\right) - \frac{\partial L}{\partial q_k} = Q_k + Q'_k \qquad for\ k = 1,2,\dots,n$$

12) The Lagrange equation found on the previous step includes "λ". "λ" must be found out in order to solve equation of motion. To do that, write the obtained Lagrange equation in the form of:

$$\hat{M}(\bar{q})\ddot{\bar{q}} - \bar{C}(\bar{q},\dot{\bar{q}}) = \hat{\emptyset}(\bar{q})\bar{\lambda} + \hat{A}\bar{F} \tag{2-35}$$

$$\hat{M}(\bar{q})\ddot{\bar{q}} = \bar{C}(\bar{q},\dot{\bar{q}}) + \hat{\emptyset}(\bar{q})\bar{\lambda} + \hat{A}\bar{F}$$

$$\ddot{\bar{q}} = \left[\hat{M}(\bar{q})\right]^{-1}\bar{C}(\bar{q},\dot{\bar{q}}) + \left[\hat{M}(\bar{q})\right]^{-1}\hat{\emptyset}(\bar{q})\bar{\lambda} + \left[\hat{M}(\bar{q})\right]^{-1}\hat{A}\bar{F}$$

$$\ddot{\bar{q}} = \bar{D} + \hat{E}\bar{\lambda} + \hat{G}\bar{F} \tag{2-36}$$

where $\bar{D} = \left[\widehat{M}(\bar{q})\right]^{-1}\bar{C}(\bar{q},\dot{\bar{q}})$, $\hat{E} = \left[\widehat{M}(\bar{q})\right]^{-1}\widehat{\emptyset}(\bar{q})$ and $\hat{G} = \left[\widehat{M}(\bar{q})\right]^{-1}\hat{A}$.

This final form of equation of motion can be decomposed as:

$$\ddot{\bar{q}} = \begin{bmatrix}\ddot{\bar{\theta}}\\ \ddot{\bar{r}}\end{bmatrix} = \begin{bmatrix}\bar{D}_\theta\\ \bar{D}_r\end{bmatrix} + \begin{bmatrix}\hat{E}_\theta\\ \hat{E}_r\end{bmatrix}\bar{\lambda} + \begin{bmatrix}\hat{G}_\theta\\ \hat{G}_r\end{bmatrix}\bar{F} \tag{2-37}$$

This set of equations are written in the following form in order to eliminate $\bar{\lambda}$ and $\bar{r}$:

$$\ddot{\bar{\theta}} = \bar{D}_\theta + \hat{E}_\theta\bar{\lambda} + \hat{G}_\theta\bar{F} \tag{2-38}$$

$$\ddot{\bar{r}} = \bar{D}_r + \hat{E}_r\bar{\lambda} + \hat{G}_r\bar{F} \tag{2-39}$$

13) Using the acceleration level kinematic relation and the Lagrange equation for $\ddot{\bar{r}}$, find out $\bar{\lambda}$:

$$\ddot{\bar{r}} = \hat{R}\ddot{\bar{\theta}} + \bar{m} = \bar{D}_r + \hat{E}_r\bar{\lambda} + \hat{G}_r\bar{F} \tag{2-40}$$

$$\bar{\lambda} = \hat{E}_r^{-1}\left[\hat{R}\ddot{\bar{\theta}} + \bar{m} - \bar{D}_r - \hat{G}_r\bar{F}\right] \tag{2-41}$$

14) Express $\bar{r}$ and $\dot{\bar{r}}$ in terms of $\bar{\theta}$ and $\dot{\bar{\theta}}$ in order to express equation of motion in terms of cable segment angles only.

15) Plug $\bar{\lambda}$ expression found before into the equation of motion:

$$\ddot{\bar{\theta}} = \bar{D}_\theta + \hat{E}_\theta\hat{E}_r^{-1}\left[\hat{R}\ddot{\bar{\theta}} + \bar{m} - \bar{D}_r - \hat{G}_r\bar{F}\right] + \hat{G}_\theta\bar{F} \tag{2-42}$$

$\left[\hat{I} - \hat{E}_\theta\hat{E}_r^{-1}\hat{R}\right]\ddot{\bar{\theta}} = \bar{D}_\theta + \hat{E}_\theta\hat{E}_r^{-1}\left[\bar{m} - \bar{D}_r - \hat{G}_r\bar{F}\right] + \hat{G}_\theta\bar{F}$ where $\hat{I}$ is identity matrix.

$$\ddot{\bar{\theta}} = \hat{\beta}\left[\bar{D}_\theta + \hat{E}_\theta \hat{E}_r{}^{-1}\left[\bar{m} - \bar{D}_r - \hat{G}_r\bar{F}\right] + \hat{G}_\theta\bar{F}\right] \tag{2-43}$$

where

$$\hat{\beta} = \left[\hat{I} - \hat{E}_\theta \hat{E}_r{}^{-1}\hat{R}\right]^{-1} \tag{2-44}$$

Note that this is the final form of equation of motion that is utilized to simulate motion of two-cable planar parallel cable robot.

2.5 Determination of the Number of Segments for Realistic Cable Modeling

Discretization or segmentation of cables for dynamic modeling brings a new issue to be addressed: How many segments are required for each discrete cable so that they can reflect adequately realistic behavior of a continuous cable? An appropriate approach to deal with this problem is essential in order to deduce that developed lumped-mass dynamic model represents the cable robot accurately.

In study of Collard, Lamaury and Gouttefarde [49], this topic is discussed by comparison of 12-meter constant lengths of the 6 cables discretized into one to ten segments. Their static equilibrium with given cable lengths, dynamic response in case of payload elevation and natural frequencies are analyzed all of which are based on convergence of acquired results.

In this research, modal analysis of a separately modeled single cable is carried out by applying the system parameters observed in the cable robot. This method is considered as a proof of concept for comprehensive dynamic modeling of cable manipulator by defining discretized single cable as a decision maker for determination of number of segments. Therefore, workspace for a planar cable robot is specified first, which is displayed in Figure 2.7 in order to examine the system parameters that each cable is exposed to. These parameters can be listed as cable length, cable mass and tensions appeared on the cable, which play a great role on the values of natural frequencies of cables.

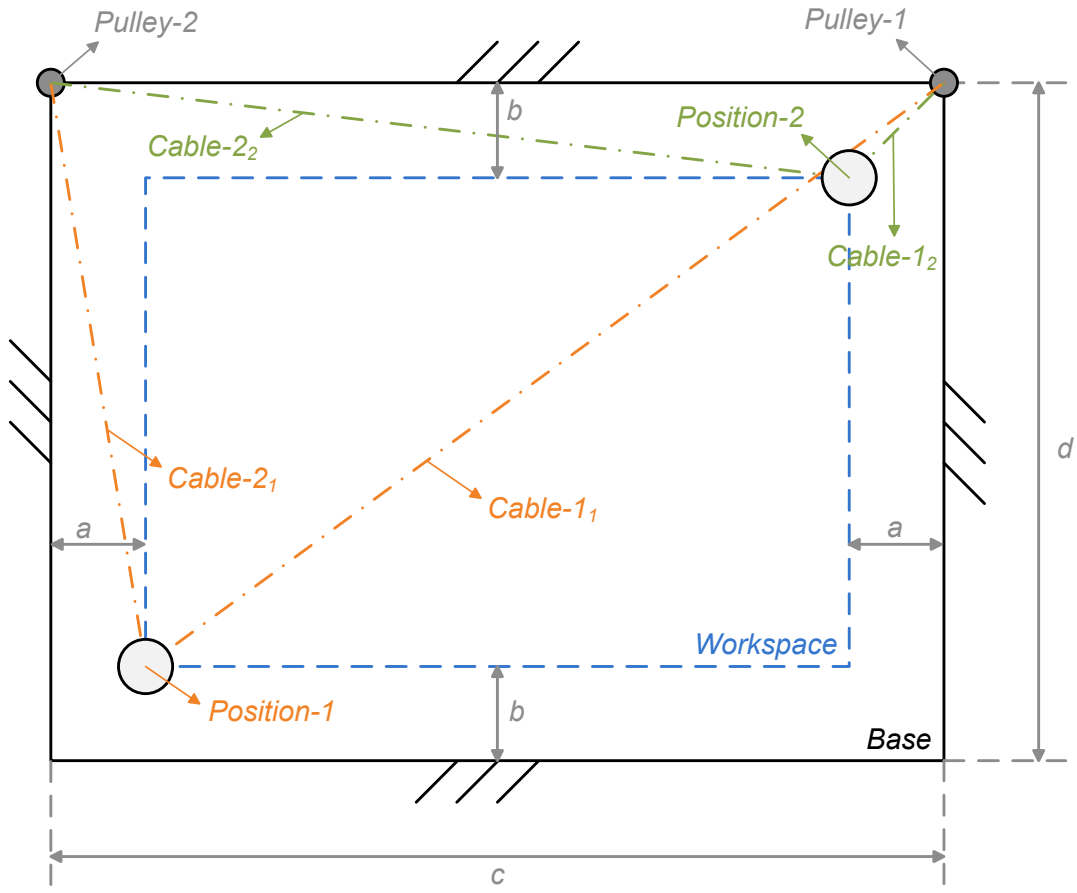

Figure 2.7: Specified Workspace of the Planar Cable Robot

Dimensions of this workspace are assigned as follows:

Table 1: Specified Workspace Dimensions

Specified Workspace Parameters	**Value (Unit)**
d (Height of the Base)	10 (m)
c (Width of the Base)	5 (m)
b (Height Offset)	1.2 (m)
a (Width Offset)	0.5 (m)
Coordinates of Position-1 (x,y)	-4.5 , -8.8 (m,m)
Coordinates of Position-2 (x,y)	-0.5 , -1.2 (m,m)
Coordinates of Pulley-1 (x,y)	0 , 0 (m,m)
Coordinates of Pulley-2 (x,y)	-5 , 0 (m,m)

To be more descriptive for the notation used in Figure 2.7, $Cable - i_j$ means i^{th} cable of j^{th} position.

After the introduction of the workspace of planar cable robot, it is necessary also to specify its other parameters like payload, diameter of the cable and density of the cable material used. Cable length and consequently cable mass depend on the location of payload within the workspace.

Table 2: Assigned System Parameters

Assigned System Parameter	**Value (Unit)**
Mass of the End-Effector/Payload	3 (kg)
Diameter of the Cable	1.59 (mm)
Density of the Cable Material	7.8 (g/cm^3)

It should be noted that assigned parameters listed in Table 2 are meaningful not only for a workspace of this kind but also for large scale applications of cable robots. In researches [29], [23], [50], [51] and [52], where larger workspaces are also studied, cable mass to payload ratio ranges between 0.01 and 0.09 for the longest cable obtained within the specified workspace. This ratio is about 0.05 in this thesis. Therefore, it can be inferred that methods developed within this thesis might also be used for large scale applications since they have approximately similar order of cable dynamics dominance.

In order to involve all the extremities in terms of lengths, masses and tensions of cables, positions of payload located at the corners of the workspace envelope are taken into consideration. These corner positions are indicated with “Position-1” and “Position-2” in Figure 2.7. Although, there exist four corner locations of the workspace, it is sufficient to deal with the two diagonal ones since the other two constitute just the symmetrical configurations and have the same cable properties. According to this approach, Position-1 is analyzed firstly which has the longest and the heaviest cable with minimum tension. It can be intuitively concluded that this configuration gives the opportunity of observing cable with low natural frequency.

Position-2, as the diagonal location relative to Position-1, is analyzed secondly. The shortest cable of this position is the point of interest since there appears the highest tension on it. Therefore, it has vital importance in terms of strength of the cable and has a great role to determine cable diameter.

Resulting parameters related with cable can be simply derived as follows to be used in the natural frequency calculation:

Coordinates of Position-1:

$$x_{Position-1} = -4.5\ m\ ,\ y_{Position-1} = -8.8\ m$$

Resulting cable length between Position-1 and Pulley-1:

$$l_{Cable-1} = \sqrt{(x_{Position-1} - x_{Pulley-1})^2 + (y_{Position-1} - y_{Pulley-1})^2}$$

$$l_{Cable-1} = 9.88\ m$$

Resulting cable length between Position-1 and Pulley-2:

$$l_{Cable-2} = \sqrt{(x_{Position-1} - x_{Pulley-2})^2 + (y_{Position-1} - y_{Pulley-2})^2}$$

$$l_{Cable-2} = 8.81\ m$$

It is assumed that cable forms a straight line between payload and pulley. This assumption is valid only for cable length and cable mass calculation which is required for modal analysis of a single cable. It is a known fact that cable normally forms a point loaded catenary curve in this situation. However, it is accurate enough to assume it a straight line since purpose in this approach is to sense the order of magnitude of relation between natural frequencies and discretization level of a cable.

Angles of the cables making with the horizontal axis can be derived using the geometry of the workspace:

$$tan\theta_{P11} = \frac{y_{Position-1} - y_{Pulley-1}}{x_{Position-1} - x_{Pulley-1}}$$

where $x_{Pulley-1} = 0$ and $y_{Pulley-1} = 0$

$$\theta_{P11} = atan\left(\frac{y_{Position-1}}{x_{Position-1}}\right) = 62.92°$$

Similarly, the angle of Cable-2 can also be found out:

$$tan\theta_{P12} = \frac{y_{Position-1} - y_{Pulley-2}}{x_{Position-1} - x_{Pulley-2}}$$

since $y_{Pulley-2} = 0$

$$\theta_{P12} = atan\left(\frac{y_{Position-1}}{x_{Position-1} - x_{Pulley-2}}\right) = 86.75°$$

Tensions observed at Position-1 can be calculated using static equilibrium at this configuration:

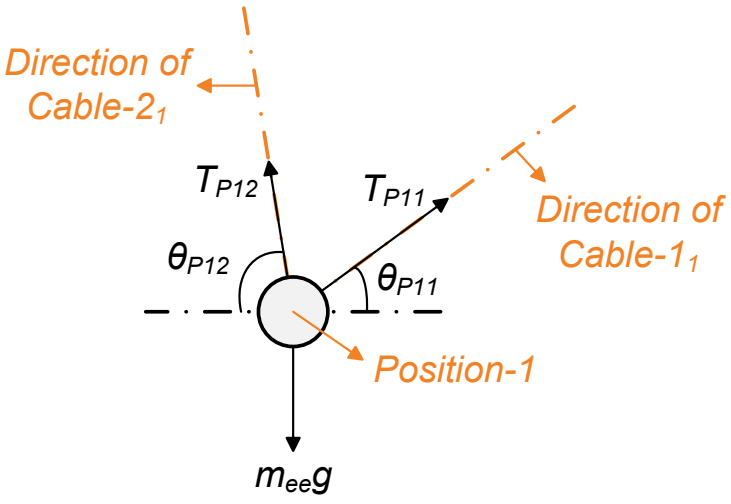

Figure 2.8: Free Body Diagram for Position-1

Force equilibrium along x-axis:

$$T_{P11}cos\theta_{P11} = T_{P12}cos\theta_{P12}$$

Force equilibrium along y-axis:

$$T_{P11}sin\theta_{P11} + T_{P12}sin\theta_{P12} = m_{ee}g$$

In this notation, T_{Pji} represents the tension of ith cable at jth position, θ_{Pji} is the angle between ith cable and the horizontal axis at jth position and m_{ee} is the mass of the end-effector or payload. It is clear that tensions calculated from these equilibrium equations do not contain effect of the cable masses. However, they are not ignorable which leads to somehow count them in. For ease of calculation, tension components of the weights of cables are directly added to the tensions obtained from above equations.

$$T'_{P11} = T_{P11} + m_{Cable-1}gsin\theta_{P11}$$

$$T'_{P12} = T_{P12} + m_{Cable-2}gsin\theta_{P12}$$

Same calculations are repeated for Position-2, which has the coordinates of:

$$x_{Position-2} = -0.5\ m\ ,\ y_{Position-2} = -1.2\ m$$

Resulting cable length between Position-2 and Pulley-1:

$$l_{Cable-1} = \sqrt{(x_{Position-2} - x_{Pulley-1})^2 + (y_{Position-2} - y_{Pulley-1})^2}$$

$$l_{Cable-1} = 1.3\ m$$

Resulting cable length between Position-2 and Pulley-2:

$$l_{Cable-2} = \sqrt{(x_{Position-2} - x_{Pulley-2})^2 + (y_{Position-2} - y_{Pulley-2})^2}$$

$$l_{Cable-2} = 4.66\ m$$

Angles of the cables making with the horizontal axis can be derived using the geometry of the workspace:

$$tan\theta_{P21} = \frac{y_{Position-2} - y_{Pulley-1}}{x_{Position-2} - x_{Pulley-1}}$$

where $x_{Pulley-1} = 0$ and $y_{Pulley-1} = 0$

$$\theta_{P21} = atan\left(\frac{y_{Position-1}}{x_{Position-1}}\right) = 86.75°$$

Similarly, the angle of Cable-2 can also be found out:

$$tan\theta_{P22} = \frac{y_{Position-2} - y_{Pulley-2}}{x_{Position-2} - x_{Pulley-2}}$$

since $y_{Pulley-2} = 0$

$$\theta_{P22} = atan\left(\frac{y_{Position-2}}{x_{Position-2} - x_{Pulley-2}}\right) = 14.93°$$

Tensions observed at Position-2 can be calculated using static equilibrium at this configuration:

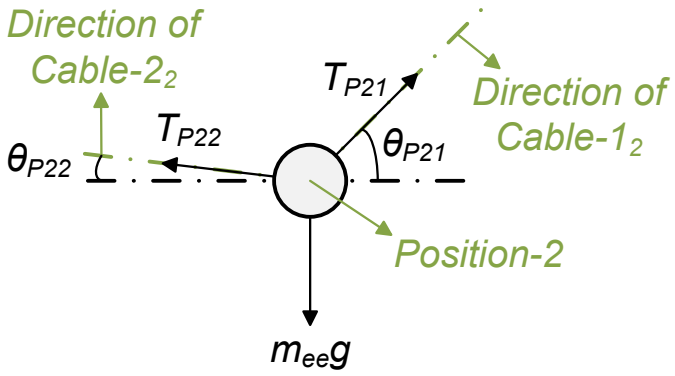

Figure 2.9: Free Body Diagram for Position-2

Force equilibrium along x-axis:

$$T_{P21}cos\theta_{P21} = T_{P22}cos\theta_{P22}$$

Force equilibrium along y-axis:

$$T_{P21}sin\theta_{P21} + T_{P22}sin\theta_{P22} = m_{ee}g$$

Tensions including tensioning effect of the cables:

$$T'_{P21} = T_{P21} + m_{Cable-1}gsin\theta_{P21}$$

$$T'_{P22} = T_{P22} + m_{Cable-2}gsin\theta_{P22}$$

After performing all the calculations based on the method described above, resulting system parameters are obtained and listed below:

Table 3: Resulting System Parameters

Resulting System Parameter			**Value (Unit)**
Cable Length	*@ Position-1*	Cable-1	9.88 (m)
		Cable-2	8.81 (m)
	@ Position-2	Cable-1	1.3 (m)
		Cable-2	4.66 (m)
Cable Mass	*@ Position-1*	Cable-1	0.1531 (kg)
		Cable-2	0.1365 (kg)
	@ Position-2	Cable-1	0.02 (kg)
		Cable-2	0.072 (kg)
Cable Tension	*@ Position-1*	Cable-1	4.64 (N)
		Cable-2	27.86 (N)
	@ Position-2	Cable-1	28.87 (N)
		Cable-2	11.60 (N)

According to Table 3, the most critical condition in terms of cable strength occurs at Position-2 for Cable-1 as expected. Referring to the catalog of CarlStahl™ [53] [54], it is better for optimal life time to select a cable which has the strength of 10 times of the load on it. Diameter of the cable indicated in Table 2, is selected considering this rule of thumb.

From Table 3, it is clear that natural frequencies of Cable-1 at Position-1 need to be analyzed since it has the highest length and mass but the lowest tension within this specified workspace. In this respect, this cable is taken out from the cable robot with the tension on it by considering the two ends are fixed at that instant and its transverse vibration is studied. It is aimed to examine the change in the natural frequencies as the number of segments of this single cable increases. If there is observed no considerable change of natural frequencies despite the increase of level of discretization, then it can be concluded that the number of segments where the last considerable change is presented, is enough to represent the dynamics of the cable accurately in the cable robot model. However, there is one more open issue of this approach: How many natural frequencies should be investigated? In order to answer this question, Fourier expansion of a square wave position reference is taken into account. Since a square wave command reflects the most aggressive response expectation from the cable robot and it scans high frequency range, there is no need to consider any other type of motion.

Fourier expansions of reference commands of 1 m movement from Position-1 in both x and y directions are obtained and illustrated below:

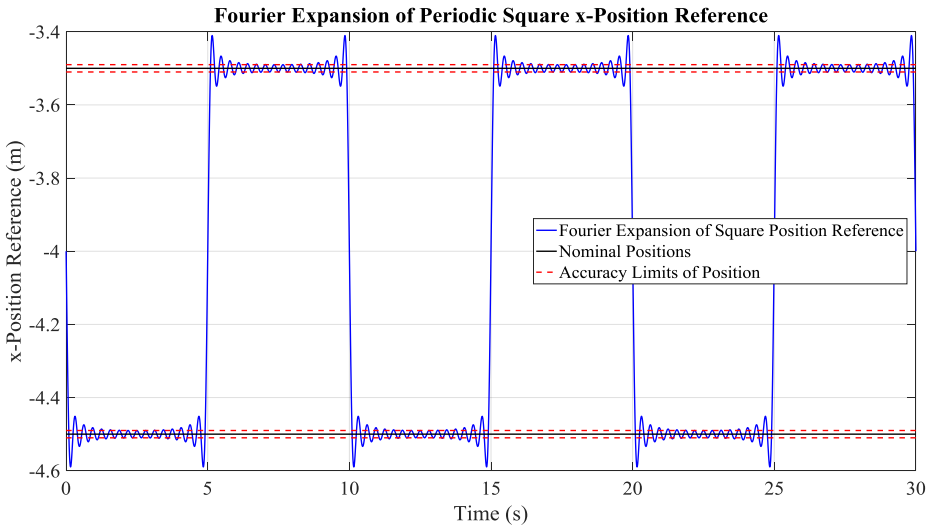

Figure 2.10: Fourier Expansion of Square Wave Position Reference in x-Direction

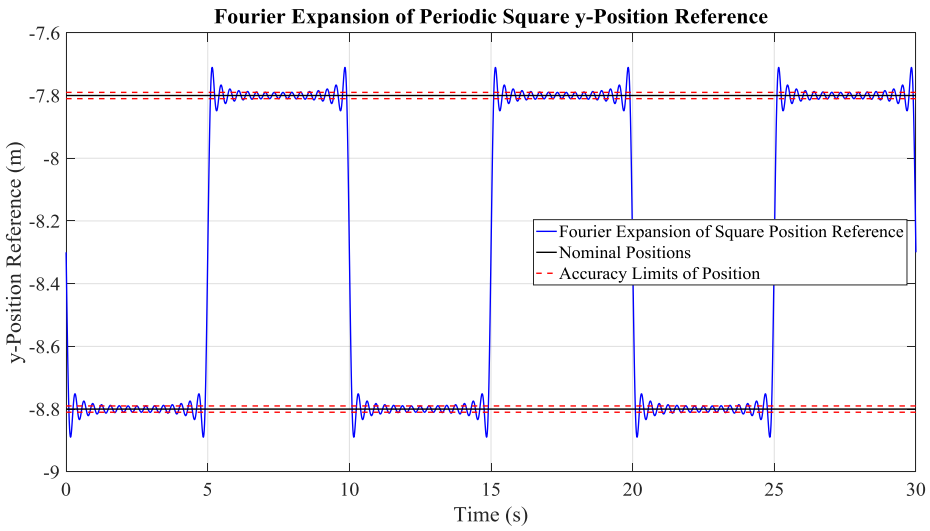

Figure 2.11: Fourier Expansion of Square Wave Position Reference in y-Direction

As shown in Figure 2.10 and Figure 2.11, accuracy limit of 1% error is defined for position references and Fourier expansion with first 16 odd terms is derived so that it stays within this limit range. It is important to note that overshoots and undershoots resulting from Gibbs phenomenon are ignored since they do not disappear even if number of terms included in Fourier expansion is increased. Frequency of the highest term of resulting Fourier expansion is the decision maker for the upper limit of frequency that should be examined.

Frequency of the highest term:

$$\omega_{highest} = \frac{k_{final}}{T} = 3.1\ Hz$$

where k_{final} is the index of the highest term and T is the period of square wave.

It is sufficient to analyze the natural frequencies up to value of $\omega_{highest}$. In order to find out natural frequencies of the single cable, regarding eigenvalue problem of it needs to be built. Thus there is a requirement for derivation of linearized form of equations of motion.

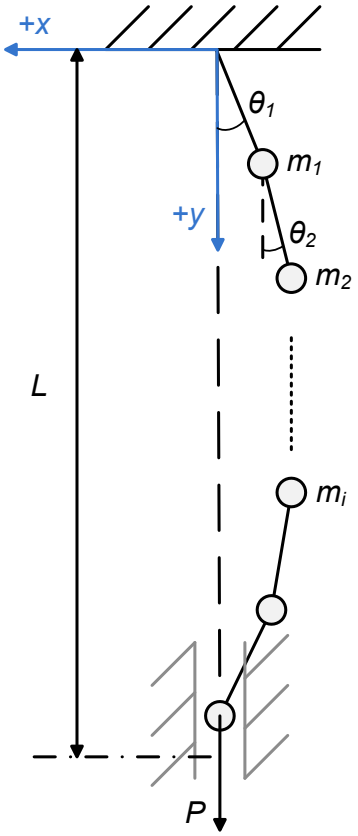

Figure 2.12: Discretized Single Cable

As shown in Figure 2.12, single cable is divided into N number of segments which have equal lengths and a tensioning force, P, is applied such that tip point moves vertically as if it is in a prismatic joint. Total mass of cable is uniformly distributed to the nodes formed by connection of the segments. Equations of motion for this segmented cable are obtained using constrained Lagrange dynamics details of

which are described in Section 2.4.3 of this thesis. At this step, it is not preferred to write down all the details of derivation for kinematics and dynamics since it becomes nothing but just repetition of the equations presented for cable robot before. The only remarkable difference is the constraint equation, which can be simply stated as:

$$x_{Tip} = 0$$

The constraint implies that tip point of the cable where tensioning force is applied, is not allowed to move in x-direction.

The general form of the constrained Lagrange equations is already written as

$$\dot{P}_k - \frac{\partial K}{\partial q_k} + \frac{\partial D}{\partial \dot{q}_k} + \frac{\partial U}{\partial q_k} = Q_k + Q'_k \qquad for\ k = 1,2,\dots,n$$

They can also be represented in general matrix form:

$$\widehat{M}(\bar{q})\ddot{\bar{q}} + \widehat{N}(\bar{q},\dot{\bar{q}})\dot{\bar{q}} + \bar{g}(\bar{q}) = \bar{\tau} \tag{2-45}$$

It is clear that Eqn. (2-45) is nonlinear and cannot be written in eigenvalue problem form. Therefore, a linearization step is necessary and it is wise to apply it before deriving the final form of the equations of motion not to deal with more complex expressions. Linearization steps at energy level are simply summarized as follows:

Kinetic and Potential Energy, K and U: After obtaining kinetic and potential energy, firstly substitute $sin\theta \approx \theta$ and $cos\theta \approx 1 - {\theta^2}/{2}$. Then, drop out 3rd and higher order terms, i.e. *quadrate* it, because with derivative operations, $\frac{\partial K}{\partial q_k}$ and $\frac{\partial U}{\partial q_k}$, final forms of them become linear.

Time Derivative of Generalized Momentum, $\dot{P}$: Use *quadrated* kinetic energy to find out $\dot{P}$ and since it appears as it is in the final form of the equations of motion, drop out 2nd and higher order terms to linearize it

Generalized Force, Q: Similar to $\dot{P}$, generalized force takes place directly in the final form of dynamic equations. For this reason, it should be dropped out 2nd and higher order terms after substitution of $sin\theta \approx \theta$ and $cos\theta \approx 1 - {\theta^2}/{2}$.

Generalized Constraint Force, $\dot{Q}$: Derivation of generalized constraint force is directly related with the velocity level constraint equation. Hence constraint equation is required to be linearized to be used in this step, which implies that 2nd and higher order terms after substitution of $sin\theta \approx \theta$ and $cos\theta \approx 1 - {\theta^2}/{2}$. Then,

its virtual form is utilized to form the virtual work of constraint force that results in generalized constraint forces including Lagrange multiplier(s).

It is assumed that all joints within the segmented single cable are frictionless and bodies included are not exposed to any dissipation effect. Therefore, $\frac{\partial D}{\partial \dot{q}_k}$ expression vanishes to zero.

After linearization operation, equations of motion are written in linear form and eigenvalue problem is obtained:

$$\left(\widehat{K} - \omega^2 \widehat{M}\right)\{\varphi\} = \bar{0}$$

In this thesis, Cable-1 of Position-1 is divided from 2 to 15 segments and for each case eigenvalue problem is solved by using Matlab's® *eig* command to obtain natural frequencies. Results of this analysis are presented on the following graphs on which impact of the number of segments on the natural frequencies is also illustrated.

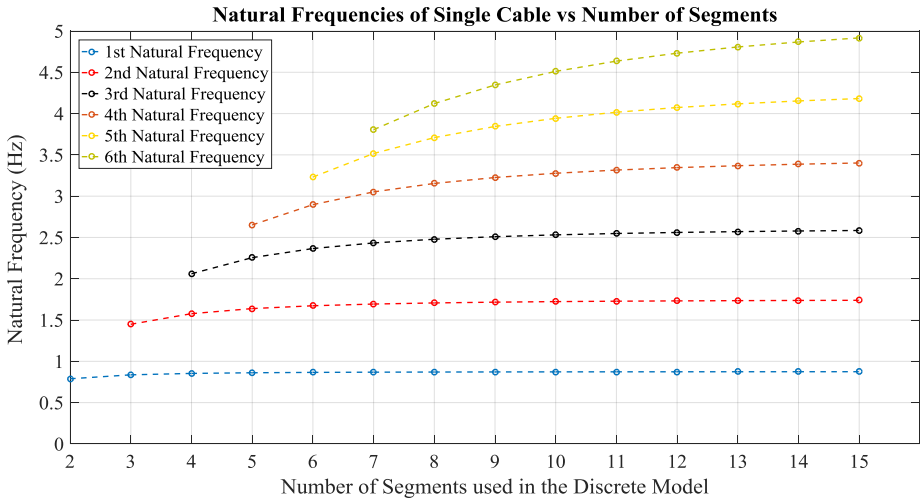

Figure 2.13: Natural Frequencies of Single Cable vs Number of Segments used in the Discrete Model

These graphs indicate that it is accurate enough to consider first 5 natural frequencies of the single cable since the 5th natural frequency is greater than the maximum frequency included in Fourier expansion of square wave, i.e. $\omega_{highest}$. At this stage, convergence rate of the first 5 natural frequencies are analyzed depending on the number of segments. For this purpose, a limit of 3% is specified for the change in the natural frequencies. In other words, if an increase in the segment number causes a percentage change smaller than 3% in the natural frequency, then it is concluded that there is no need to increase the number of segmentation anymore since it causes ignorable impact. Based on this strategy, percentage change of natural frequencies with respect to level of discretization is illustrated on the below figures with the help of its simple formulation:

$$Percentage\ Change = \frac{\omega_{i,j+1} - \omega_{i,j}}{\omega_{i,j+1}} * 100$$

where $\omega_{i,j}$ is the ith natural frequency of j-segmented single cable.

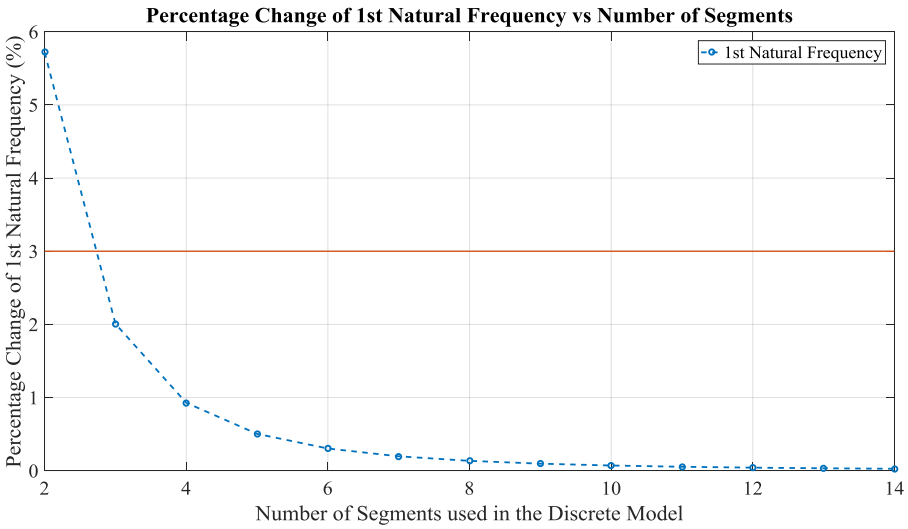

Figure 2.14: Percentage Change of 1st Natural Frequency vs Number of Segments used in the Discrete Model

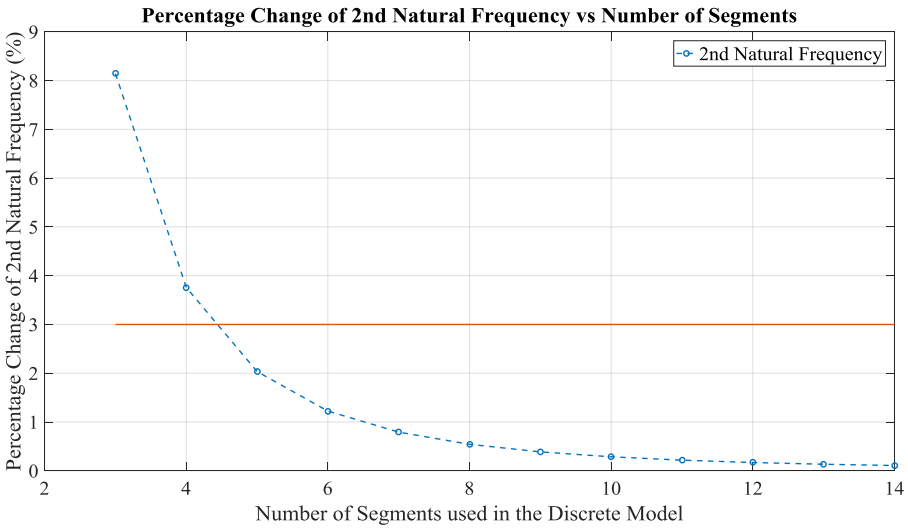

Figure 2.15: Percentage Change of 2nd Natural Frequency vs Number of Segments used in the Discrete Model

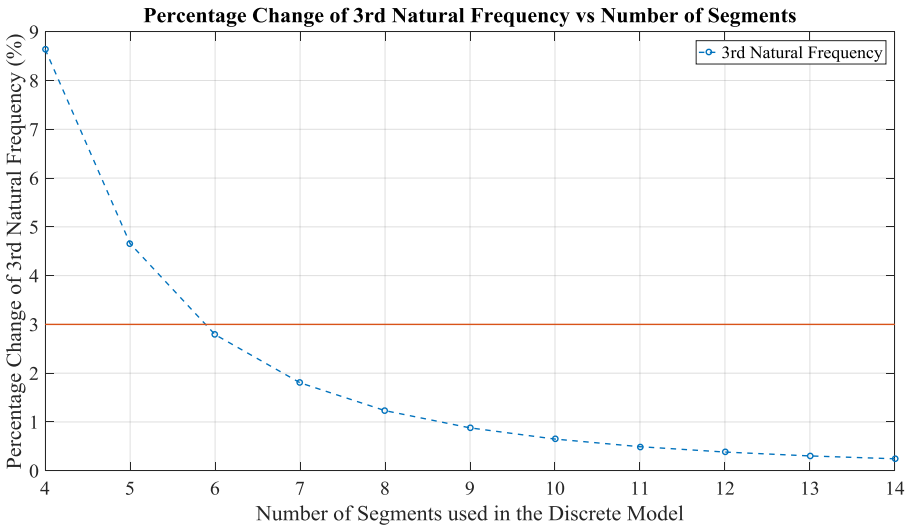

Figure 2.16: Percentage Change of 3rd Natural Frequency vs Number of Segments used in the Discrete Model

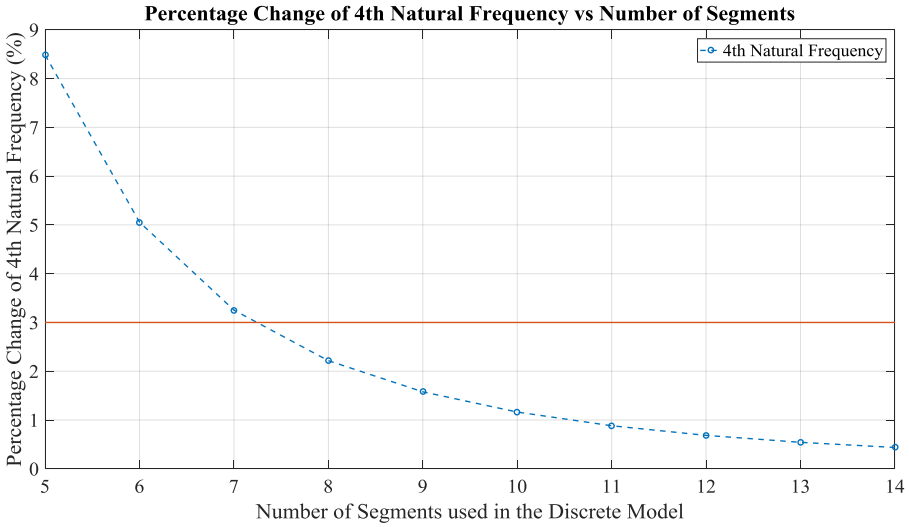

Figure 2.17: Percentage Change of 4th Natural Frequency vs Number of Segments used in the Discrete Model

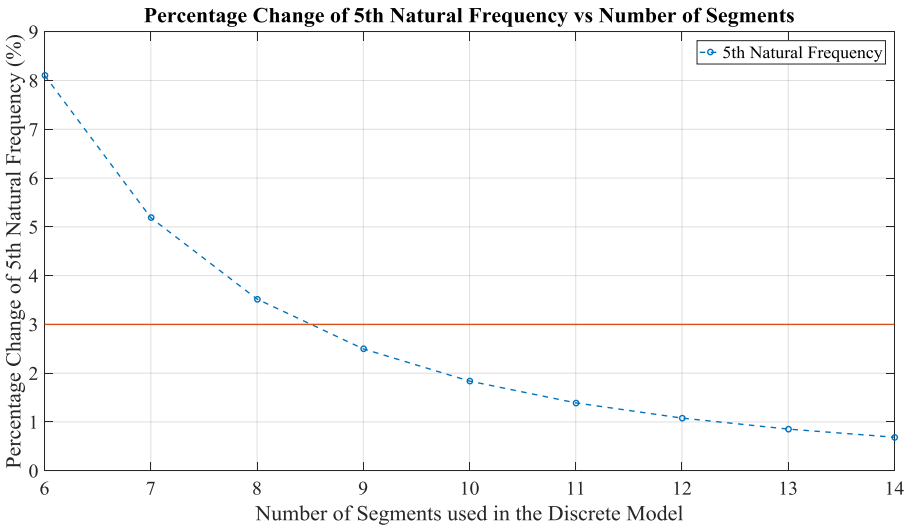

Figure 2.18: Percentage Change of 5th Natural Frequency vs Number of Segments used in the Discrete Model

Convergence rates displayed in the above figures show that Cable-1 at Position-1 is represented with 10 segments in realistic manner for the defined workspace because percentage changes of 4^{th} and 5^{th} natural frequencies are below 3% after 8 and 9-segment discretization respectively. Since this configuration is the most critical one in terms of required segment number, it is concluded that cables of this planar cable robot need maximum 10-segment discretization to perform a task within this workspace. (It should be noted that the approximation presented in this section is employed just to have meaningful foresight about the system.)

As already stated, cable is modeled with segmentation and resulting discrete cable includes segments connected with frictionless revolute joints. This feature causes the discrete cable to be able to bend such that it has sharp corner during motion. This is actually not the case in a real cable; however, according to the catalogs of CarlStahl™ [53] and [54], recommended minimum pulley diameter to maximize cable life is 25 times of cable diameter for 7x19 cable construction. This information concludes that ~39.75 mm diameter pulley is proper for 1.59 mm diameter cable. Meaning that, Ø1.59 mm cable is able to bend around Ø39.75 mm pulley. If this pulley diameter is compared to the length of the cable used in the manipulator, it is relatively very small. For this reason, locating a revolute joint

between cable segments is a reasonable assumption. Moreover, assuming each segment as a rigid element is also an acceptable assumption since low-stretch cables are supplied in the market.

2.6 Modeling and Control Algorithm for a General Case

A set of Matlab® scripts and functions are developed which can be used for any specified workspace and any combination of segment numbers of cables. These scripts and functions generate all the required Matlab® functions to be used in the modeling and control analysis. The diagram given in Figure 2.19 describes how it works and what it expects from the user. Names of the Matlab® scripts or functions are put inside the blocks of flowchart and their purpose of use is described below:

- *Data Set (User Interface)*: This is the cluster of values determined by the user within a script that can be considered as user interface. It includes dimensions of the workspace to find out extreme points, amplitude of square wave position commands to be used in *Fourier Expansion* script, desired period of square wave, error range for acceptable resulting Fourier expansion, mass of carried object at end-effector, diameter of the cables, density of cable material, convergence limit of natural frequencies of single cable, state estimation method, type of command and controller parameters.
- *Fourier Expansion*: In this script, Fourier expansion of the square wave which is selected as a sample command is completed by satisfying the accuracy error range specified by user. The frequency of the highest order term included in Fourier expansion is found out to determine the frequency limit.
- *Natural Frequency*: This script calculates the natural frequencies of a single cable through the mass and stiffness matrices gathered from linearized equations of motions. This analysis is repeated by increasing the number of segments until maximum natural frequency of the cable reaches the frequency value coming from *Fourier Expansion* block. This block finally determines the required number of segments for discretization by evaluating

the convergence rate of the highest natural frequency compared to the number of segments.

- *Equation Check OK?*: It is checked whether equations for modeling and control analysis are built before or not. If yes, it directly starts the simulations. In opposite case, it activates *Equation Deriver*.
- *Equation Deriver*: This block is responsible for symbolic derivation of all equations to be used in modeling and control analysis of cable robot. They include kinematic relations, equations of motion derived by constrained Lagrange dynamics and inverse dynamics controller input. At the end of this script, it generates all these equations in separate Matlab® functions which can be used in numerical operations throughout simulations. It is important to note that *Equation Deriver* completes its task based on the number of segments sent by *Natural Frequency* script.
- *Simulation*: Simulation script is formed by all Matlab® functions generated by *Equation Deriver*. It uses them according to the preferred estimators and commands defined by user (detailed analysis of these simulations is the topic of Chapter 4).

Information about data transmission lines:

- Line-1: From *Data Set (User Interface)*, workspace dimensions, amplitude and period of square wave and error range for acceptable resulting Fourier expansion values are transmitted to *Fourier Expansion* script.
- Line-2: From *Data Set (User Interface)*, workspace dimensions, cable diameter, density of cable material, mass of carried object at end-effector and convergence limit of natural frequencies of single cable values are transmitted to *Natural Frequency* script.
- Line-3: The maximum frequency obtained in *Fourier Expansion* script is transmitted to *Natural Frequency* script.
- Line-4: Resulting number of segments coming from *Natural Frequency* is sent to *Equation Check OK?* block.

- Line-5: Details of commands, state estimation methods and controller parameters preferred by user are transmitted to be utilized in *Simulator*. Moreover, masses of cables and payload are also provided with this line.

In the following chapter, all the terms and techniques mentioned here about controller are explained thoroughly.

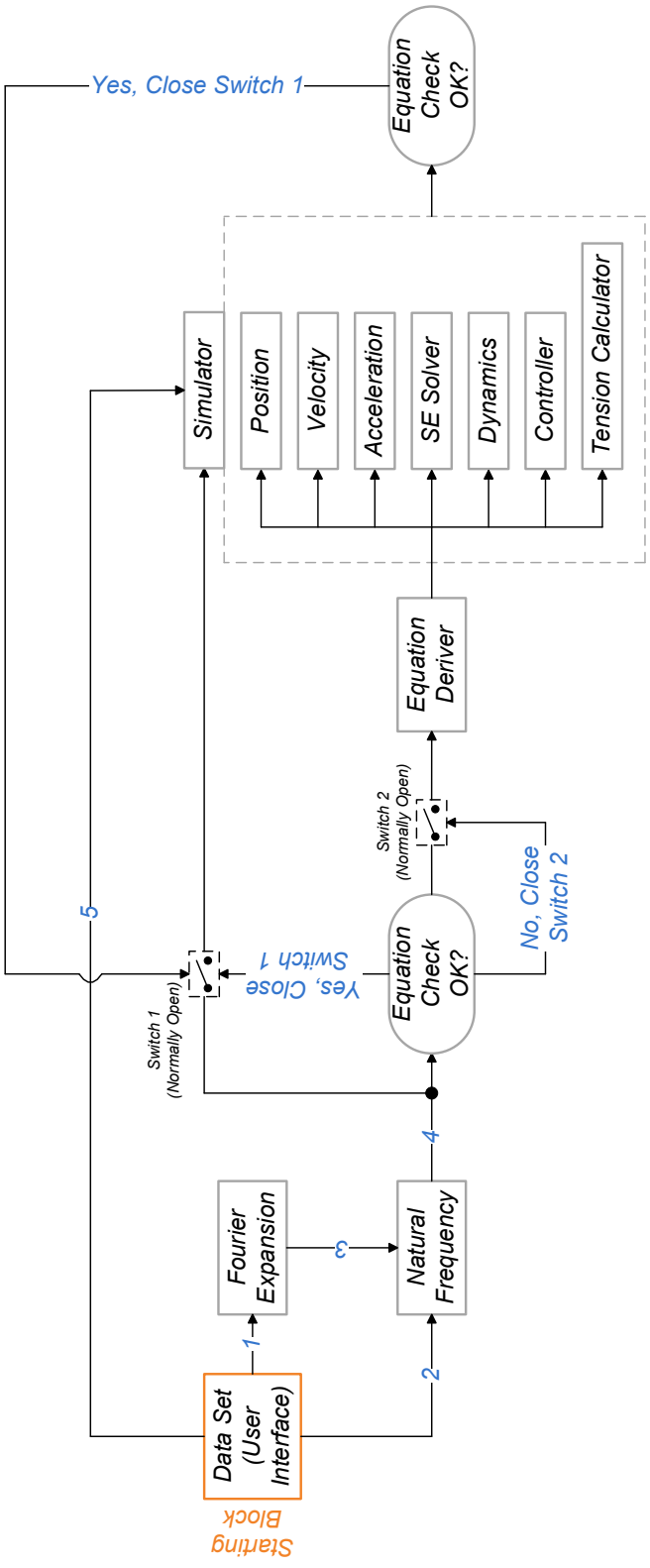

Figure 2.19: Diagram of Modeling and Control Algorithm for a General Case

CHAPTER 3

CONTROLLER DESIGN

Control problem of a manipulator is simply stated as determination of actuator forces or torques that provides manipulator to track the reference commands including both transient and steady-state periods. This problem might contain following a commanded motion while having no contact with an object or performing a reference motion having contact with environment taking place as constraint. In order to deal with different types of control problems, there are several control strategies to implement, which have considerable impacts on system performance [55].

Treating a manipulator as construction of n independent joints and controlling each axis of these joints as single-input/single-output system is the most straightforward strategy among all. In this technique, coupling effects of joints are introduced as disturbance inputs or neglected in relatively small motion of manipulator [55]. However, in order to enhance productivity of manipulators better dynamic characteristics are needed, which leads designers to develop new control strategies. These strategies are relatively more complex but provide high quality in terms of dynamical performance since they include realistic dynamic models [56].

Depending on the demanded motion or construction characteristics of manipulator, nonlinear coupling terms might have effects on performance of the system. For this reason, it may not be obtained satisfactory tracking performance from manipulator since taking these terms as disturbance instead of complete elimination of them may cause high errors of positioning. Therefore, it becomes inevitable to build up a controller that utilizes the dynamic model of the system so that it is able to cancel adverse effects of nonlinear coupling terms [55]. Although there exist several dynamic model-based control algorithms, inverse dynamics control is one of the

mostly implemented ones and presents good tracking results in many robotic applications. In this thesis, motion demands of two-cable parallel cable manipulator are met by using inverse dynamics control based on its mathematical model developed.

3.1 Inverse Dynamics Control

Inverse dynamics scheme is a special application of feedback linearization technique which is based on direct use of dynamic model of manipulator. With the help of complete model of manipulator, this control strategy eliminates nonlinear effects of gravity, Coriolis and centrifugal force, friction, and the manipulator inertia tensor. Since robot dynamics are used within feedback, linearized and decoupled control problem ends up and regular linear controllers can easily be adapted to it. Thus it results in better trajectory tracking performance because linear controllers are applied to exact linearized system dynamics [57] [56] [55].

In this thesis, inverse dynamics controller is implemented in task space; however, it is preferred to give background information about both joint and task space application.

3.1.1 Joint Space Inverse Dynamics Control [48]

Dynamic equations of an n-link rigid robot can be stated in matrix form

$$\widehat{M}(\bar{q})\ddot{\bar{q}} + \widehat{N}(\bar{q},\dot{\bar{q}})\dot{\bar{q}} + \bar{g}(\bar{q}) = \bar{\tau} \tag{3-1}$$

The basic idea of inverse dynamics approach is to find out a nonlinear feedback control law

$$\bar{\tau} = f(\bar{q},\dot{\bar{q}},t) \tag{3-2}$$

which gives a linear closed-loop system when plugged into equations of motion. For a manipulator, this type of control law can be easily chosen by inspecting the dynamic equations.

$$\bar{\tau} = \widehat{M}(\bar{q})\bar{u}_q + \widehat{N}(\bar{q}, \dot{\bar{q}})\dot{\bar{q}} + \bar{g}(\bar{q}) \tag{3-3}$$

then, by combining the equations of motion and control law

$$\widehat{M}(\bar{q})\ddot{\bar{q}} + \widehat{N}(\bar{q}, \dot{\bar{q}})\dot{\bar{q}} + \bar{g}(\bar{q}) = \widehat{M}(\bar{q})\bar{u}_q + \widehat{N}(\bar{q}, \dot{\bar{q}})\dot{\bar{q}} + \bar{g}(\bar{q}) \tag{3-4}$$

It reduces to

$$\ddot{\bar{q}} = \bar{u}_q \tag{3-5}$$

where $\bar{u}_q$ represents a new input, explicit form of which is not proposed yet. Inverse dynamics control formulated in Eq. (3-3) provides a facilitative result, which is given by Eq. (3-5), named double integrator system.

It is wise to design $\bar{u}_q$ as PD controller since control problem is converted to control of linear second order system

$$\bar{u}_q = \ddot{\bar{q}}^* + \widehat{K}_d(\dot{\bar{q}}^* - \dot{\bar{q}}) + \widehat{K}_p(\bar{q}^* - \bar{q}) \tag{3-6}$$

where,

$\bar{q}^*$: Desired Generalized Coordinate Vector

$\bar{q}$: Actual Generalized Coordinate Vector

$\dot{\bar{q}}^*$: Desired Generalized Velocity Vector

$\dot{\bar{q}}$: Actual Generalized Velocity Vector

$\ddot{\bar{q}}^*$: Desired Generalized Acceleration Vector

$\ddot{\bar{q}}$: Actual Generalized Acceleration Vector

$\widehat{K}_d$: Derivative Gain Matrix

$\widehat{K}_p$: Proportional Gain Matrix

Combining Eq. (3-5) and (3-6)

$$\bar{u}_q = \ddot{\bar{q}}^* + \hat{K}_d(\dot{\bar{q}}^* - \dot{\bar{q}}) + \hat{K}_p(\bar{q}^* - \bar{q})$$
$$= \ddot{\bar{q}} \;\Rightarrow\; (\ddot{\bar{q}}^* - \ddot{\bar{q}}) + \hat{K}_d(\dot{\bar{q}}^* - \dot{\bar{q}}) + \hat{K}_p(\bar{q}^* - \bar{q}) = 0$$

Then joint space error dynamics become:

$$\ddot{\bar{e}}_q + \hat{K}_d\dot{\bar{e}}_q + \hat{K}_p\bar{e}_q = 0 \tag{3-7}$$

It can be observed that this second order differential equation helps out to interpret error dynamics of the closed loop system. Error,$\bar{e}_q$ asymptotically approaches zero by proper selection of $\hat{K}_p$ and $\hat{K}_d$ values. K_{pi} and K_{di} can be related in critically damped case of any joint i as:

$$K_{di}{}^2 = 4K_{pi} \tag{3-8}$$

This control algorithm summarized so far is illustrated on the following diagram.

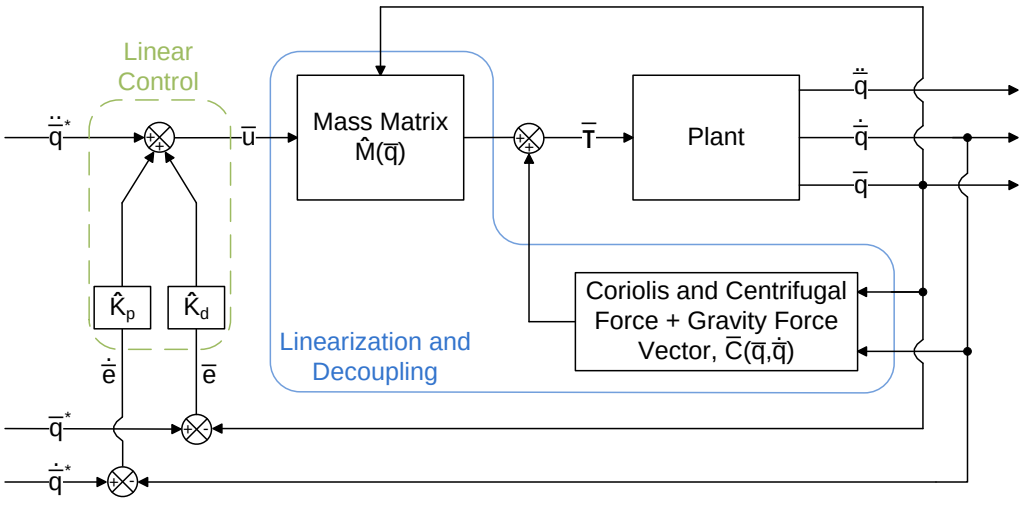

Figure 3.1: Joint Space Inverse Dynamics Control Architecture

3.1.2 Task Space Inverse Dynamics Control [48]

In order to track motion references in task space, linear control portion of control architecture which is indicated in Figure 3.1 needs to be updated while keeping the linearization/decoupling part the same. This implies that new type of $\bar{u}_q$ is obtained in task space that is represented by $\bar{u}_X$. Let $\bar{X} \in R^6$ represent the end-effector pose. Since $\bar{X}$ is a function of the joint variables $\bar{q}$, it can be written that

$$\dot{\bar{X}} = \hat{J}(\bar{q})\dot{\bar{q}} \tag{3-9}$$

$$\ddot{\bar{X}} = \hat{J}(\bar{q})\ddot{\bar{q}} + \dot{\hat{J}}(\bar{q})\dot{\bar{q}} \tag{3-10}$$

where $\hat{J}(\bar{q})$ is the Jacobian matrix.

By using joint space relation stated in Eq. (3-5) and acceleration equation (Eq.(3-10)) $\bar{u}_X$ is written as

$$\bar{u}_X = \hat{J}(\bar{q})\bar{u}_q + \dot{\hat{J}}(\bar{q})\dot{\bar{q}} \tag{3-11}$$

which results in the double integrator system in task space coordinates as follows

$$\ddot{\bar{X}} = \bar{u}_X \tag{3-12}$$

For given desired task space trajectory $\bar{X}^*$, $\bar{u}_X$ is chosen as (It should be noted that $\bar{X}^*$ satisfies smoothness and boundedness assumptions similar to the joint space trajectory $\bar{q}^*$)

$$\bar{u}_X = \ddot{\bar{X}}^* + \hat{K}_d\left(\dot{\bar{X}}^* - \dot{\bar{X}}\right) + \hat{K}_p(\bar{X}^* - \bar{X}) = \ddot{\bar{X}} \tag{3-13}$$

Error dynamics of task space takes the form of

$$\ddot{\bar{e}}_X + \hat{K}_d \dot{\bar{e}}_X + \hat{K}_p \bar{e}_X = 0 \tag{3-14}$$

It can be concluded that by simply modifying the linear control portion of joint space inverse dynamics control and keeping the linearization/decoupling part unchanged, control architecture is adapted to task space tracking. This procedure again ends up with a similar second order differential equation describing error dynamics of system. With proper selection of $\hat{K}_p$ and $\hat{K}_d$ values, error, $\bar{e}_X$ asymptotically approaches zero.

3.2 Implementation of Inverse Dynamics Control on Two-Cable Planar Parallel Cable Manipulator

After brief introduction of inverse dynamics concept for both joint and task spaces, it is time to implement this scheme on two-cable planar parallel cable manipulator. In this application, main goal is to control x and y Cartesian coordinates of end-effector which is assumed to be a point mass. Thus it does not have orientation and x and y coordinates are enough to constitute its pose in this model.

Controller is expected to generate required forces applied to 1st segments of two cables that are selected as specified variables of system.

In previous chapter, dynamic model of two-cable planar parallel manipulator is expressed with the help of Lagrange equations of motion. Final form of these equations can be stated in the following format:

$$\hat{M}(\bar{q})\ddot{\bar{q}} + \hat{N}(\bar{q}, \dot{\bar{q}})\dot{\bar{q}} + \bar{g}(\bar{q}) = \hat{A}\bar{F} \tag{3-15}$$

where,

$\hat{M}$: Mass/Inertia Matrix

$\bar{q}$: Generalized Coordinate Vector

$\hat{N}(\bar{q}, \dot{\bar{q}})\dot{\bar{q}}$: Coriolis and Centrifugal Force Vector

$\bar{g}$: Gravity Force Vector

$\bar{F}$: Generalized Force Vector

$\hat{A}$: Generalized Force Coefficient Matrix

In more compact form:

$$\hat{M}(\bar{q})\ddot{\bar{q}} + \bar{C}(\bar{q}, \dot{\bar{q}}) = \hat{A}\bar{F} \tag{3-16}$$

where,

$\bar{C}$: Coriolis and Centrifugal Force + Gravity Force Vector

It is aimed to control the cable robot in a desired manner so that it can accomplish the defined task like picking up an object and transporting it by following a proposed path. For this purpose, inverse dynamics control is utilized in order to cancel out nonlinear effects appear in the equations of motion and gain accurate trajectory tracking performance.

In order to achieve nonlinear to linear conversion, it is wise to select control input in this form:

$$\hat{M}(q)\bar{u} + \bar{C}(\bar{q}, \dot{\bar{q}}) = \bar{T} \tag{3-17}$$

After selection of $\bar{T}$, elimination of nonlinear terms and derivation of linear equation are completed:

$$\hat{M}(q)\ddot{\bar{q}} + \bar{C}(\bar{q}, \dot{\bar{q}}) = \hat{M}(q)\bar{u} + \bar{C}(\bar{q}, \dot{\bar{q}}) \Rightarrow \ddot{\bar{q}} = \bar{u} \tag{3-18}$$

It is obvious that inverse dynamics control is an effective method to be able to not only linearize equations of motion but also decouple them. This final form is linear anymore; therefore, linear controllers can be applied easily. However, in two-cable planar parallel cable manipulator it is aimed to control x and y coordinates of end-effector. It means that joint space variables, which are cable segment angles, $\bar{\theta}$, are

not point of interest. For this reason, inverse dynamics controller should be proposed for task space.

$$\bar{u}_p = \ddot{\bar{p}}^* + \hat{K}_d(\dot{\bar{p}}^* - \dot{\bar{p}}) + \hat{K}_p(\bar{p}^* - \bar{p}) = \ddot{\bar{p}} \tag{3-19}$$

where,

$\bar{p}^*$: Desired x and y Coordinates Vector of End-effector (Vector Dimension:2x1)

$\bar{p}$: Actual x and y Coordinates Vector of End-effector (Vector Dimension:2x1)

$\dot{\bar{p}}^*$: Desired x and y Velocity Vector of End-effector (Vector Dimension:2x1)

$\dot{\bar{p}}$: Actual x and y Velocity Vector of End-effector (Vector Dimension:2x1)

$\ddot{\bar{p}}^*$: Desired x and y Acceleration Vector of End-effector (Vector Dimension:2x1)

$\ddot{\bar{p}}$: Actual x and y Acceleration Vector of End-effector (Vector Dimension:2x1)

$\hat{K}_d$: Derivative Gain Matrix (Matrix Dimension:2x2)

$\hat{K}_p$: Proportional Gain Matrix (Matrix Dimension:2x2)

Acceleration equation of cable manipulator is obtained, which is similar to Eq. (3-10), in previous chapter as Eq. (2-33):

$$\ddot{\bar{p}} = \dot{\hat{J}}(\bar{q})\dot{\bar{\theta}} + \hat{J}(\bar{q})\ddot{\bar{\theta}} \tag{3-20}$$

Combination of Eq. (3-13) and (3-14) gives the following formulation

$$\ddot{\bar{p}} = \ddot{\bar{p}}^* + \hat{K}_d(\dot{\bar{p}}^* - \dot{\bar{p}}) + \hat{K}_p(\bar{p}^* - \bar{p}) = \dot{\hat{J}}(\bar{q})\dot{\bar{\theta}} + \hat{J}(\bar{q})\ddot{\bar{\theta}} \tag{3-21}$$

Moreover, explicit form of the equations of motion is also obtained as Eq. (2-43):

$$\ddot{\bar{\theta}} = \hat{\beta}\left[\bar{D}_\theta + \hat{E}_\theta \hat{E}_r{}^{-1}\left[\bar{m} - \bar{D}_r - \hat{G}_r\bar{F}\right] + \hat{G}_\theta\bar{F}\right]$$

$$\text{where } \hat{\beta} = \left[\hat{I} - \hat{E}_\theta \hat{E}_r{}^{-1}\hat{R}\right]^{-1}$$

which can be rewritten as

$$\ddot{\bar{\theta}} = \hat{\beta}\left[\bar{D}_\theta + \hat{E}_\theta \hat{E}_r{}^{-1}(\bar{m} - \bar{D}_r) - \hat{E}_\theta \hat{E}_r{}^{-1}\hat{G}_r\bar{F} + \hat{G}_\theta\bar{F}\right]$$

$$\ddot{\bar{\theta}} = \hat{\beta}\left[\bar{D}_\theta + \hat{E}_\theta \hat{E}_r{}^{-1}(\bar{m} - \bar{D}_r)\right] + \hat{\beta}\left[-\hat{E}_\theta \hat{E}_r{}^{-1}\hat{G}_r + \hat{G}_\theta\right]\bar{F} \tag{3-22}$$

Combined closed-loop equations can be obtained by plugging this final form of Eq. (2-43), which is Eq. (3-16), into Eq. (3-15). It is important to note that in this derivation jacobian matrix, $\hat{J}(\bar{q})$, cannot be inverted since it is not square. Its dimension for this system is $2xN_{total}$.

$$\begin{aligned}&\ddot{\bar{p}}^* + \widehat{K_d}(\dot{\bar{p}}^* - \dot{\bar{p}}) + \widehat{K_p}(\bar{p}^* - \bar{p}) \\ &= \dot{\hat{J}}(\bar{q})\dot{\bar{\theta}} + \hat{J}(\bar{q})\underbrace{\left[\hat{\beta}\left[\bar{D}_\theta + \hat{E}_\theta \hat{E}_r{}^{-1}(\bar{m} - \bar{D}_r)\right] + \hat{\beta}\left[-\hat{E}_\theta \hat{E}_r{}^{-1}\hat{G}_r + \hat{G}_\theta\right]\bar{F}\right]}_{\ddot{\bar{\theta}} from\ eqautions\ of\ motion}\end{aligned} \tag{3-23}$$

Since controller outputs are selected as two forces applied along the 1st segments of two cables that are represented with a force vector, $\bar{F}$, they are solved from Eq. (3-17):

$$\begin{aligned}\bar{F} = \hat{\varepsilon}\Big[&\ddot{\bar{p}}^* + \hat{K}_d(\dot{\bar{p}}^* - \dot{\bar{p}}) + \hat{K}_p(\bar{p}^* - \bar{p}) - \dot{\hat{J}}(\bar{q})\dot{\bar{\theta}} \\ &- \hat{J}(\bar{q})\hat{\beta}\left[\bar{D}_\theta + \hat{E}_\theta \hat{E}_r{}^{-1}(\bar{m} - \bar{D}_r)\right]\Big]\end{aligned} \tag{3-24}$$

where $\hat{\varepsilon} = \left[\hat{\beta}\left(-\hat{E}_\theta \hat{E}_r{}^{-1}\hat{G}_r + \hat{G}_\theta\right)\right]^{-1}$

Force vector, $\bar{F}$, found in Eq. (3-18) is now ready to be fed into plant for tracking of desired trajectory.

In order to visualize it better, block diagram of inverse dynamics control implementation of two-cable planar parallel cable robot is presented in implicit form.

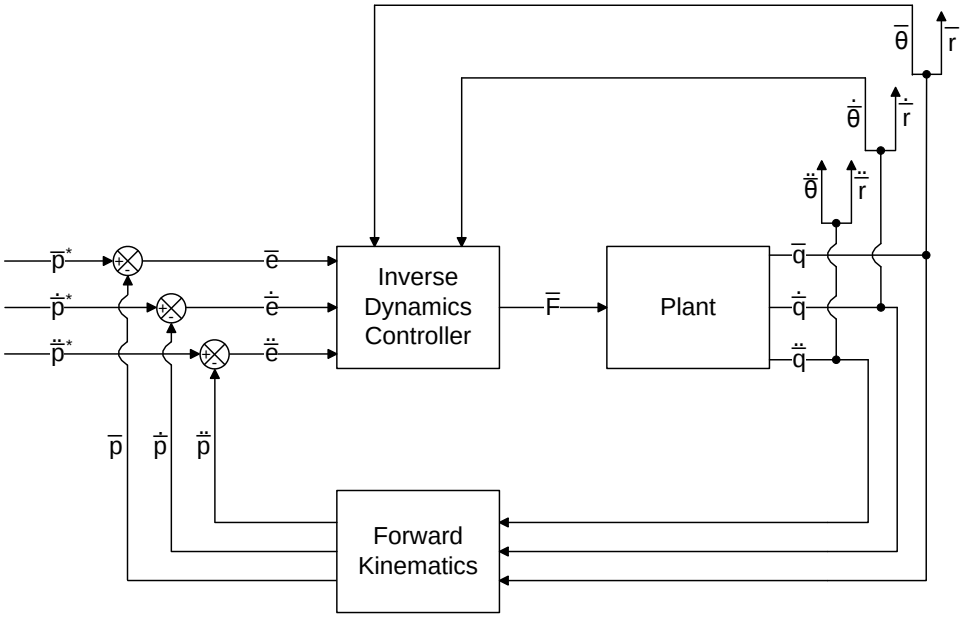

Figure 3.2: Implicit Control Diagram of Two-Cable Planar Parallel Manipulator

From this block diagram illustrated in Figure 3.2, it is clear that execution of inverse dynamics control needs vector of cable segment angles and its derivative, $\bar{\theta}$ and $\dot{\bar{\theta}}$. Achieving these parameters by measuring is not practical on a continuous cable. Therefore, they should be calculated with the help of known system parameters and mathematical models. However, calculation complexity should be handled by controller hardware within controller step time since calculation of system parameters is required to be done on-line in every control loop. Hence two main approaches are developed in this thesis to find out cable segment angles and their derivative(s) in an acceptable time span:

- Lower-Order Model Approach
- Pseudo-Static Approach

Unlike cable segment angles, it is feasible to measure 1st cable segment lengths, $\bar{r}$, by simply measuring rotation of pulley on which cables are wrapped. By this means, it is reasonable to assume 1st cable segment lengths, $\bar{r}$, are measurable and there is no need for additional mathematical operation or model-based estimation to obtain them. However, derivative(s) of $\bar{r}$ are required to be found out with

numerical differentiation unless there is located a sensor that measure directly $\dot{\bar{r}}$ or $\ddot{\bar{r}}$.

3.2.1 Lower-Order Model Approach for Inverse Dynamics Control

One of the proposed methods to make accurate estimation of cable segment angles, $\bar{\theta}$, is to run a lower order dynamic model, which is again constructed by using Lagrange dynamics method presented in chapter 2, during controller action and find out these angles to be used in inverse dynamics controller. While a proper model of cable, which is assumed to be good enough to represent a continuous cable, has $N_{total,h}$ number of segments, a low-order model has $N_{total,l}$ number of segments where $N_{total,l} < N_{total,h}$. Using low-order model decreases the number of equations of motion, which helps out to reduce online calculation time of segment angles and gives opportunity of assigning smaller step times for controller. It is worth remarking that both plant simulator, i.e. higher-order model, and lower-order model represent the same system by differing only on the level of discretization of cables. The figure stated below helps to visualize it clearly.

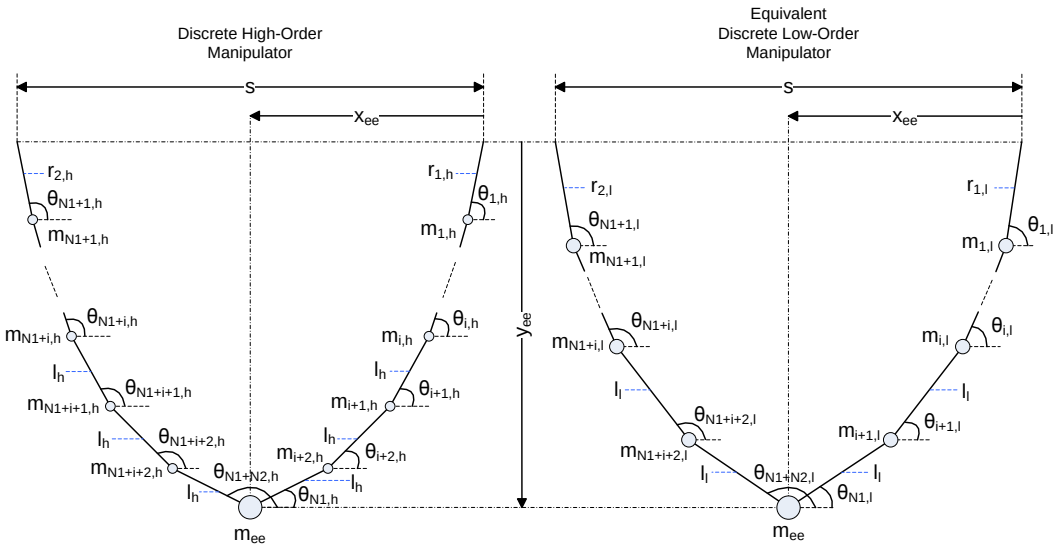

Figure 3.3: Discrete Plant Simulator (Higher-Order Model) of Two-Cable Planar Parallel Manipulator and its Equivalent Lower-Order Model

As a first step, system parameters belonging to lower-order model that are listed below have to be determined:

- Node mass, m_l
- 1st segment lengths, $\bar{r_l} = [r_{1,l}, r_{2,l}]$, at the beginning of task
- Constant segment length, l_l
- Cable segment angles, $\bar{\theta_l}$

These variables can be obtained by solving static equilibrium equations of lower-order system under conditions of specified x and y positions of end-effector, x_{ee} and y_{ee}, with total cable masses. In other words, low-order system can be expressed with its variables such that it has same x and y coordinates of end-effector with higher-order model and total mass of each cable is the same as cables of higher-order model.

Number of segments of right and left cables for higher-order system: $N_{1,h}$ and $N_{2,h}$ $N_{1,h}$ and $N_{2,h}$ define the order of higher-order system.

Desired order difference between two models: δ_{order}

Number of segments of right and left cables for lower-order system:

$$N_{1,l} = N_{1,h} - \delta_{order} \text{ and } N_{2,l} = N_{2,h} - \delta_{order}$$

Total masses of right and left cables, which are the same for both higher and lower-order systems: $m_{cable,right}$ and $m_{cable,left}$

Node masses of higher and lower-order models for right and left cables:

Higher-order node masses: $m_{node,right,h} = \frac{m_{cable,right}}{N_{1,h}-1}$ and $m_{node,left,h} = \frac{m_{cable,left}}{N_{2,h}-1}$

Lower-order node masses: $m_{node,right,l} = \frac{m_{cable,right}}{N_{1,l}-1}$ and $m_{node,left,l} = \frac{m_{cable,left}}{N_{2,l}-1}$

After finding node masses, other unknown system parameters of low-order model can be solved from static equilibrium problem which is described in previous chapter. This solution should satisfy x, y coordinates of end-effector which are specified for high-order system already. With the help of Eq. (2-15):

$$p_{N1,low,right} = r_{1,l}e_1 + \sum_{j=2}^{N1,l} l_l e_j = [x_{ee} \;\; y_{ee}]$$

With static equilibrium solution, all starting parameters of lower-order model are known. Therefore, dynamic simulation of cable manipulator can be run with implementation of inverse dynamics controller in case of lower-order model approach for controller.

3.2.1.1 Lower-Order Angle Generator Model and Lower-Order Controller

Lower-order model generates $N_{total,l}$ number of angles, $\bar{\theta}_{e,l}$, for cable manipulator meaning that controller has to be also lower-order. Therefore, the first method which is worth to try is using lower-order model as a segment angle generator and lower-order controller that uses the segment angles coming from lower-order model. The procedure of lower-order model approach can be summarized as follows:

1) Feed reference (desired) end-effector position, velocity and acceleration vectors, i.e. $\bar{p}^*$, $\dot{\bar{p}}^*$, and $\ddot{\bar{p}}^*$.

2) Calculate end-effector position, velocity and acceleration error vectors, i.e. $\bar{e}$, $\dot{\bar{e}}$, and $\ddot{\bar{e}}$ by using actual and desired end-effector position, velocity and acceleration. Note that starting or parking position of the cable robot is static-equilibrium position since it is assumed that cable manipulator is stationary at the beginning of defined task. In other words, initial velocity and acceleration vectors of end-effector are zero vectors. If system has capability of measuring

end-effector position, it can be directly used during trajectory tracking instead of obtaining it by forward kinematics calculation using cable segment angles, $\bar{\theta}$.

$$\bar{e} = \bar{p}^* - \bar{p}$$
$$\dot{\bar{e}} = \dot{\bar{p}}^* - \dot{\bar{p}}$$
$$\ddot{\bar{e}} = \ddot{\bar{p}}^* - \ddot{\bar{p}}$$

3) Feed the error vectors, i.e. $\bar{e}$, $\dot{\bar{e}}$, and $\ddot{\bar{e}}$, found on previous step to the controller and calculate the resulting controller output force vector, $\bar{F}$, by using inverse dynamics controller technique.

4) Give controller output force vector, $\bar{\bar{F}}$, to the plant. In this study, response of the plant is found out by running mathematical model of it, i.e. by simulating the cable manipulator, since there is no physical system available.

5) Plant simulation gives the results for actual values of $\bar{\theta}$ and $\bar{r}$. From these vectors, $\bar{r}$ can be directly used in any calculation requiring variable lengths of the 1st cable segments since it is measurable.

6) Parallel to plant simulation, solve lower-order model of the cable robot at that instant in order to estimate the cable segment angles used in lower-order controller. In this step, controller output force vector, $\bar{F}$, that is used in plant simulation is also fed to this lower-order model. Obtain estimated $\bar{\theta}_e$ and $\dot{\bar{\theta}}_e$ vectors to provide controller.

7) If it is not taken any position, velocity or acceleration measurement on end-effector, they should be calculate by using estimated cable segment angles, angular velocities and accelerations $\bar{\theta}_e$, $\dot{\bar{\theta}}_e$ and $\ddot{\bar{\theta}}_e$ acquired from lower-order model.

Detailed block diagram of lower-order angle generator model and lower-order controller approach including all the steps described above is displayed below. Approach is divided into two cases in terms of position measurement capability of end-effector, both of which are presented and studied.

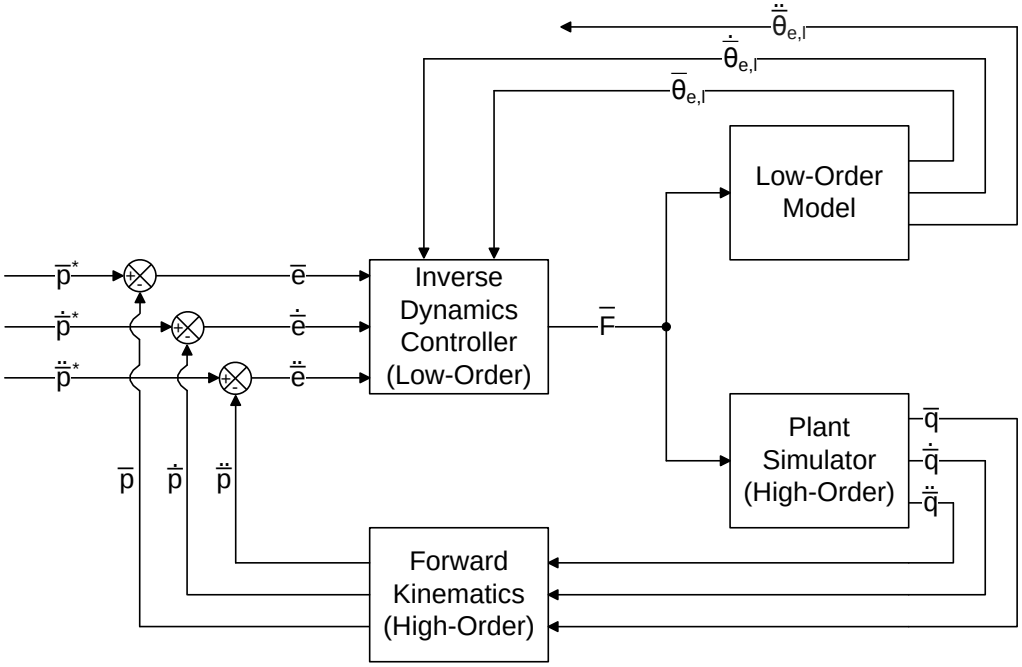

Figure 3.4: Lower-Order Angle Generator Model and Lower-Order Inverse Dynamics Controller Approach with Measured End-Effector Pose

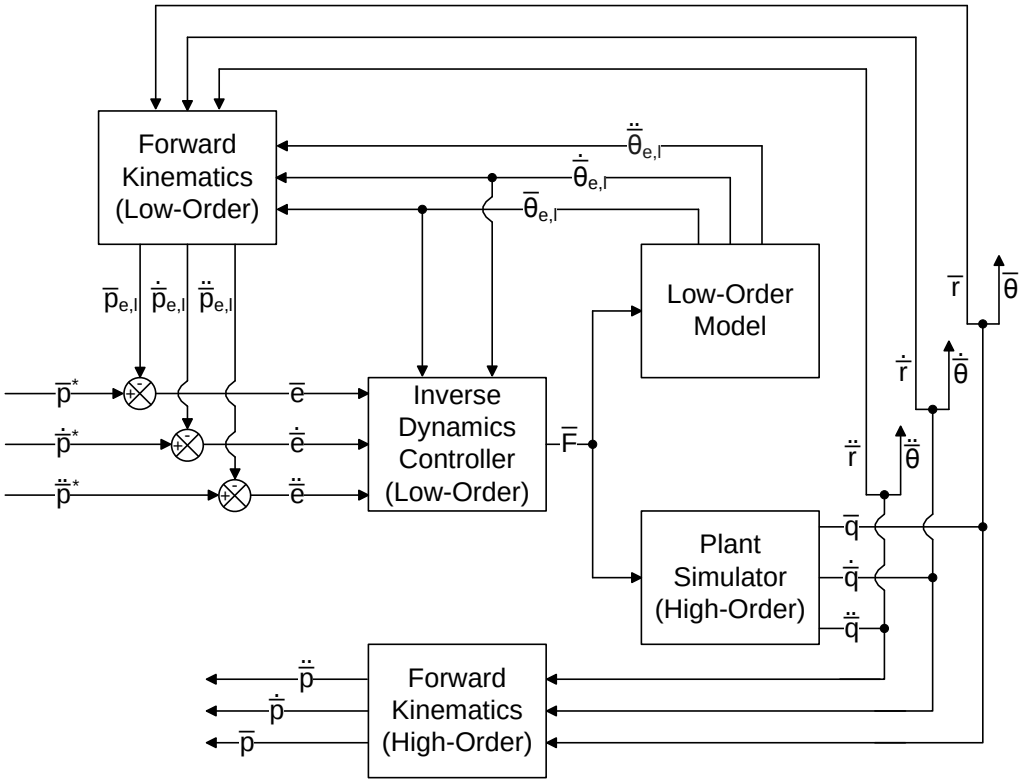

Figure 3.5: Lower-Order Angle Generator Model and Lower-Order Inverse Dynamics Controller Approach with Estimated End-Effector Pose

In case of estimated end-effector pose, the only measured system variable is the length of 1st segments, $\bar{r}$. This measured value is used to update the 1st segment length vector of lower-order model, $\bar{r}_l$ by using the following formulation.

$$\overline{\delta r} = \bar{r}_{i+1} - \bar{r}_i$$

$$\bar{r}_{l,i+1} = \bar{r}_{l,i} + \overline{\delta r}$$

3.2.1.2 Lower-Order Angle Generator Model and High-Order Controller

In case of a need for keeping controller as high order, there should be developed a method to estimate $N_{total,h}$ number of segment angles for cable manipulator by using $N_{total,l}$ number of them gathered with the help of lower-order simplified system model (Note that $N_{total,l} < N_{total,h}$). In order to provide ease of

methodology and keep calculation time as short as possible, it is logical to use two curves that are fit to the sample segment nodes of each cable obtained from lower-order model. These curves represent the approximate shapes of each cable during motion and are employed to estimate node positions of high-order model, which is assumed to be accurate enough to represent the plant having continuous cables. Since high-order controller needs $N_{total,h}$ number of segment angles and also their first derivatives, these estimated node positions assist to develop approximate angle values to be used in high-order inverse dynamics controller.

In order to increase fidelity level of fitted curve, first segment node positions of each cable for high-order system are also added to the sample nodes thanks to measurability of 1st segment lengths. Nevertheless their exact positions cannot be determined without their segment angle values making with the horizontal axis. There are proposed two ways for their determination, one of which is direct measurement of the angle by utilizing a method like the one presented in study [58] where cable is passed through groves opened on the mechanical parts that are free to rotate with the help of bearings and there are placed two encoders at the rotation axis to measure angular position. As it is seen in Figure 3.6, two angles of rotation can be measured in 3D space. It is sufficient to use only one axis rotation measurement of a similar concept to determine angles of 1st segments for each cable in planar manipulator application.

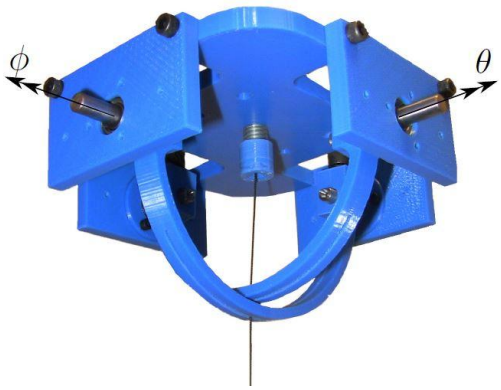

Figure 3.6: Measurement Method of Cable Angles [58]

Despite representation of the same system of high and lower-order models, 1st segments of cables within them do not have to be collinear. In Figure 3.7, this situation is visualized by overlapping actuator and end-effector points of each model. Due to variation of segment node mass values and number of them contained in models, there exists an angle difference, $\delta\theta$, between 1st segments.

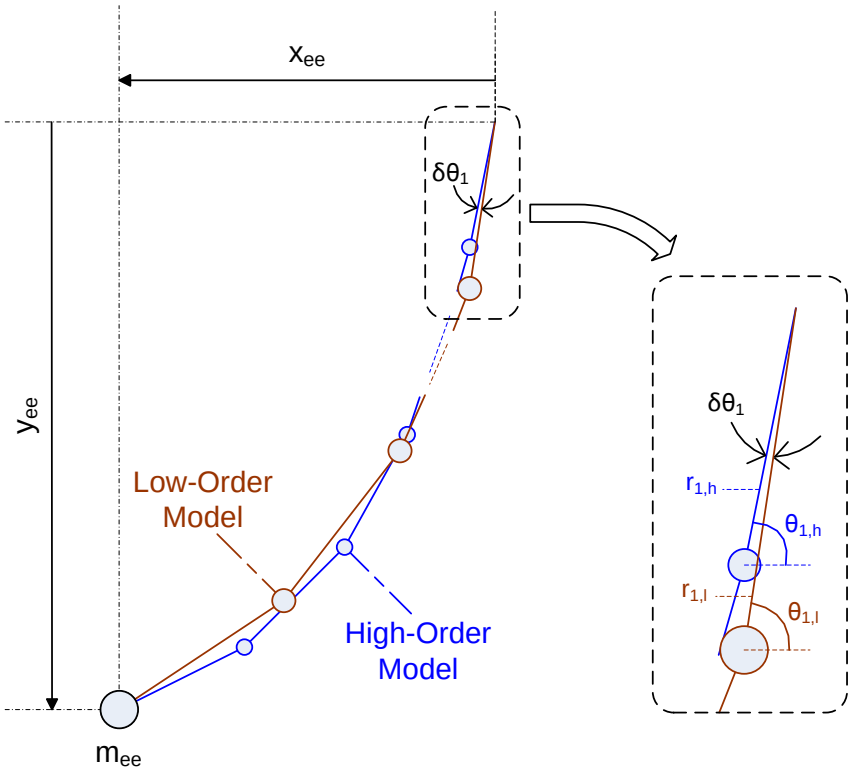

Figure 3.7: Overlapped High and Lower-Order Segment Nodes for Right-Cable

As an alternative approach to measurement, direction of 1st segment lengths of high-order model can be regarded as collinear with the 1st segments of lower-order system for simplicity. Effect of this assumption on manipulator performance is analyzed in next chapter with various simulations.

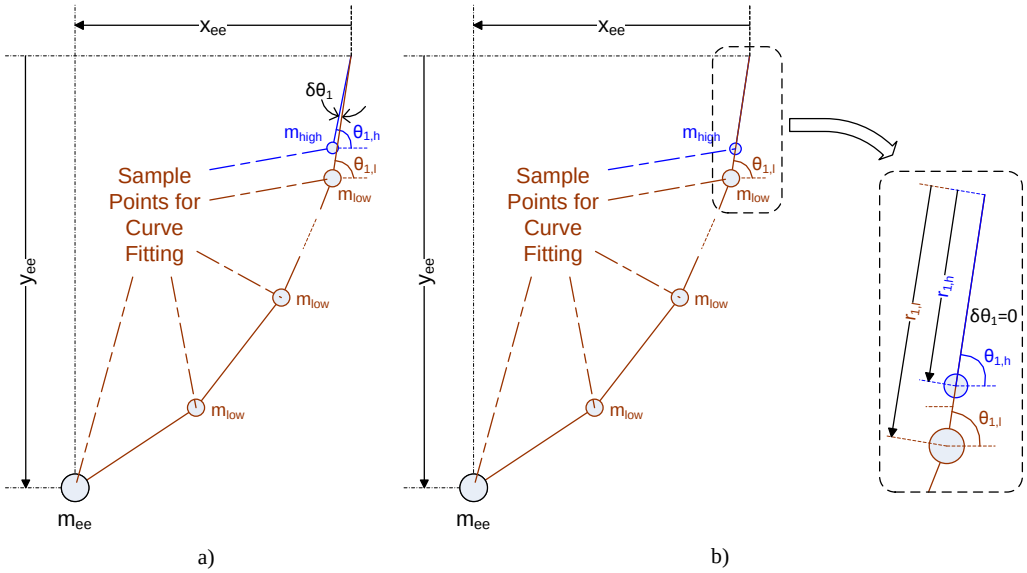

Figure 3.8: Sample Points for Curve Fitting in case of a) measured 1st segment angle b) collinear $r_{1,h}$ and $r_{1,l}$

Detailed block diagram of lower-order angle generator model and high-order controller approach is displayed below. Approach is divided into two cases in terms of position measurement capability of end-effector, both of which are presented and studied.

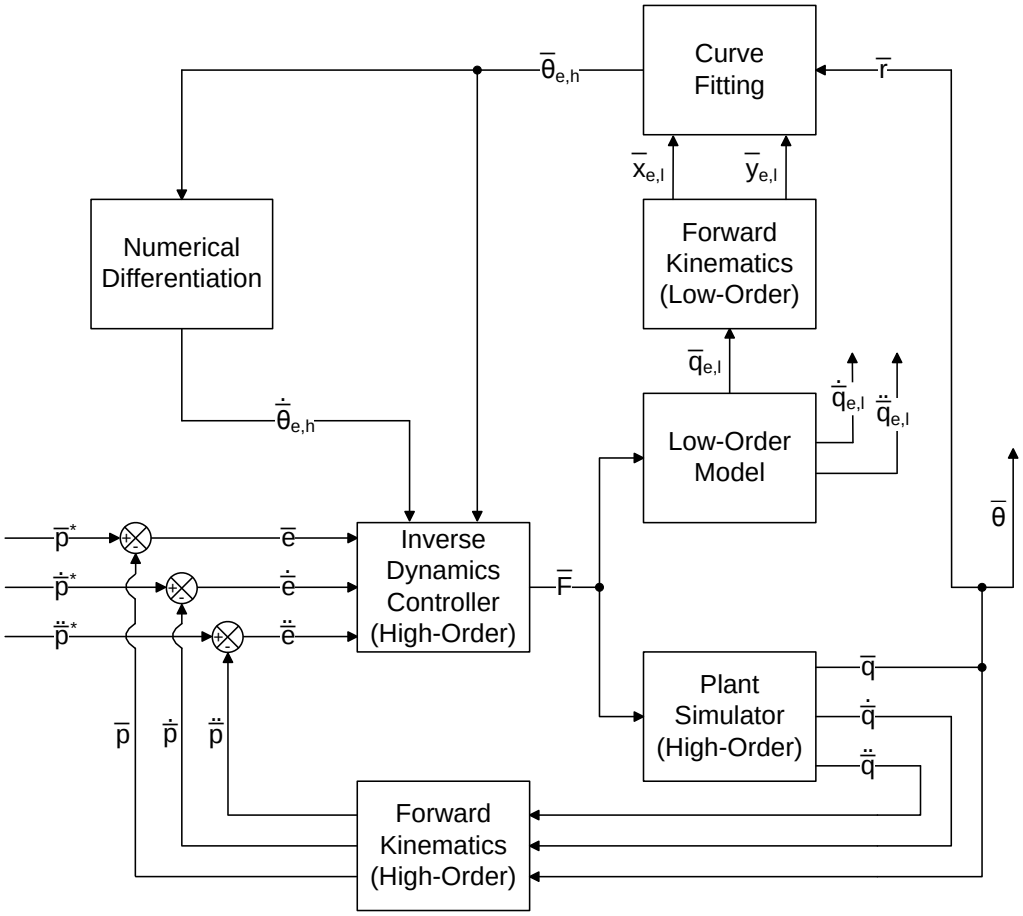

Figure 3.9: Lower-Order Angle Generator Model and High-Order Inverse Dynamics Controller Approach with Measured End-Effector Pose

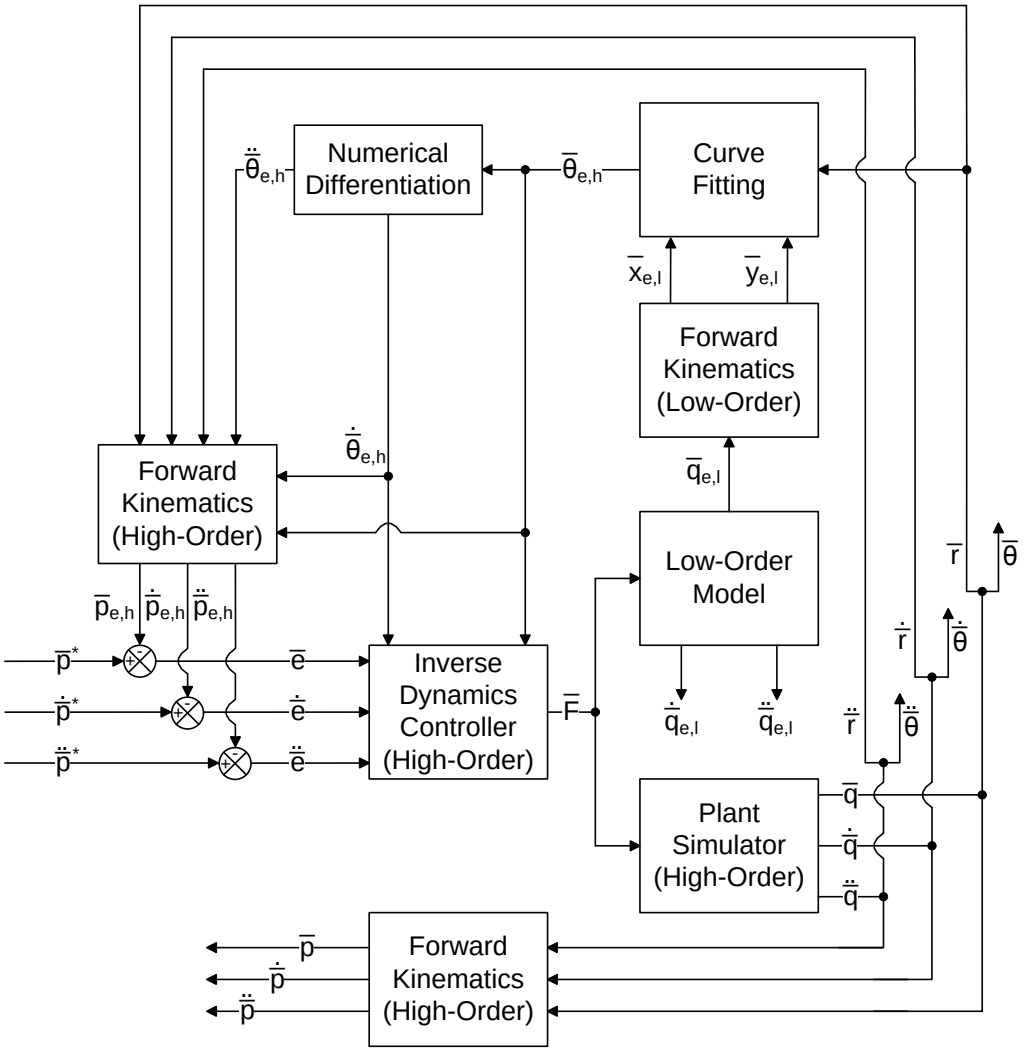

Figure 3.10: Lower-Order Angle Generator Model and High-Order Inverse Dynamics Controller Approach with Estimated End-Effector Pose

As it is seen in Figure 3.9 and Figure 3.10, "Curve Fitting" block needs x and y Cartesian positions of segment nodes, $\bar{x}_{e,l}$ and $\bar{y}_{e,l}$, belonging to lower-order model, which can be derived by virtue of lower-order forward kinematics making use of $\bar{q}_{e,l} = [\bar{\theta}_{e,l}, \bar{r}_{e,l}]$. In this notation, $\bar{\theta}_{e,l}$ and $\bar{r}_{\mathrm{e,l}}$ symbolize segment angle vector of lower-order model and lengths of 1st segments vector of lower-order model respectively. Furthermore, measured 1st segment lengths, $\bar{r}$, to determine the 1st sample points of curve fitting are fed. Although it is not shown explicitly on block diagrams, it is proposed two options for finding these 1st sample points of each cable, $\bar{x}_{1,l}$ and $\bar{y}_{1,l}$:

$$\bar{x}_{1,l} = \sigma_l \bar{r}\, cos\left(\bar{\theta}_{e,l,1}\right) + \sigma_h \bar{r} cos\,(\bar{\theta}_1)$$
$$\bar{y}_{1,l} = \sigma_l \bar{r}\, sin\left(\bar{\theta}_{e,l,1}\right) + \sigma_h \bar{r} sin\,(\bar{\theta}_1)$$

In this formulation, σ_l and σ_h work as a switch operator meaning that $\sigma_l = 1$ and $\sigma_h = 0$ in case of colinearity assumption of $r_{1,l}$ and $r_{1,h}$; however, $\sigma_l = 0$ and $\sigma_h = 1$ for measured $\bar{\theta}_1$.

Sample points except for $\bar{x}_{1,l}$ and $\bar{y}_{1,l}$ are taken from position level forward kinematics of lower-order model and they are indicated with $\bar{x}_{e,l}$ and $\bar{y}_{e,l}$. As a result, cluster of sample points, $\bar{x}_{sample}$ and $\bar{y}_{sample}$, are formed.

$$\bar{x}_{sample} = [\bar{x}_{1,l} \quad \bar{x}_{e,l}]$$
$$\bar{y}_{sample} = [\bar{y}_{1,l} \quad \bar{y}_{e,l}]$$

For curve fitting and data interpolation, two basic methods are studied by utilizing Matlab's® "*spline*" and "*polyfit*" commands where "*spline*" uses a cubic spline interpolation and "*polyfit*" fits "n" degree polynomial and gives its coefficients [59]. Interpolant values, $\bar{x}_{interpolant}$, as inputs to these commands are calculated by dividing range of $\bar{x}_{sample}$ into $N_{1,h}$ and $N_{2,h}$ intervals for right and left cables respectively. First and last elements of $\bar{x}_{interpolant}$ are the same as $\bar{x}_{sample}$, which are first segment node and end-effector node.

After finding estimated y position values, $\bar{y}_{estimated}$, corresponding to $\bar{x}_{interpolant}$, estimated high-order cable segment angles are easily obtained. For "*spline*" operation, these angles are calculated as follows:

$$\theta_{e,h,i+1} = tan^{-1}\left[\frac{y_{estimated,i+1} - y_{estimated,i}}{x_{sample,i+1} - x_{sample,i}}\right]$$

Since "*polyfit*" results the coefficients of fitted polynomial, segment angles are found out by taking the inverse tangent of the slope of interested point. Slope of

resulting polynomial, $f(\bar{x}_{interpolant})$, is found by simply taking the first derivative of it.

$$\bar{\theta}_{e,h} = tan^{-1}[f'(\bar{x}_{interpolant})]$$

Apart from angular positions, inverse dynamics controller also requires angular velocities, $\dot{\bar{\theta}}_{e,h}$, which are figured out by numerical differentiation of $\bar{\theta}_{e,h}$.

$$\dot{\bar{\theta}}_{e,i} = \frac{(\bar{\theta}_{e,i+1} - \bar{\theta}_{e,i})}{\Delta t}$$

Similarly, angular accelerations can also be derived with numerical differentiation.

$$\ddot{\bar{\theta}}_{e,i} = \frac{\left(\dot{\bar{\theta}}_{e,i+1} - \dot{\bar{\theta}}_{e,i}\right)}{\Delta t}$$

In a condition of unmeasured end-effector pose which is presented in Figure 3.10, $\bar{\theta}_{e,h}$, $\dot{\bar{\theta}}_{e,h}$, and $\ddot{\bar{\theta}}_{e,h}$ are provided with measured $\bar{r}$, $\dot{\bar{r}}$ and $\ddot{\bar{r}}$ so that estimated end-effector position, velocity and acceleration, i.e. $\bar{p}_{\mathrm{e,h}}$, $\dot{\bar{p}}_{\mathrm{e},h}$, and $\ddot{\bar{p}}_{\mathrm{e},h}$, can be determined thanks to high-order forward kinematic equations to close control loop.

3.2.2 Pseudo-Static Approach for Inverse Dynamics Control

Another method to provide cable segment angles, $\bar{\theta}$, is to use pseudo-static approach. In this technique, instead of trying to measure cable segment angles, $\bar{\theta}$, or gathering them from dynamic simulation of cable robot, they are planned to be obtained from static equilibrium solution by assuming that manipulator is at its static equilibrium position at that instant. A static solver is required to be run by taking measurable 1st cable segment lengths, $\bar{r}$, as inputs to this solver in every control loop and corresponding angle results of the solver are provided to inverse dynamics controller for the next control loop. Estimated cable segment angular

velocities are figured out by numerical differentiation of segment angles which are the results of static equilibrium solution.

This approach has advantage in terms of calculation time during controller action. Instead of solving system of differential equations of plant, solving set of algebraic equations that are static force equilibrium equations, takes shorter time. The procedure of quasi-static approach can be summarized as follows:

1) Feed reference (desired) end-effector position, velocity and acceleration vectors, i.e. $\bar{p}^*$, $\dot{\bar{p}}^*$, and $\ddot{\bar{p}}^*$.

2) Calculate end-effector position, velocity and acceleration error vectors, i.e. $\bar{e}$, $\dot{\bar{e}}$, and $\ddot{\bar{e}}$ by using actual and desired end-effector position, velocity and acceleration. Note that starting or parking position of the cable robot is static-equilibrium position since it is assumed that cable manipulator is stationary at the beginning of defined task. In other words, initial velocity and acceleration vectors of end-effector are zero vectors. If system has capability of measuring end-effector position, it can be directly used during trajectory tracking instead of obtaining it by forward kinematics calculation using cable segment angles, $\bar{\theta}$.

$$\bar{e} = \bar{p}^* - \bar{p}$$
$$\dot{\bar{e}} = \dot{\bar{p}}^* - \dot{\bar{p}}$$
$$\ddot{\bar{e}} = \ddot{\bar{p}}^* - \ddot{\bar{p}}$$

3) Feed the error vectors, i.e. $\bar{e}$, $\dot{\bar{e}}$, and $\ddot{\bar{e}}$, found on previous step to the controller and calculate the resulting controller output force vector, $\bar{\bar{F}}$, by using inverse dynamics controller technique.

4) Give controller output force vector, $\bar{F}$, to the plant. In this study, response of the plant is found out by running mathematical model of it, i.e. by simulating the cable manipulator, since there is no physical system available.
5) Plant simulation gives the results for actual values of $\bar{\theta}$ and $\bar{r}$. From these vectors, $\bar{r}$ can be directly used in any calculation requiring variable lengths of the 1st cable segments since it is measurable.

6) Solve static equilibrium of the cable manipulator at that instant in order to estimate the cable segment angles, $\bar{\theta}$, used in controller. In this step, it assumed that the motion is slow enough to estimate cable segment angles, $\bar{\theta}$, with the help of static equilibrium solver. This assumption does not imply that manipulator is capable of tracking only slow motion tasks. In relatively aggressive trajectories, it is expected to have higher errors but pseudo-static approach still helps to obtain satisfactory performance which is examined in next chapter of thesis with simulation results.

7) Calculate estimated 1st derivative of cable segment angles, $\dot{\bar{\theta}}_e$, with numerical differentiation employing current and previous estimated cable segment angle values, $\bar{\theta}_e$, and also time step of controller algorithm.

$$\dot{\bar{\theta}}_{e,i} = \frac{\left(\bar{\theta}_{e,i+1} - \bar{\theta}_{e,i}\right)}{\Delta t}$$

8) If it is not taken any position measurement on end-effector, it should be calculated by using estimated cable segment angles, $\bar{\theta}_e$, to be used in error calculation of next loop.

Detailed block diagram of pseudo-static approach including all the steps described above is displayed below. Approach is divided into two cases in terms of position measurement capability of end-effector, both of which are presented and studied.

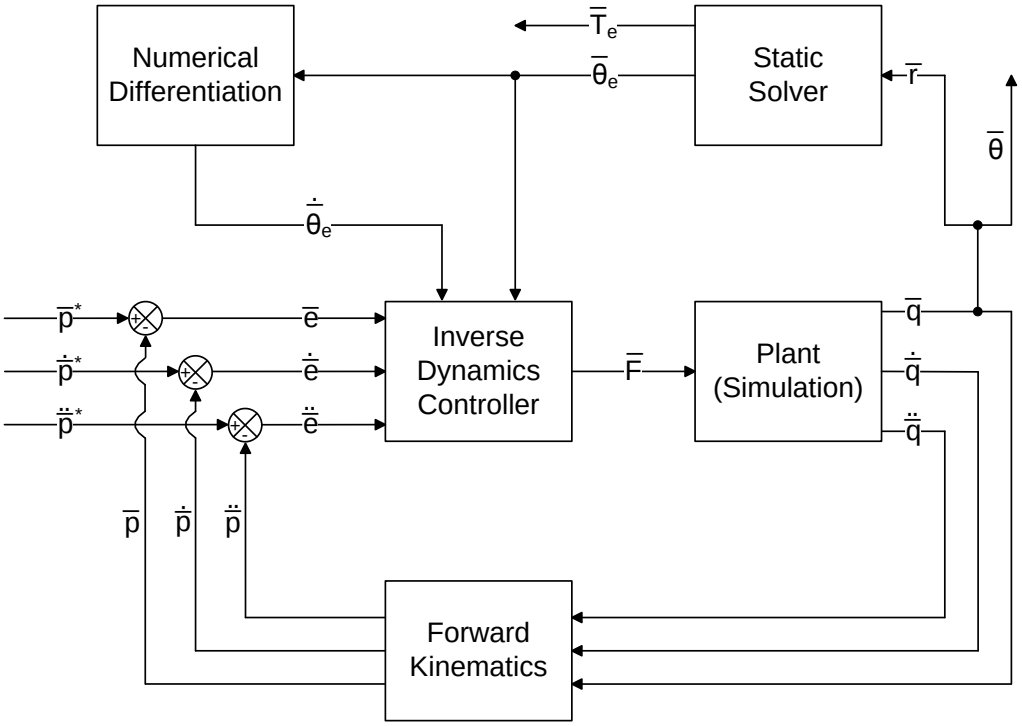

Figure 3.11: Pseudo-Static Approach for Inverse Dynamics Control with Measured End-Effector Pose

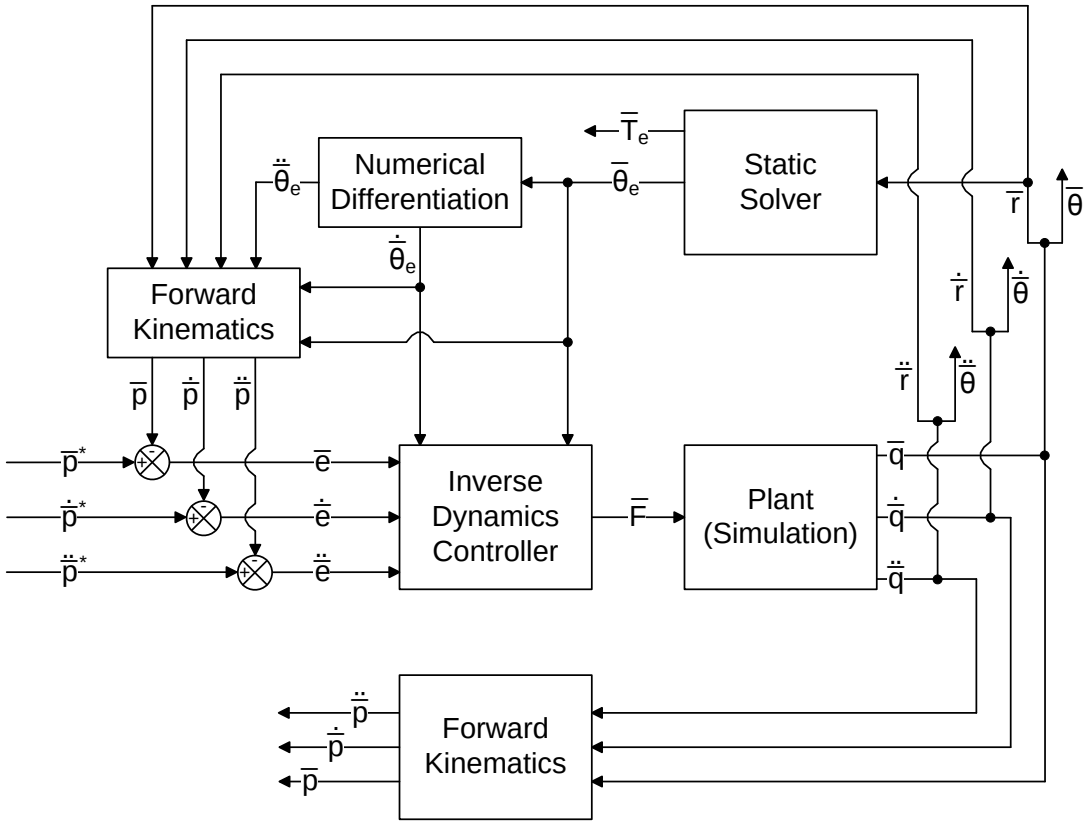

Figure 3.12: Pseudo-Static Approach for Inverse Dynamics Control with Estimated End-Effector Pose

Static solver gives not only estimated cable segment angles, $\bar{\theta}_e$, but also tensions of segments at static equilibrium, $\bar{T}_e$.

Similar to calculation of angular velocities, angular accelerations can also be derived with numerical differentiation.

$$\ddot{\bar{\theta}}_{e,i} = \frac{\left(\dot{\bar{\theta}}_{e,i+1} - \dot{\bar{\theta}}_{e,i}\right)}{\Delta t}$$

In a condition of unmeasured end-effector pose which is presented in Figure 3.12, $\bar{\theta}_e$, $\dot{\bar{\theta}}_e$, and $\ddot{\bar{\theta}}_e$ are provided with measured $\bar{r}$, $\dot{\bar{r}}$ and $\ddot{\bar{r}}$ so that estimated end-effector position, velocity and acceleration, i.e. $\bar{p}_e$, $\dot{\bar{p}}_e$, and $\ddot{\bar{p}}_e$, can be determined thanks to forward kinematic equations to close control loop.

3.3 Tension Monitoring and Control of Two-Cable Planar Parallel Cable Manipulator

Tension monitoring and control is one of the most important and also challenging issues of cable manipulators that should be addressed with some applicable precautions within control algorithm. Due to natural structure of a cable, it can apply only pulling force; therefore, tensions appeared on cables should not decrease below a certain limit in order to prevent slackness during operation of manipulator. Otherwise, slack cables become out of control which causes poor trajectory tracking performance.

Dynamic equilibrium equations are derived in order to monitor cable tensions in every loop of control action which are stated below:

For right cable:

Along x-axis: $F_{x,r,i} = m_i a_{i,x} \rightarrow T_i \cos\theta_i - T_{i+1} \cos\theta_{i+1} = m_i a_{i,x}$

Along y-axis: $F_{y,r,i} = m_i a_{i,y} \rightarrow T_i \sin\theta_i - T_{i+1} \sin\theta_{i+1} - m_i g = m_i a_{i,y}$

where $i = 1,2, \dots, (N_1 - 1)$

For left cable:

Along x-axis: $F_{x,l,j} = m_j a_{j,x} \rightarrow -T_j \cos(\pi - \theta_j) + T_{j+1} \cos(\pi - \theta_{j+1}) = m_j a_{j,x}$

Along y-axis: $F_{y,l,j} = m_j a_{j,y} \rightarrow T_j \sin(\pi - \theta_j) - T_{j+1} \sin(\pi - \theta_{j+1}) - m_j g = m_j a_{j,y}$

where $j = (N_1 + 1), (N_1 + 2), \dots, (N_{total} - 1)$

For tension monitoring, tension values should be calculated from these dynamic equilibrium equations, where cable segment angles, $\bar{\theta}$, segment node accelerations are known. Thus segment tensions become the only unknowns for tension

monitoring problem. There exist total of $N_1 + N_2$ tensions, which can be figured out as follows:

It is a need to multiply x-axis dynamic equilibrium equations with "$-\sin\theta_i$" and y-axis equilibrium equations with "$cos\,\theta_i$" and then sum them up which results in following formulation for right cable:

$$T_{i+1} = \frac{m_i\left(a_{i,y}\,cos\,\theta_i - a_{i,x}\,sin\,\theta_i + g\,cos\,\theta_i\right)}{sin\,(\theta_i - \theta_{i+1})}$$

where $i = 1,2,\dots,(N_1 - 1)$

1st segment tension of right cable, T_1, is already known since it is equal to the control input F_1.

Segment tension values of left cable are developed with similar approach meaning that x-axis dynamic equilibrium equations are multiplied with "$sin(\pi - \theta_i)$" and y-axis equilibrium equations are multiplied with "$cos(\pi - \theta_i)$" and then summed:

$$T_{j+1} = \frac{m_j\left(a_{j,y}\,cos(\pi - \theta_j) + a_{j,x}\,sin\left(\pi - \theta_j\right) + g\,cos(\pi - \theta_j)\right)}{sin\left(\theta_{j+1} - \theta_j\right)}$$

where $j = (N_1 + 1), (N_1 + 2), \dots, (N_{total} - 1)$

1st segment tension of left cable, T_{N+1}, is already known since it is equal to the control input F_2.

Determination of tension of each segment provides detection of slack segments in case of going below a tension limit, T_{limit}. In this situation, desired trajectory profile needs to be updated so that segment tensions can be kept at certain tension. In other words, segment tensions, $\bar{T}$, can be hold on desired level not to lose its control in exchange for trajectory tracking performance. For this reason, available performance which is directly related with the acceleration accomplished by manipulator in a case of limited segment tension requires to be calculated. For this

stage, dynamic equilibrium equations become again point of interest to be able to find out available accelerations of segment nodes, $\bar{a}'$. However, unlike tension monitoring, cable segment angles, $\bar{\theta}$ are also unknown besides node accelerations. To be more descriptive, "$2x(N_{total}-1)$" number of node accelerations and "N_{total}" segment angles are all unknown but there exist total of "$2x(N_{total}-1)$" dynamic equilibrium equations. In this study, it is proposed an optimization algorithm to deal with this problem. By utilizing optimization, it is aimed to minimize the difference between desired and available node accelerations, i.e. $\bar{a}^*$ and $\bar{a}'$, under the constraint of tension limit, T_{limit}. This approach helps to keep not only loss of tracking performance at minimum but also segment tensions at desired level.

Formulations for available segment node accelerations, $\bar{a}'$, are derived in the following form:

For right-cable along x and y axes:

$$a'_{i,x} = \frac{T'_i \cos\theta_i - T'_{i+1}\cos\theta_{i+1}}{m_i}$$

$$a'_{i,y} = \frac{T'_i \sin\theta_i - T'_{i+1}\sin\theta_{i+1} - m_i g}{m_i}$$

where $i = 1,2,\dots,(N_1-1)$

For left-cable along x and y axes:

$$a'_{j,x} = \frac{-T'_j \cos(\pi-\theta_j) + T'_{j+1}\cos(\pi-\theta_{i+1})}{m_j}$$

$$a'_{j,y} = \frac{T'_j \sin(\pi-\theta_i) - T'_{j+1}\sin(\pi-\theta_{i+1}) - m_j g}{m_j}$$

where $j = (N_1+1),(N_1+2),\dots,(N_{total}-1)$

For end-effector node along x and y axes:

$$a'_{ee,x} = \frac{T'_{N1}\, cos\, \theta_{N1} - T'_{Ntotal}\, cos(\pi - \theta_{Ntotal})}{m_{ee}}$$

$$a'_{ee,y} = \frac{T'_{N1}\, sin\, \theta_{N1} + T'_{Ntotal}\, sin(\pi - \theta_{Ntotal}) - m_{ee}g}{m_{ee}}$$

Now, problem turns into constrained nonlinear multivariable problem where objective is to minimize the deviation from desired acceleration vector of segment nodes, $\bar{a}^*$, by satisfying the condition of $\bar{T}' \geq \bar{T}_{limit}$. Note that it is desired to monitor tensions of all segments of cable, since anyone of them might become critical depending on the dynamics of motion. Hence optimization problem becomes multiobjective because all node accelerations are taken into account within dynamic equilibrium equations.

By considering all these important points, objective functions are created as stated below:

Objective function for the 1st segment node along x and y axes, $\bar{f}_1 = [f_{1,x} \quad f_{1,y}]^T$:

$$f_{1,x} = \left(a^*_{1,x} - a'_{1,x}(T'_1, T'_2)\right)^2$$

$$f_{1,y} = \left(a^*_{1,y} - a'_{1,y}(T'_1, T'_2)\right)^2$$

$$\bar{f}_1 = [f_{1,x} \quad f_{1,y}]^T$$

Objective function for the 2nd segment node along x and y axes, $\bar{f}_2 = [f_{2,x} \quad f_{2,y}]^T$:

$$f_{2,x} = \left(a^*_{2,x} - a'_{2,x}(T'_2, T'_3)\right)^2$$

$$f_{2,y} = \left(a^*_{2,y} - a'_{2,y}(T'_2, T'_3)\right)^2$$

$$\bar{f}_2 = [f_{2,x} \quad f_{2,y}]^T$$

….

….

Objective function for the (N_{total}-1)th segment node along x and y axes, $\bar{f}_{(Nt-1)} = [f_{(Nt-1),x} \quad f_{(Nt-1),y}]^T$:

$$f_{(Nt-1),x} = \left(a^*_{(Nt-1),x} - a'_{(Nt-1),x}(T'_{Nt-1}, T'_{Nt})\right)^2$$

$$f_{(Nt-1),y} = \left(a^*_{(Nt-1),y} - a'_{(Nt-1),y}(T'_{Nt-1}, T'_{Nt})\right)^2$$

$$\bar{f}_{Nt-1} = [f_{(Nt-1),x} \quad f_{(Nt-1),y}]^T$$

("N_t" stands for "N_{total}")

These objective functions can be turned into aggregate single objective function, $f(\bar{T}')$, with the help of assigned weights, $w_{i,x}$ and $w_{i,y}$.

$$\bar{w}_i = [w_{i,x} \quad w_{i,y}]$$

$$f(\bar{T}') = \sum_{i=1}^{Nt-1} \bar{w}_i \bar{f}_i$$

$$f(\bar{T}') = w_{1,x}f_{1,x} + w_{1,y}f_{1,y} + w_{2,x}f_{2,x} + w_{2,y}f_{2,y} + \cdots + w_{Nt-1,x}f_{Nt-1,x} + w_{Nt-1,y}f_{Nt-1,y}$$

Finalized structure of optimization problem can be stated as

$$min\{\, f(\bar{T}')\,\} \quad s.t. \quad \bar{T}' \geq \bar{T}_{limit}$$

This minimization problem is handled by using Matlab's® "*fmincon*" function which finds $\bar{T}'$ minimizing the constrained nonlinear multivariable function $f(\bar{T}')$ [60] [61]. It is wise to select weights of end-efector node objective functions as high as possible since main concern is to keep end-effector tracking result as close as possible to desired path. The constraint for weights included in single aggregate objective function is formed:

$$\sum_{i=1}^{Nt-1} w_{i,x} + \sum_{i=1}^{Nt-1} w_{i,y} = 1$$

Solution of optimization problem provides $\bar{T}'$ first two elements of which become required segment forces of 1st segments, $\bar{F}'$. The resultant algorithm of tension monitoring and control is presented on the below figure.

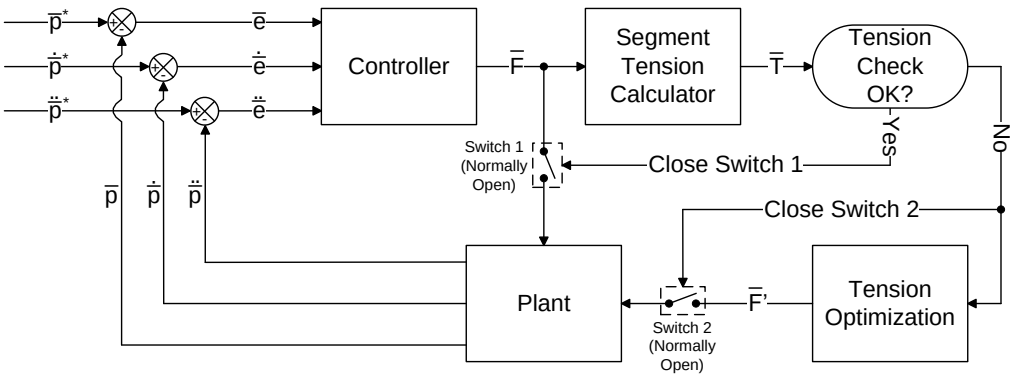

Figure 3.13: Tension Monitoring and Control Algorithm

As Figure 3.13 illustrates, before directly feeding force vector generated by inverse dynamics controller, $\bar{F}$, to the plant, resulting tensions of segments are calculated in block "*Segment Tension Calculator*" and checked whether they contain any slack segment in block "*Tension Check*". If no, i.e. tension check returns the result as "*Yes"* to *"OK?"*, then regular operation of control algorithm is maintained by feeding $\bar{F}$ to plant. In opposite case, updated set of 1st segment forces, $\bar{F}'$, needs to be developed such that it eliminates segment slackness by minimizing the loss of trajectory tracking performance. Minimization stage is completed in the block named "*Tension Optimization*" in Figure 3.13.

All segment angle estimation methods implemented on inverse dynamics control strategy proposed in this chapter are tested with different trajectories and system parameters in order to evaluate their performance by simulations which are presented in the next chapter in detail.

3.4 Candidates for Measurement Methods of System Variables

As a nature of control applications, a system variable or a set of system variables obviously have to be measured. Therefore, it is important to ensure that the variables defined to be used as feedback, are measurable with adequate accuracy. In the block diagrams of inverse dynamics controller presented in this chapter, 1st segment lengths of cables, end-effector pose and tensions of cables are proposed as measured parameters. In this section, possible methods and equipments to be employed to reply this need are indicated. Most of these methods are already used in an application and encountered in the literature. Since it is clear that measurement of rotation of pulleys is the most straightforward and easiest way to implement, it is not mentioned about measurement of 1st segment length.

3.4.1 Measurement of End-Effector Pose

In most of the applications, it is preferred to use vision based feedback of end-effector pose. Details of this method are expressed below with the examples successful applications:

In research [29], two cameras are utilized in order to measure pose of 6-DOF end-effector. This method of measurement is accomplished by tracking the lasers attached to the corners of triangular end-effector.

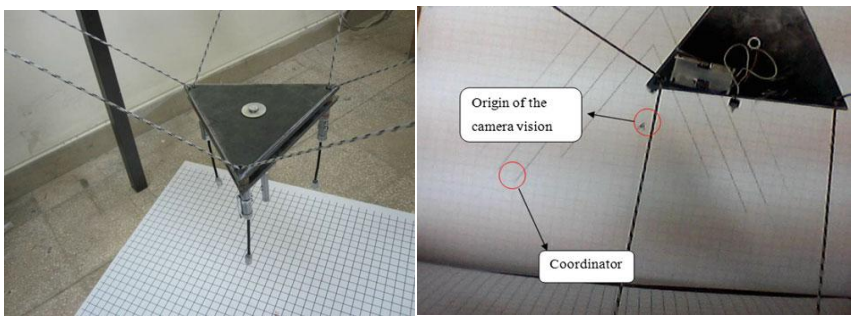

Figure 3.14: Triangular End-Effector Measured by Two Cameras in Study [29]

In study of Lytle, *et al*. [34], site measurement system (SMS) is selected to measure pose of the RoboCrane with accuracy of millimeters. For this purpose, there are placed three receivers at the corners of triangular platform of the RoboCrane with four laser transmitters distributed to the workspace.

Figure 3.15: An SMS Laser Transmitter and an SMS Optical Reciever used in Study [34]

In their studies [41] and [62] R. Babaghasabha, *et.al.* conducted a series of experiments on a fully constrained planar cable robot with four cables. In order to measure the pose of end-effector, it is used a CCD camera located at a distance of 1.12 m from the motion plane. A square mark is placed on the end-effector corners of which are sensed by the camera.

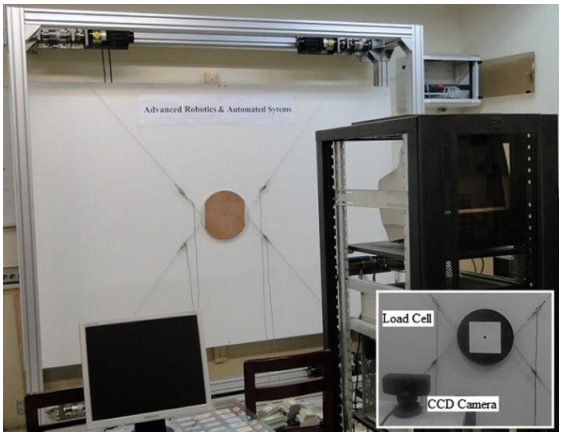

Figure 3.16: Vision Based Feedback of End-Effector Pose used in Study [41]

In their studies [63] and [64], Dallej, et al. proposed a visual servoing method for cable-driven parallel manipulator with 8 cables. The concept is illustrated on the following figure by them.

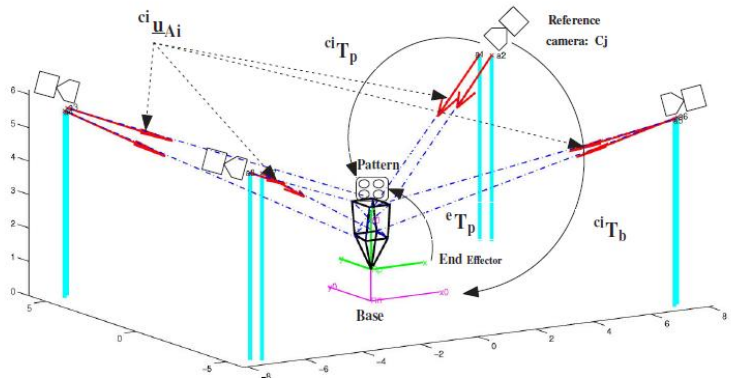

Figure 3.17: Vision-Based Servoing Proposed in Study [64]

In studies of Dallej et al. [65] and [66], there are introduced 3D visual servoing methods to control some rigid link parallel manipulators. In addition, 3D visual servoing methods are implemented to a serial manipulators by placing a visual sensor on the end-effector, some examples of which are described in studies [67], [68] and [69].

In the research [70], there are conducted some experiments on 5 m scaled version of FAST and pose measurement of the feed cabin (end-effector) is completed with three laser ranging equipments. Another example for laser equipment use is completed by Jin et al.. In their study, they used 2D laser scanner to measure end-effector of a planar cable robot with 4 cables [71].

As a different approach, an indirect measurement of end-effector pose is also employed based on the measurement of inclination angles of the cables with a method shown in Figure 3.6 [38]. By using these angles and knowing cable lengths and actuator positions, end-effector pose is calculated through kinematic relations.

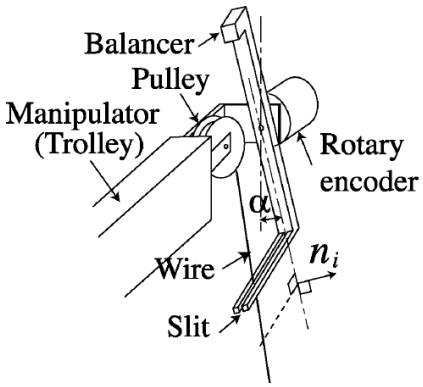

Figure 3.18: Method for Measurement of Cable Angle proposed in Study [38]

3.4.2 Measurement of Cable Angles

Measured cable angles are treated as angles of 1st segments which can be used both in inverse dynamics controller and also curve fitting stage of angle estimator mentioned in Section 3.2.1.2.

In Section 3.2.1.2, it is already introduced a cable angle measurement method proposed by Fortin-Côté et al. in their study [58].

Instead of direct measurement of the cable angle, it is proposed an estimation method which is based on the reaction force observer in the research [72]. In case of sensorless applications, this method might be a good alternative; however, it has to be verified through experiments.

An interesting method is introduced by Peshkin in his patent filed in 1999 [73]. The idea is based on energizing the cable with alternating current to generate magnetic field. There are also placed coils near the cable and they do not intersect with the magnetic field of the cable at initial configuration. Once cable is deflected, it induces a voltage on the coil and corresponding cable angle can be determined with the help of this voltage value.

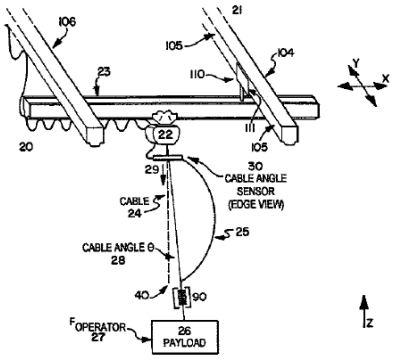

Figure 3.19: Non-Contacting Angle Sensor proposed by Peshkin [73]

3.4.3 Measurement of Cable Tension

Tension control algorithm developed in Section 3.3 checks tensions of all cable segments; therefore, tension calculator supplies N number of tension values for a cable containing N number of segments. Hence tension measurement is not sufficient to complete this tension control algorithm without any extra online calculation. However, it becomes still beneficial to have a measured tension value of the system which can be regarded as the tension of 1st cable segment or can be compared with the tension obtained from tension calculator. That's why, possible tension measurement methods encountered in the literature are presented in this section.

Load cells that are located at the pulleys of cable robot are used to sense tension of cables in order to verify simulation results and determine payload capacity, in study [29]. In another study, load cells are again used for tension measurement but this time, they are located near the cable attachment points of the end-effector [41]. In another application that utilizes load cell, it is placed within the actuator structure [71].

Kim and Park proposed an alternative approach to determine cable tension in their research [74]. They used accelerometers to measure the natural frequencies of the cable and then used the resulting values to estimate the tensions using the proper

formulations. However, it might not be practical to locate a sensor on a cable for cable robot applications since they proposed this method for constructions like bridges.

CHAPTER 4

SIMULATIONS

In this chapter, the proposed control strategy and related segment angle estimation methods to be employed in it are implemented on a simulation under different conditions and scenarios. Furthermore, some of these challenging conditions are selected to test tension monitoring and control algorithm. Before presenting the results and evaluating the performance, it is beneficial to introduce these conditions and scenarios.

4.1 Simulation Scenarios and Conditions

4.1.1 Parking Positions of the Cable Robot

It has vital importance to observe the performance of the cable robot at different regions of the workspace. Hence simulations are completed with three different initial positions, which are called parking positions of the cable robot. While vertical coordinates (y coordinates) of these positions are specified at the top, middle and the bottom of the height of the workspace, horizontal coordinates (x coordinates) are located at the midpoint of its width.

Table 4: Parking Positions of the Cable Robot

Parking Positions of the Cable Robot	Value (Unit)
1st Parking Position (x,y)	-2.5 , -1.2 (m,m)
2nd Parking Position (x,y)	-2.5 , -5 (m,m)
3rd Parking Position (x,y)	-2.5 , -8.8 (m,m)

4.1.2 Types of Reference Commands

Simulations are carried out with three types of references; square wave position command, deployment motion command and circular motion command. Each reference command is labeled with a specific name so that it is completely defined with a unique, compact name in figures. All the labels are indicated in *Command Label* part of the Table 5, Table 6 and Table 7.

4.1.2.1 Square Wave Position Command

First command to be used on the simulation is the square wave position command composed of two successive step functions. For each starting position of the cable robot, there are defined square wave commands having different amplitudes all of which are described on the following table.

Table 5: Details of Square Wave Position Commands

Initial End-Effector Position	**Motion Direction /Command Label**	**@ Time (s) – Desired Coordinates (x,y)**
1st Parking Position @ t=0:(-2.5 m , -1.2 m)	in y direction (pure vertical motion) / **S-P1-y**	@ t=0 – (-2.5 m , -1.5 m) @ t=5 – (-2.5 m , -1.2 m) @ t=10 – (-2.5 m , -1.2 m) Amplitude of Steps = 0.3 m
	in x direction (pure horizontal motion) / **S-P1-x**	@ t=0 – (-2.25 m , -1.2 m) @ t=5 – (-2.5 m , -1.2 m) @ t=10 – (-2.5 m , -1.2 m) Amplitude of Steps = 0.25 m
2nd Parking Position @ t=0:(-2.5 m , -5 m)	in y direction (pure vertical motion) / **S-P2-y**	@ t=0 – (-2.5 m , -5.5 m) @ t=5 – (-2.5 m , -5 m) @ t=10 – (-2.5 m , -5 m) Amplitude of Steps = 0.5 m
	in x direction (pure horizontal motion) / **S-P2-x**	@ t=0 – (-2 m , -5 m) @ t=5 – (-2.5 m , -5 m) @ t=10 – (-2.5 m , -5 m) Amplitude of Steps = 0.5 m
3rd Parking Position @ t=0:(-2.5 m , -8.8 m)	in y direction (pure vertical motion) / **S-P3-y**	@ t=0 – (-2.5 m , -7.8 m) @ t=5 – (-2.5 m , -8.8 m) @ t=10 – (-2.5 m , -8.8 m) Amplitude of Steps = 1 m
	in x direction (pure horizontal motion) / **S-P3-x**	@ t=0 – (-1.5 m , -8.8 m) @ t=5 – (-2.5 m , -8.8 m) @ t=10 – (-2.5 m , -8.8 m) Amplitude of Steps = 1 m

4.1.2.2 Deployment Motion Command

A quintic polynomial is utilized to generate a deployment motion profile. This polynomial is simply formulated as follows:

$$P(t) = a_5 t^5 + a_4 t^4 + a_3 t^3 + a_2 t^2 + a_1 t + a_0$$

For a motion that is planned to be completed in T seconds, following conditions are defined so that coefficients (a_i) of the quintic polynomial can be found out.

$\ddot{P}(0) = \ddot{P}(T) = 0$: Zero desired acceleration at the beginning and end of the deployment motion
$\dot{P}(0) = \dot{P}(T) = 0$: Zero desired velocity at the beginning and end of the deployment motion
$P(0) = P_{initial}$ and $P(T) = P_{final}$

Similar to the square wave command, deployment motion commands are also proposed with different amplitudes for each starting (parking) position of the end-effector of the cable robot.

Table 6: Details of Deployment Motion Commands

Initial End-Effector Position	**Motion Direction /Command Label**	**@ Time (s) – Desired Coordinates (x,y)**
1st Parking Position @ t=0:(-2.5 m , -1.2 m)	in y direction (pure vertical motion) / **D-P1-y**	@ t=1 – (-2.5 m , -1.5 m) Amplitude of Motion = 0.3 m
	in x direction (pure horizontal motion) / **D-P1-x**	@ t=1 – (-2.25 m , -1.2 m) Amplitude of Motion = 0.25 m
2nd Parking Position @ t=0:(-2.5 m , -5 m)	in y direction (pure vertical motion) / **D-P2-y**	@ t=1 – (-2.5 m , -5.5 m) Amplitude of Motion = 0.5 m
	in x direction (pure horizontal motion) / **D-P2-x**	@ t=1 – (-2 m , -5 m) Amplitude of Motion = 0.5 m
3rd Parking Position @ t=0:(-2.5 m , -8.8 m)	in y direction (pure vertical motion) / **D-P3-y**	@ t=1 – (-2.5 m , -7.8 m) Amplitude of Motion = 1 m
	in x direction (pure horizontal motion) / **D-P3-x**	@ t=1.5 – (-1.5 m , -8.8 m) Amplitude of Motion = 1 m

4.1.2.3 Circular Motion Command

As the third and the last command, circular path tracking ability of the cable robot is tested under circular motion command. For each starting position of motion, different diameters of the desired circular path are defined. Moreover, variety of desired angular speeds of motion with counter-clockwise rotation direction is planned to be examined in simulations.

Table 7: Details of Circular Motion Commands

Initial End-Effector Position	**Diameter of Desired Circular Path (Unit)**	**Desired Angular Speed of Motion (Unit) - Command Label**
1st Parking Position @ t=0:(-2.5 m , -1.2 m)	0.3 m	18 deg/s - **C-P1-1**
		36 deg/s - **C-P1-2**
		72 deg/s - **C-P1-3**
2nd Parking Position @ t=0:(-2.5 m , -5 m)	0.5 m	18 deg/s - **C-P2-1**
		36 deg/s - **C-P2-2**
		72 deg/s - **C-P2-3**
3rd Parking Position @ t=0:(-2.5 m , -8.8 m)	1 m	18 deg/s - **C-P3-1**
		36 deg/s - **C-P3-2**
		72 deg/s - **C-P3-3**

4.2 Simulation Results

In this section, simulation results are presented in order to evaluate the performance of the inverse dynamics controller proposed in Chapter 3. In the first subsection, controller is operated as if cable segment angles are somehow measured or they are calculated with the help of comprehensive plant model developed in Chapter 2. In addition to that, pose of end-effector is assumed to be measured or calculated by using measured segment angles and lengths of first segments. Secondly, lower-order model approach developed in Section 3.2.1 is utilized and corresponding system responses are visualized. In addition, the effect of order of lower-order model on the accuracy of system response is also investigated. For lower-order angle generator model with higher-order controller approach, effect of angle measurement of the first segments is indicated with few simulations. Lastly, performance of the pseudo-static approach described in Section 3.2.2 is presented. For all approaches, it is examined to determine whether measurement of end-effector position has considerable positive effects on the system performance by running simulations for some different scenarios.

Apart from cable segment estimation methods, tension monitoring and control technique explained in Section 3.3 is also analyzed through few simulations under different types of reference commands.

Segment number determination approach developed in Section 2.5 ends up with the result that it is accurate enough for the plant model to divide cables into 6, 8 and 9 segments for the simulations starting from 1st, 2nd and 3rd parking positions, respectively. Because of that, all the simulations are carried out with these corresponding numbers of segments in order to reduce simulation times.

4.2.1 Measured Segment Angles or Direct Use of the Plant Model Simulations

At first stage of simulations, controller is tested with measured end-effector pose. Segment angles are also assumed to be sensed or obtained from higher-order system with online calculation.

4.2.1.1 Response under Square Wave Position Command

Responses of the cable robot under different square wave position commands are illustrated in the following figures for the case of measured cable segment angles or direct use of the plant model.

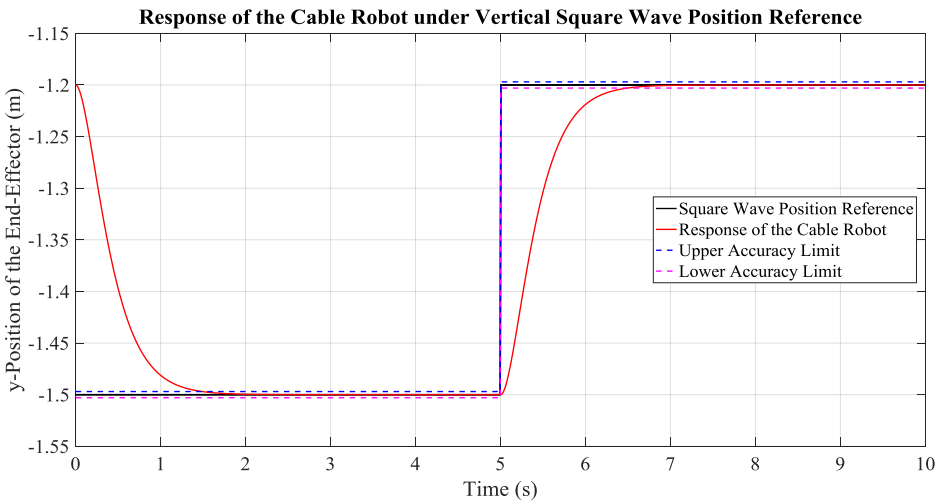

Figure 4.1: Response of the Cable Robot under Command “S-P1-y”

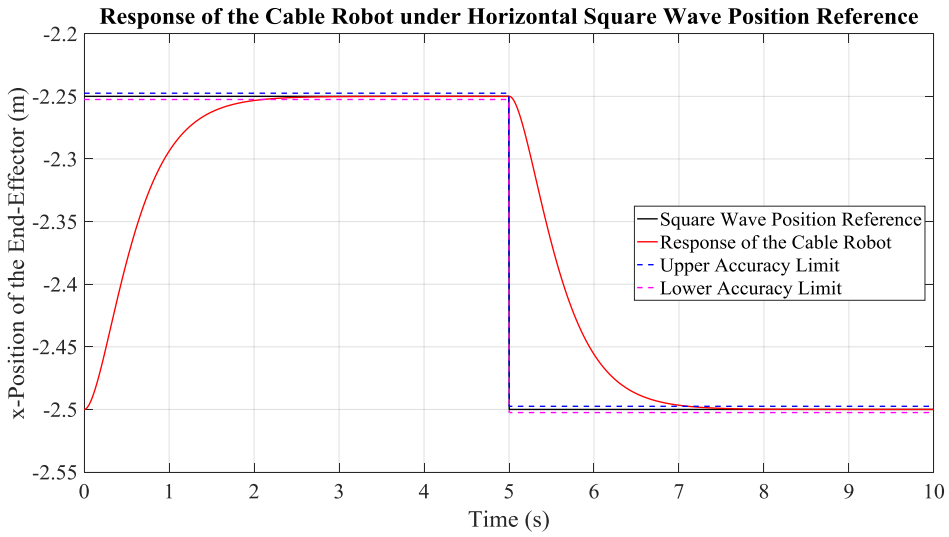

Figure 4.2: Response of the Cable Robot under Command “S-P1-x”

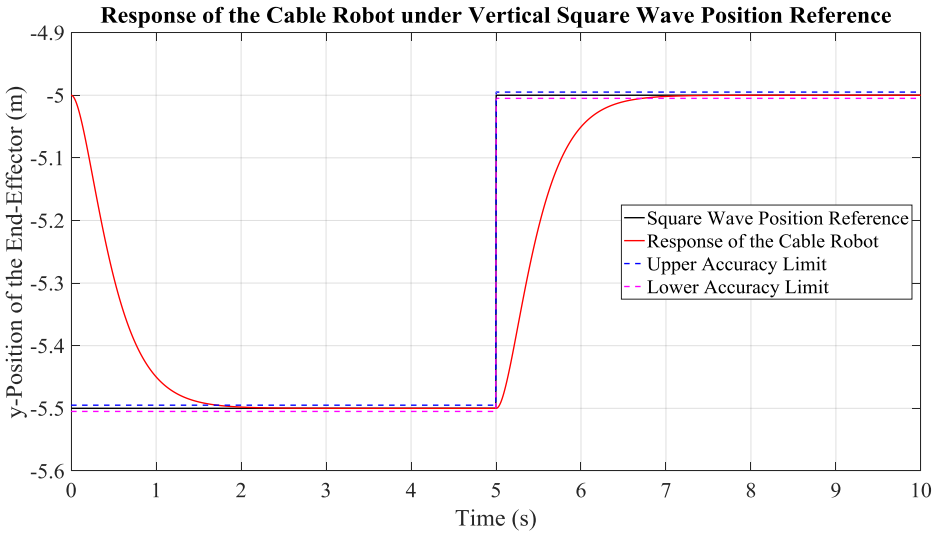

Figure 4.3: Response of the Cable Robot under Command “S-P2-y”

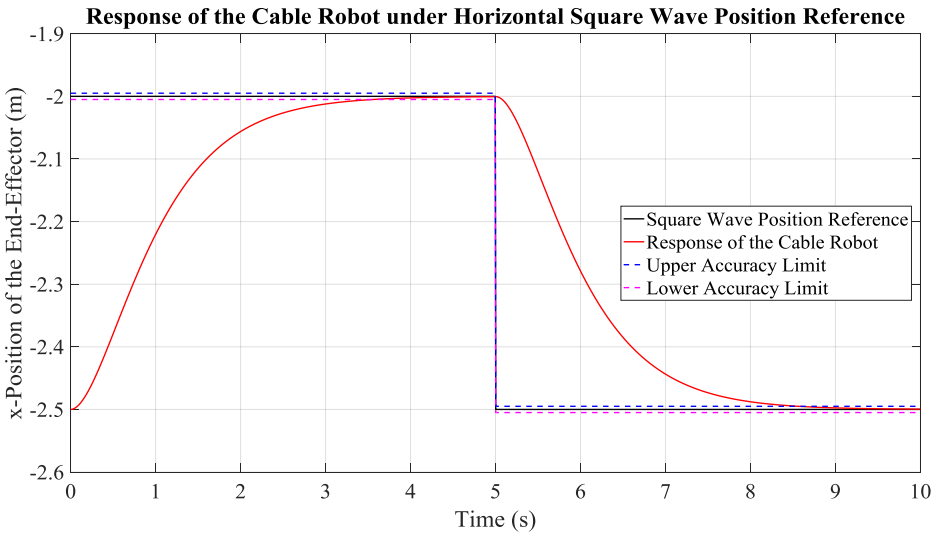

Figure 4.4: Response of the Cable Robot under Command “S-P2-x”

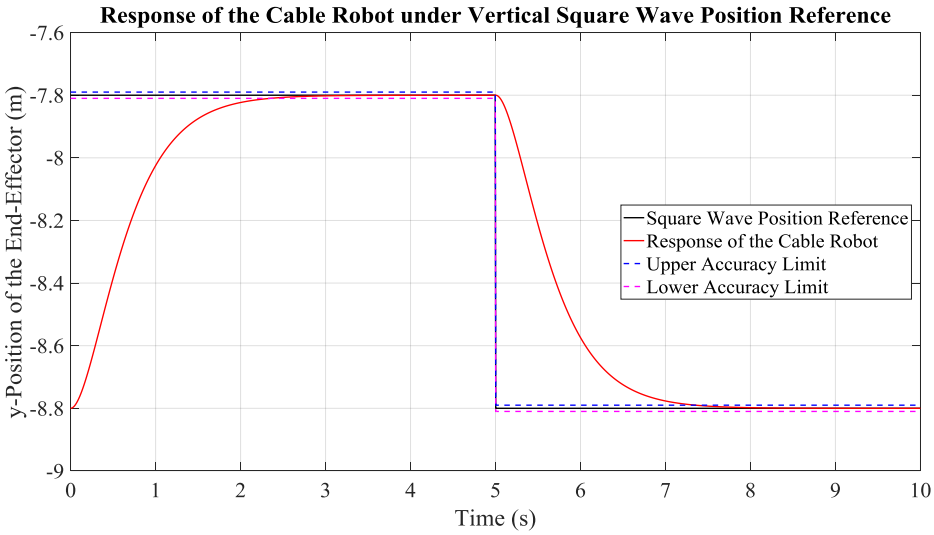

Figure 4.5: Response of the Cable Robot under Command “S-P3-y”

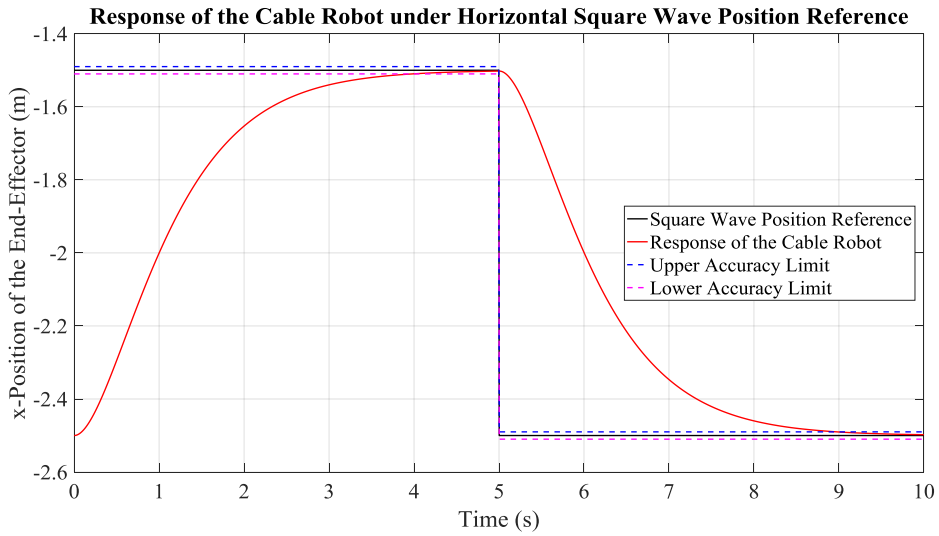

Figure 4.6: Response of the Cable Robot under Command “S-P3-x”

4.2.1.2 Response under Deployment Motion Command

Responses of the cable robot under different deployment motion commands are illustrated in the following figures for the case of measured cable segment angles or direct use of the plant model.

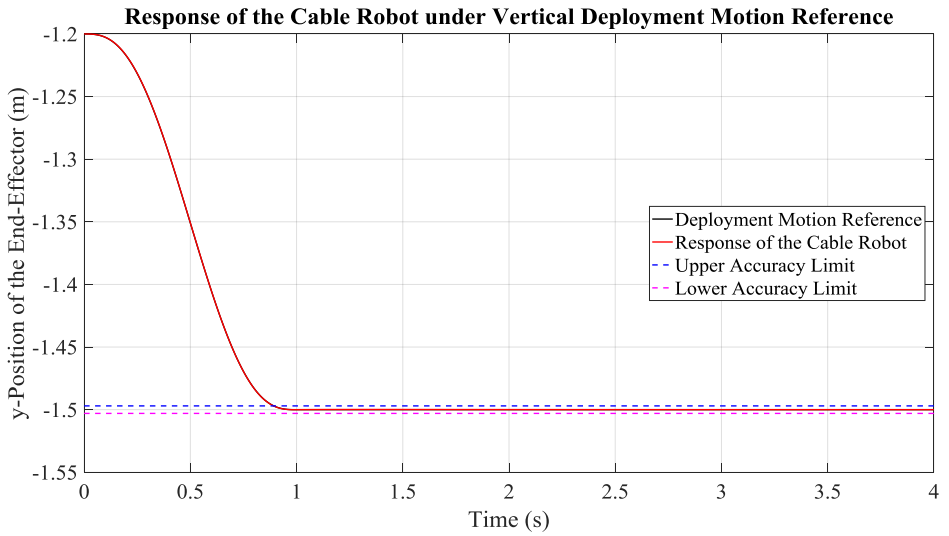

Figure 4.7: Response of the Cable Robot under Command “D-P1-y”

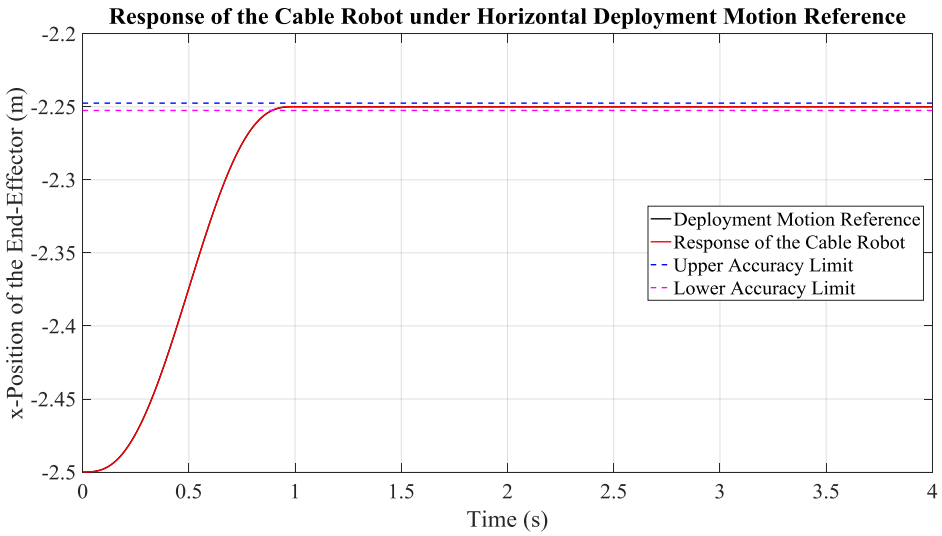

Figure 4.8: Response of the Cable Robot under Command “D-P1-x”

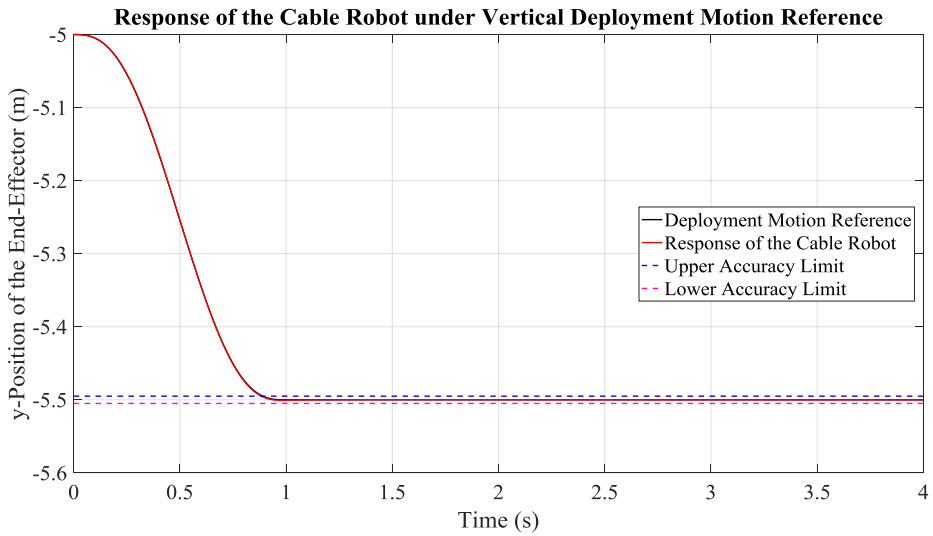

Figure 4.9: Response of the Cable Robot under Command “D-P2-y”

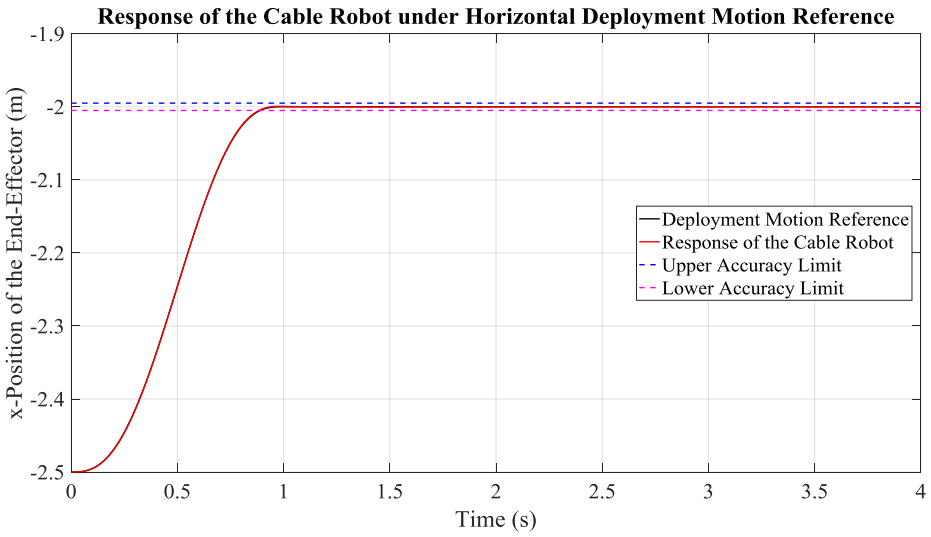

Figure 4.10: Response of the Cable Robot under Command "D-P2-x"

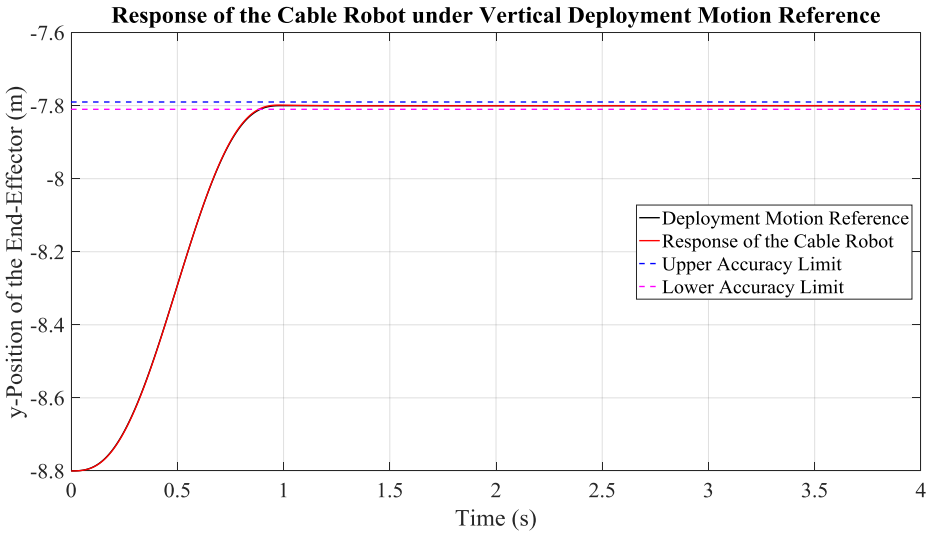

Figure 4.11: Response of the Cable Robot under Command "D-P3-y"

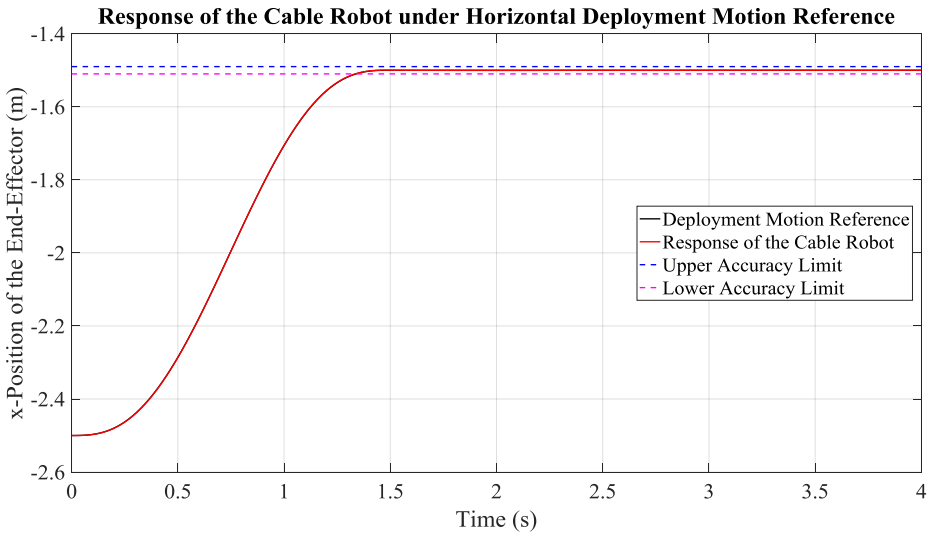

Figure 4.12: Response of the Cable Robot under Command "D-P3-x"

4.2.1.3 Response under Circular Motion Command

Responses of the cable robot under different circular motion commands are illustrated in the following figures for the case of measured cable segment angles or direct use of the plant model.

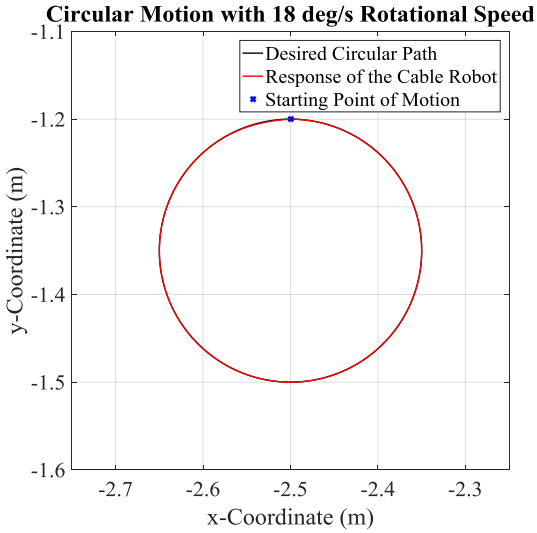

Figure 4.13: Response of the Cable Robot under Command "C-P1-1"

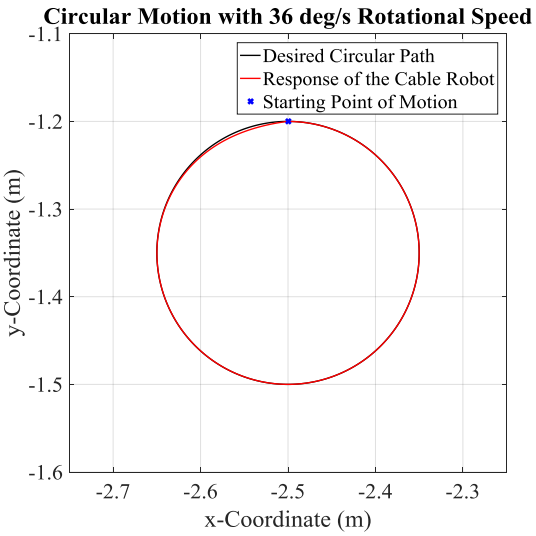

Figure 4.14: Response of the Cable Robot under Command “C-P1-2”

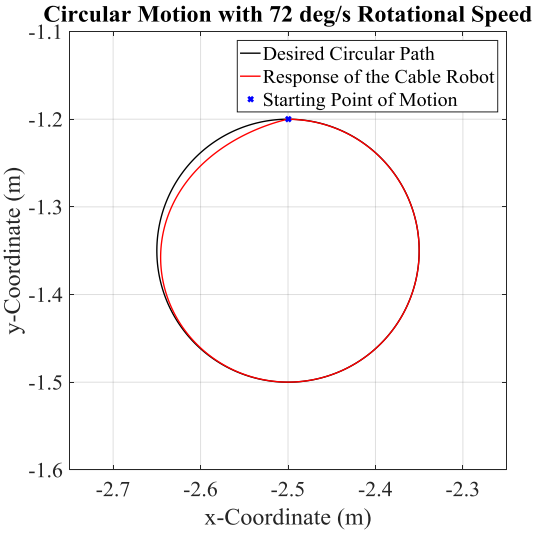

Figure 4.15: Response of the Cable Robot under Command “C-P1-3”

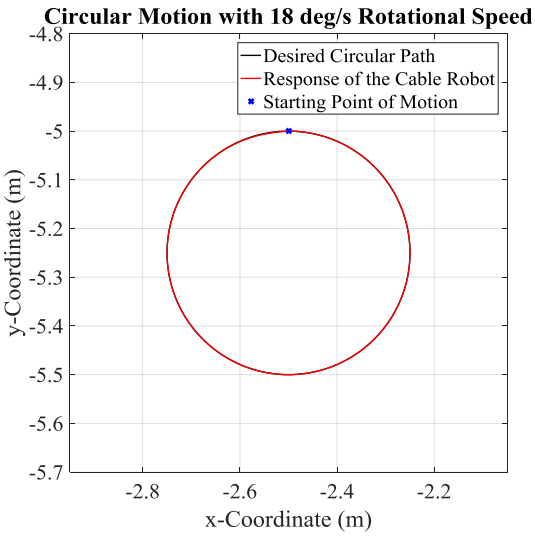

Figure 4.16: Response of the Cable Robot under Command “C-P2-1”

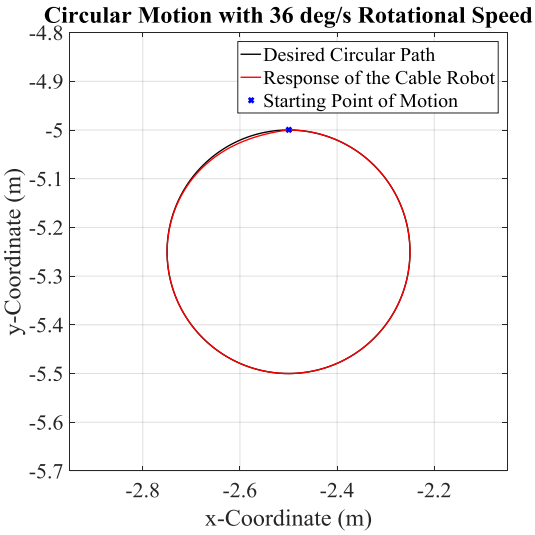

Figure 4.17: Response of the Cable Robot under Command “C-P2-2”

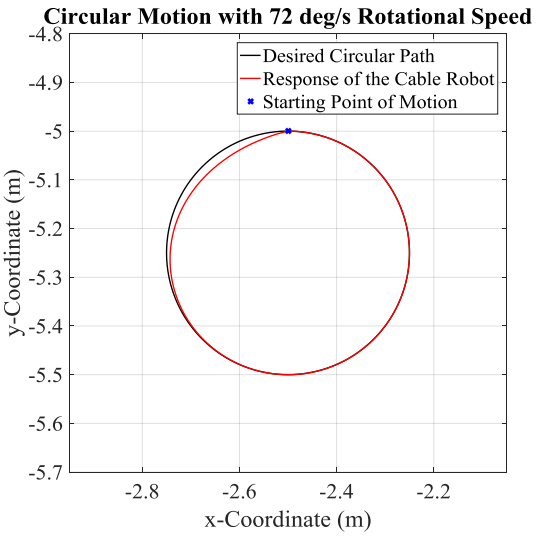

Figure 4.18: Response of the Cable Robot under Command “C-P2-3”

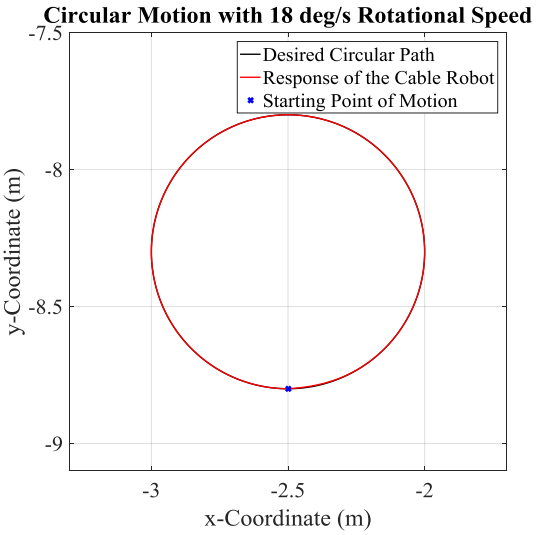

Figure 4.19: Response of the Cable Robot under Command “C-P3-1”

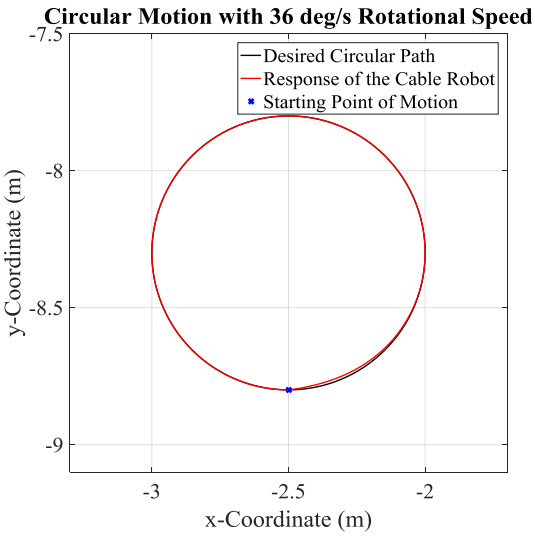

Figure 4.20: Response of the Cable Robot under Command “C-P3-2”

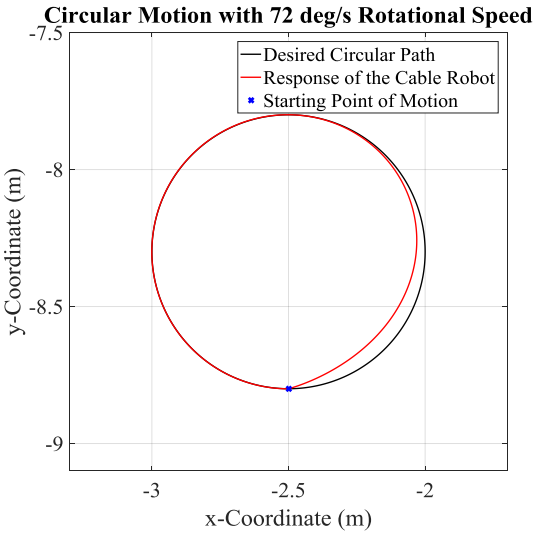

Figure 4.21: Response of the Cable Robot under Command “C-P3-3”

4.2.2 Lower-Order Model Approach Simulations

4.2.2.1 Lower-Order Angle Generator Model and Lower-Order Controller Simulations

In this section, simulations are completed with lower-order angle estimator and lower-order controller. End-effector pose is assumed to be measured at this step.

4.2.2.1.1 Response under Square Wave Position Command

Responses of the cable robot under different square wave position commands are illustrated in the following figures for the case of lower-order segment angle generator and lower-order controller with measured end-effector pose.

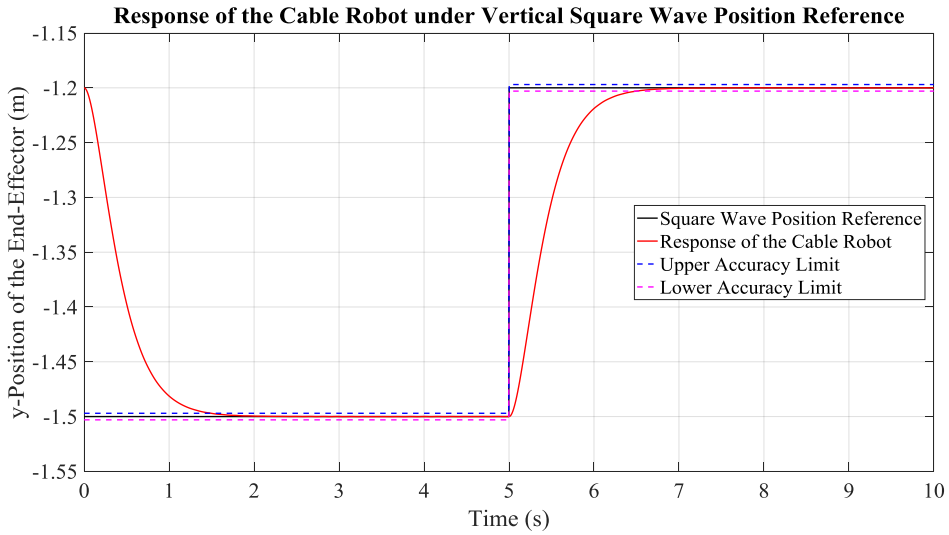

Figure 4.22: Response of the Cable Robot under Command "S-P1-y"

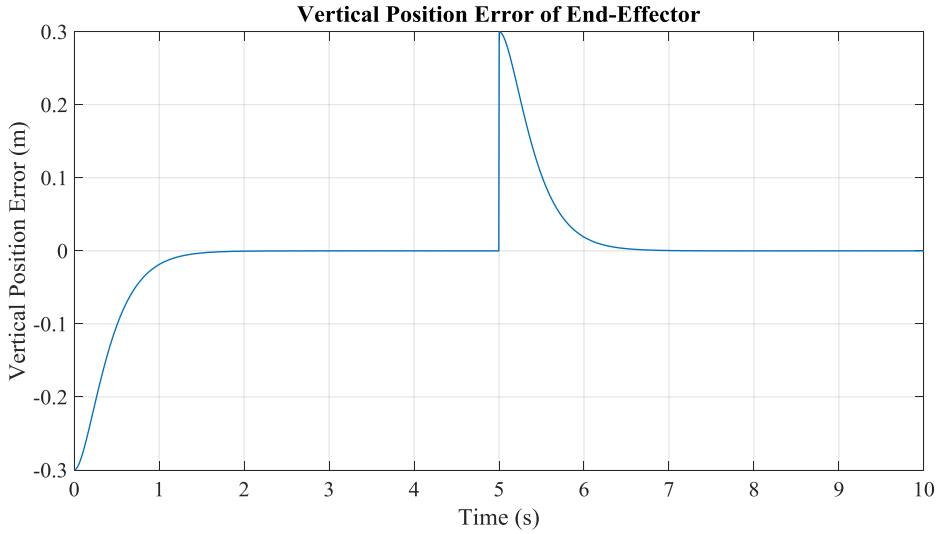

Figure 4.23: Position Error under Command "S-P1-y"

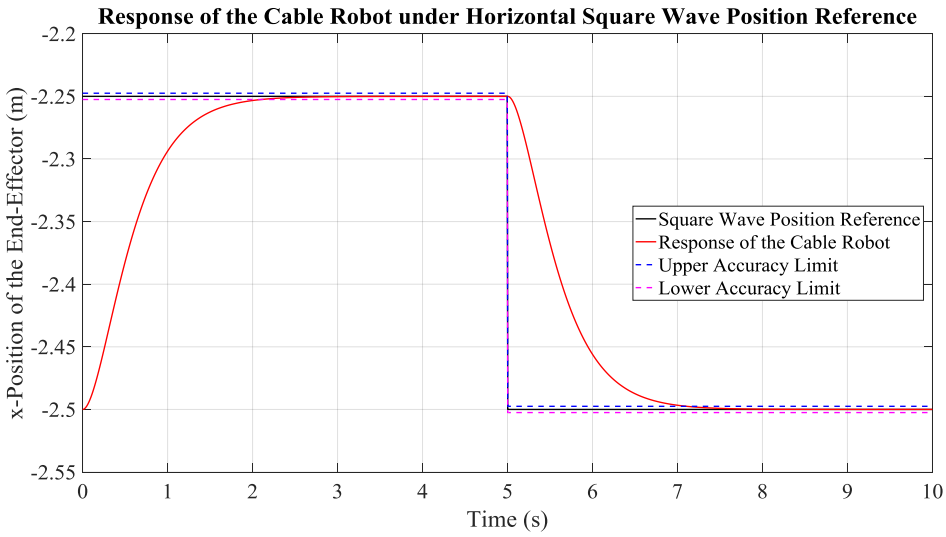

Figure 4.24: Response of the Cable Robot under Command “S-P1-x”

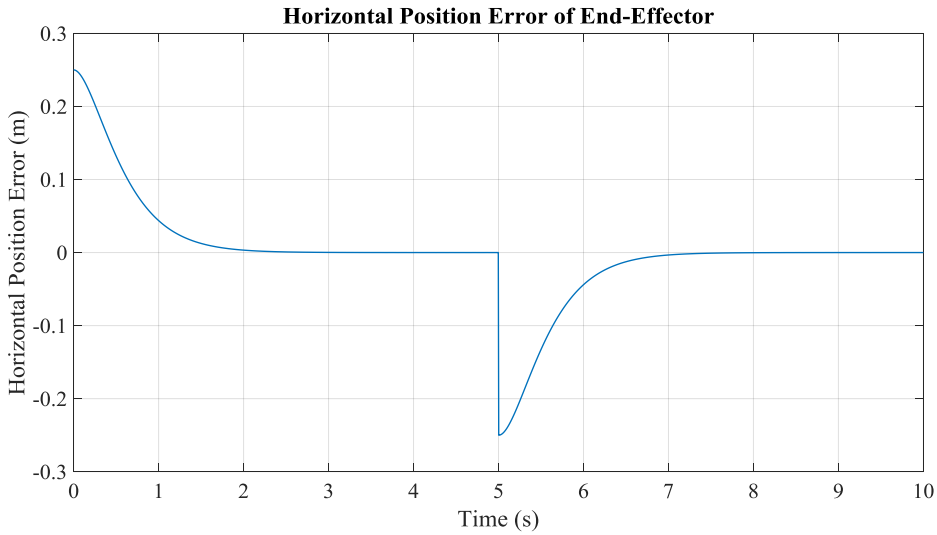

Figure 4.25: Position Error under Command “S-P1-x”

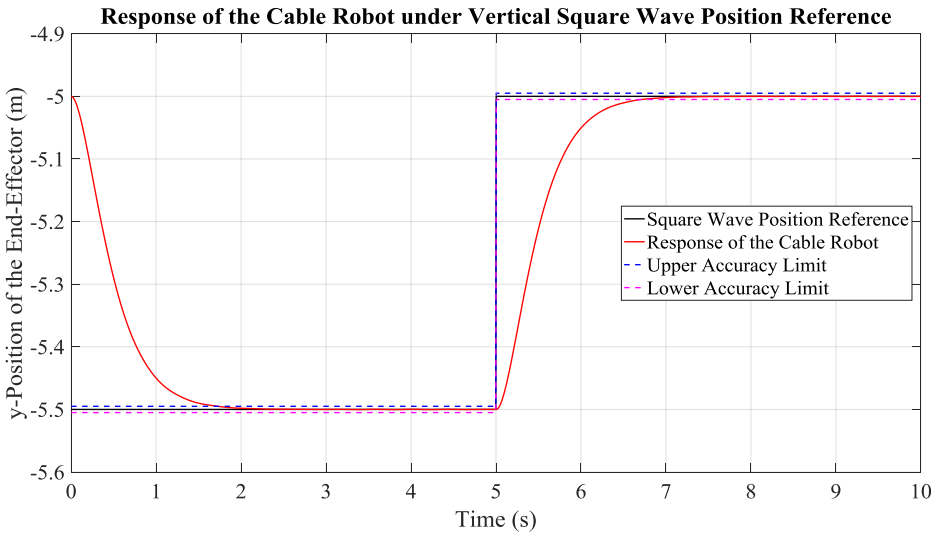

Figure 4.26: Response of the Cable Robot under Command “S-P2-y”

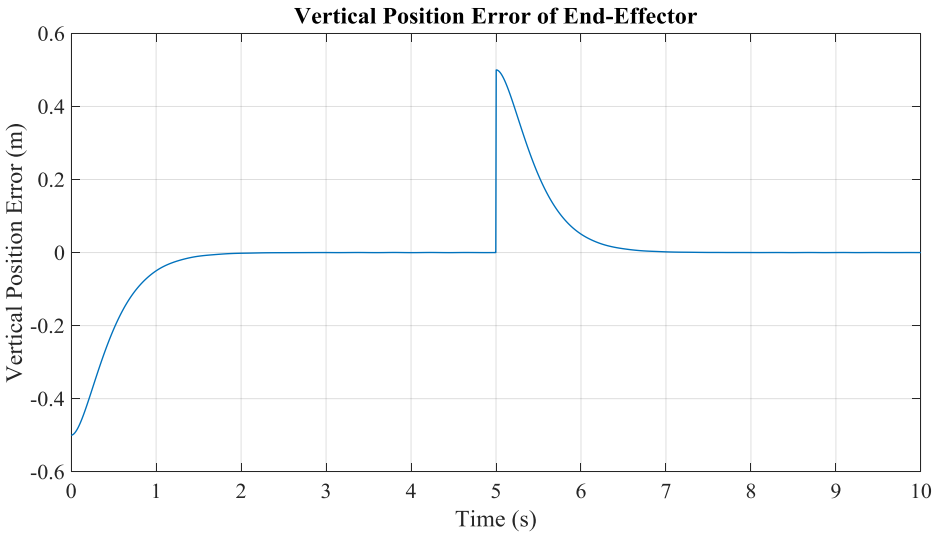

Figure 4.27: Position Error under Command “S-P2-y”

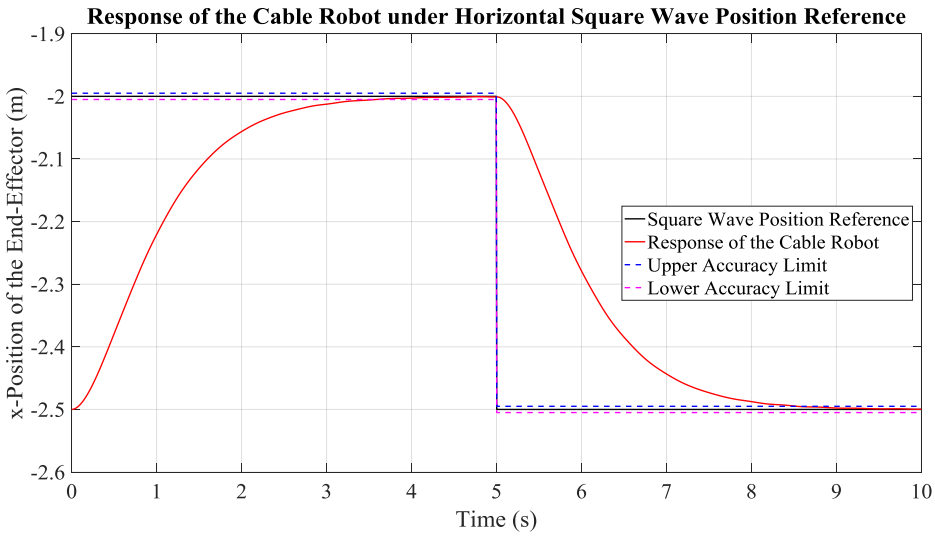

Figure 4.28: Response of the Cable Robot under Command “S-P2-x”

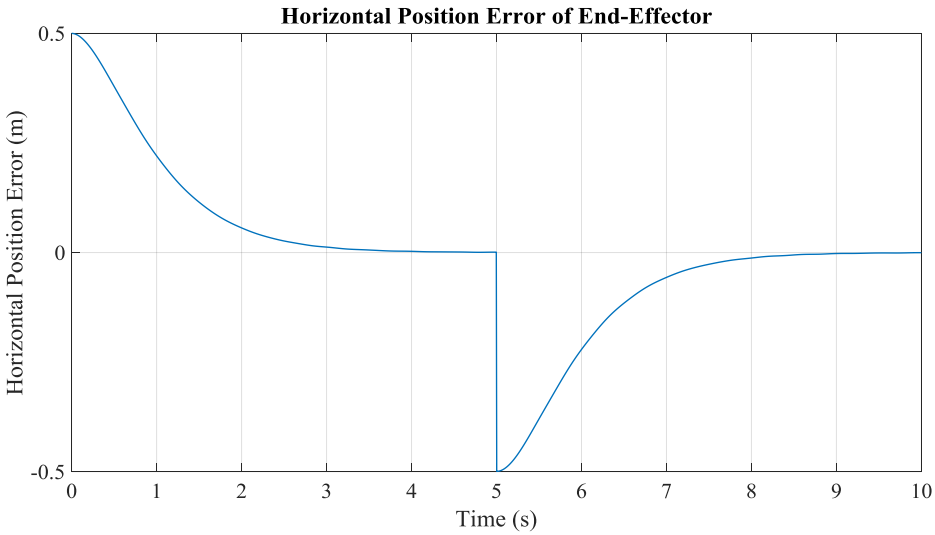

Figure 4.29: Position Error under Command “S-P2-x”

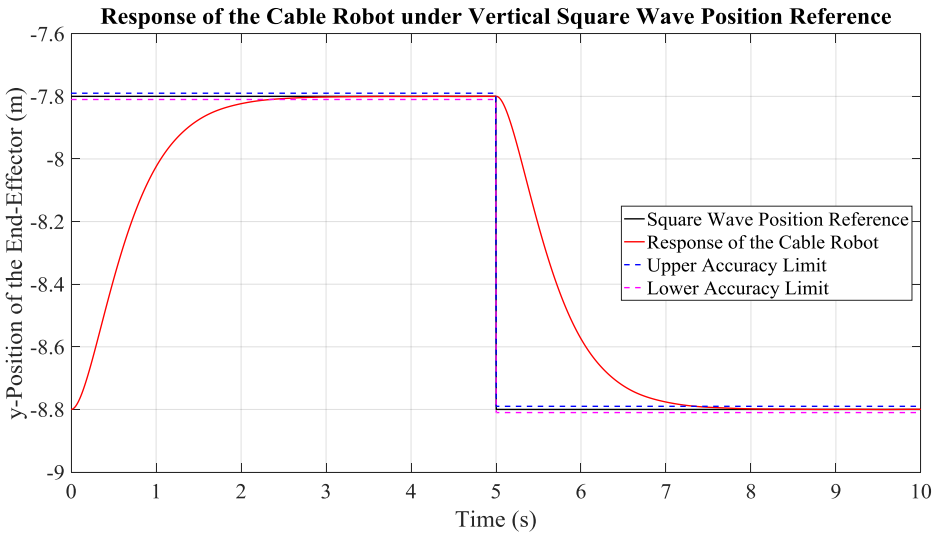

Figure 4.30: Response of the Cable Robot under Command “S-P3-y”

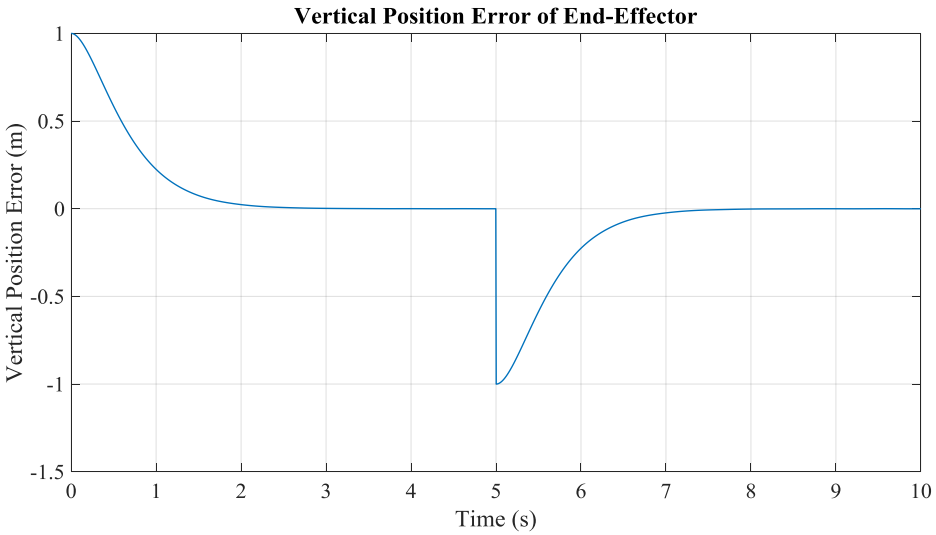

Figure 4.31: Position Error under Command “S-P3-y”

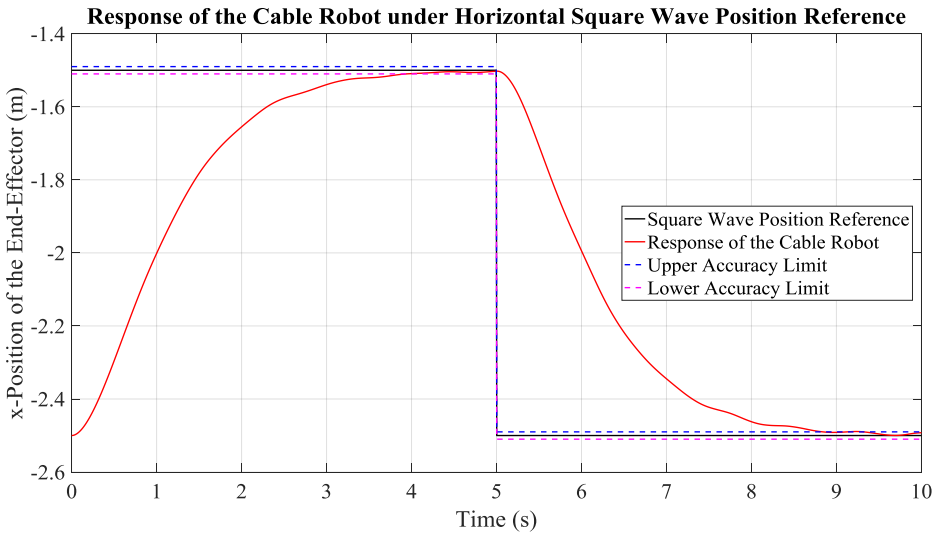

Figure 4.32: Response of the Cable Robot under Command “S-P3-x”

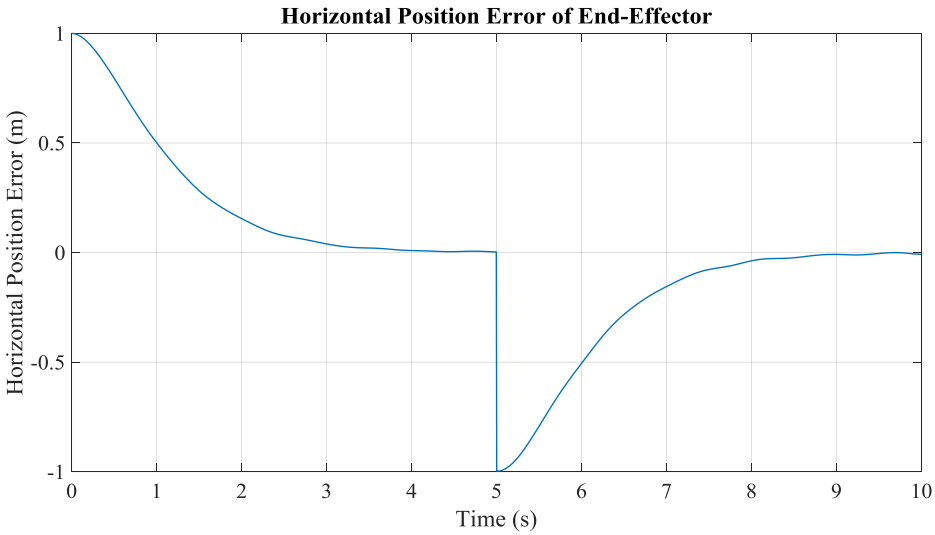

Figure 4.33: Position Error under Command “S-P3-x”

4.2.2.1.2 Response under Deployment Motion Command

Responses of the cable robot under different deployment motion commands are illustrated in the following figures for the case of lower-order segment angle generator and lower-order controller with measured end-effector pose.

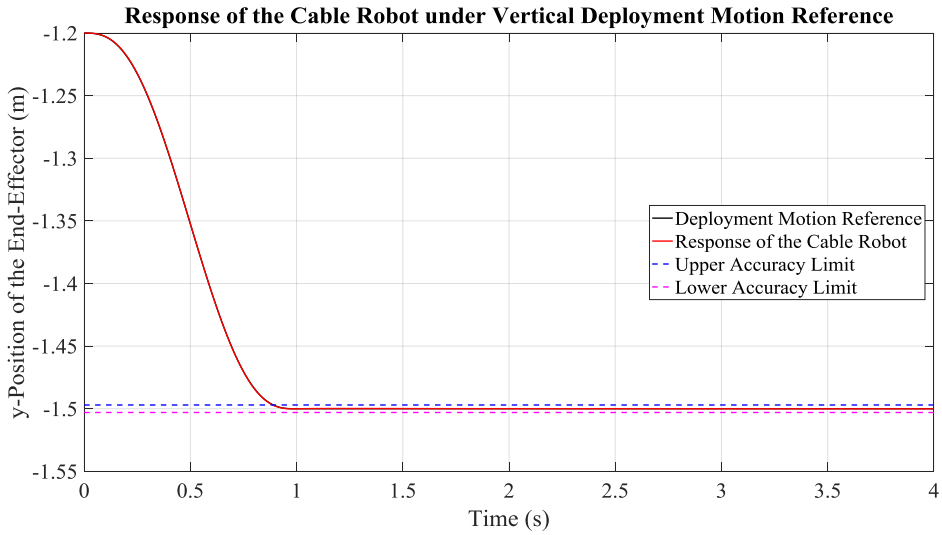

Figure 4.34: Response of the Cable Robot under Command "D-P1-y"

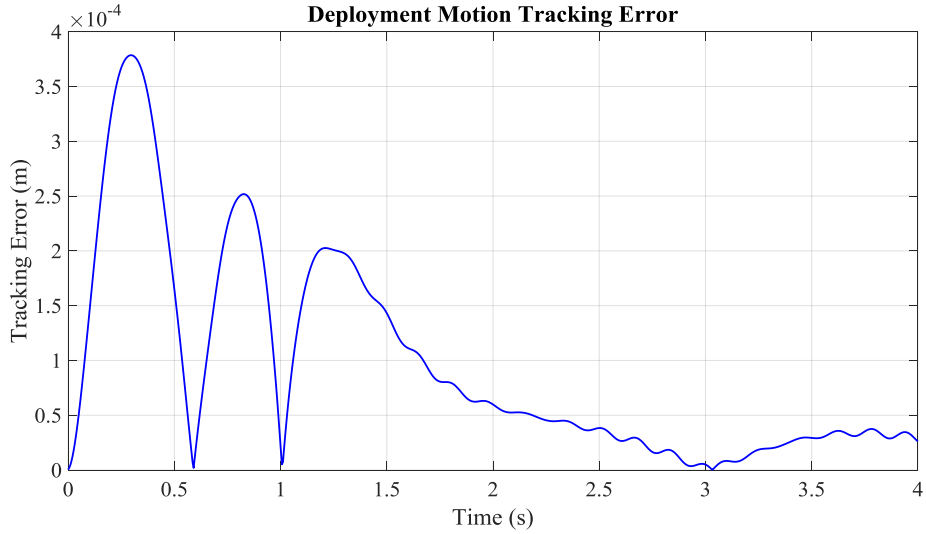

Figure 4.35: Deployment Motion Tracking Error under Command "D-P1-y"

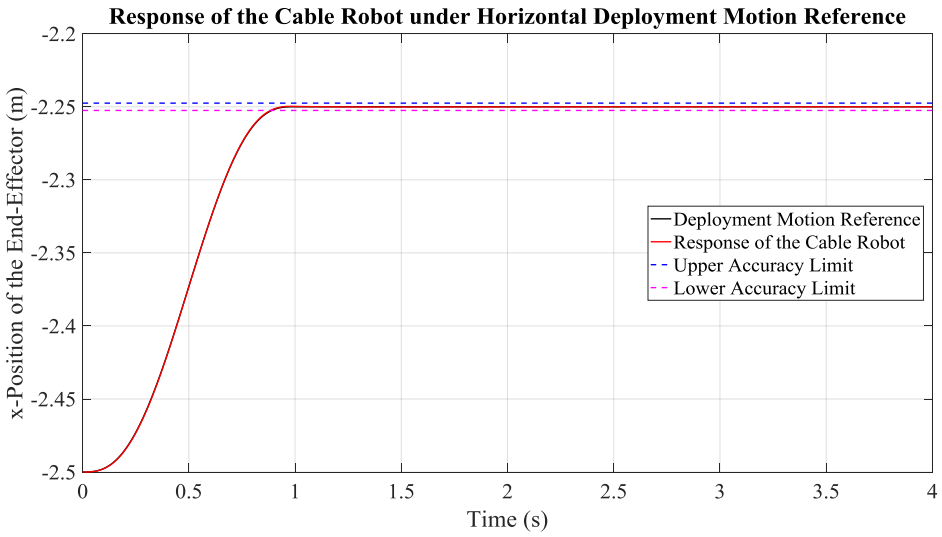

Figure 4.36: Response of the Cable Robot under Command “D-P1-x”

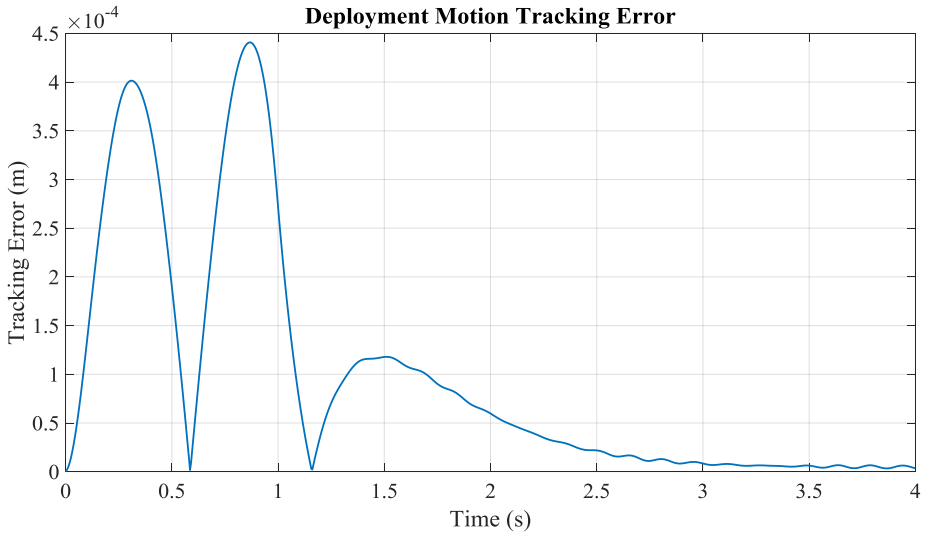

Figure 4.37: Deployment Motion Tracking Error under Command “D-P1-x”

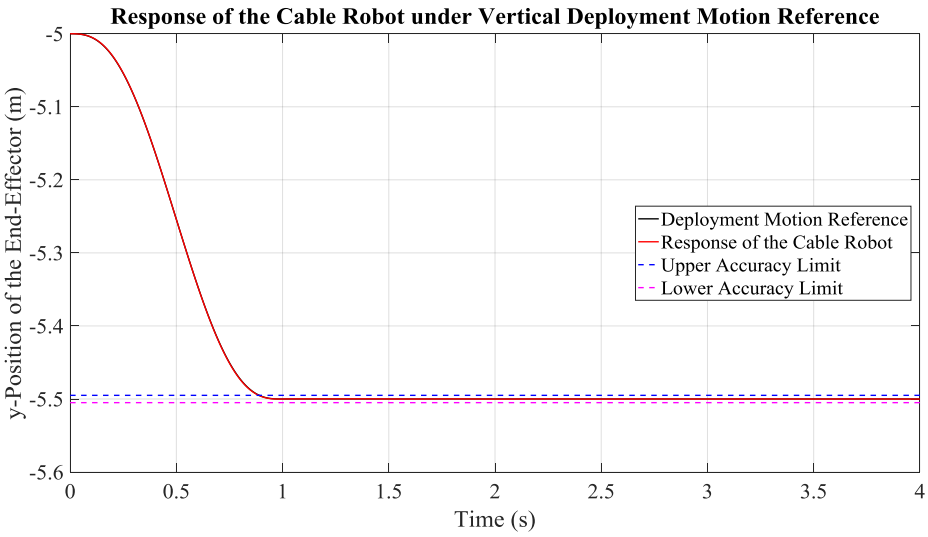

Figure 4.38: Response of the Cable Robot under Command “D-P2-y”

Figure 4.39: Deployment Motion Tracking Error under Command “D-P2-y”

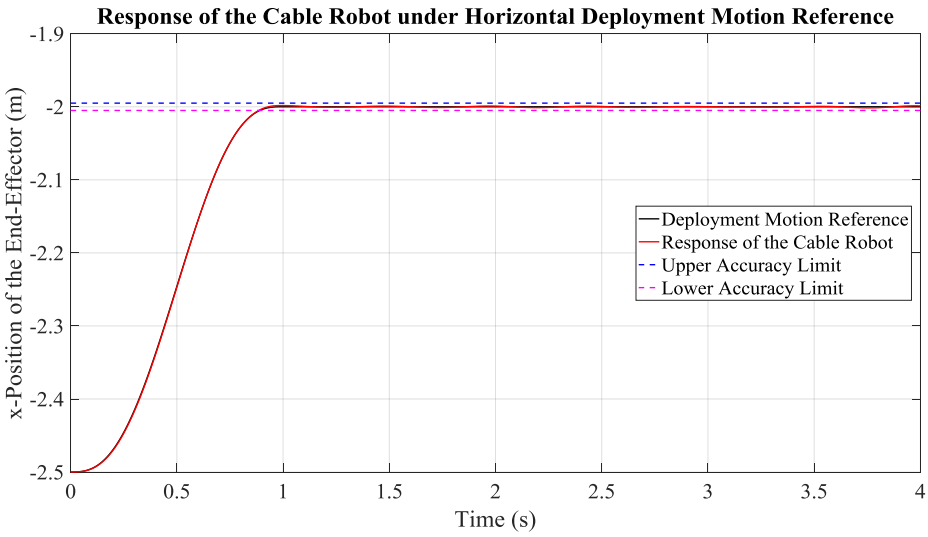

Figure 4.40: Response of the Cable Robot under Command “D-P2-x”

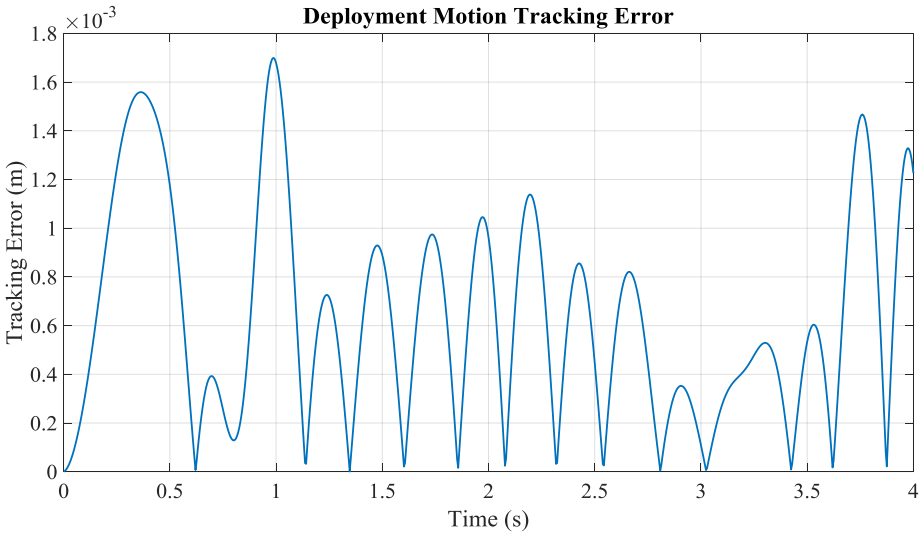

Figure 4.41: Deployment Motion Tracking Error under Command “D-P2-x”

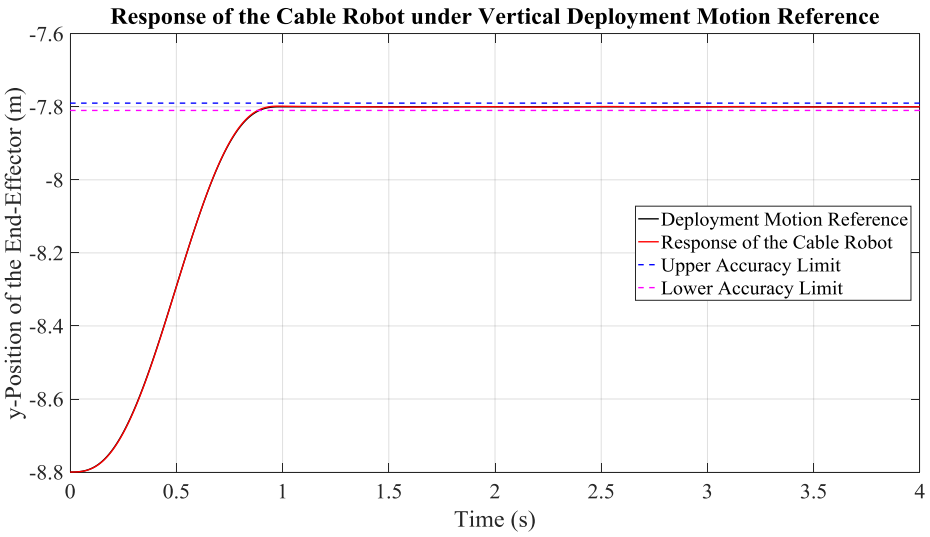

Figure 4.42: Response of the Cable Robot under Command “D-P3-y”

Figure 4.43: Deployment Motion Tracking Error under Command “D-P3-y”

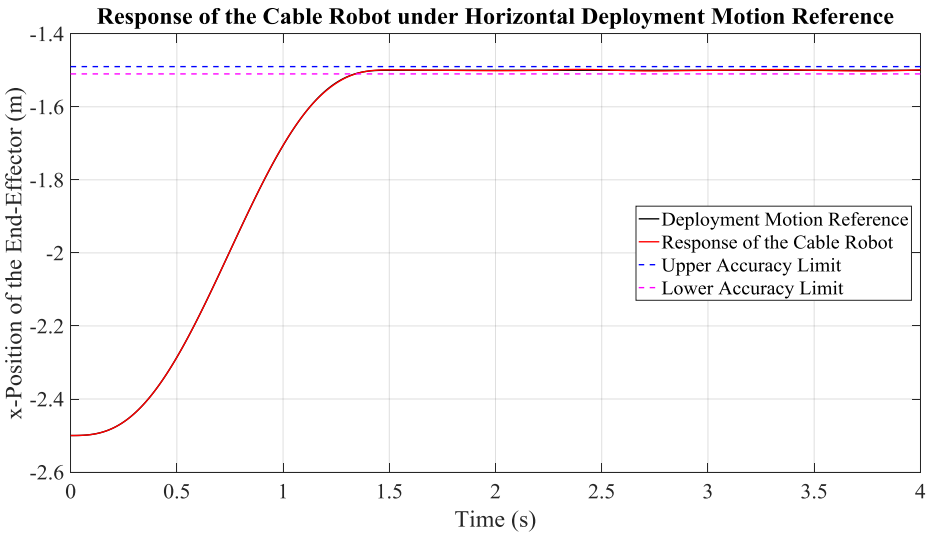

Figure 4.44: Response of the Cable Robot under Command “D-P3-x”

Figure 4.45: Deployment Motion Tracking Error under Command “D-P3-x”

4.2.2.1.3 Response under Circular Motion Command

Responses of the cable robot under different circular motion commands are illustrated in the following figures for the case of lower-order segment angle generator and lower-order controller with measured end-effector pose.

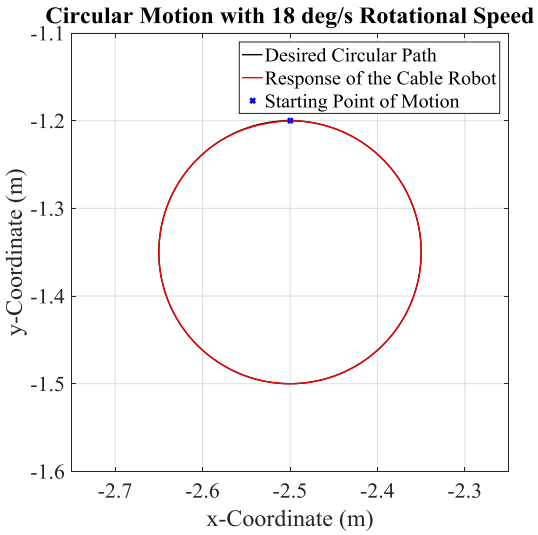

Figure 4.46: Response of the Cable Robot under Command "C-P1-1"

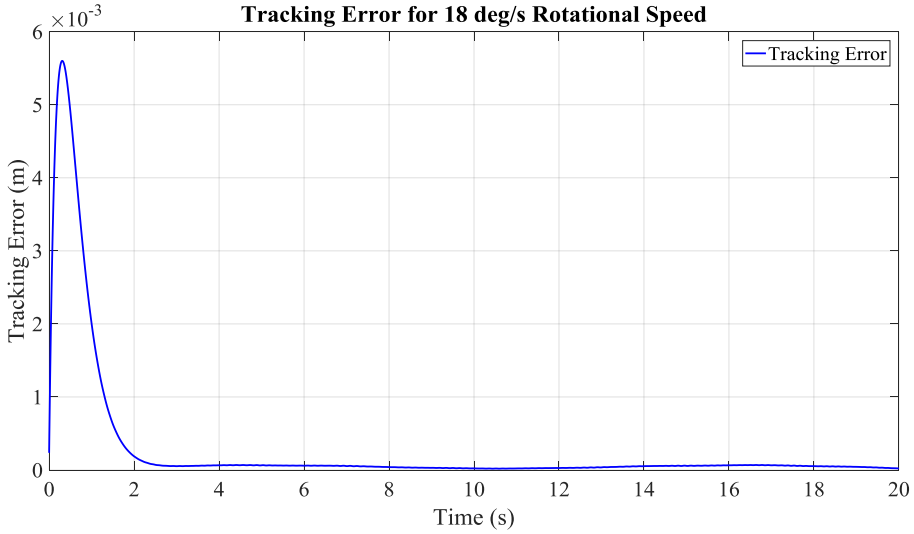

Figure 4.47: Circular Motion Tracking Error under Command "C-P1-1"

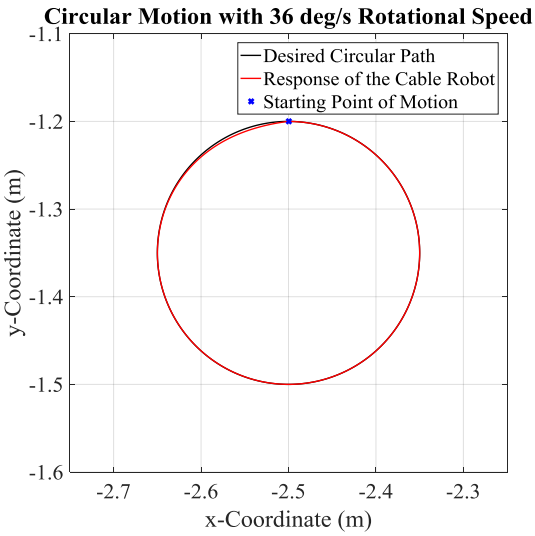

Figure 4.48: Response of the Cable Robot under Command “C-P1-2”

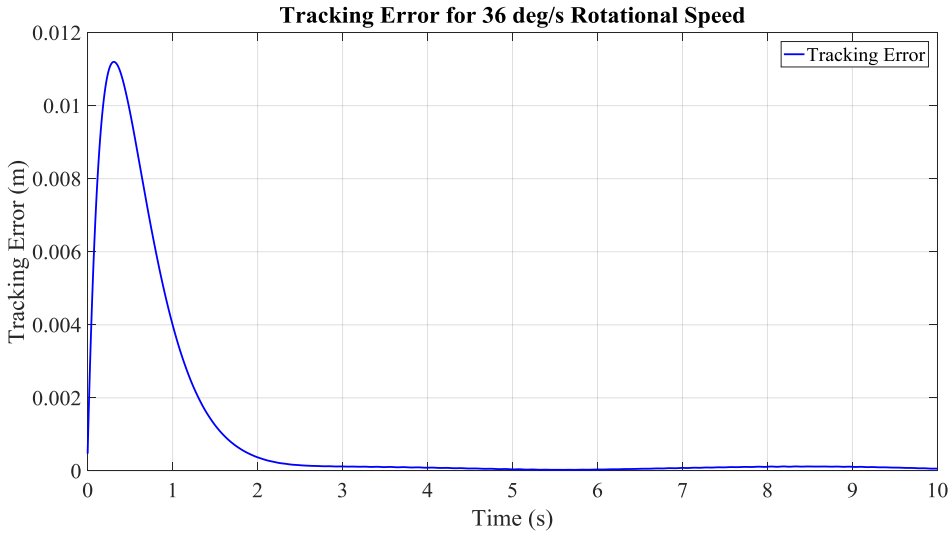

Figure 4.49: Circular Motion Tracking Error under Command “C-P1-2”

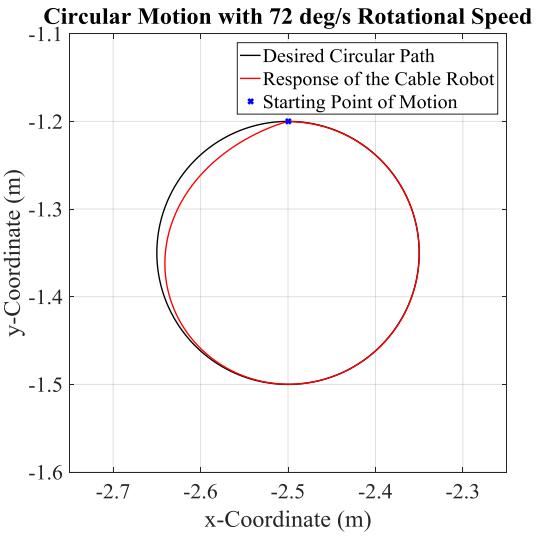

Figure 4.50: Response of the Cable Robot under Command “C-P1-3”

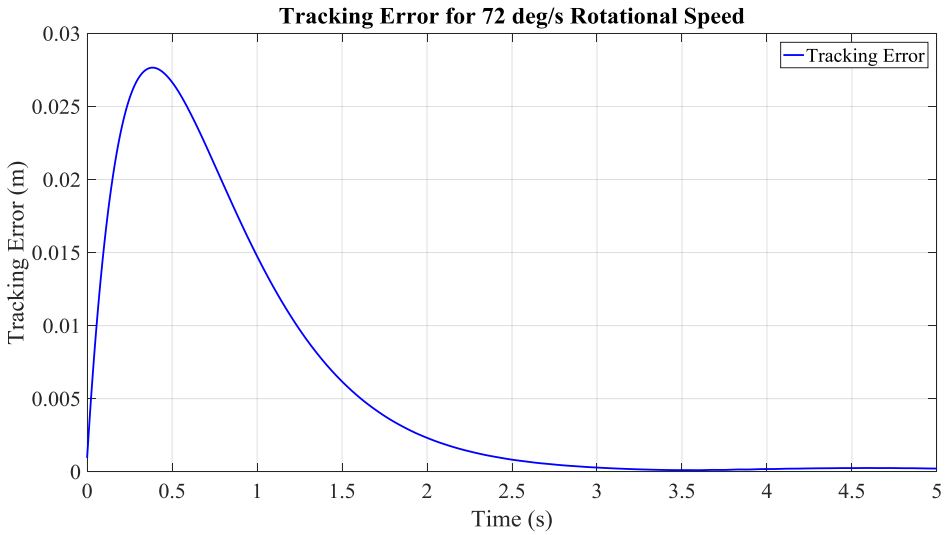

Figure 4.51: Circular Motion Tracking Error under Command “C-P1-3”

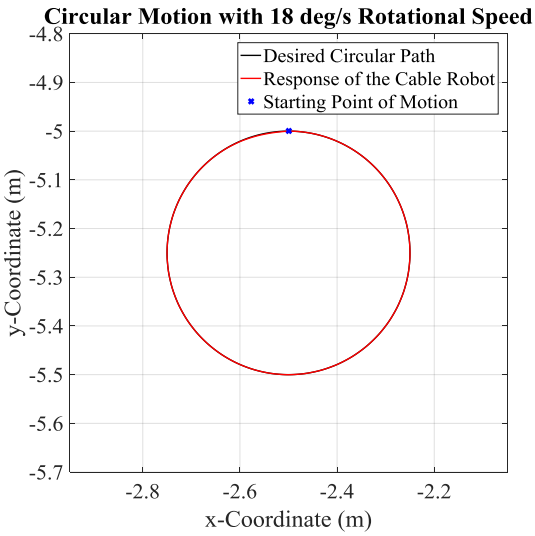

Figure 4.52: Response of the Cable Robot under Command “C-P2-1”

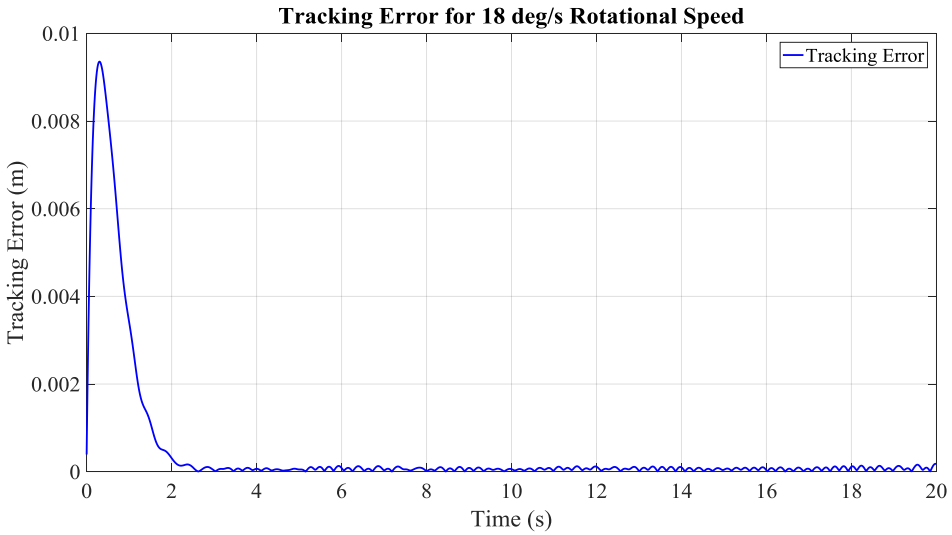

Figure 4.53: Circular Motion Tracking Error under Command “C-P2-1”

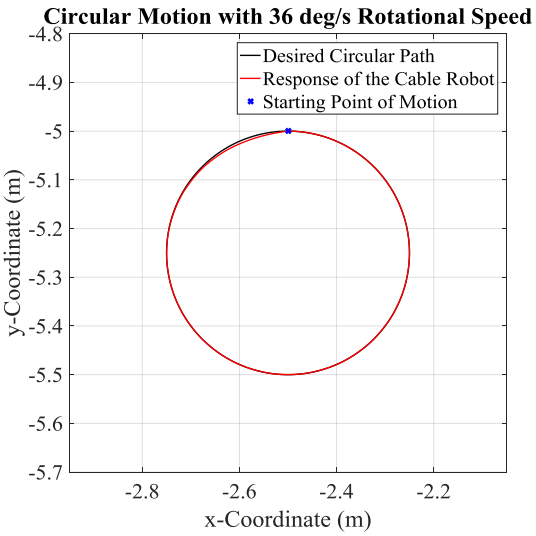

Figure 4.54: Response of the Cable Robot under Command “C-P2-2”

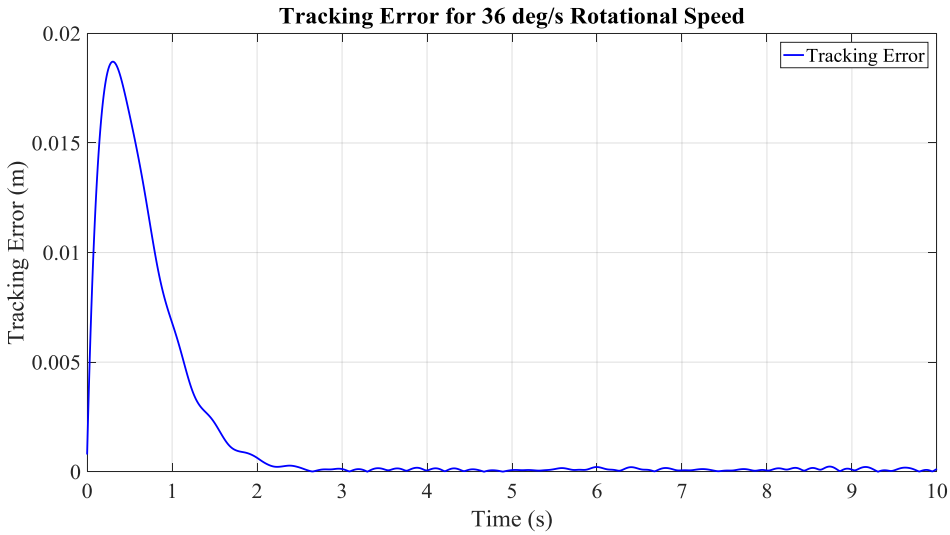

Figure 4.55: Circular Motion Tracking Error under Command “C-P2-2”

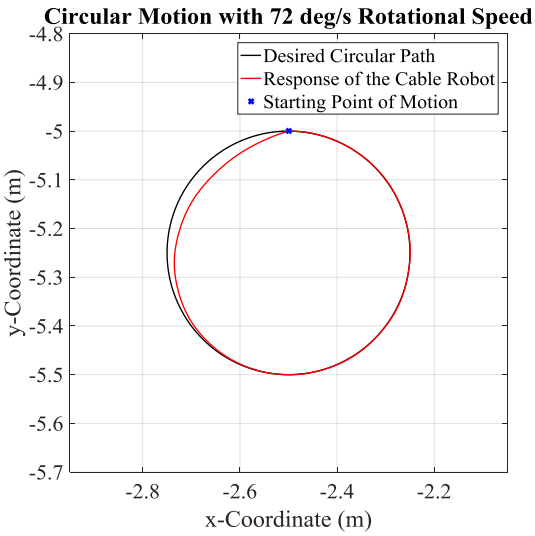

Figure 4.56: Response of the Cable Robot under Command “C-P2-3”

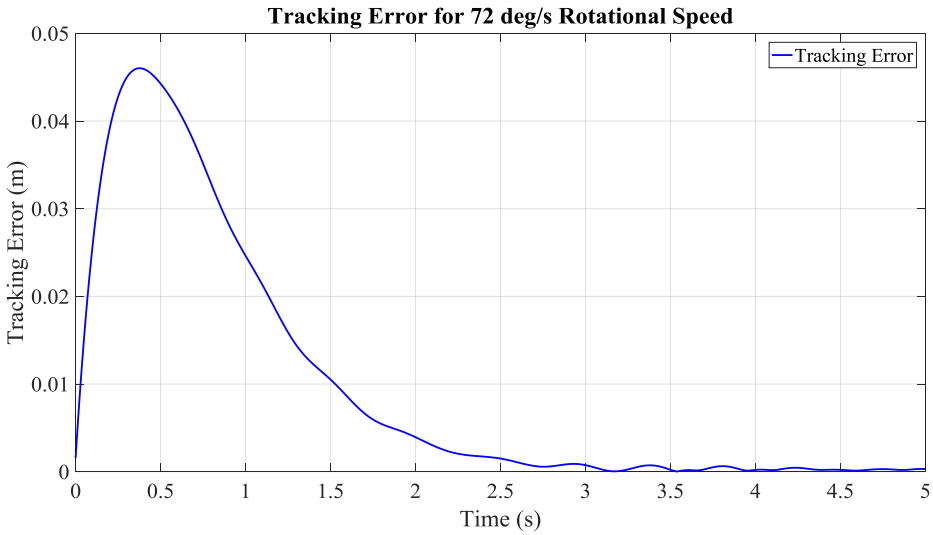

Figure 4.57: Circular Motion Tracking Error under Command “C-P2-3”

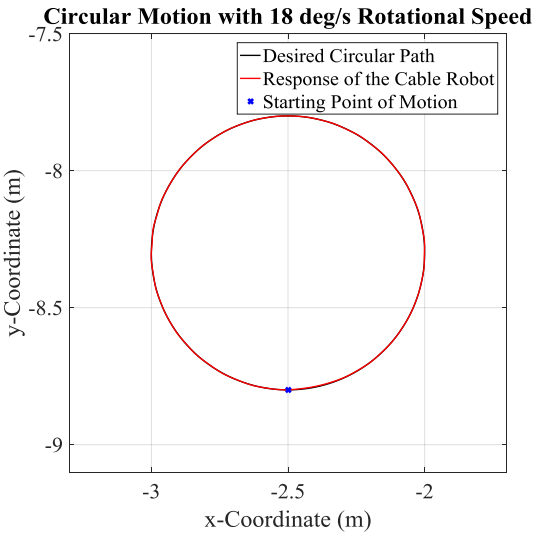

Figure 4.58: Response of the Cable Robot under Command “C-P3-1”

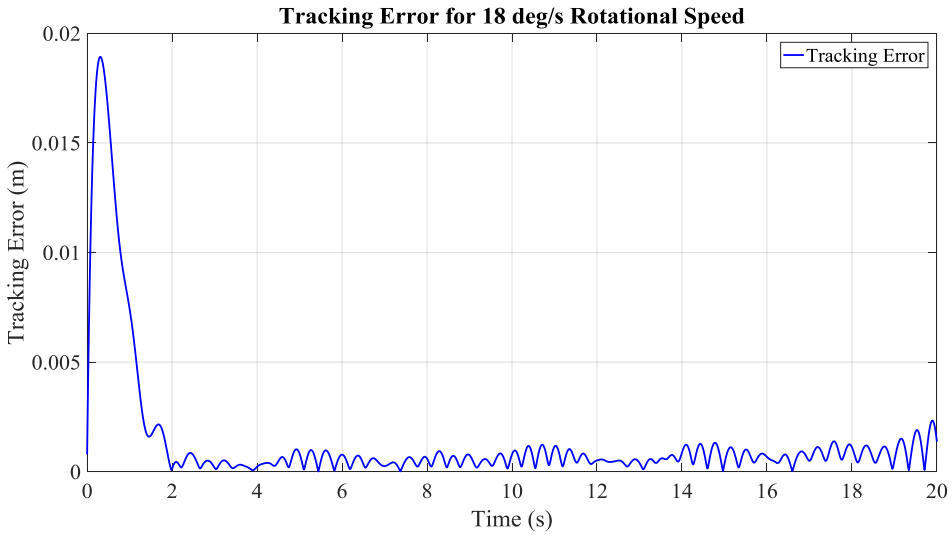

Figure 4.59: Circular Motion Tracking Error under Command “C-P3-1”

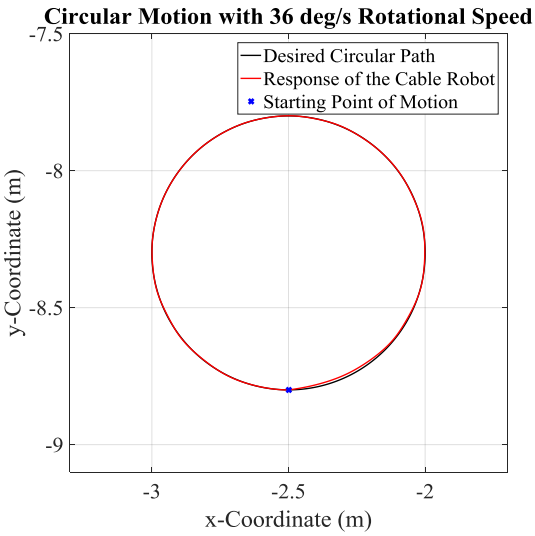

Figure 4.60: Response of the Cable Robot under Command “C-P3-2”

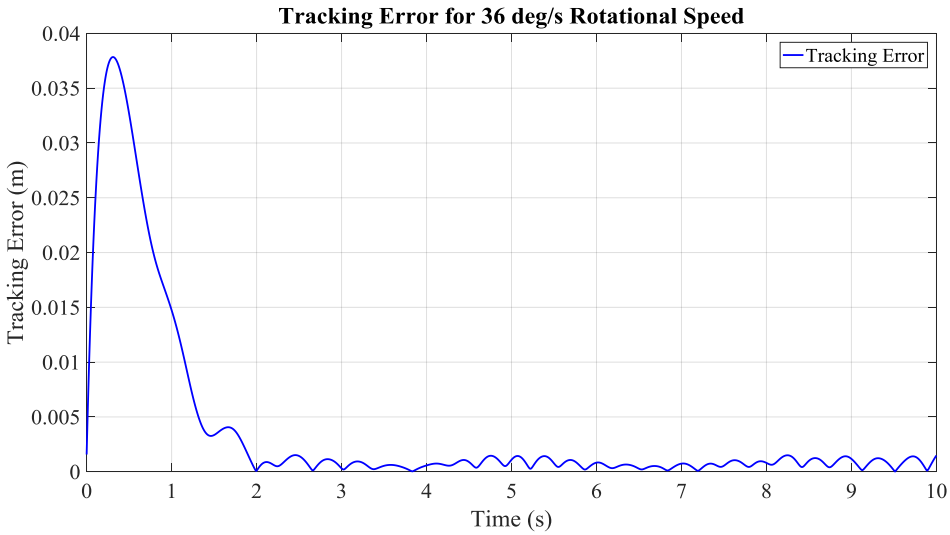

Figure 4.61: Circular Motion Tracking Error under Command “C-P3-2”

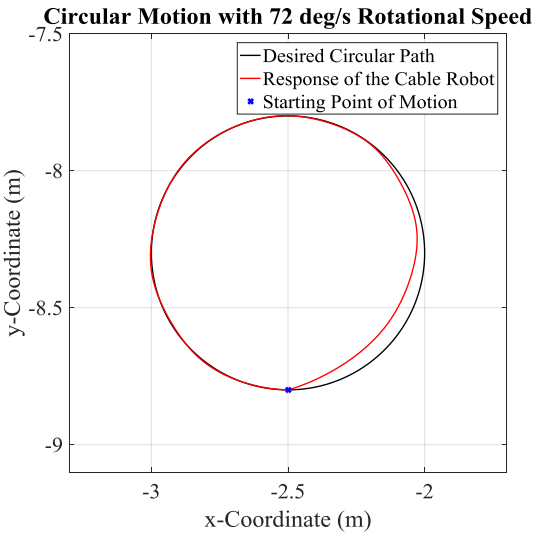

Figure 4.62: Response of the Cable Robot under Command "C-P3-3"

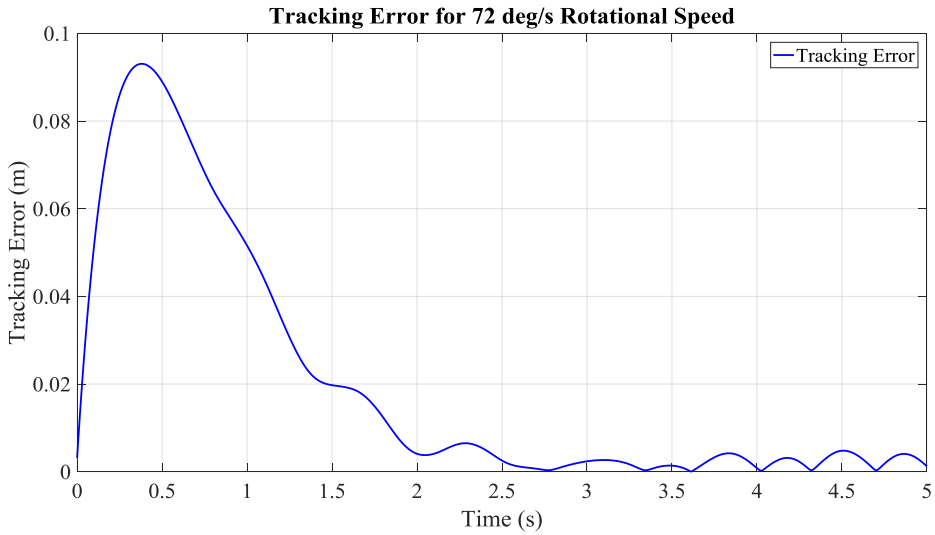

Figure 4.63: Circular Motion Tracking Error under Command "C-P3-3"

4.2.2.2 Effect of Measurement of End-Effector Position for Lower-Order Angle Generator with Lower-Order Controller Approach

In all simulations completed so far, it is assumed that position of end-effector is measured by using a proper method. In this subsection, it is aimed to observe the results of the opposite case. In other words, position of end-effector is found out with the help of estimated cable segment angles from lower-order model, measured

1st segment lengths ($\bar{r}$) and forward kinematics. Thus in this subsection, commands *D-P1-y* and *C-P1-1* are employed to illustrate the impact of end-effector measurement on the system performance.

Responses of the cable robot under these commands in case of estimated end-effector position where lower-order model is utilized as segment angle generator:

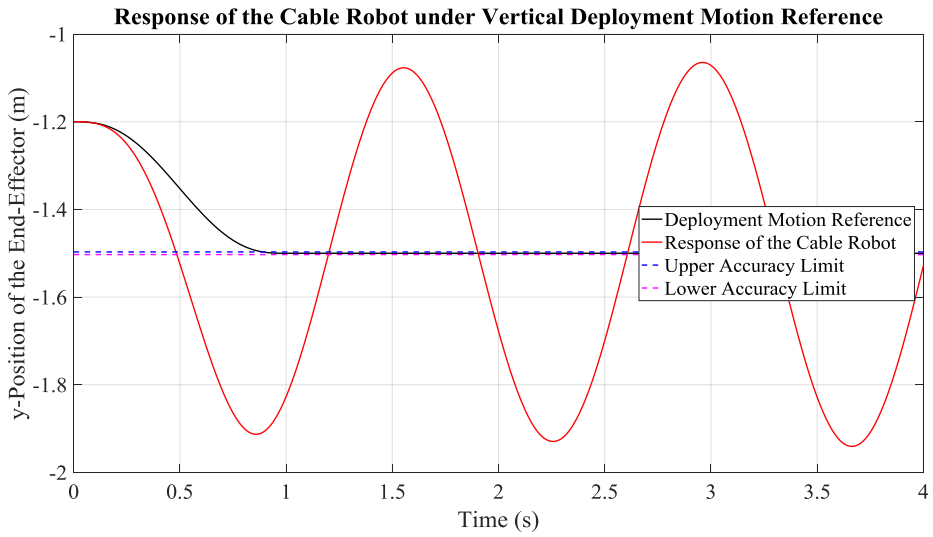

Figure 4.64: Response of the Cable Robot under Command "D-P1-y"

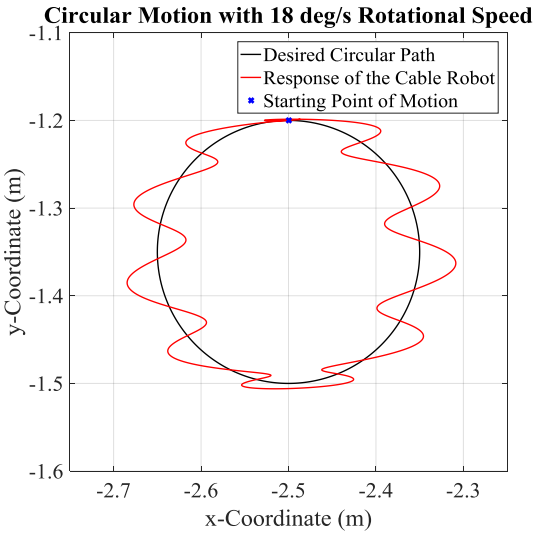

Figure 4.65: Response of the Cable Robot under Command "C-P1-1"

These results imply that measurement of end-effector in addition to the measurement of 1st segment lengths of cables is a must to obtain satisfactory performance from lower-order angle generator model with lower-order controller approach.

4.2.2.3 Lower-Order Angle Generator Model and Higher-Order Controller Simulations

In this section, simulations are completed with lower-order angle estimator and higher-order controller. End-effector pose is assumed to be measured at this step.

4.2.2.3.1 Response under Square Wave Position Command

Responses of the cable robot under different square wave position commands are illustrated in the following figures for the case of lower-order angle generator model and higher-order controller.

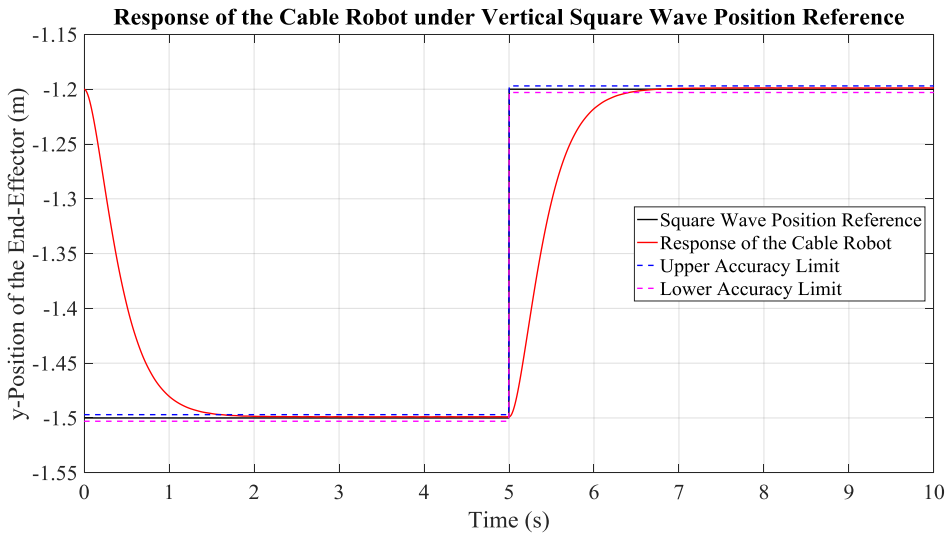

Figure 4.66: Response of the Cable Robot under Command "S-P1-y"

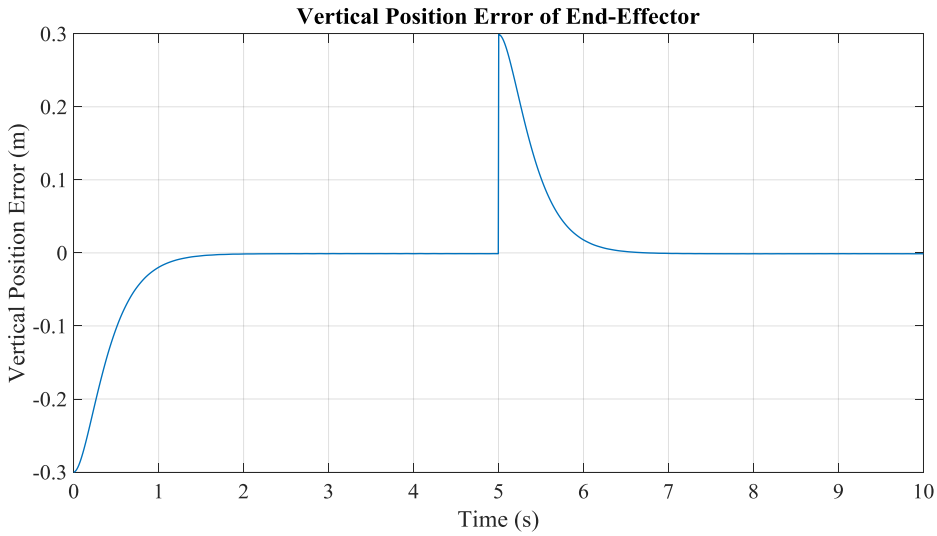

Figure 4.67: Position Error under Command “S-P1-y”

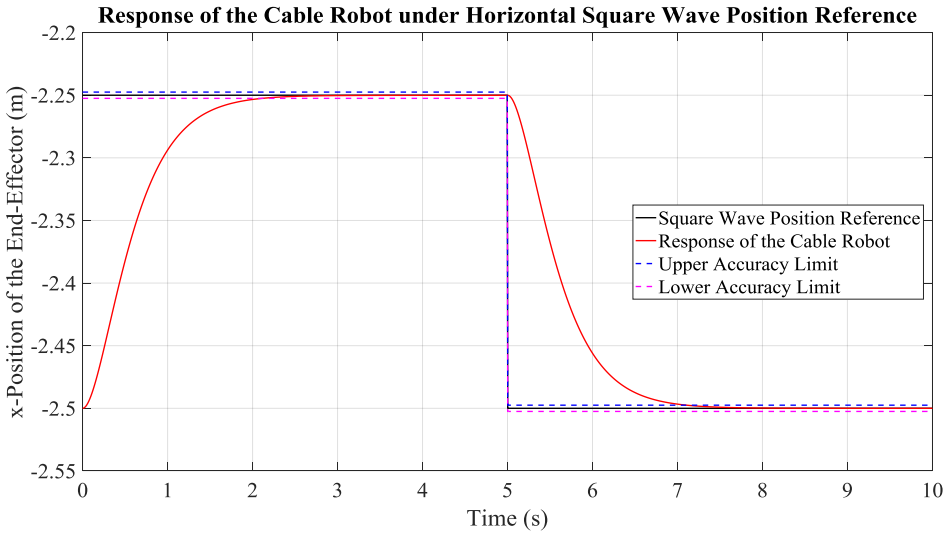

Figure 4.68: Response of the Cable Robot under Command “S-P1-x”

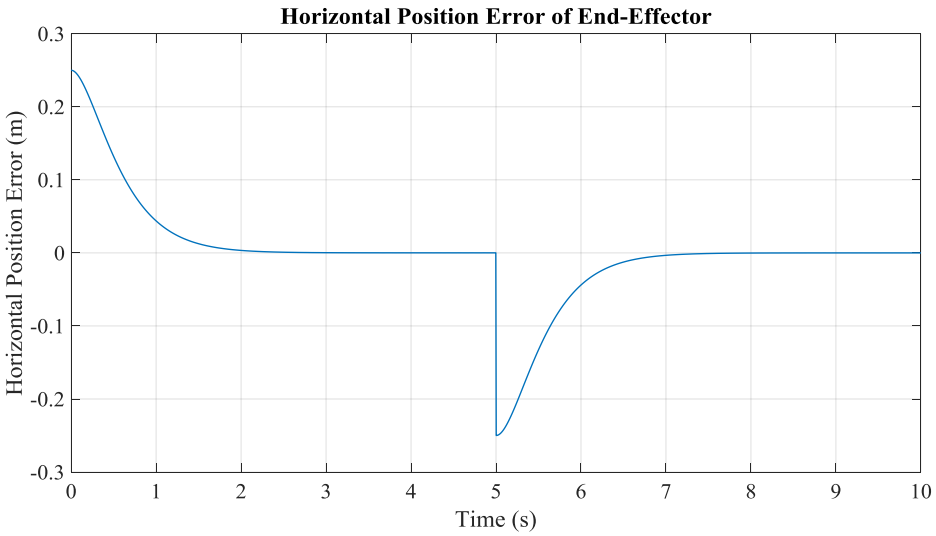

Figure 4.69: Position Error under Command “S-P1-x”

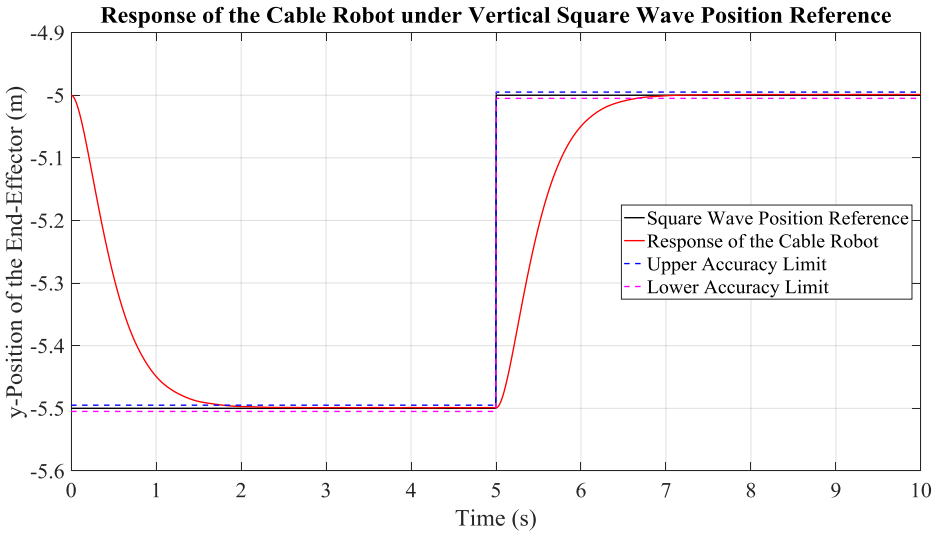

Figure 4.70: Response of the Cable Robot under Command “S-P2-y”

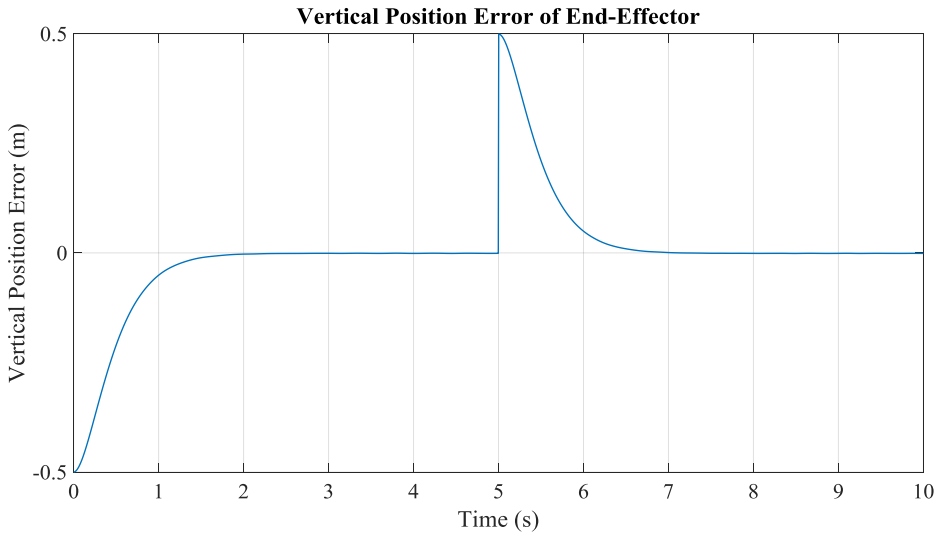

Figure 4.71: Position Error under Command “S-P2-y”

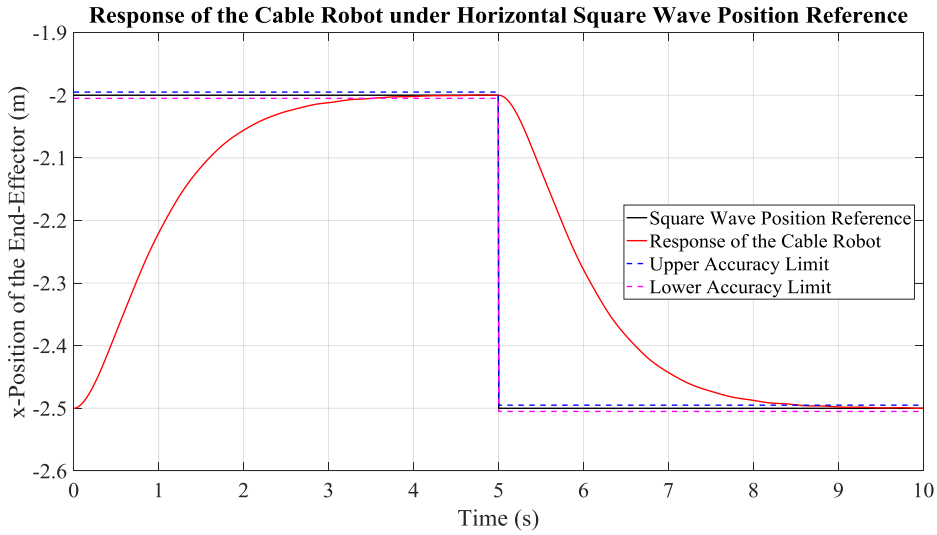

Figure 4.72: Response of the Cable Robot under Command “S-P2-x”

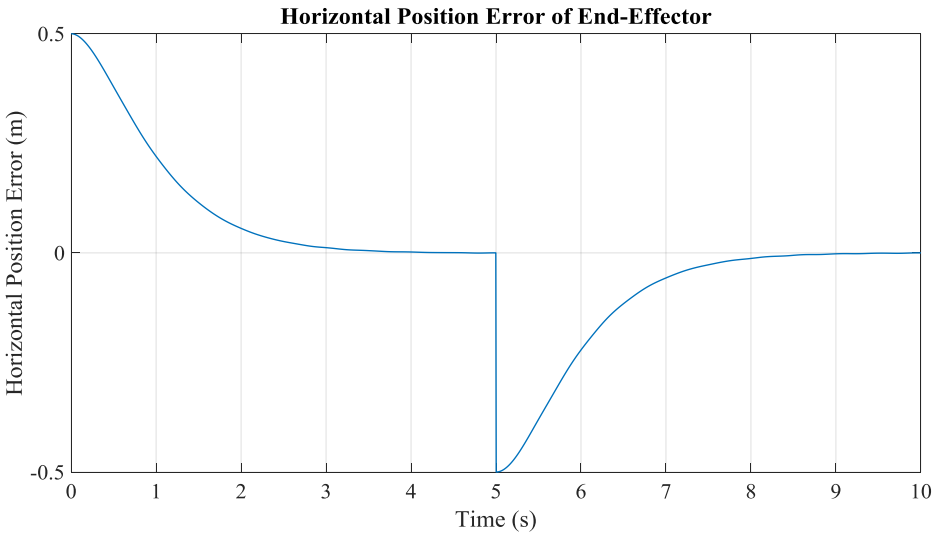

Figure 4.73: Position Error under Command “S-P2-x”

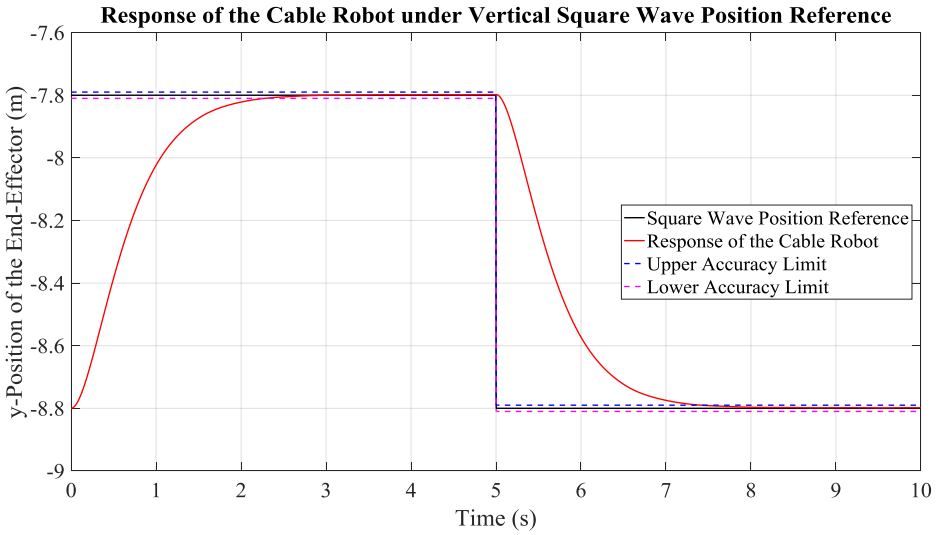

Figure 4.74: Response of the Cable Robot under Command “S-P3-y”

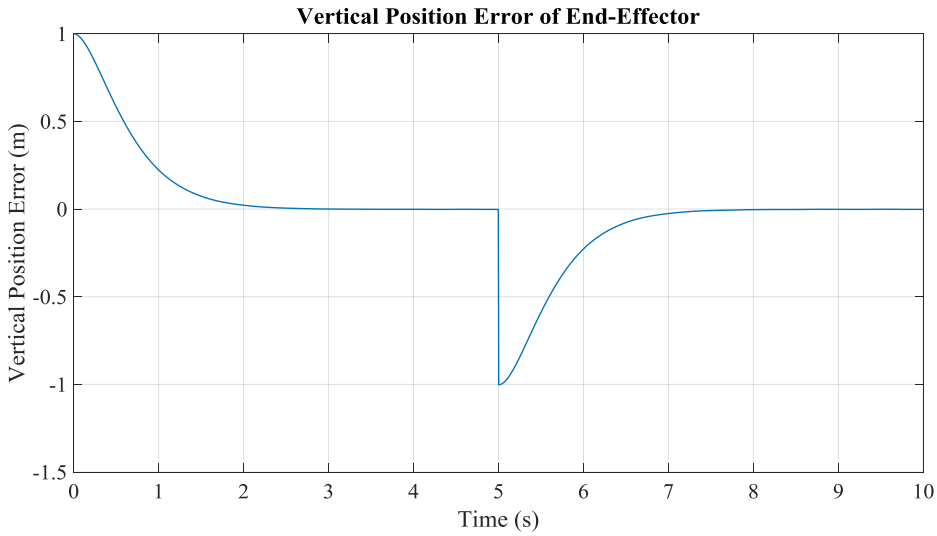

Figure 4.75: Position Error under Command “S-P3-y”

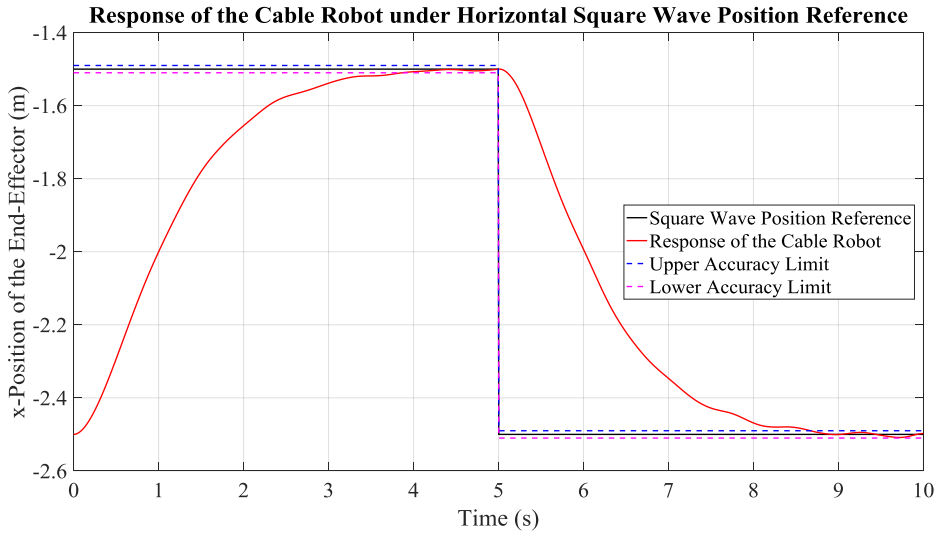

Figure 4.76: Response of the Cable Robot under Command “S-P3-x”

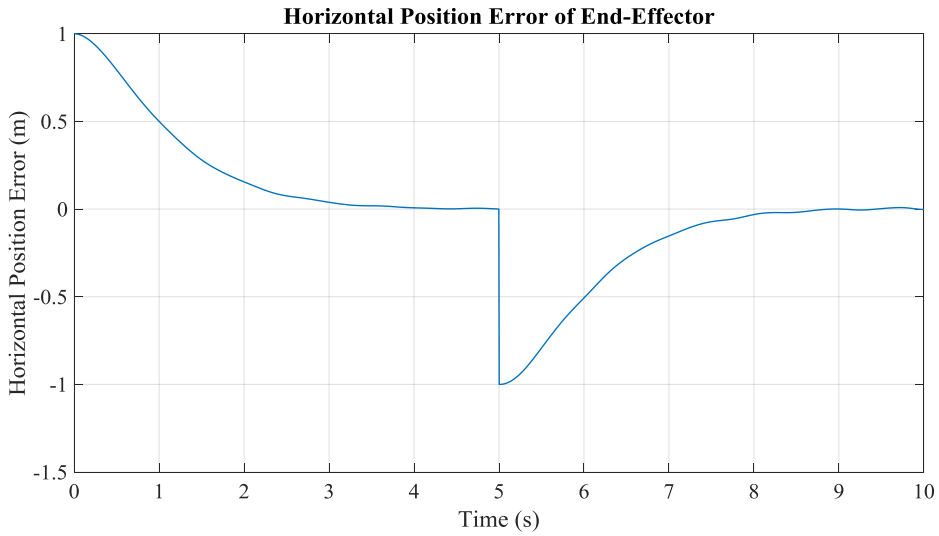

Figure 4.77: Position Error under Command “S-P3-x”

4.2.2.3.2 Response under Deployment Motion Command

Responses of the cable robot under different deployment motion commands are illustrated in the following figures for the case of lower-order angle generator model and higher-order controller.

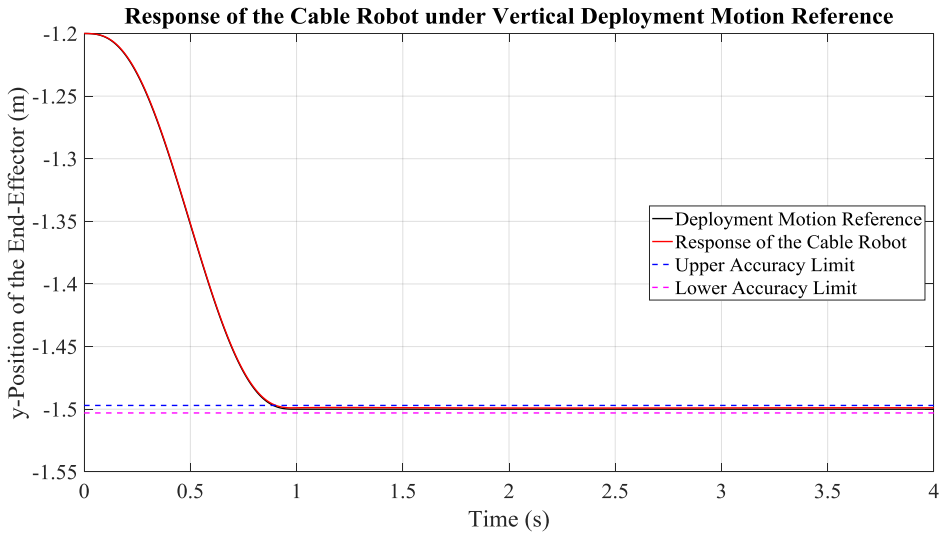

Figure 4.78: Response of the Cable Robot under Command “D-P1-y”

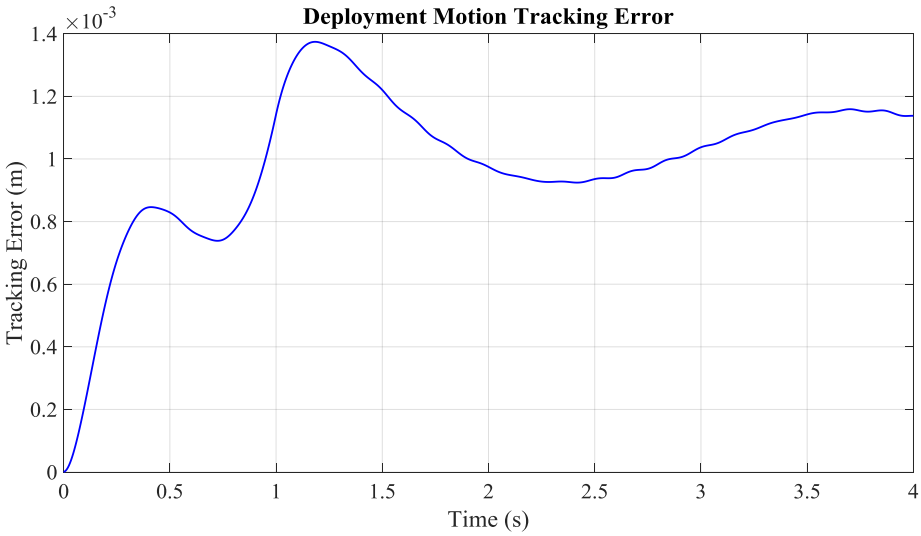

Figure 4.79: Deployment Motion Tracking Error under Command “D-P1-y”

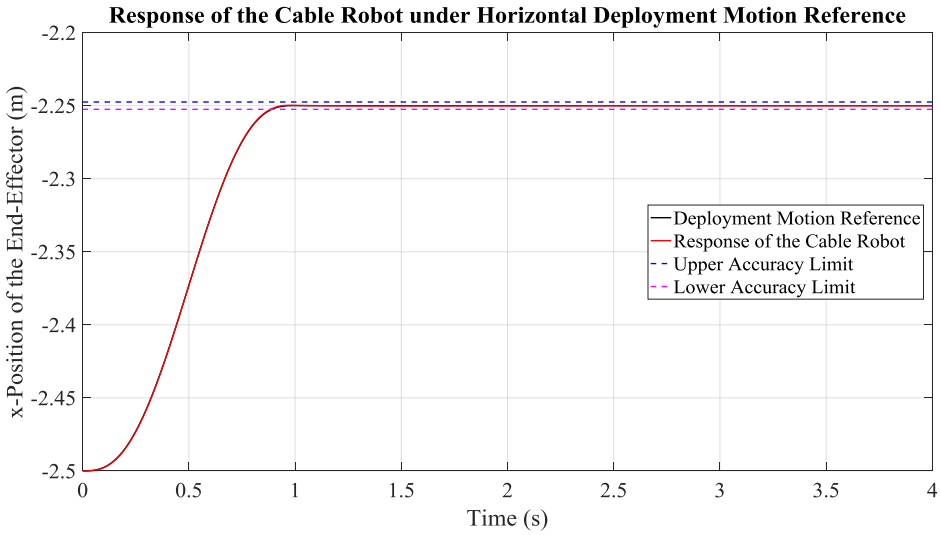

Figure 4.80: Response of the Cable Robot under Command “D-P1-x”

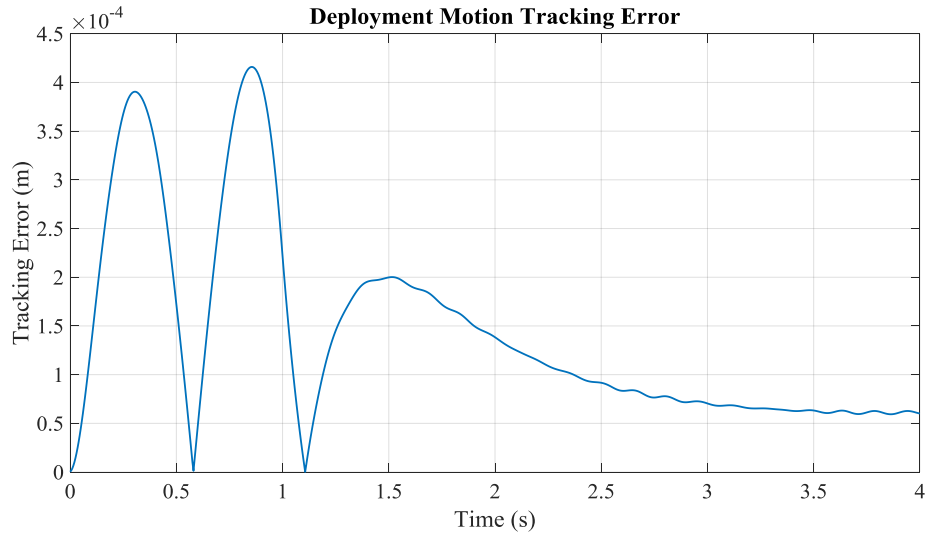

Figure 4.81: Deployment Motion Tracking Error under Command “D-P1-x”

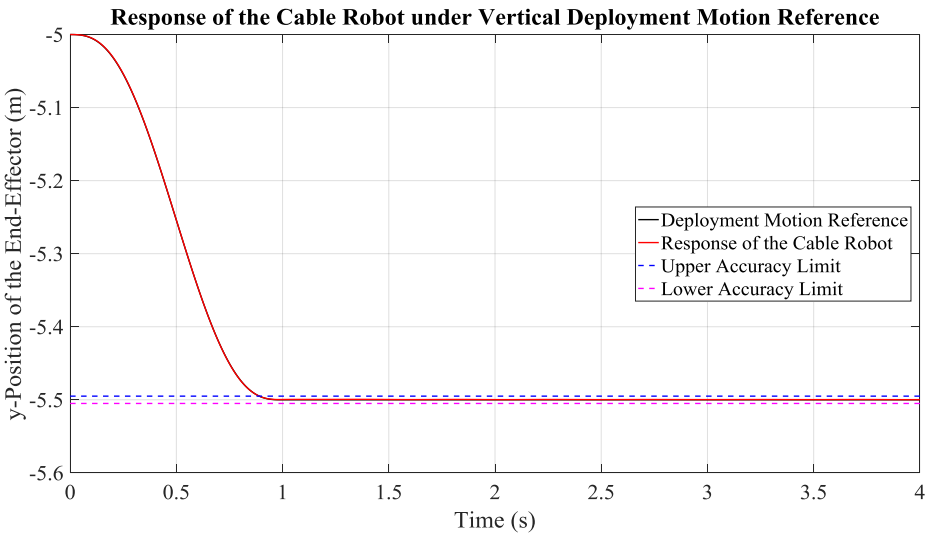

Figure 4.82: Response of the Cable Robot under Command “D-P2-y”

Figure 4.83: Deployment Motion Tracking Error under Command “D-P2-y”

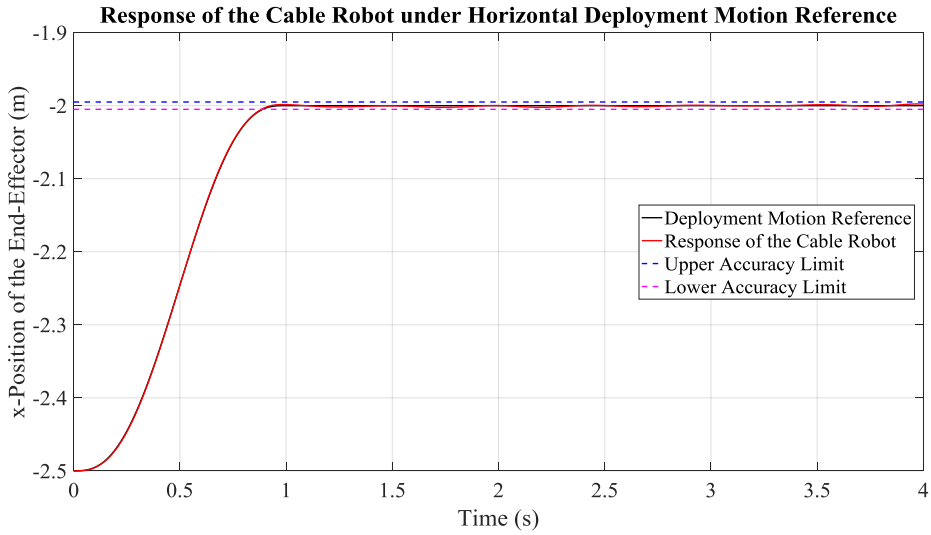

Figure 4.84: Response of the Cable Robot under Command “D-P2-x”

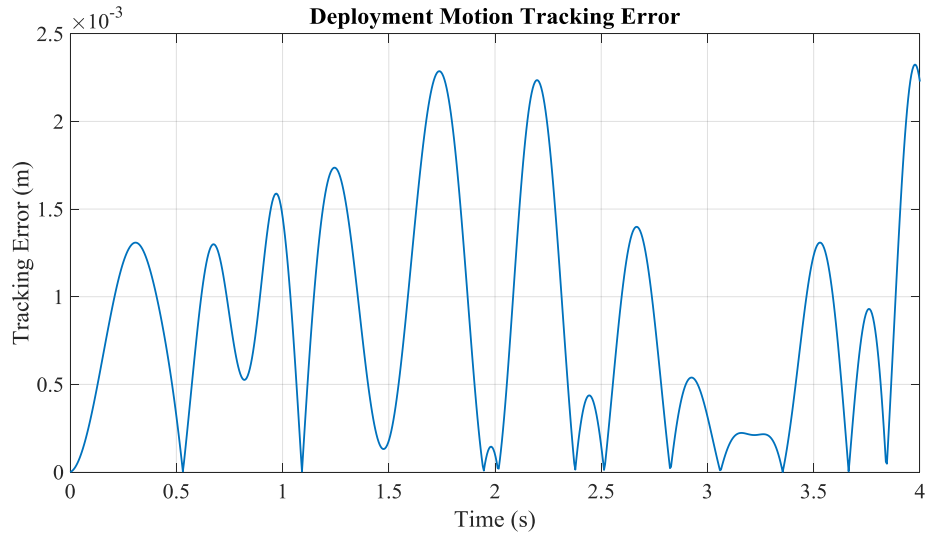

Figure 4.85: Deployment Motion Tracking Error under Command “D-P2-x”

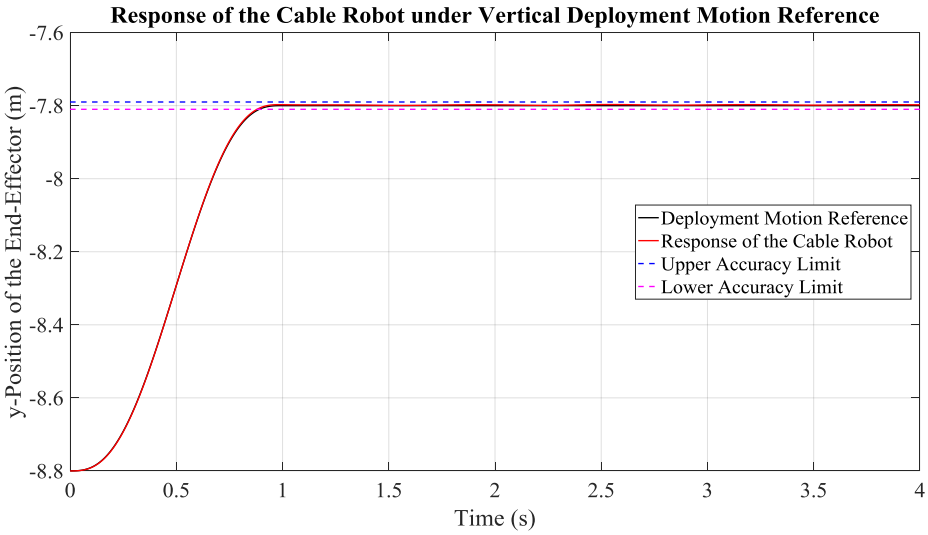

Figure 4.86: Response of the Cable Robot under Command “D-P3-y”

Figure 4.87: Deployment Motion Tracking Error under Command “D-P3-y”

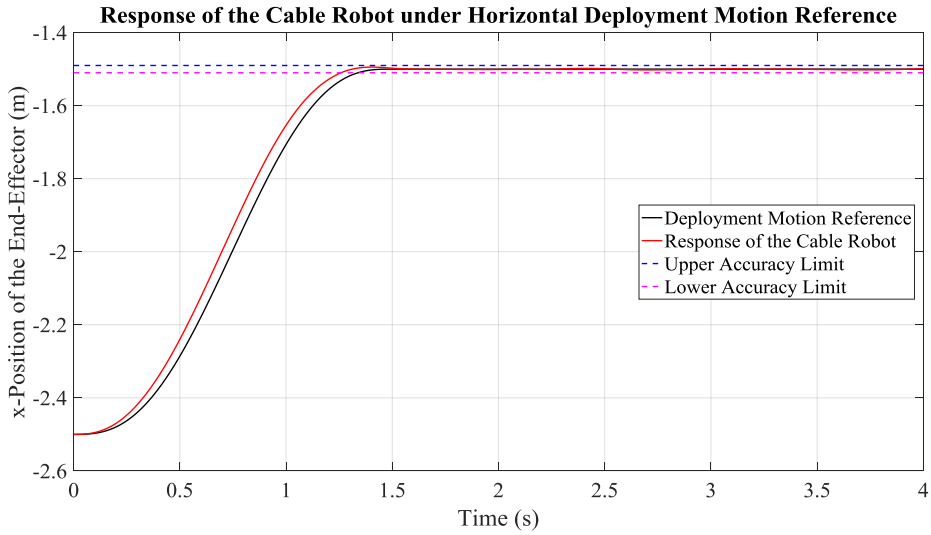

Figure 4.88: Response of the Cable Robot under Command “D-P3-x”

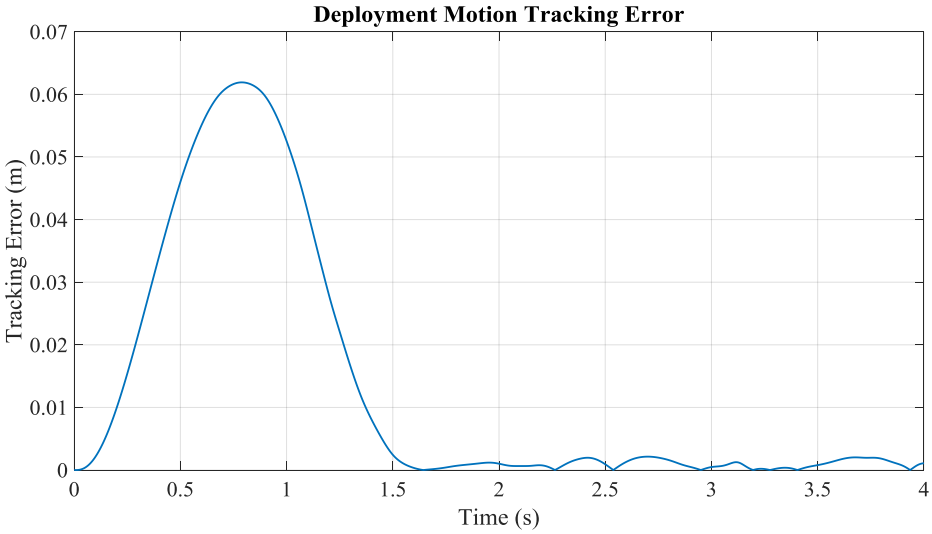

Figure 4.89: Deployment Motion Tracking Error under Command “D-P3-x”

4.2.2.3.3 Response under Circular Motion Command

Responses of the cable robot under different circular motion commands are illustrated in the following figures for the case of lower-order angle generator model and higher-order controller.

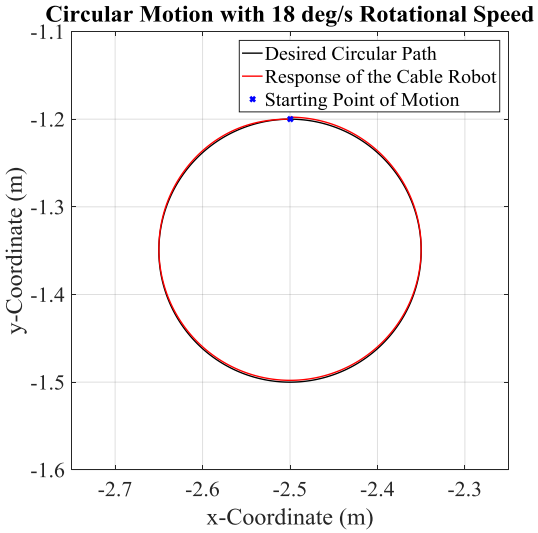

Figure 4.90: Response of the Cable Robot under Command “C-P1-1”

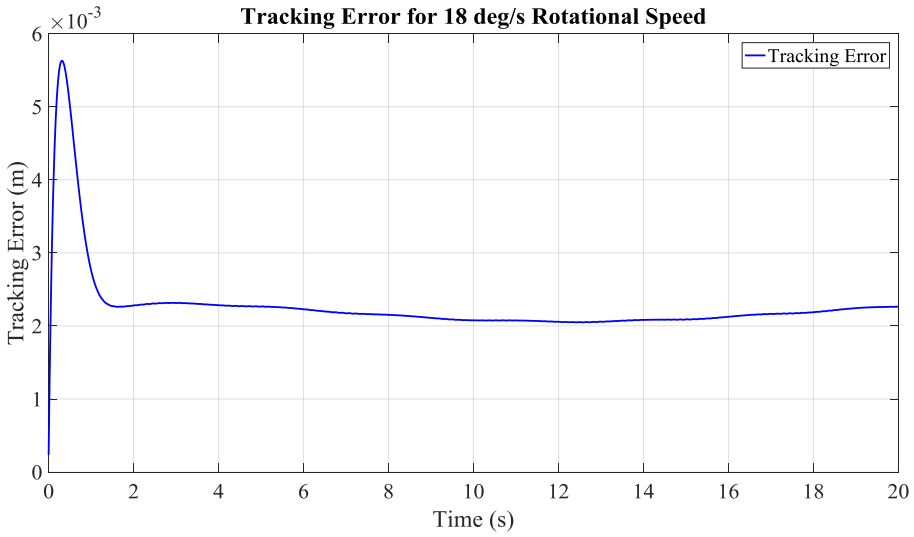

Figure 4.91: Circular Motion Tracking Error under Command “C-P1-1”

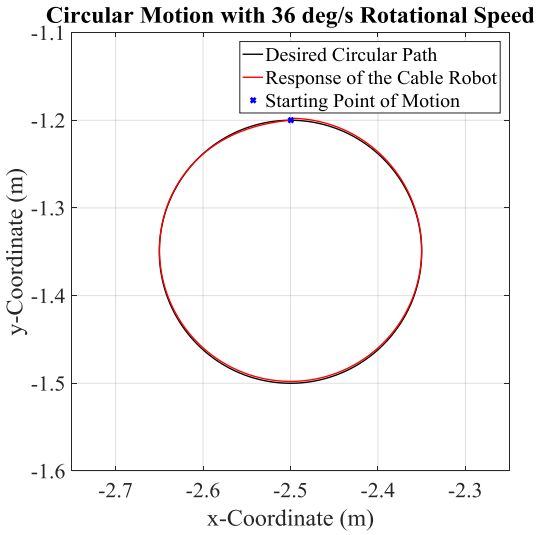

Figure 4.92: Response of the Cable Robot under Command “C-P1-2”

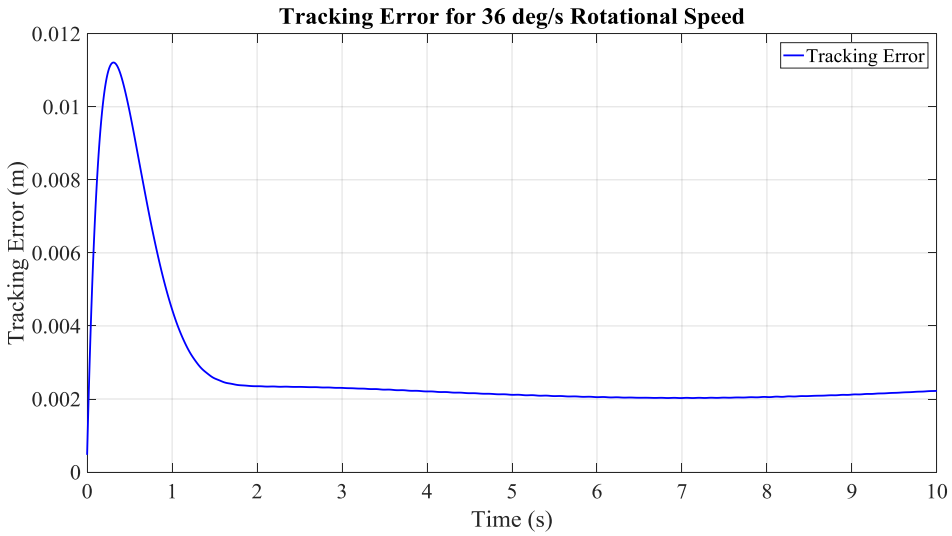

Figure 4.93: Circular Motion Tracking Error under Command “C-P1-2”

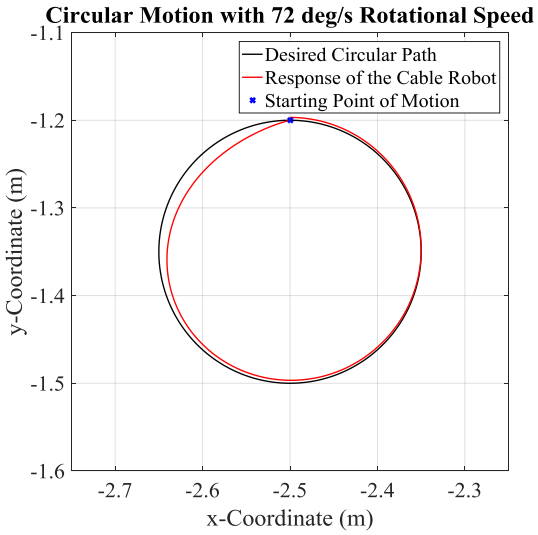

Figure 4.94: Response of the Cable Robot under Command “C-P1-3”

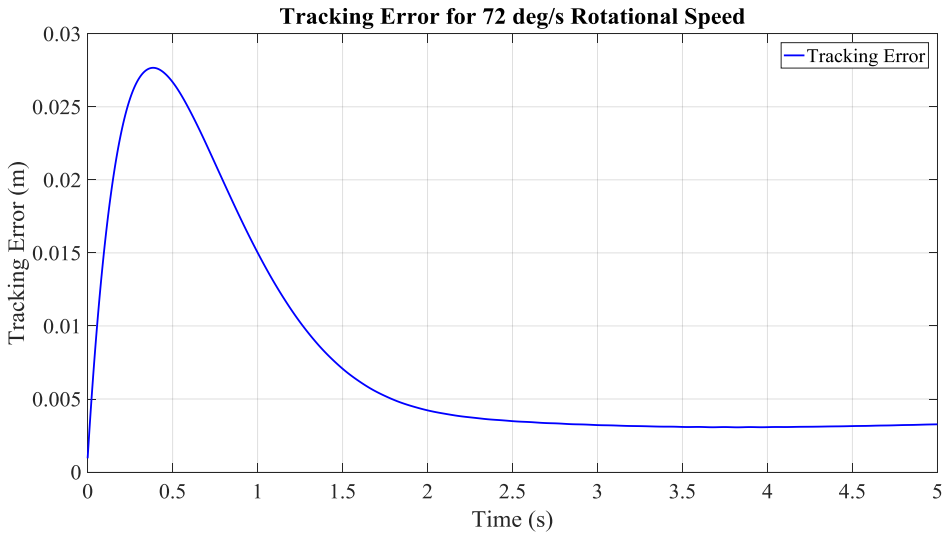

Figure 4.95: Circular Motion Tracking Error under Command “C-P1-3”

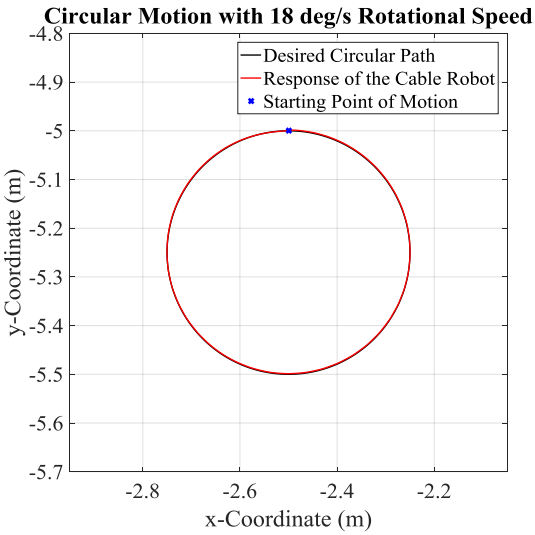

Figure 4.96: Response of the Cable Robot under Command “C-P2-1”

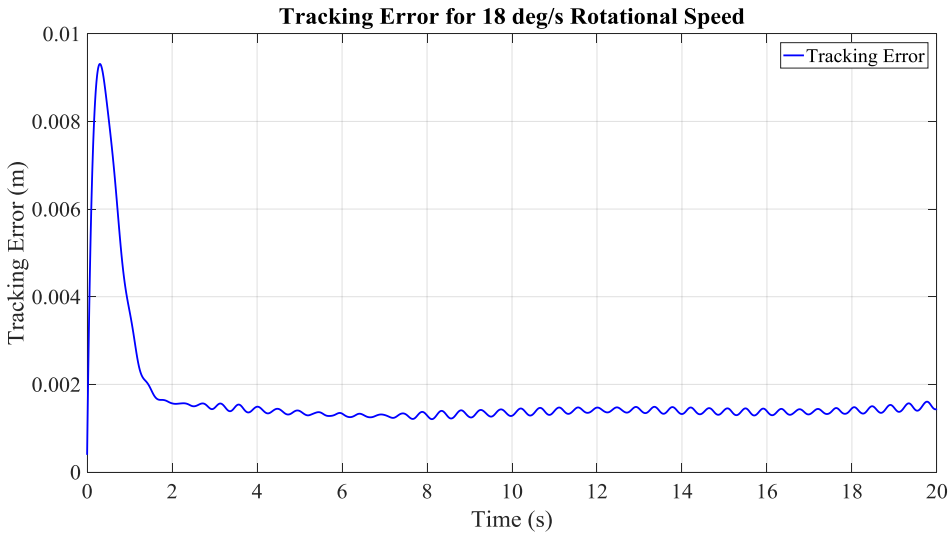

Figure 4.97: Circular Motion Tracking Error under Command “C-P2-1”

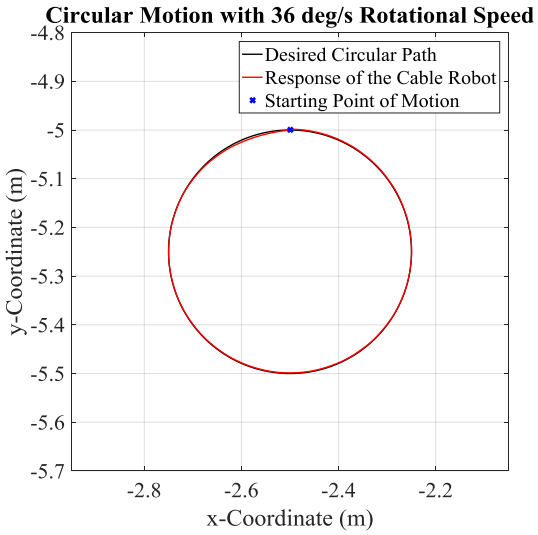

Figure 4.98: Response of the Cable Robot under Command “C-P2-2”

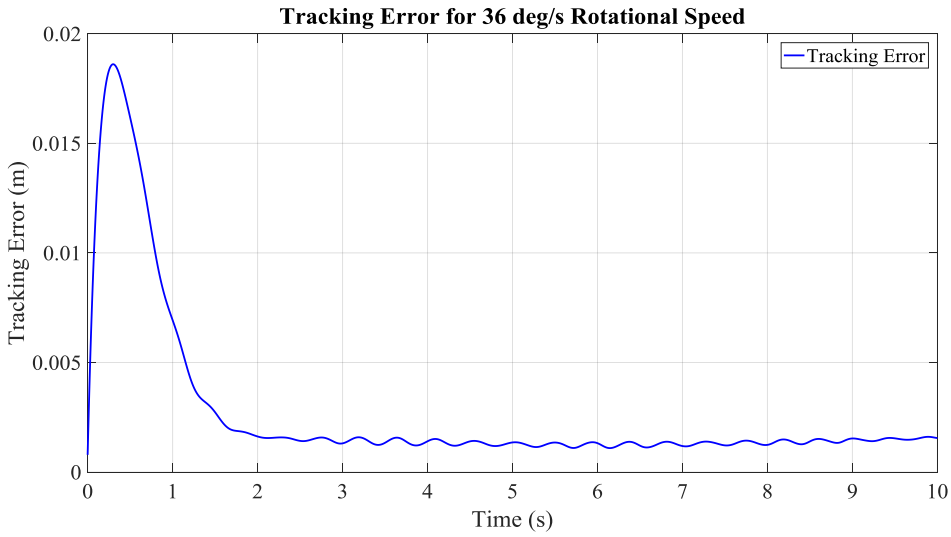

Figure 4.99: Circular Motion Tracking Error under Command "C-P2-2"

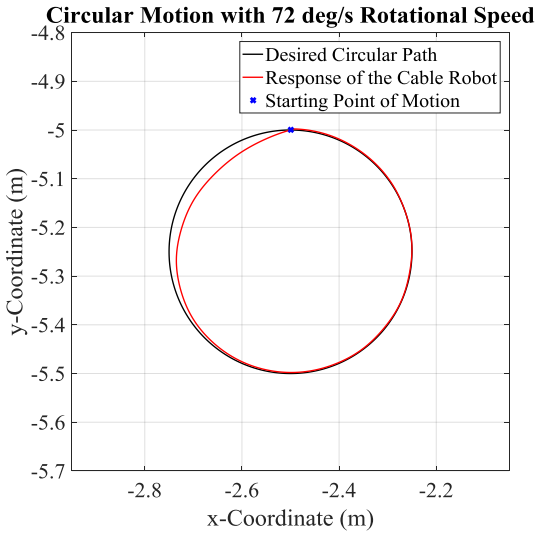

Figure 4.100: Response of the Cable Robot under Command "C-P2-3"

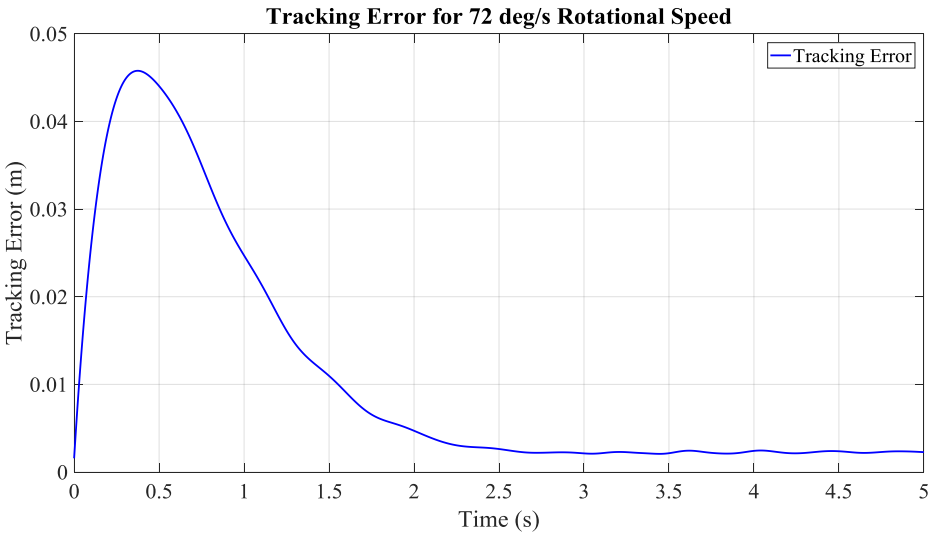

Figure 4.101: Circular Motion Tracking Error under Command “C-P2-3”

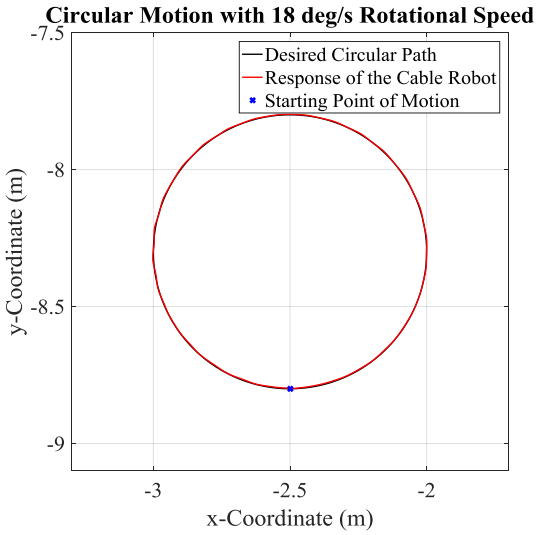

Figure 4.102: Response of the Cable Robot under Command “C-P3-1”

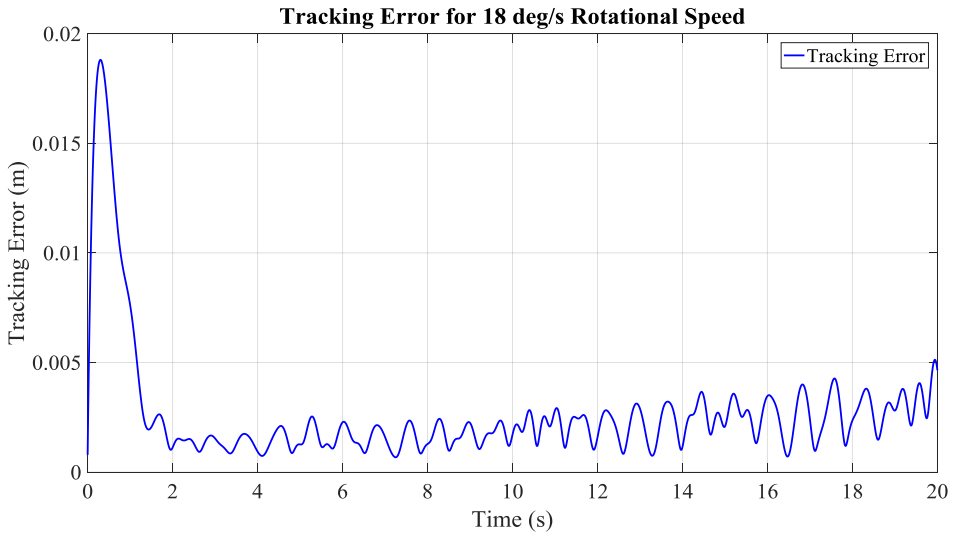

Figure 4.103: Circular Motion Tracking Error under Command “C-P3-1”

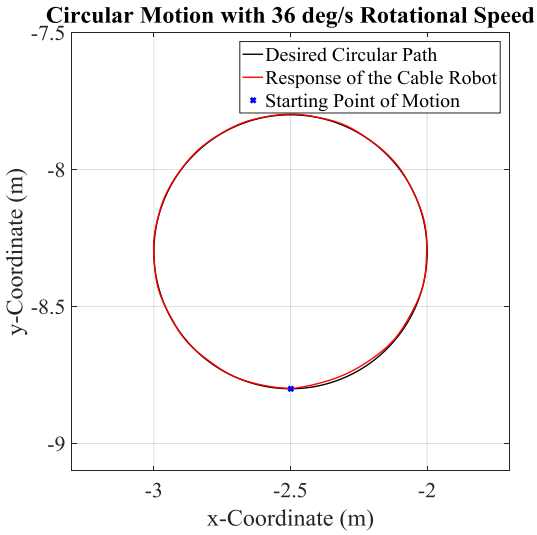

Figure 4.104: Response of the Cable Robot under Command “C-P3-2”

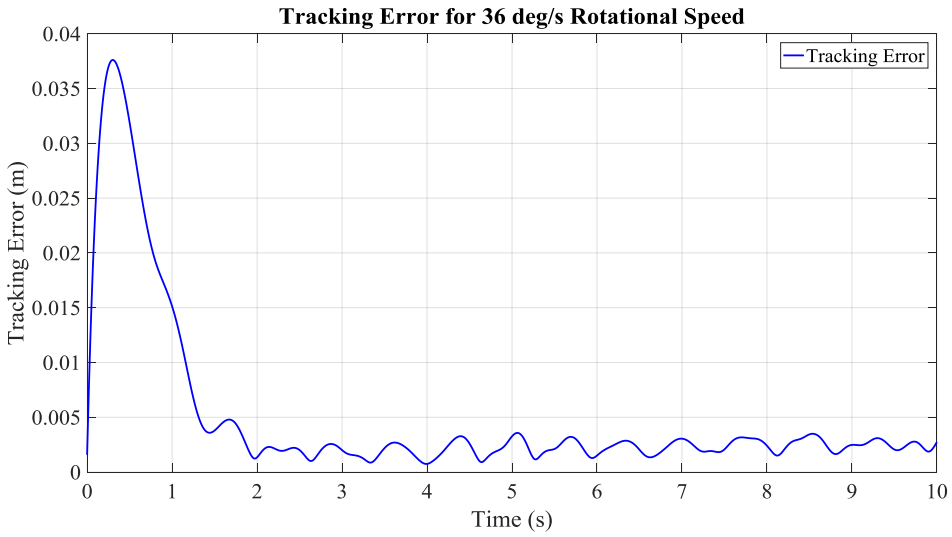

Figure 4.105: Circular Motion Tracking Error under Command “C-P3-2”

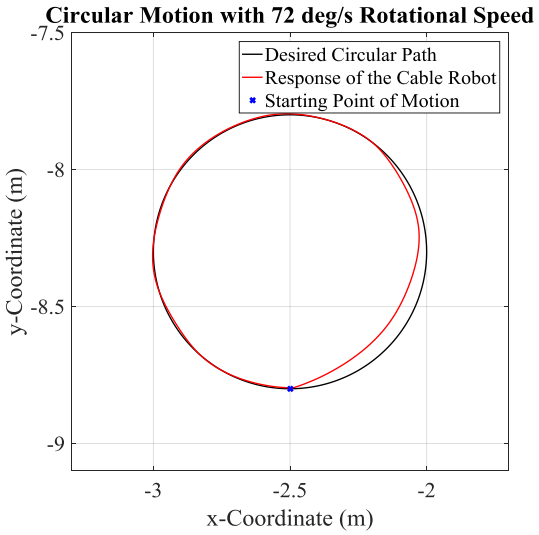

Figure 4.106: Response of the Cable Robot under Command “C-P3-3”

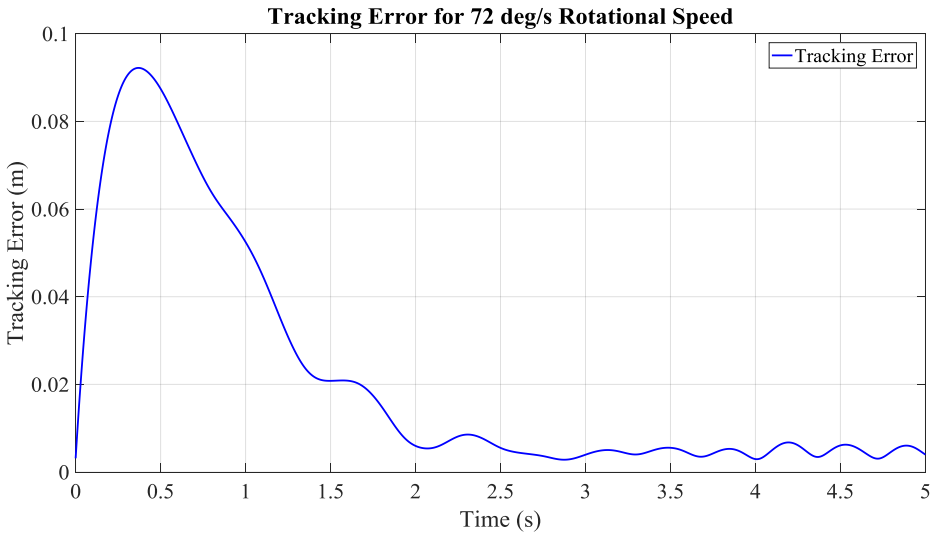

Figure 4.107: Circular Motion Tracking Error under Command "C-P3-3"

4.2.2.3.4 Effect of Order of Lower-Order Model

It is a critical topic to analyze the effect of lower-order model on the performance of the system. Hence in this subsection, the most challenging commands applied on the cable robot are employed to see this influence. For each command, order of lower-order model is increased from 3 to 7 and resulting positioning errors are displayed on the same figure as illustrated below.

Notation used in the legends of these plots: *i-i Lower-Order Model* implies that each cable is assumed to be divided into *i* number of segments for the lower-order model.

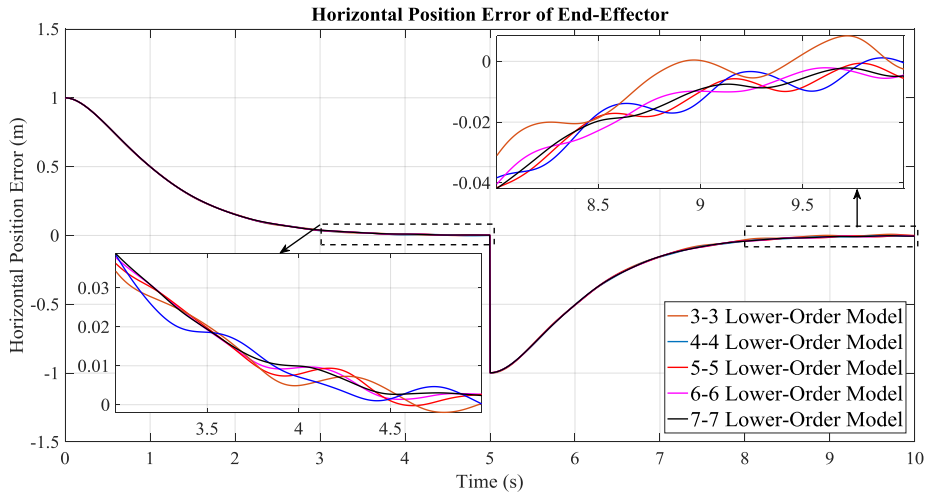

Figure 4.108: Effect of Order of Lower-Order Model on the Response of Cable Robot under Command "S-P3-x"

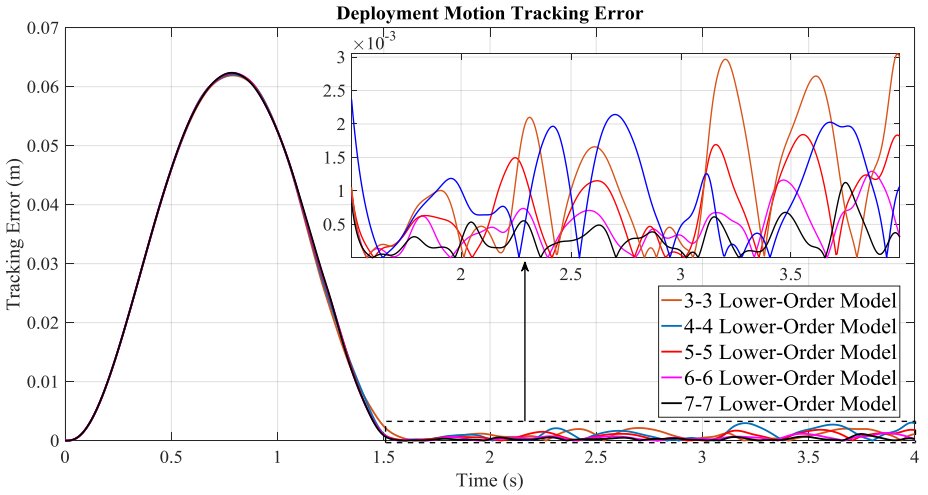

Figure 4.109: Effect of Order of Lower-Order Model on the Response of Cable Robot under Command "D-P3-x"

In Figures Figure 4.108 and Figure 4.109, it is realized that, increase in the order of lower-order model provides the smoothening effect on steady-state oscillations. However, these are not considerable positive effects since the amplitude of these oscillations are relatively small.

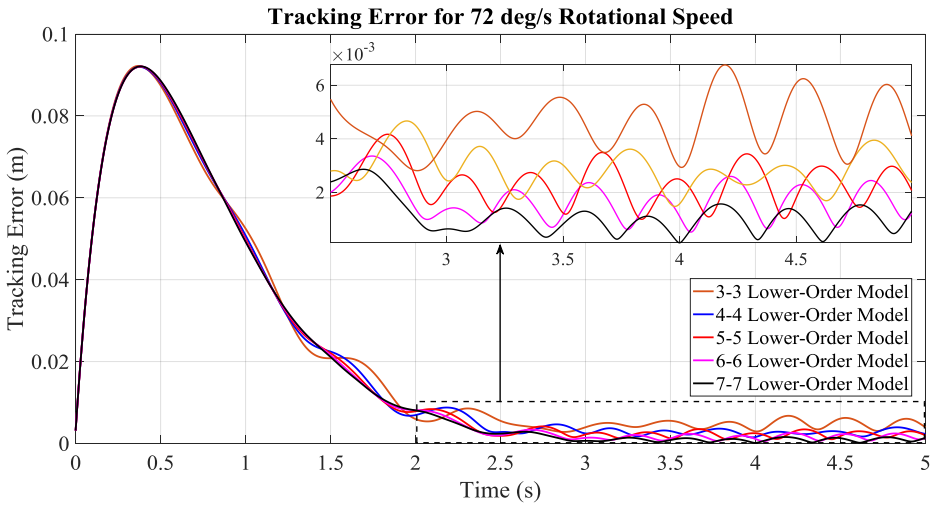

Figure 4.110: Effect of Order of Lower-Order Model on the Response of Cable Robot under Command "C-P3-3"

According to Figure 4.110, steady-state error vanishes as order of lower-order model is increased. Nevertheless, this enhancement is not a considerable one and may not be a need depending on the requirements of the task.

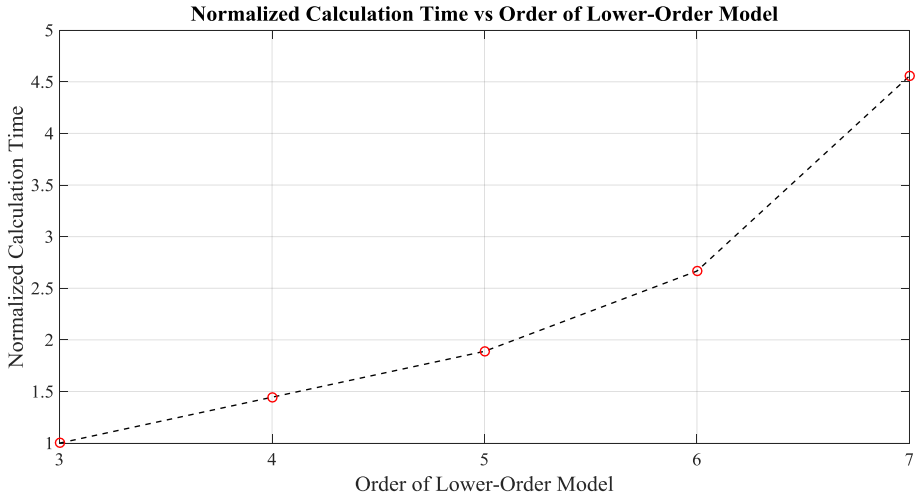

Figure 4.111: Effect of Order of Lower-Order Model on Normalized Calculation Time

In order to evaluate the profit-loss statement in case of increase in the order of lower-order model, normalized calculation time with respect to the order is presented in Figure 4.111. It is clear that it is not obtained a remarkable

enhancement in the accuracy of the cable robot which worths to have longer execution time for segment angles. Therefore, simulations completed with lower-order model having 3rd order, can be taken into account to evaluate system performance.

4.2.2.3.5 Effect of Measurement of Angles of First Segments for Curve Fitting Approach

So far, all simulations utilizing lower-order angle generator and higher-order controller, angles of 1st segments are assumed to be same with the ones calculated from lower-order model like in the Figure 3.8-b. To be able to comment about necessity of measurement of 1st segment angles and to observe its contribution to the performance of the cable robot, few simulations are carried out as if they are measured. By this means, measured 1st segment angles are directly used in curve fitting operation and vector of segment angles that is fed to the controller.

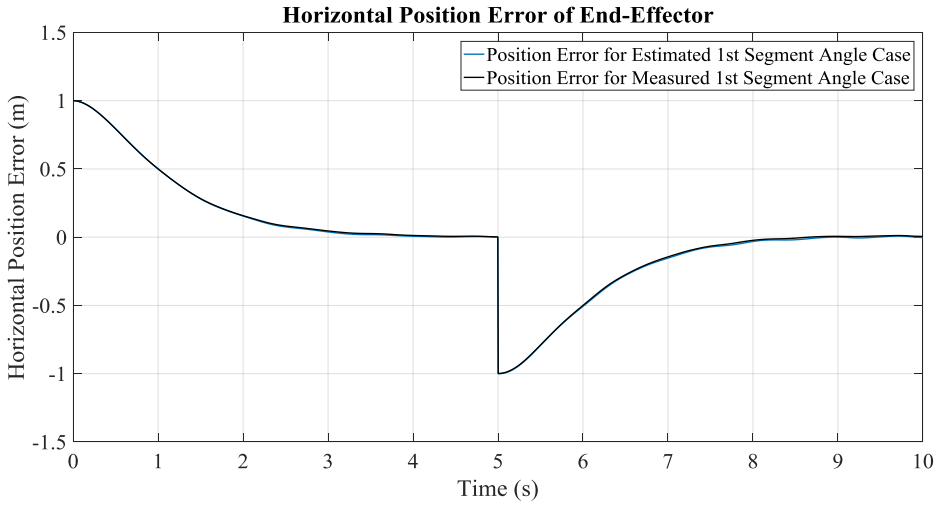

Figure 4.112: Effect of Measurement of 1st Segment Angles on the Response of Cable Robot under Command “C-P3-3”

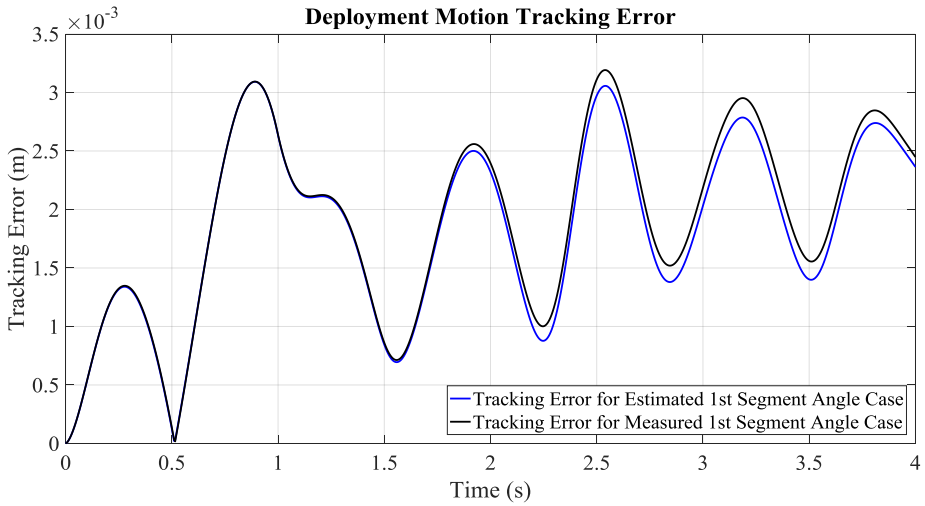

Figure 4.113: Effect of Measurement of 1st Segment Angles on the Response of Cable Robot under Command "D-P3-y"

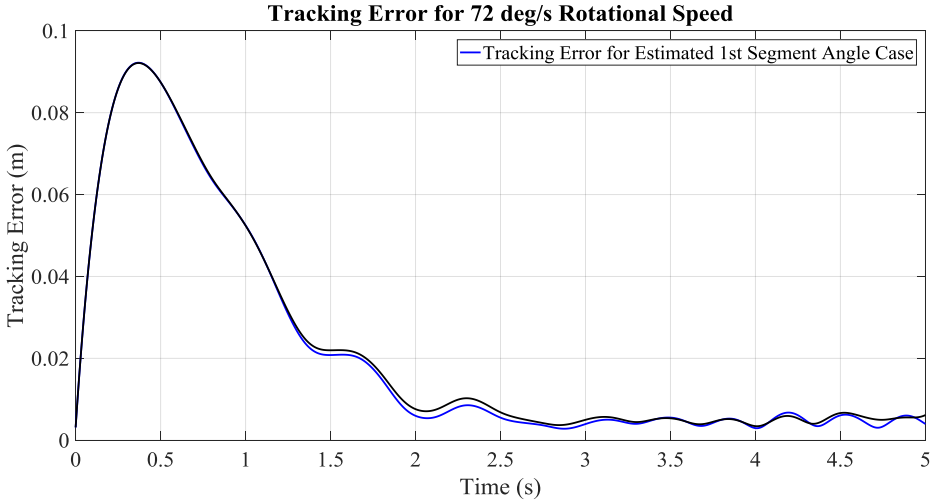

Figure 4.114: Effect of Measurement of 1st Segment Angles on the Response of Cable Robot under Command "C-P3-3"

As a result, measuring 1st segment angles does not serve significant improvement for positioning accuracy of the cable robot since it is observed almost no change between measured and estimated segment angle cases in Figure 4.112, Figure 4.113 and Figure 4.114.

4.2.3 Pseudo-Static Approach Simulations

In this section, simulations are completed with pseudo-static approximation. End-effector pose is assumed to be measured at this step.

4.2.3.1 Response under Square Wave Position Command

Responses of the cable robot under different square wave position commands are illustrated in the following figures for the case of pseudo-static angle generator.

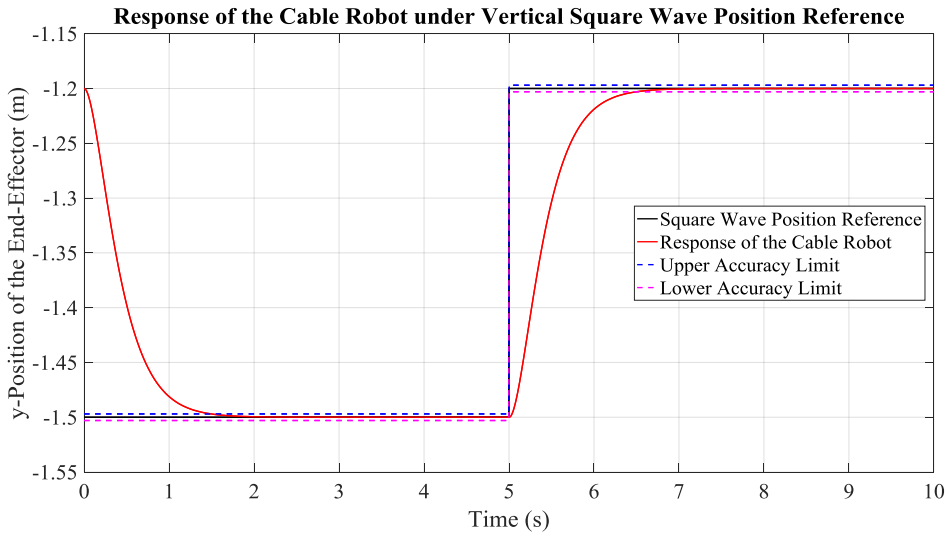

Figure 4.115: Response of the Cable Robot under Command “S-P1-y”

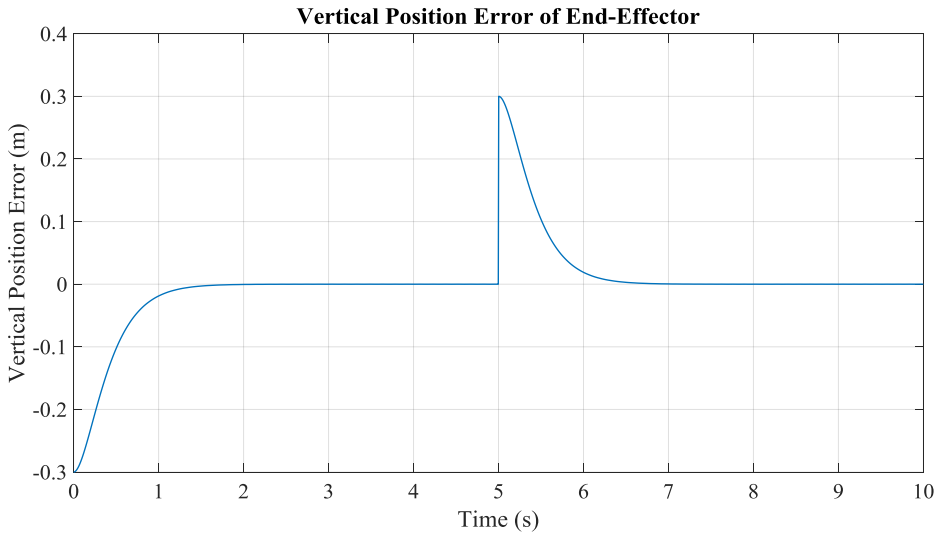

Figure 4.116: Position Error under Command “S-P1-y”

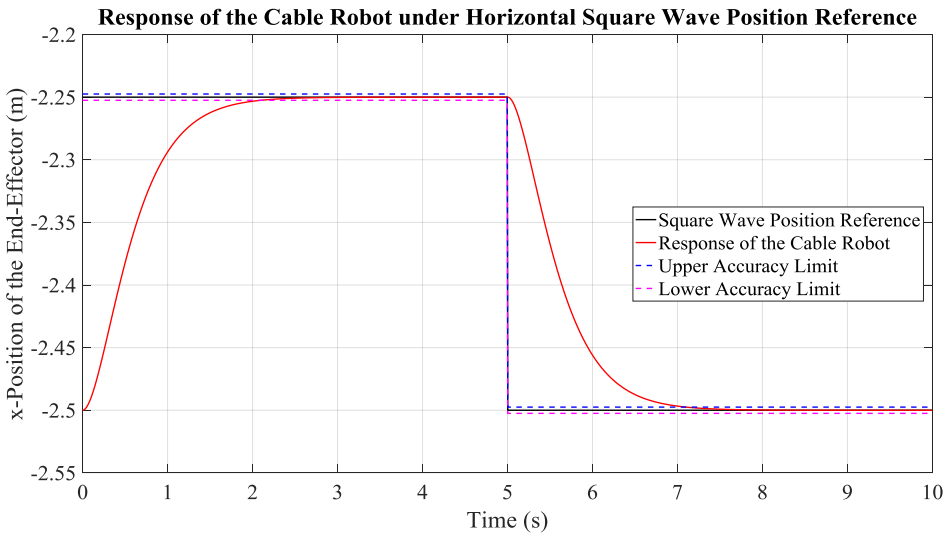

Figure 4.117: Response of the Cable Robot under Command “S-P1-x”

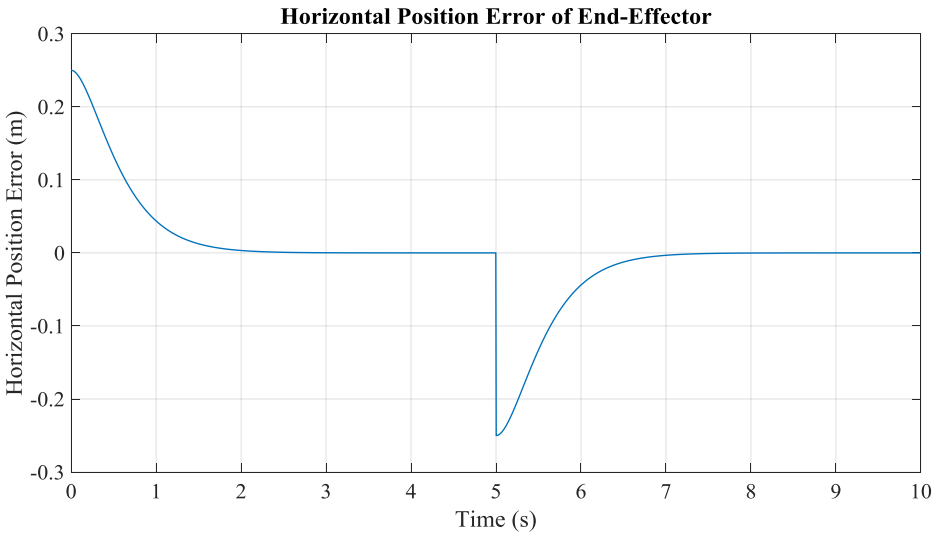

Figure 4.118: Position Error under Command “S-P1-x”

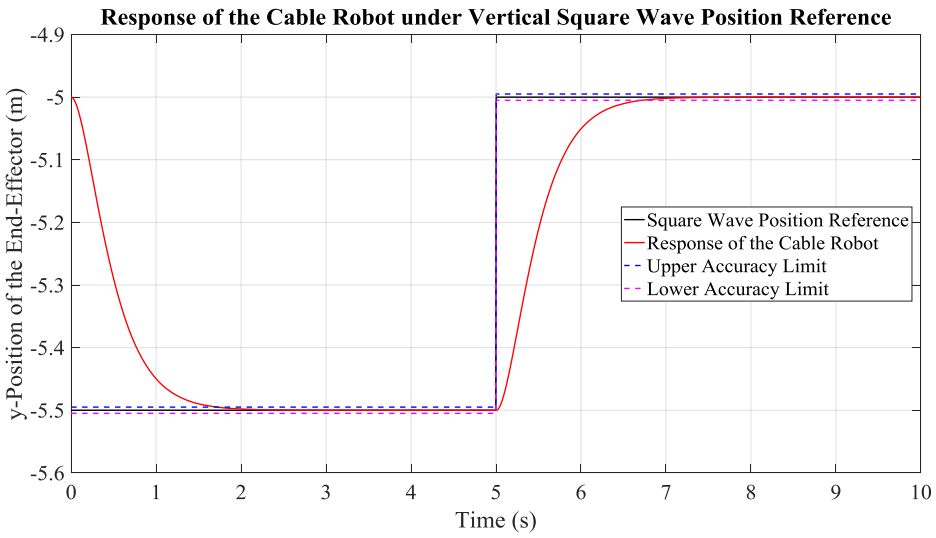

Figure 4.119: Response of the Cable Robot under Command “S-P2-y”

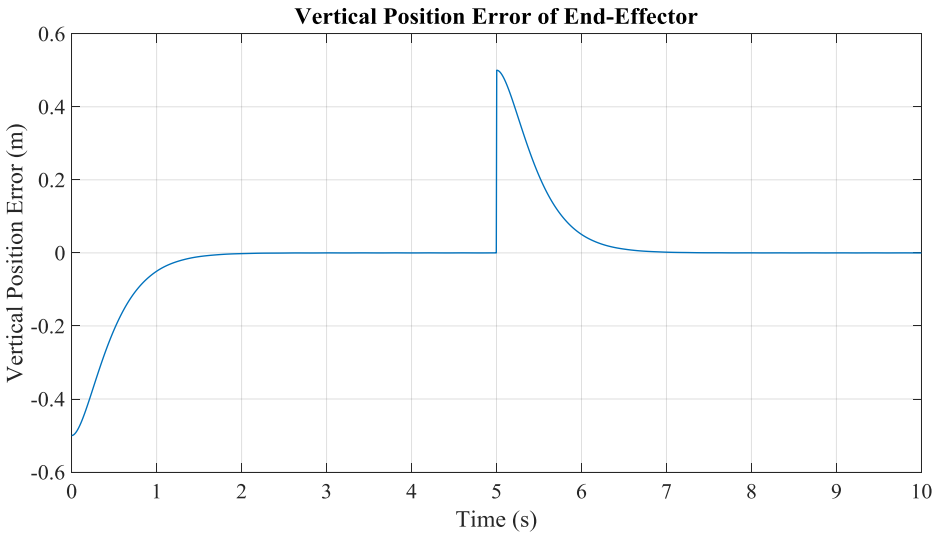

Figure 4.120: Position Error under Command “S-P2-y”

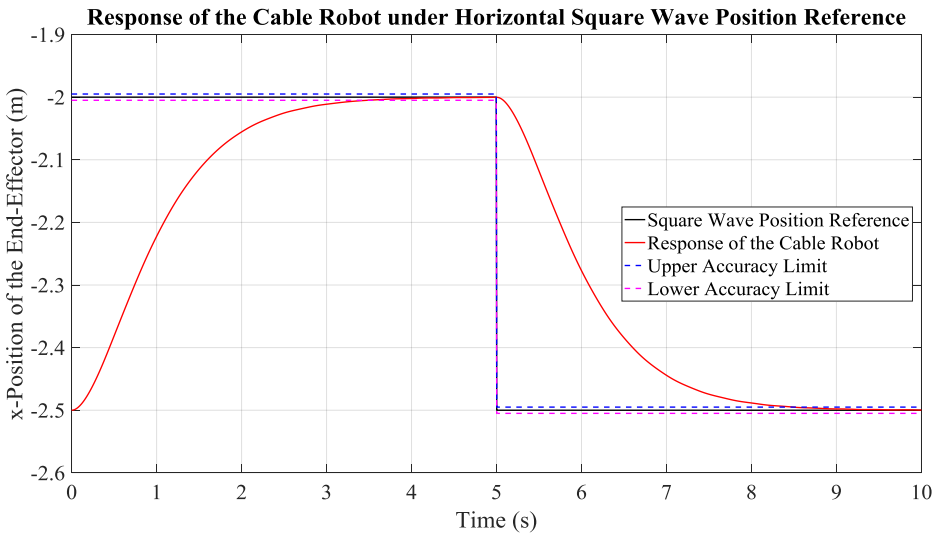

Figure 4.121: Response of the Cable Robot under Command “S-P2-x”

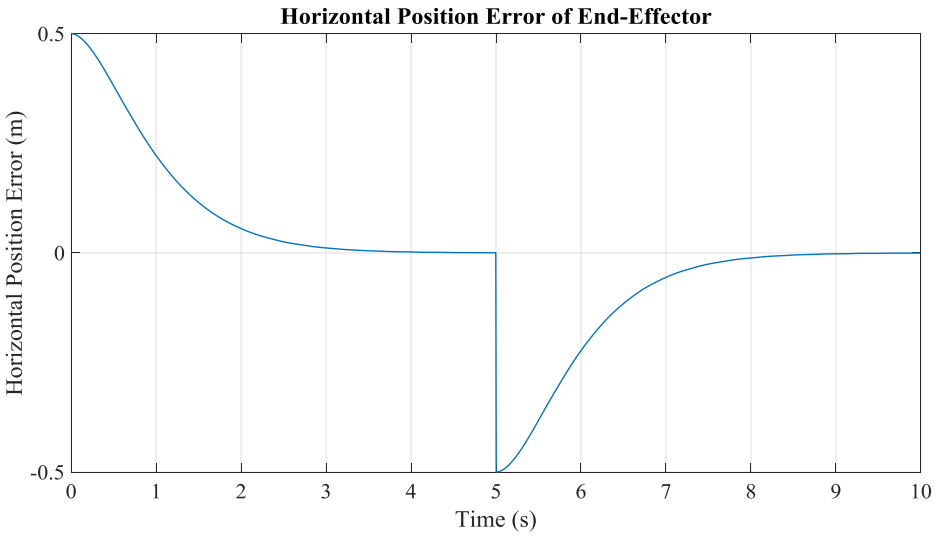

Figure 4.122: Position Error under Command “S-P2-x”

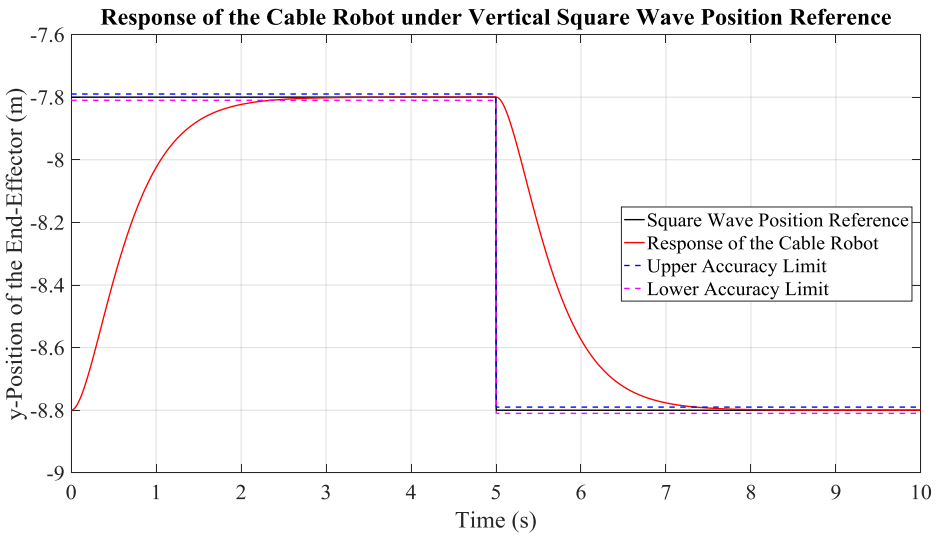

Figure 4.123: Response of the Cable Robot under Command “S-P3-y”

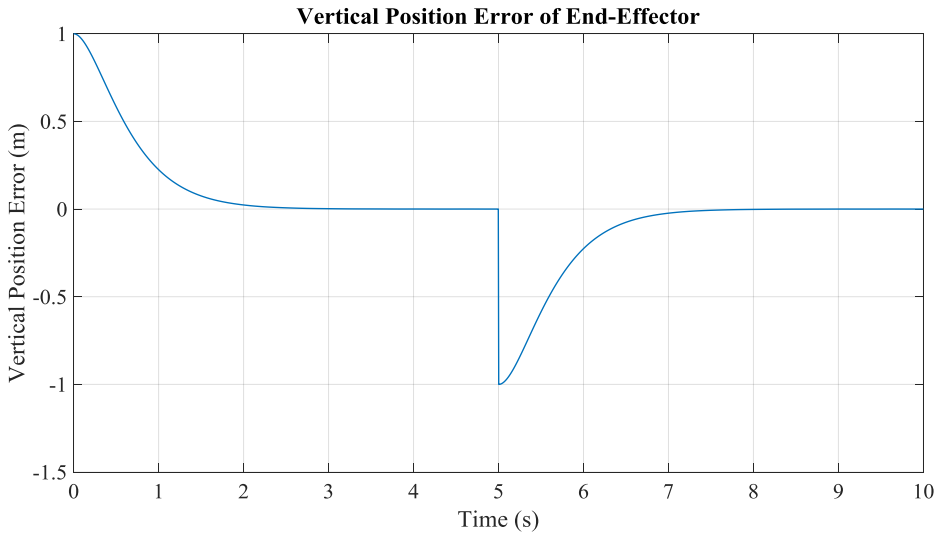

Figure 4.124: Position Error under Command “S-P3-y”

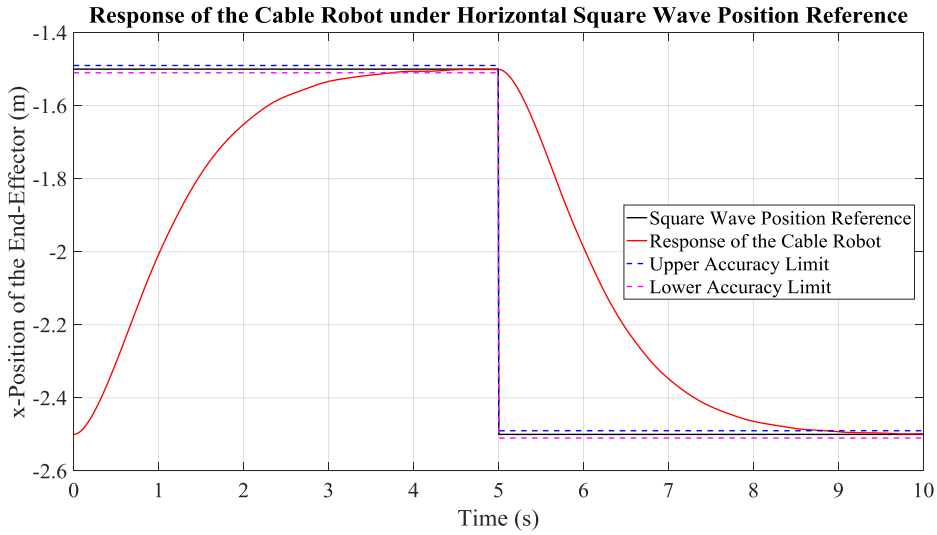

Figure 4.125: Response of the Cable Robot under Command “S-P3-x”

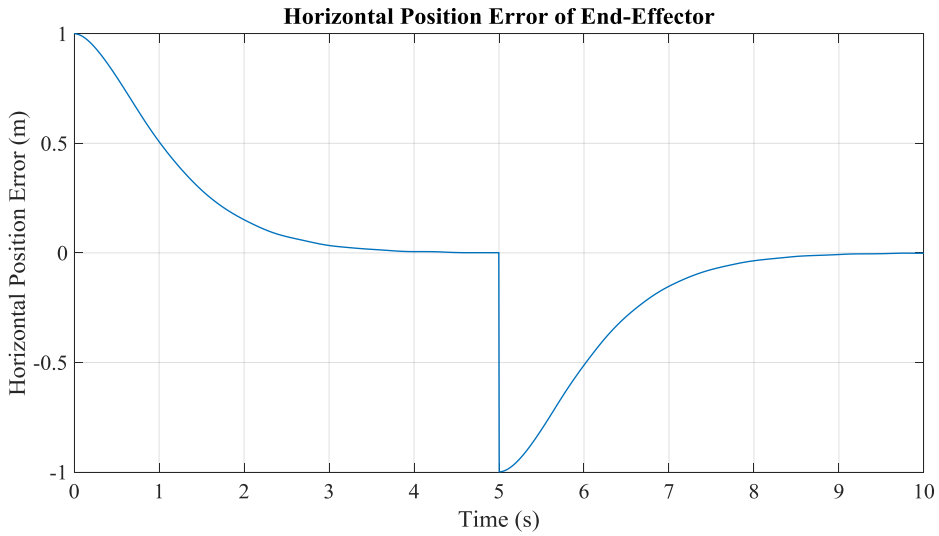

Figure 4.126: Position Error under Command “S-P3-x”

4.2.3.2 Response under Deployment Motion Command

Responses of the cable robot under different deployment motion commands are illustrated in the following figures for the case of pseudo-static angle generator.

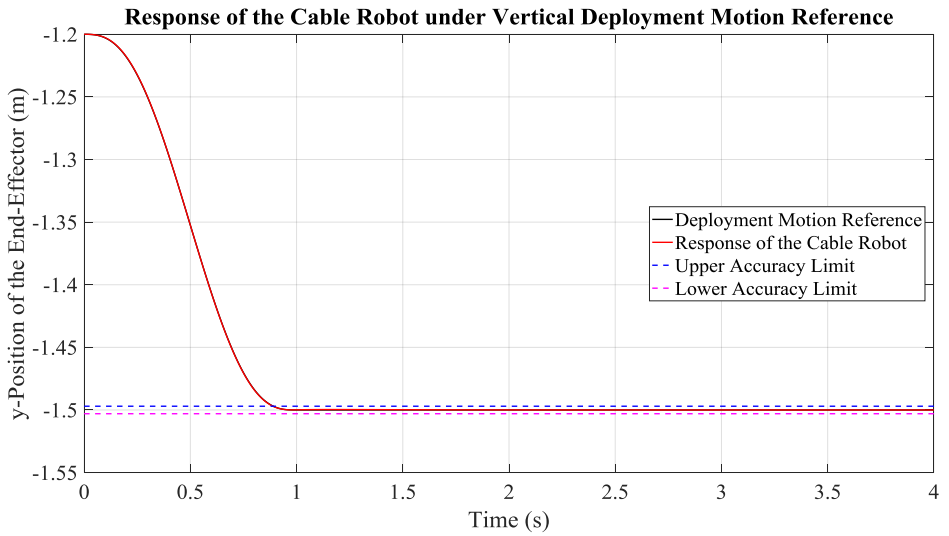

Figure 4.127: Response of the Cable Robot under Command “D-P1-y”

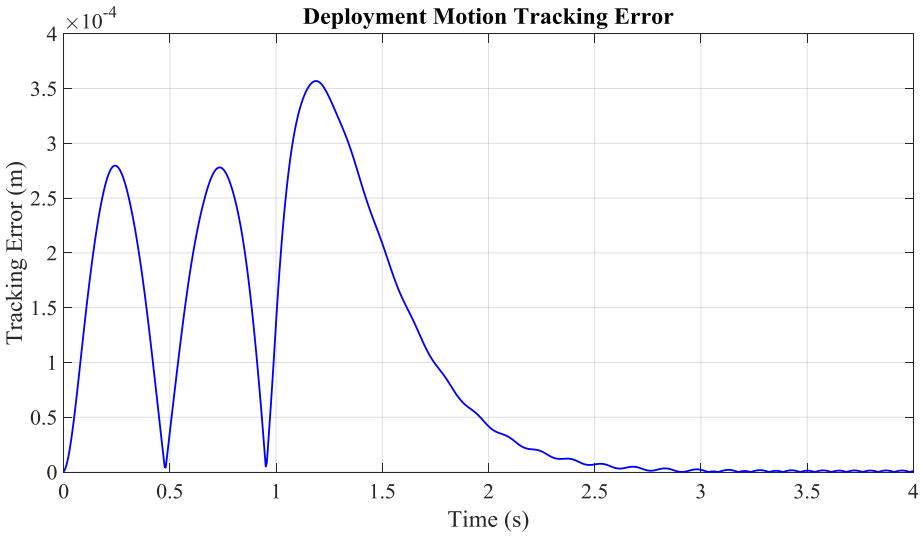

Figure 4.128: Deployment Motion Tracking Error under Command “D-P1-y”

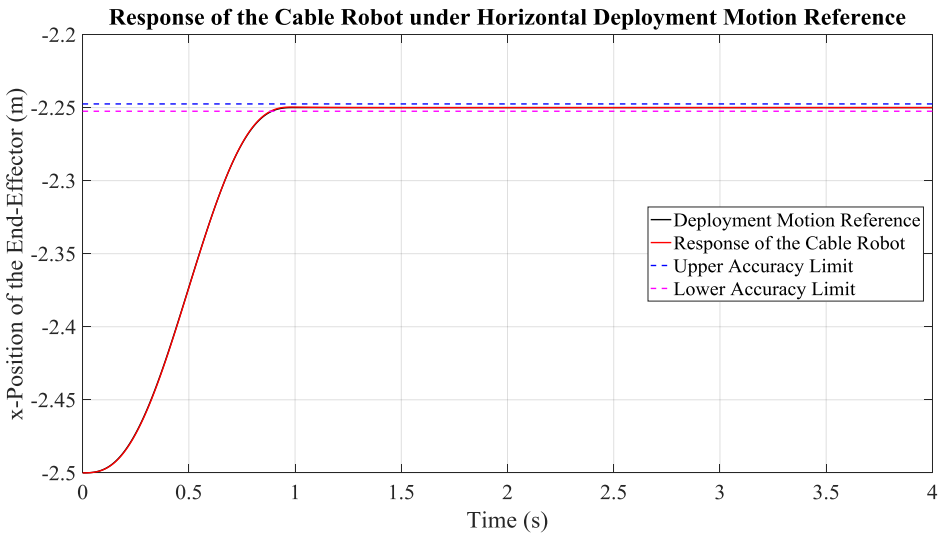

Figure 4.129: Response of the Cable Robot under Command “D-P1-x”

Figure 4.130: Deployment Motion Tracking Error under Command “D-P1-x”

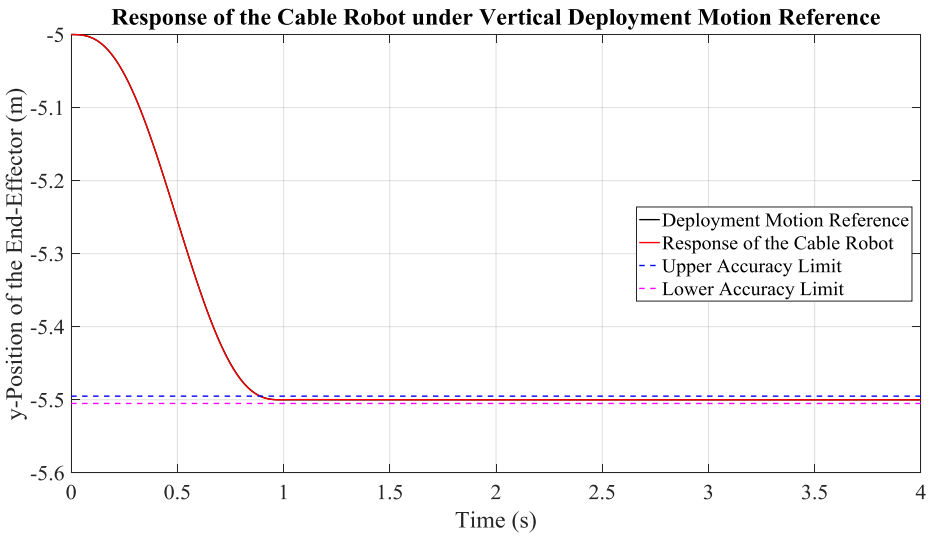

Figure 4.131: Response of the Cable Robot under Command “D-P2-y”

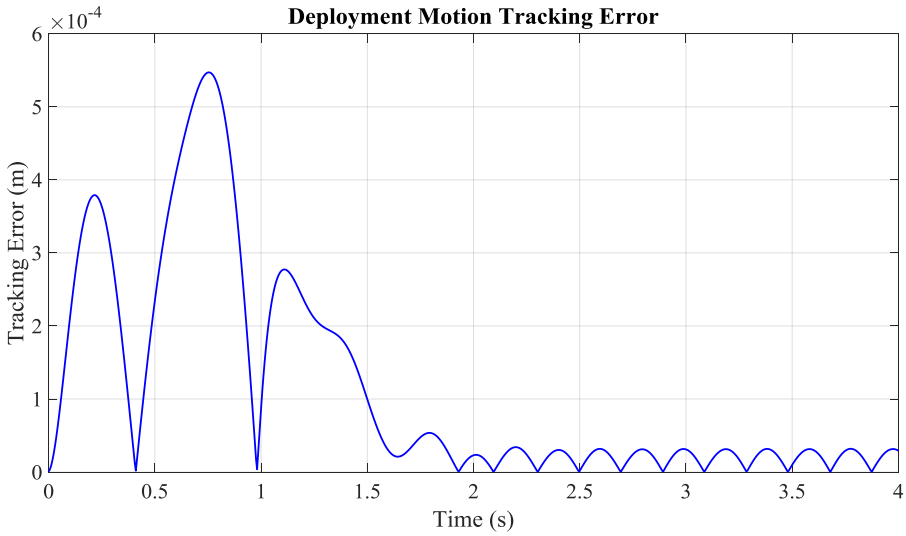

Figure 4.132: Deployment Motion Tracking Error under Command “D-P2-y”

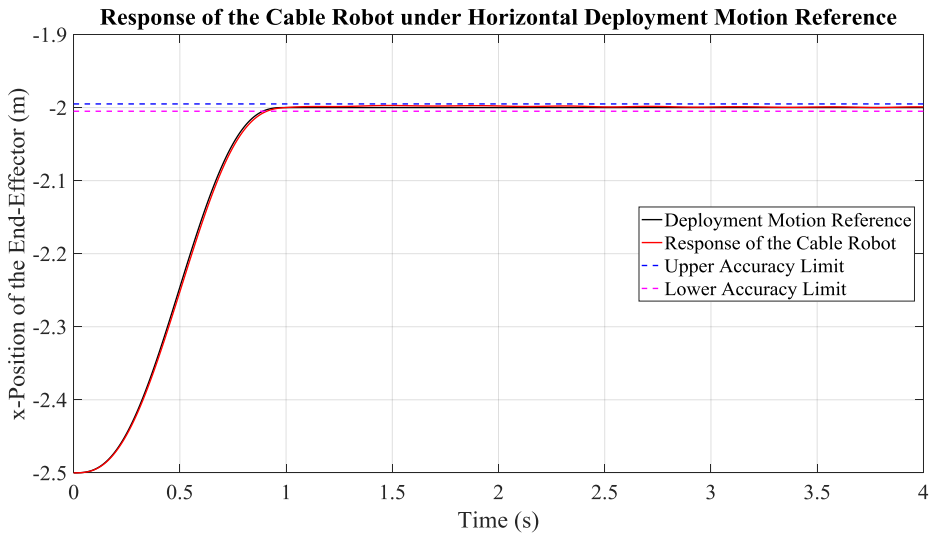

Figure 4.133: Response of the Cable Robot under Command “D-P2-x”

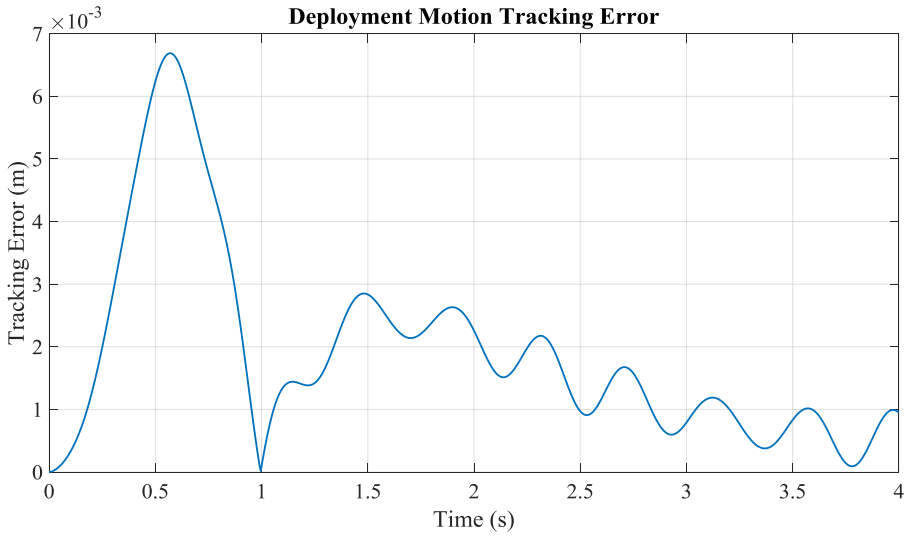

Figure 4.134: Deployment Motion Tracking Error under Command “D-P2-x”

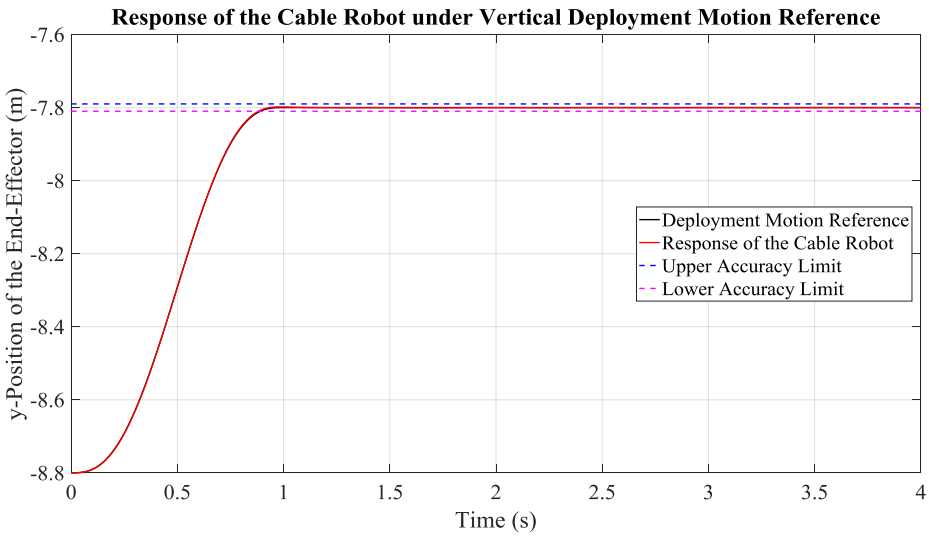

Figure 4.135: Response of the Cable Robot under Command “D-P3-y”

Figure 4.136: Deployment Motion Tracking Error under Command “D-P3-y”

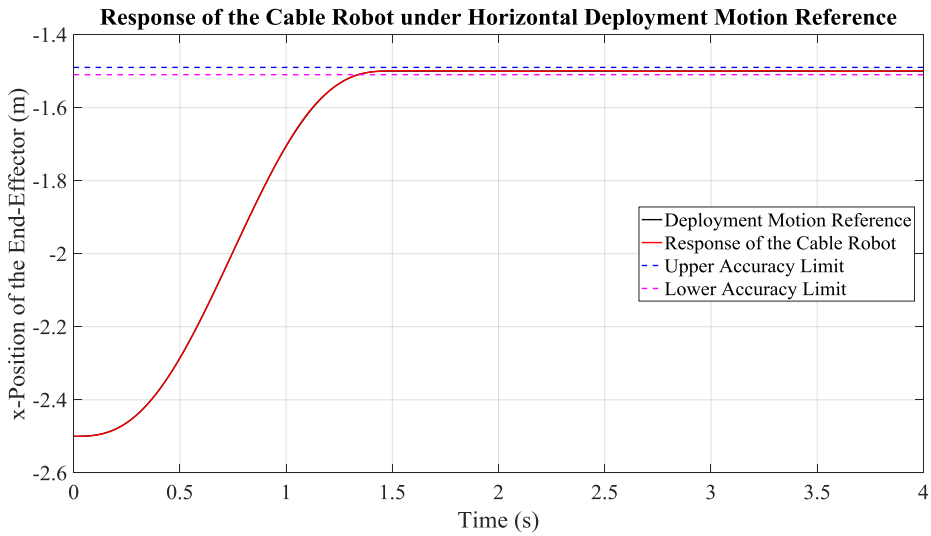

Figure 4.137: Response of the Cable Robot under Command “D-P3-x”

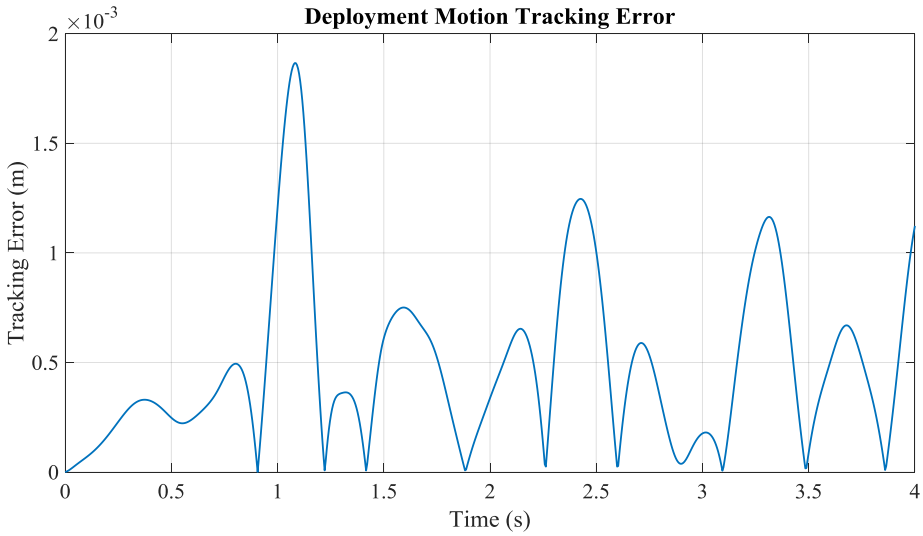

Figure 4.138: Deployment Motion Tracking Error under Command “D-P3-x”

4.2.3.3 Response under Circular Motion Command

Responses of the cable robot under different circular motion commands are illustrated in the following figures for the case of pseudo-static angle generator.

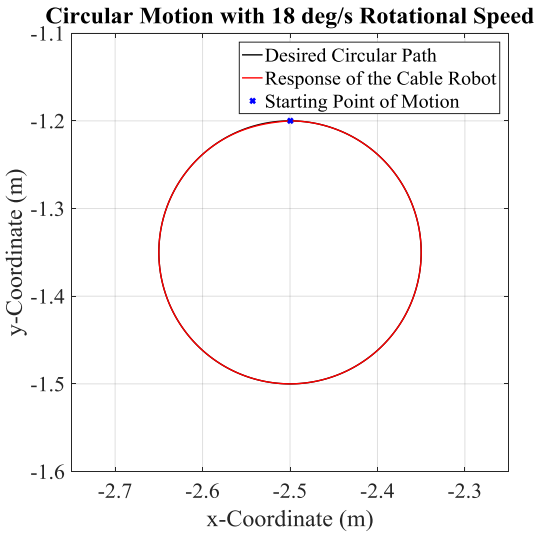

Figure 4.139: Response of the Cable Robot under Command “C-P1-1”

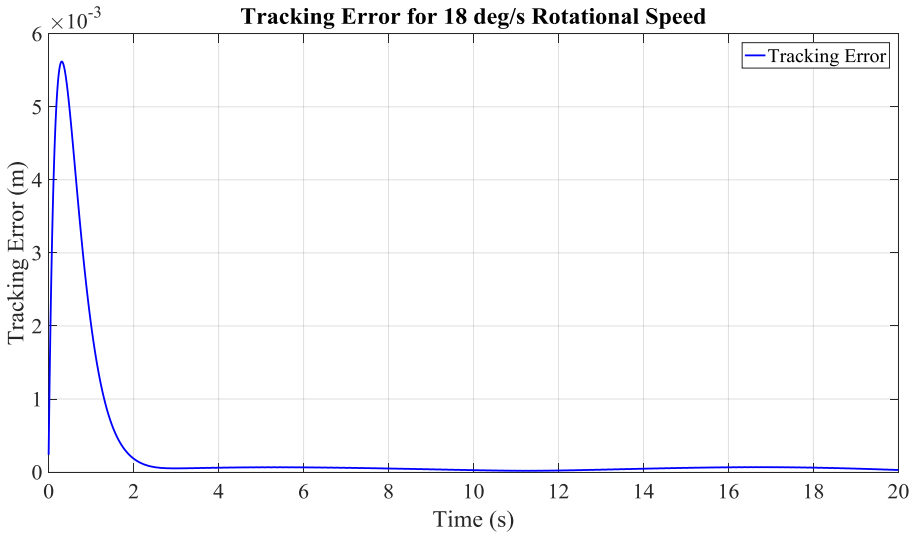

Figure 4.140: Circular Motion Tracking Error under Command “C-P1-1”

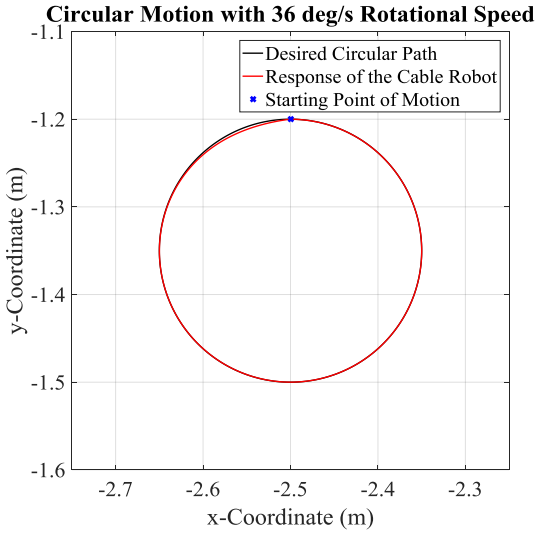

Figure 4.141: Response of the Cable Robot under Command “C-P1-2”

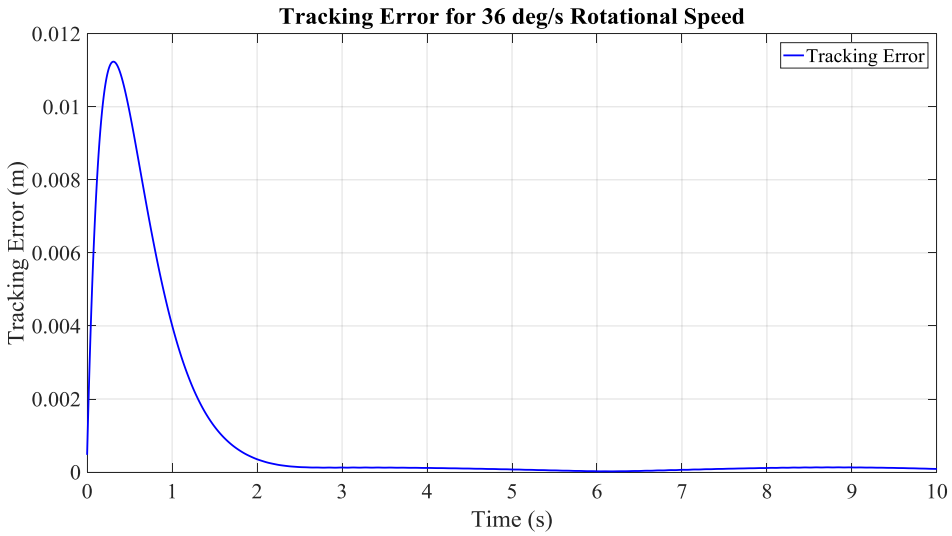

Figure 4.142: Circular Motion Tracking Error under Command “C-P1-2”

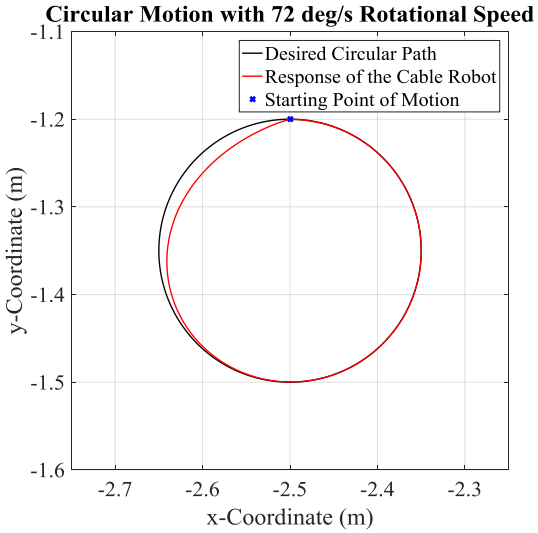

Figure 4.143: Response of the Cable Robot under Command “C-P1-3”

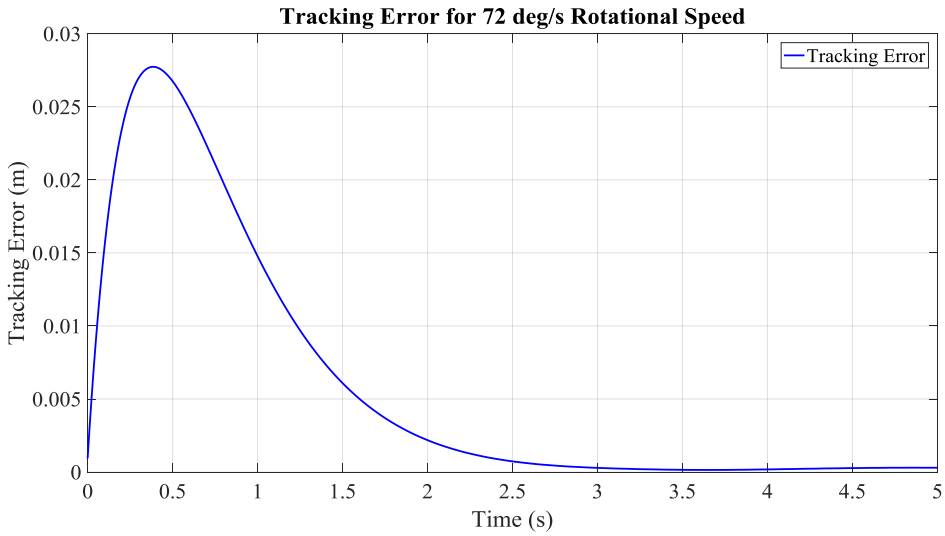

Figure 4.144: Circular Motion Tracking Error under Command “C-P1-3”

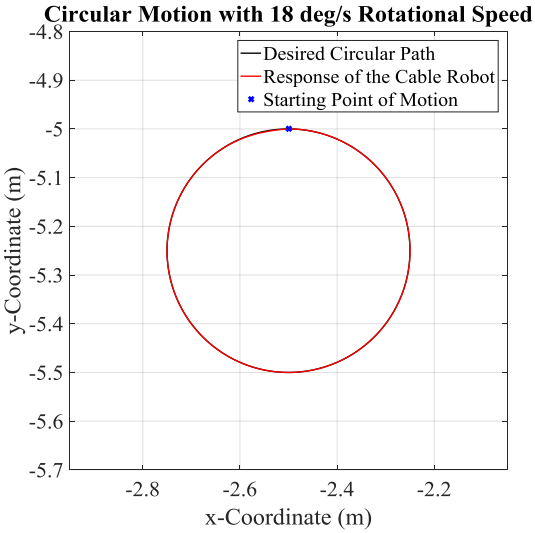

Figure 4.145: Response of the Cable Robot under Command “C-P2-1”

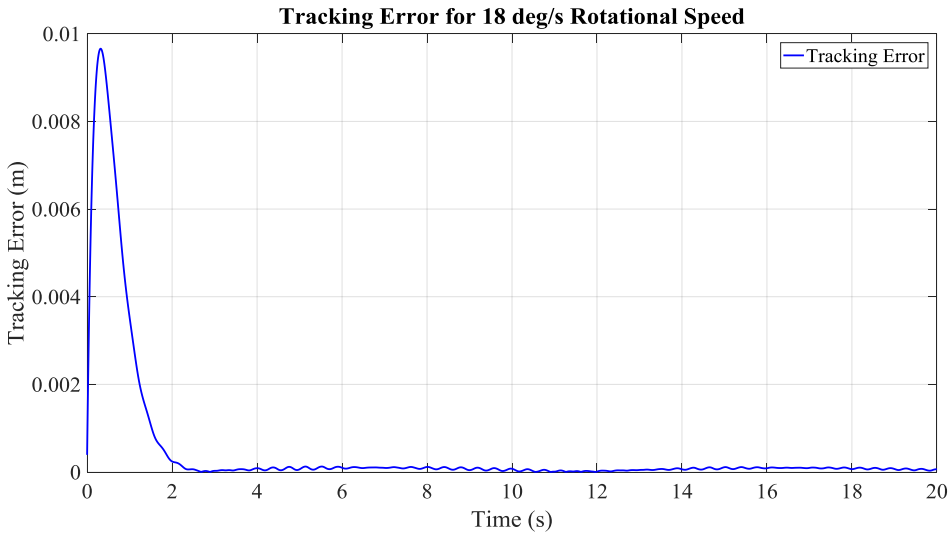

Figure 4.146: Circular Motion Tracking Error under Command “C-P2-1”

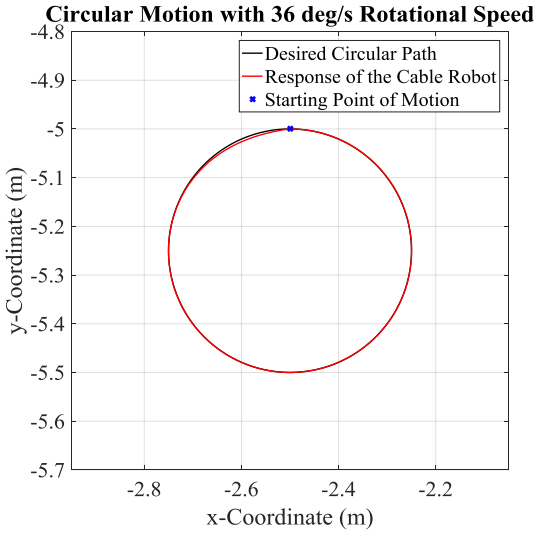

Figure 4.147: Response of the Cable Robot under Command “C-P2-2”

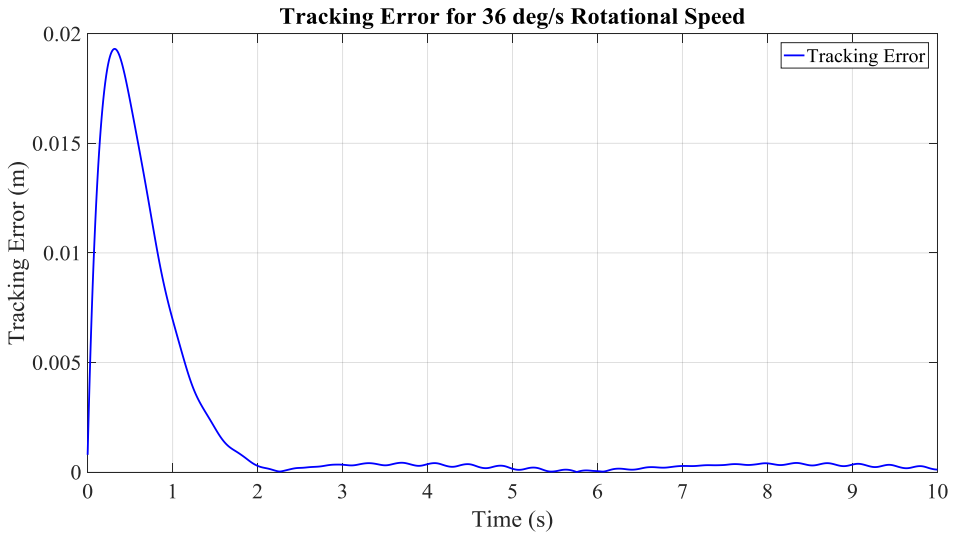

Figure 4.148: Circular Motion Tracking Error under Command “C-P2-2”

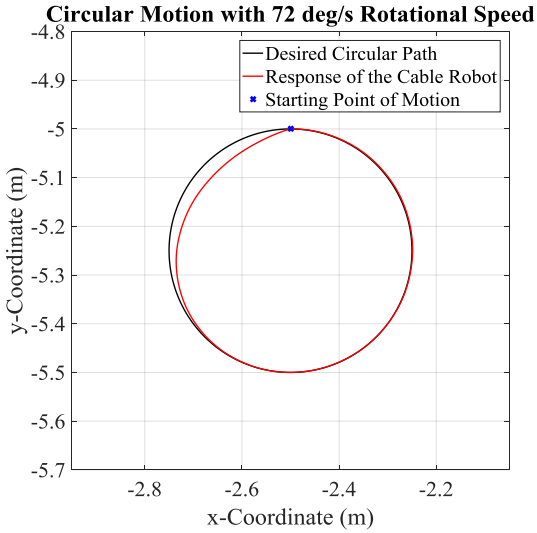

Figure 4.149: Response of the Cable Robot under Command “C-P2-3”

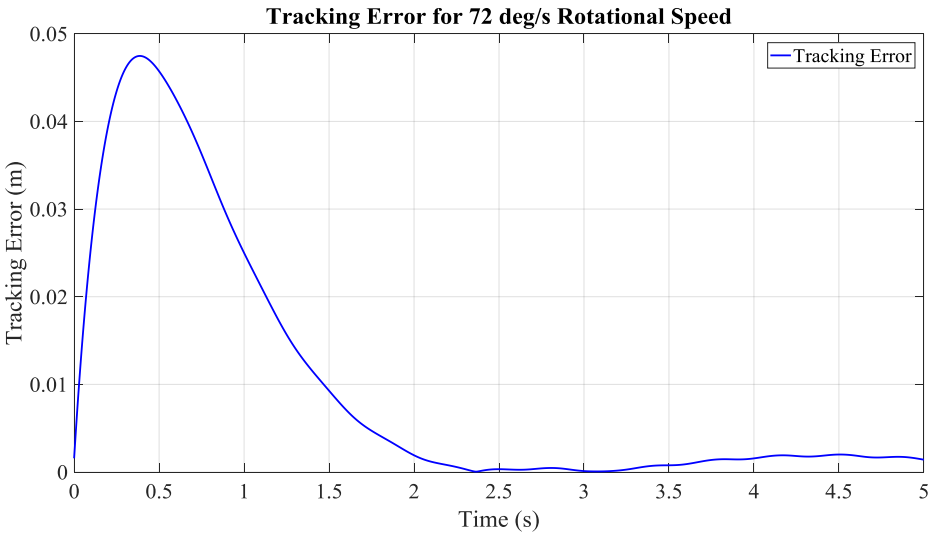

Figure 4.150: Circular Motion Tracking Error under Command “C-P2-3”

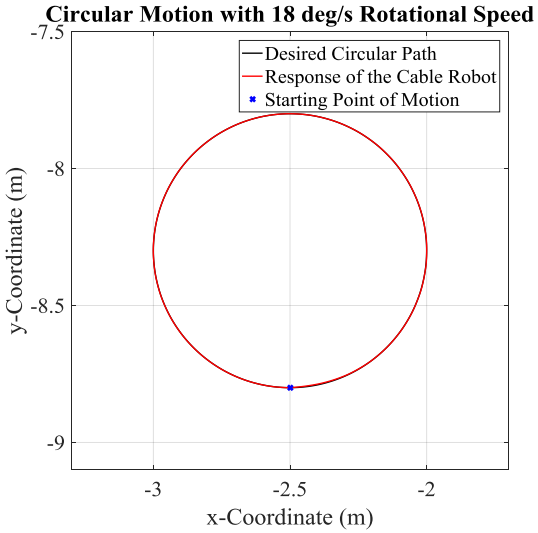

Figure 4.151: Response of the Cable Robot under Command “C-P3-1”

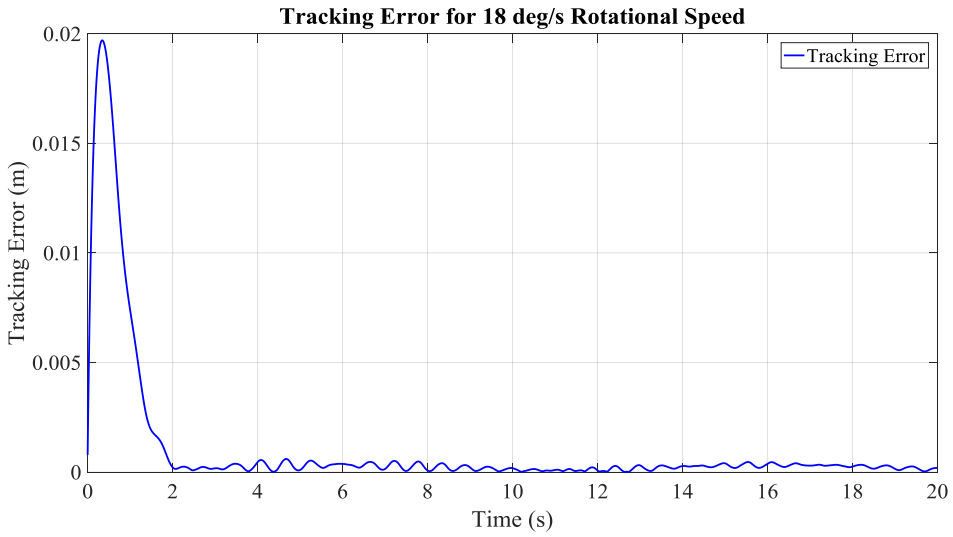

Figure 4.152: Circular Motion Tracking Error under Command “C-P3-1”

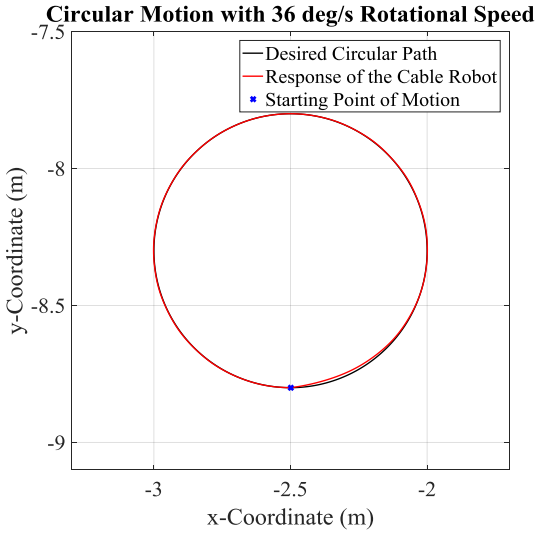

Figure 4.153: Response of the Cable Robot under Command “C-P3-2”

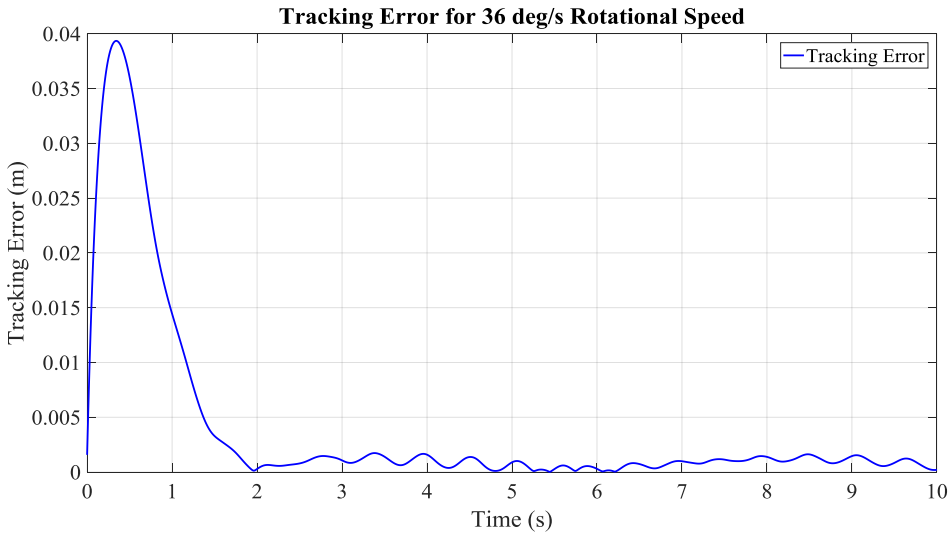

Figure 4.154: Circular Motion Tracking Error under Command “C-P3-2”

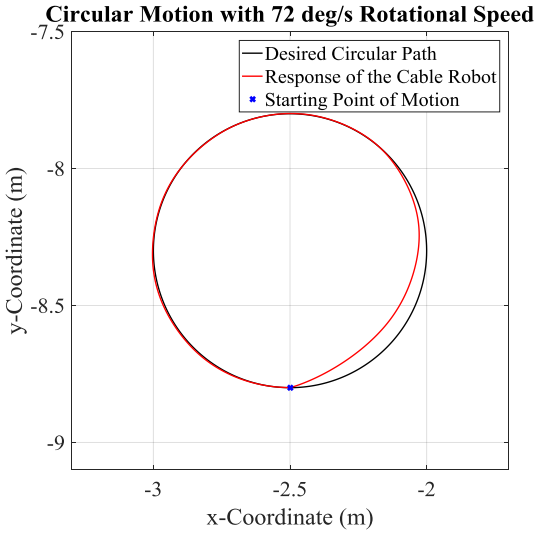

Figure 4.155: Response of the Cable Robot under Command “C-P3-3”

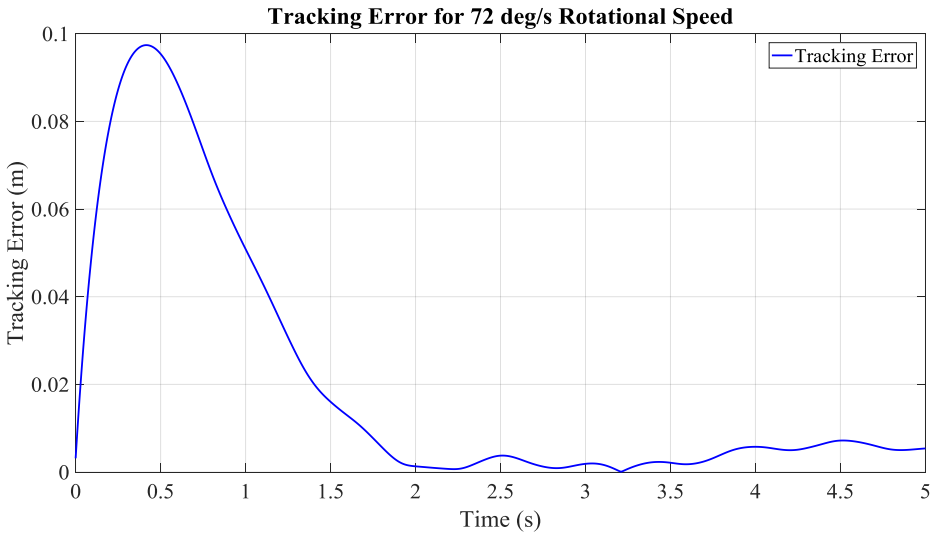

Figure 4.156: Circular Motion Tracking Error under Command "C-P3-3"

After completing all the scenarios with implementation of pseudo-static approach, it is also aimed to show the stability behavior of the cable robot. With this purpose in mind, an error formulation similar to a Lyapunov function is formed for each command type. It should be noted that these functions indicated below are not kind of mathematical proof for stability analysis, but they just help to observe corresponding error functions vanish in time or at least stay within an interval.

Error formulations for motion in x and y directions comprise sum of squares of position error and its time derivative:

$$E_x = {e_x}^2 + {\dot{e}_x}^2 \text{ and } E_y = {e_y}^2 + {\dot{e}_y}^2$$

where e_i represents the position error in i direction and $\dot{e}_i$ is the velocity error in i direction. Result of corresponding error formulations are presented in the following figures for a few square wave command examples:

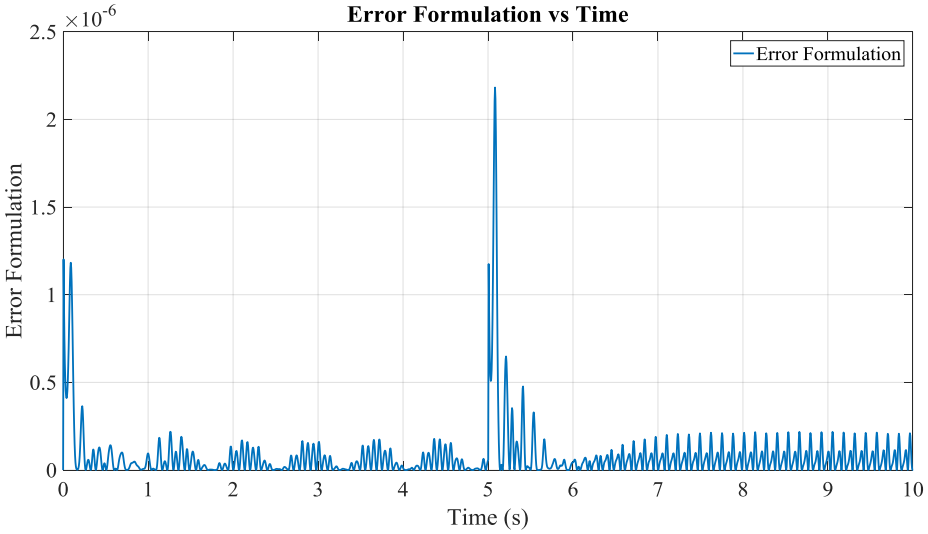

Figure 4.157: Error Formulation (E_x) vs Time for Command "S-P1-x"

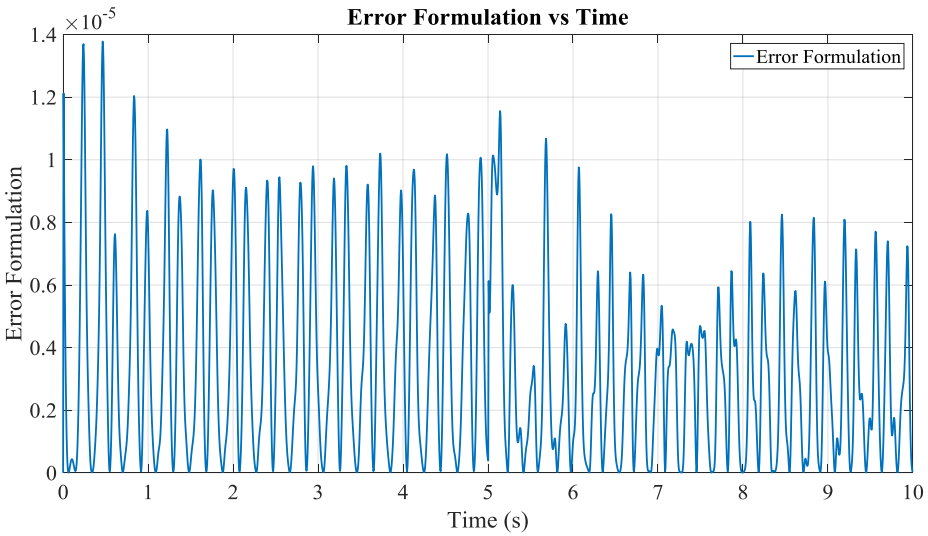

Figure 4.158: Error Formulation (E_y) vs Time for Command "S-P2-y"

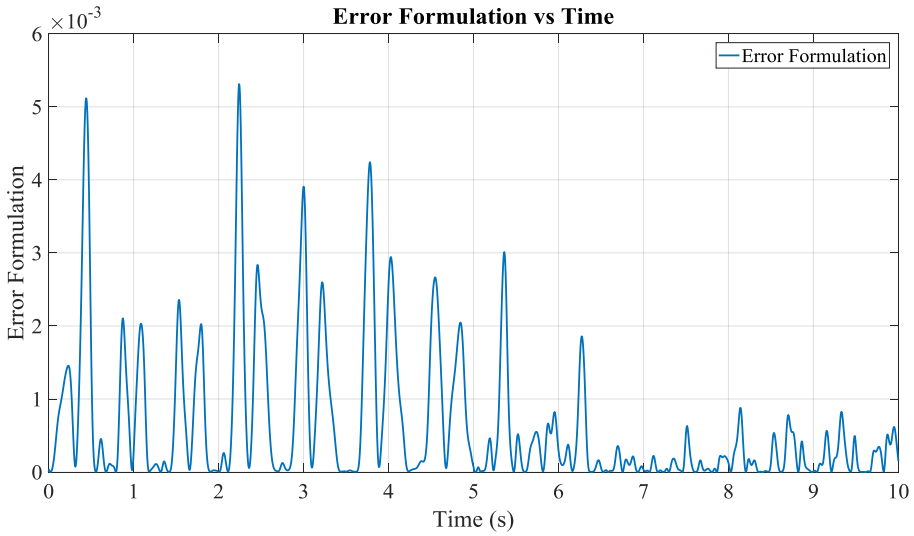

Figure 4.159: Error Formulation (E_x) vs Time for Command "S-P3-x"

These results help out to have basic information about how pseudo-static approach works out well as a segment angle estimator. It is observed that error formulation results do not amplify and vanish in time.

4.2.4 Effect of Measurement of End-Effector Position for Lower-Order Angle Generator with Higher-Order Controller and Pseudo-Static Approaches

In all simulations completed so far, it is assumed that position of end-effector is measured by using a proper method. In this subsection, it is aimed to observe the results of the opposite case. In other words, position of end-effector is found out with the help of estimated cable segment angles, measure 1st segment lengths ($\bar{r}$) and forward kinematics. Thus in this subsection, the most challenging commands applied on the cable robot are employed to illustrate the impact of end-effector measurement on the system performance.

Responses of the cable robot under challenging commands in case of estimated end-effector position where lower-order model angle generator with curve fitting operation method is employed as segment angle generator:

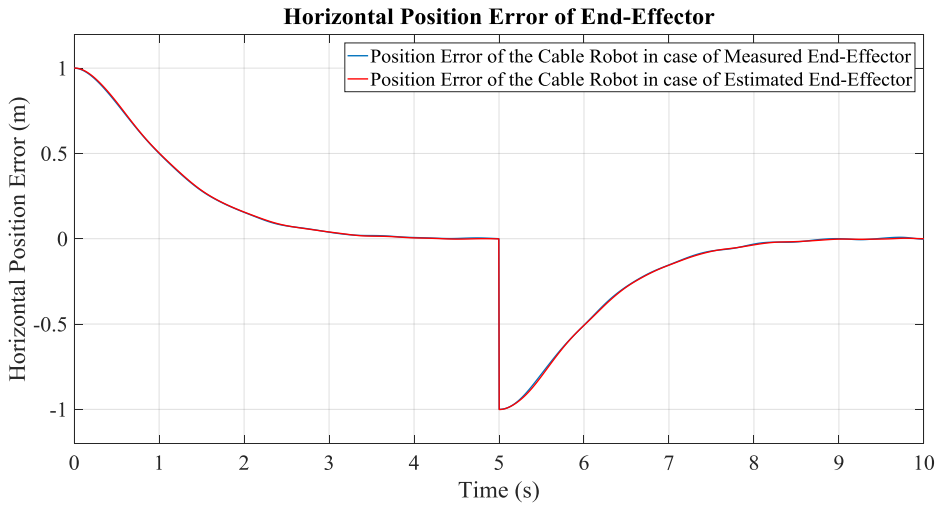

Figure 4.160: Position Error Comparison of Measured and Estimated End-Effector Case under Command "S-P3-x"

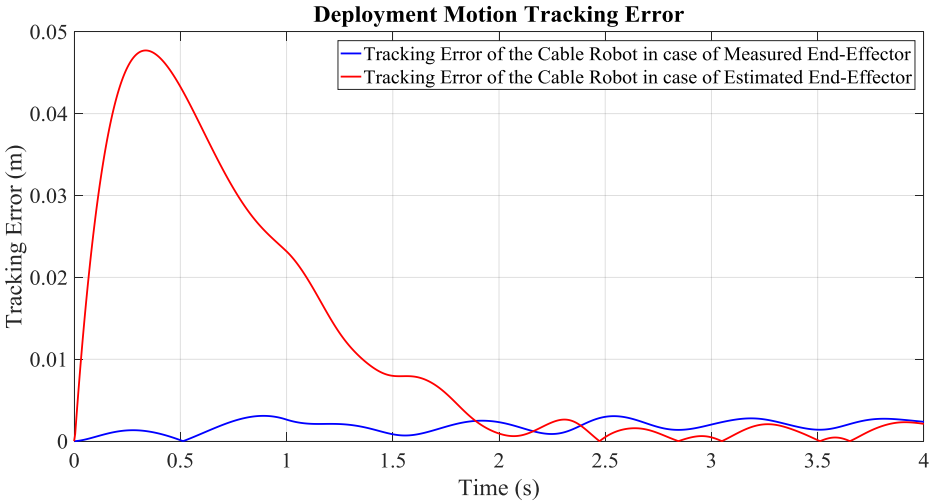

Figure 4.161: Tracking Error Comparison of Measured and Estimated End-Effector Case under Command "D-P3-y"

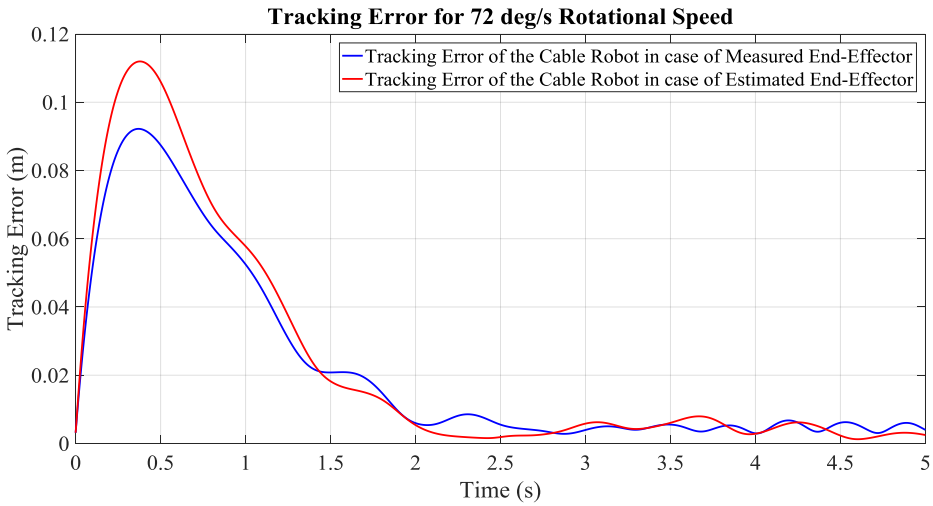

Figure 4.162: Tracking Error Comparison of Measured and Estimated End-Effector Case under Command "C-P3-3"

Responses of the cable robot under challenging commands in case of estimated end-effector position where pseudo-static approach is employed as segment angle generator:

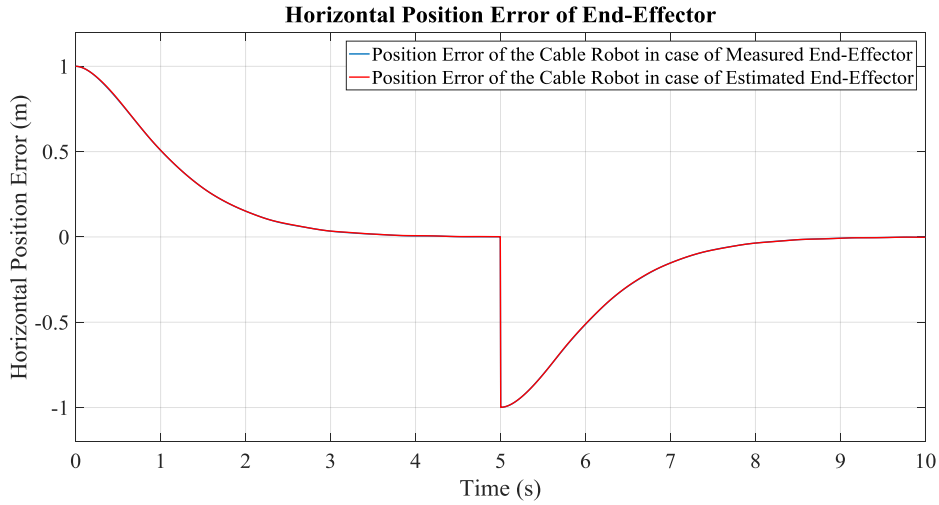

Figure 4.163: Position Error Comparison of Measured and Estimated End-Effector Case under Command "S-P3-x"

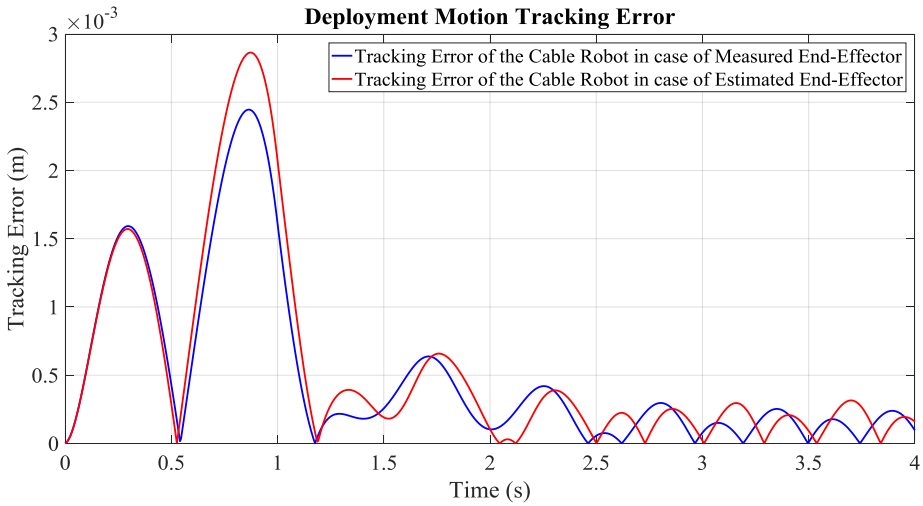

Figure 4.164: Tracking Error Comparison of Measured and Estimated End-Effector Case under Command "D-P3-y"

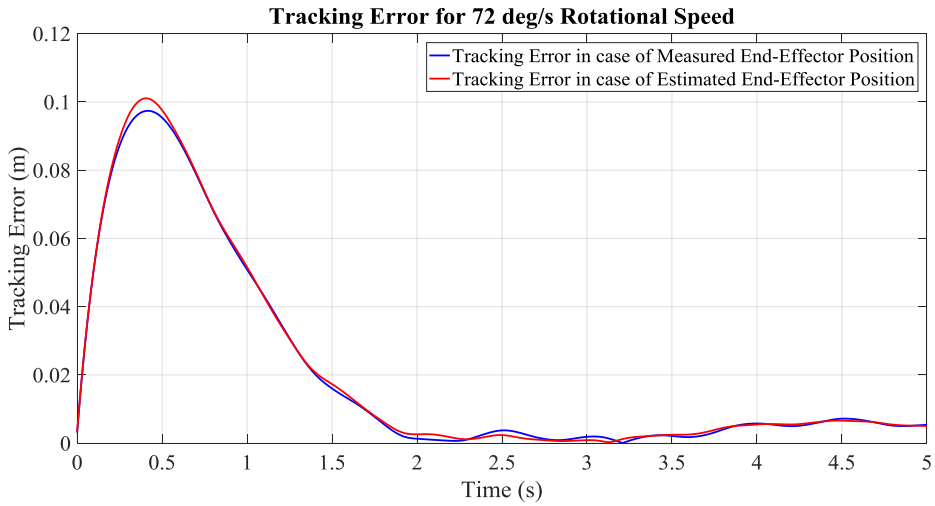

Figure 4.165: Tracking Error Comparison of Measured and Estimated End-Effector Case under Command "C-P3-3"

It is concluded that end-effector measurement enhances the accuracy of the cable robot especially in path tracking tasks like deployment and circular motions. However, it is observed that cable robot can still be able to complete the defined task with an acceptable error, which is not the case for lower-order angle generator with lower order controller. Point-to-point motion is accomplished with almost the same accuracy in case of estimated end-effector position. Therefore, it is not an

absolute necessity to employ end-effector measurement for these methods described in Sections 3.2.1.2 and 3.2.2 .

4.2.5 Tension Monitoring and Control Simulations

Performance of tension monitoring and control algorithm is presented with implementation to different and challenging scenarios in the following figures. In these simulations, there are assigned various minimum limit tension values, T_{limit}, in order to evaulate its effectiveness for different cases.

Results of square wave commands: Commands *S-P2-y* and *S-P3-y* are employed on the following examples. For the results of each command, there are presented input forces applied to the 1st segments of cable, obtained motions and resultant position errors in sequence.

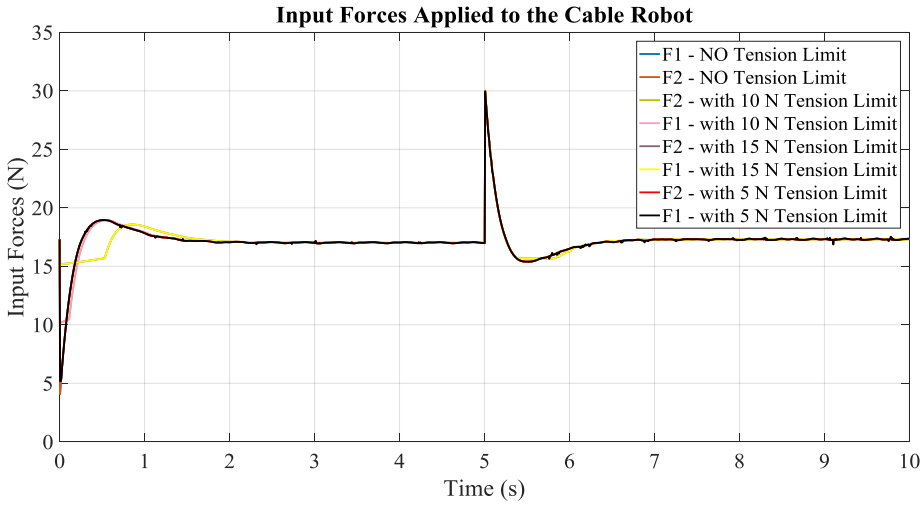

Figure 4.166: Input Forces in case of Tension Control under Command “S-P2-y”

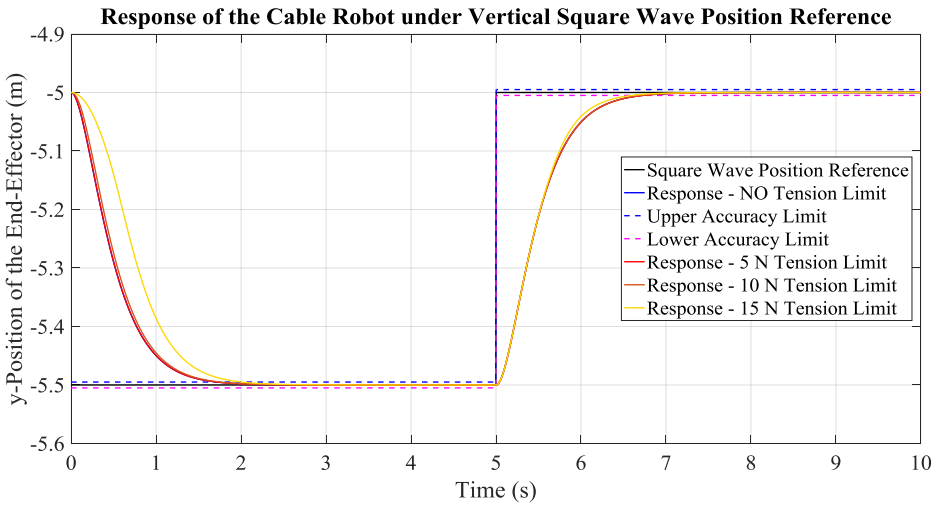

Figure 4.167: Response of the Cable Robot in case of Tension Control under Command “S-P2-y”

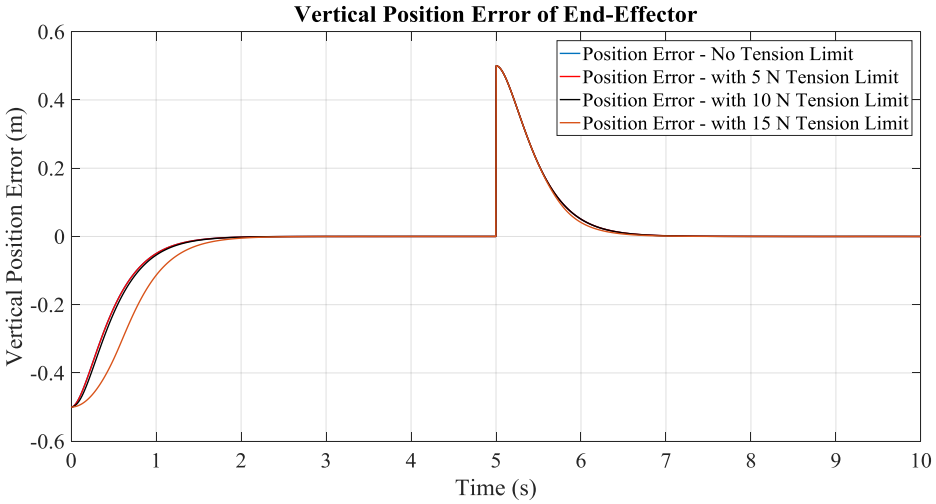

Figure 4.168: Position Error of the Cable Robot in case of Tension Control under Command “S-P2-y”

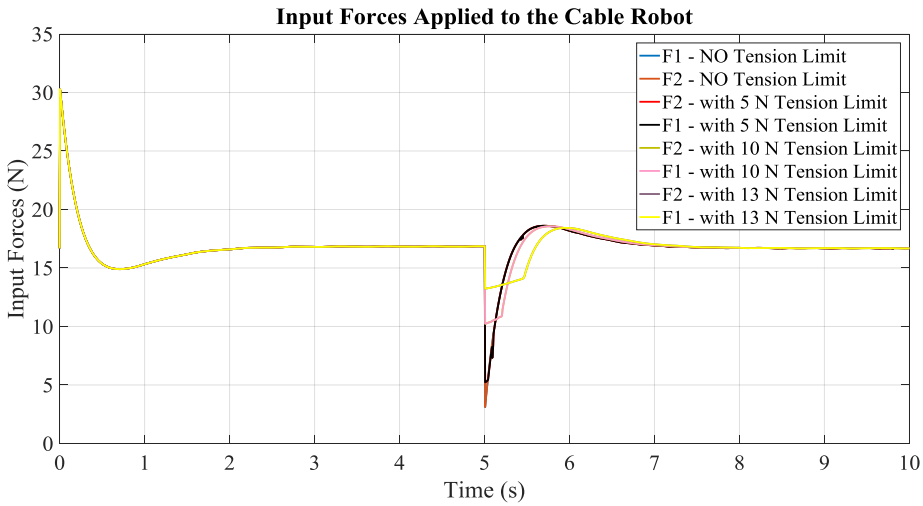

Figure 4.169: Input Forces in case of Tension Control under Command "S-P3-y"

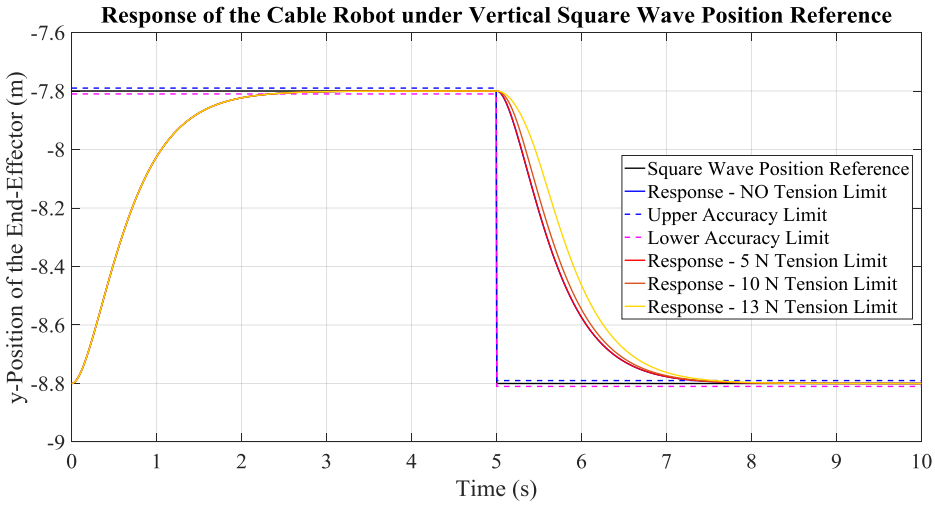

Figure 4.170: Response of the Cable Robot in case of Tension Control under Command "S-P3-y"

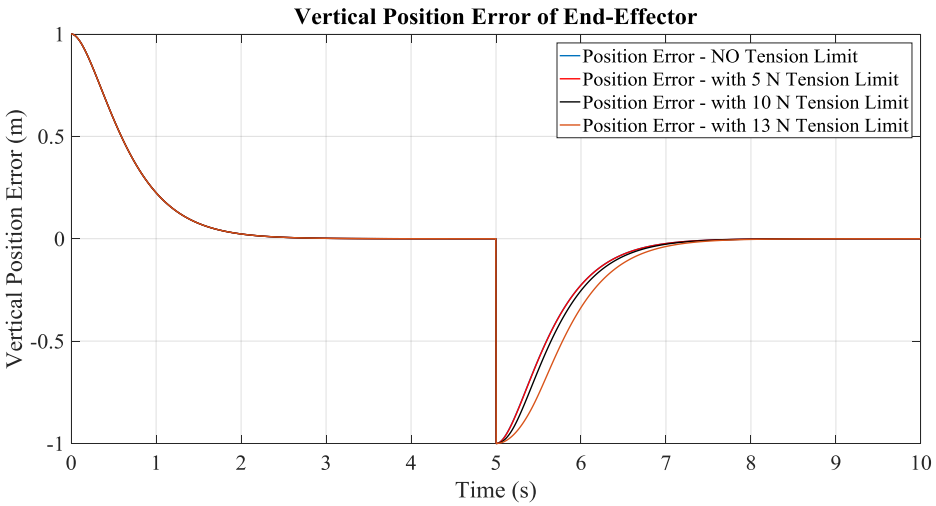

Figure 4.171: Position Error of the Cable Robot in case of Tension Control under Command "S-P3-y"

Results of circular motion commands: Commands *C-P2-3* and *C-P3-3* are employed on the following examples. For the results of each command, there are presented input forces applied to the 1st segments of cable, obtained motions and resultant position errors in sequence.

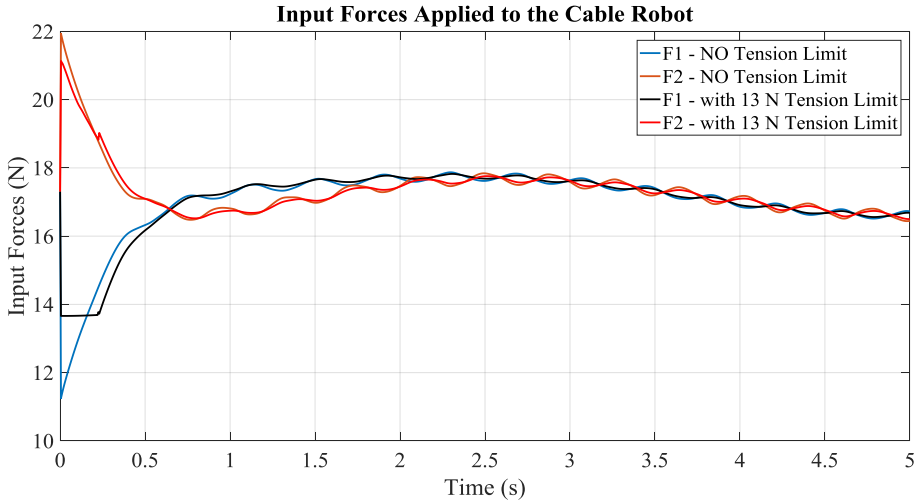

Figure 4.172: Input Forces in case of Tension Control under Command "C-P2-3"

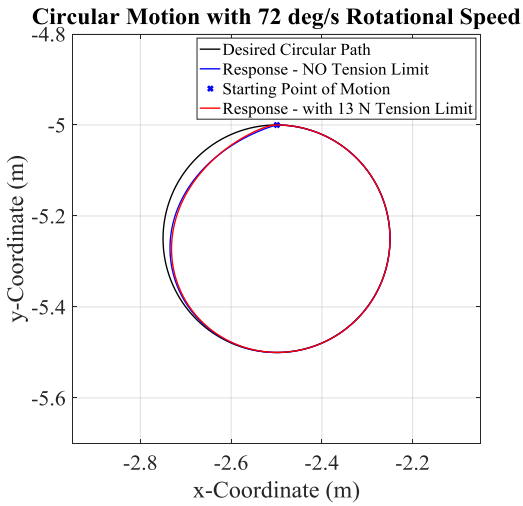

Figure 4.173: Response of the Cable Robot in case of Tension Control under Command “C-P2-3”

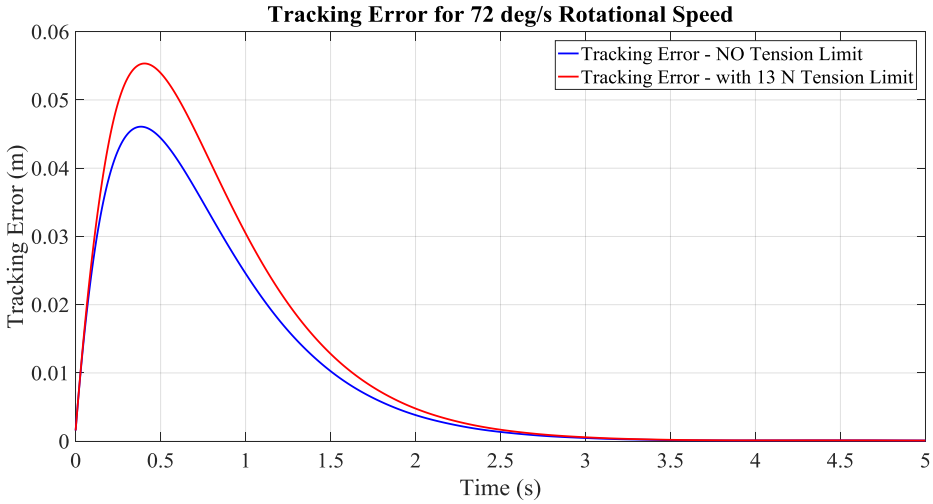

Figure 4.174: Tracking Error of the Cable Robot in case of Tension Control under Command “C-P2-3”

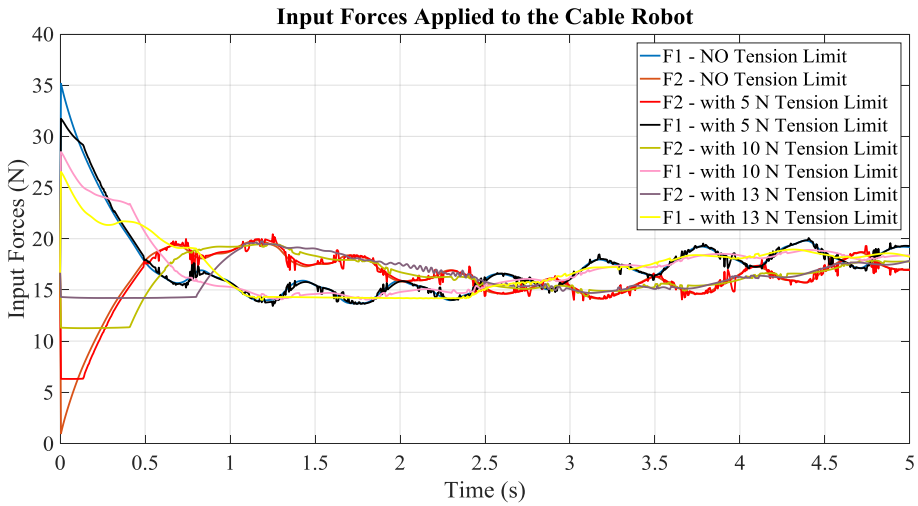

Figure 4.175: Input Forces in case of Tension Control under Command "C-P3-3"

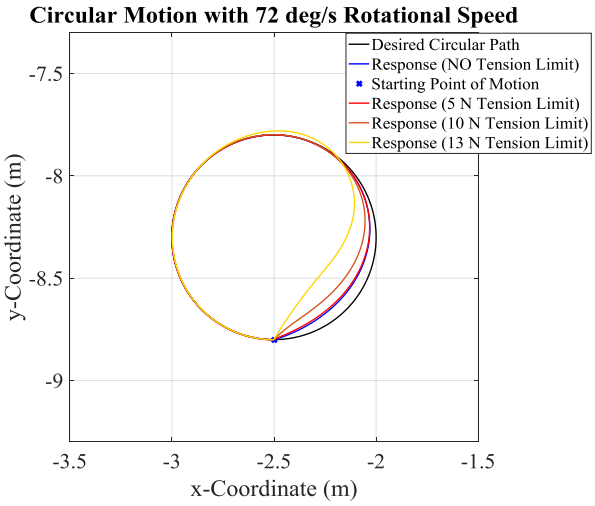

Figure 4.176: Response of the Cable Robot in case of Tension Control under Command "C-P3-3"

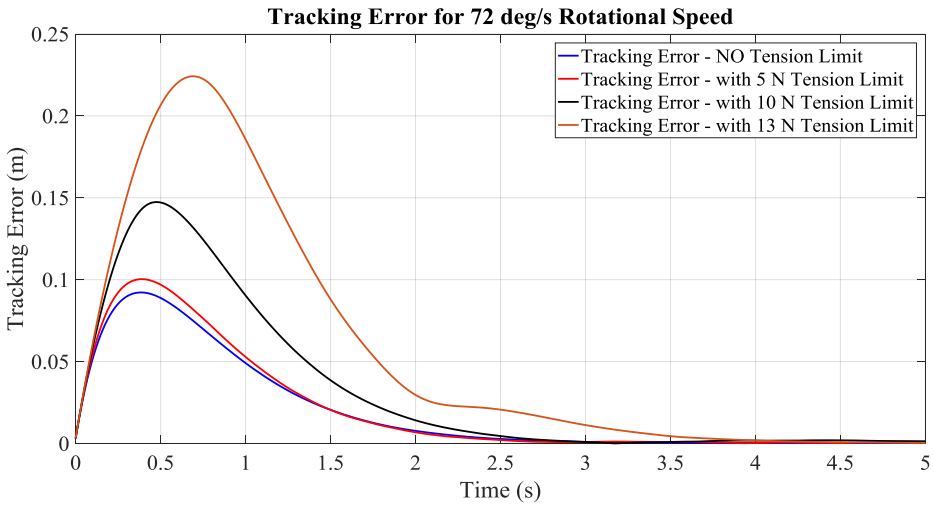

Figure 4.177: Tracking Error of the Cable Robot in case of Tension Control under Command “C-P3-3”

CHAPTER 5

CONCLUSION AND FUTURE WORK

5.1 Conclusion

The main focus of the research presented in this thesis is modeling and control of a planar cable-actuated parallel manipulator by taking dynamics and sagging of cables into consideration. For this purpose, comprehensive mathematical model is built up by discretizing each cable into rigid line elements (segments) and distributing its mass into nodes formed at intersection of these segments. Number of segments that must be used to simulate a cable in sufficiently realistic manner is determined by analyzing the natural frequencies obtained from discrete model of single cable. In this approach, convergence of first "n" number of natural frequencies is observed in specified workspace and operating conditions. The limiting frequency which determines the number n, is found out by Fourier expansion of square wave position reference. As a result of this approach, it is indicated that there occurs no considerable change for segment number greater than 9-10 in the specified workspace. Thus cables of the manipulator operating in this workspace are divided into maximum 10 segments. However, an algorithm is also developed which generates all required equations of motion for any assigned value for segment number of cables. This algorithm provides the opportunity of simulating cable robot for any desired workspace or variety of system parameters depending on the demands.

It is worth to indicate that discretized cable robot has more degrees of freedom than number of control inputs, which are forces applied on 1st cable segments. However, main concern is to control end-effector (payload) pose at the end of the day. For this reason, inverse dynamics controller is employed in task space in order to control x and y coordinates of point mass payload. This control strategy enables to use linear

conventional controllers like PID since it linearizes system nonlinearities and decouples equations of motion thanks to model-based inverse dynamics calculation carried out during motion. Although motion of end-effector is the only point of interest, it is still required to determine angles of cable segments making with horizontal axis because inverse dynamics controller needs them in every control loop for its model-based portion. Angle measurement of all segments along a cable is not feasible since a real cable always has curve-like shape meaning that it is a difficult task to capture distinct angle values on a continuous cable. Furthermore, locating a sensor on a cable constitute extra mass creating undesired inertial effect on system. Hence segment angles are preferred to be generated using mathematical model of cable robot in this thesis. As a drawback, this approach brings more calculation time that must be accomplished within one step time of control loop. Two main methods that are called lower-order model and pseudo-static approaches are described to be able to minimize the calculation load on controller hardware. Two sub-methods are introduced within the lower-order model method, first of which contains lower-order model and lower-order controller. Second one differs from the first with property of higher-order controller but still lower-order model. It becomes inevitable to develop a strategy to generate higher-order segment angles from the lower-order congeneric angles in this second sub-method. In this research, curve fitting approach is employed using lower-order node positions as candidates. Using fitted curve, high-order node positions are estimated and estimated higher-order segment angles are generated by spending less time relative to directly running higher-order dynamic model. Pseudo-static method, which is the second main approach presented in this study, is based on computing segment angles as if cable robot is at its static equilibrium at that instant. As a similar outcome to lower-order model method, this approach also reduces the execution time of solution of model-based part of inverse dynamics controller. In applications of these methods within inverse dynamics controller, it is critical to examine the effects of measured system variables. This concept is treated under two subtopics in this thesis. First of all, feasibility of system variables that are claimed to be used as feedback quantities in the control strategy is examined. A literature survey is carried out to detect similar implementations where end-effector pose, cable angles and cable tensions

are measured successfully. It is essential to note that measurement of the cable length is relatively an easy task and measurement of pulley rotation is a common methodology to meet this need. Secondly, measurement concept is explored with a what-if analysis to see what would be the results in case of some unmeasured system variables. Details of this analysis are given in Chapter 4 with all corresponding results and related evaluations are indicated on the following lines.

Designed controller and developed segment angle estimation methods are tested through several number of simulations. In order to observe their performance properly, different parking positions and command types are employed in these simulations. There are specified three different parking positions at three different heights of the workspace. All these positions are located at the midpoint of the width. However, other width positions are also investigated, since different amplitudes of the position commands are used. Moreover, parking positions close to sides of workspace are also simulated because cable robot wait at these positions and then start motion again after the first step of square wave commands. In addition to square wave position command, deployment and circular motion commands are also used in simulations in order to evaluate path tracking performance of the cable robot. For deployment motion, different displacement amplitudes are defined for each parking position. For circular motion, not only different diameter values but also various rotation speeds of motion are specified at again three different parking positions. At the first stage of simulations, cable robot is tested as if all cable segment angles are somehow measured or calculated with the help of plant model (higher-order model). Moreover, end-effector pose is also assumed to be sensed. As expected, results of the simulations under the conditions explained above are quite successful because optimum conditions are supplied. Simulations of lower-order model approach are conducted in the next stage. Results of lower-order angle estimator with lower-order controller show that this method is very effective if 1^{st} segment lengths and end-effector pose are measured. Resulting error graphs indicate that cable robot completes both point-to-point and tracking tasks accurately (pls. refer to Section 4.2.2.1). However, in case of estimated end-effector pose, method fails (pls. refer to Section 4.2.2.2). Lower-order angle

estimator with higher-order controller is the second method developed under lower-order model approach. Simulations of this method are completed with measured 1st segment lengths and measured end-effector pose firstly. Corresponding results are very satisfactory for both point-to point motion and path tracking tasks (pls. refer 4.2.2.3). Effect of order of lower-order model is another important aspect analyzed in Section 4.2.2.3.4. Results of this analysis show that it does not worth to increase the order. Because it is not obtained considerable enhancement even if the order of lower-order model is increased up to 7, but normalized calculation time is increased up to ~4.5 times of the starting value (shown in Figure 4.111). Furthermore, necessity for measurement of 1st cable segment angles is also studied. It is not observed significant improvement in case of cable angle measurement (pls. refer to Section 4.2.2.3.5). In simulations of pseudo-static approach, all tasks are completed with high accuracy, where end-effector is assumed to be measured. In order to state the stability of this approach, an error function, which is similar to a Lyapunov function is established. This method is not a mathematical proof but gives pretty good information about the system behavior. It is illustrated that defined error function vanishes eventually or at least stays within a constant range (pls. refer to Figure 4.157, Figure 4.158 and Figure 4.159). Requirement for end-effector measurement is also investigated for lower-order angle estimator with higher-order controller and pseudo-static approximations. Simulation results reveal that these methods still perform well and they can be implemented by just measurement of 1st segment lengths. In the last part of Chapter 4, tension monitoring and control algorithm is tested with challenging command and conditions. Under square wave position and circular motion commands, performance of the proposed method is analyzed with different limiting tension values. Considering the results, it is concluded that, tension control method works effectively and prevents cable slackness successfully.

5.2 Recommendations for Future Work

The methods developed in this thesis can be improved and the scope of the study can be extended. For this purpose, some of the possible additional works are listed below as suggestions for future work.

- Performance of all the developed methods is demonstrated through simulations. However, it would be beneficial to make validations with a prototype of a planar cable robot.
- As already stated, this study is conducted with implementation on a planar robot. The reason behind this choice is that it is aimed to focus on effectiveness of dynamic modeling techniques and approaches proposed for controller rather than dealing with the complexity of the system. However, 3D cable robots are more feasible to take place in the industry. Therefore, it is a need to adapt the same methods to a 3D under constrained cable-actuated parallel manipulator.
- All simulations are carried out without any disturbance of the environment in this thesis. Since cable robots have big potential to be used in outdoor and hazardous environment, analysis with disturbance should be taken into consideration.
- In addition to the segment angle estimation techniques proposed in this thesis, state estimation with Kalman filter might be good alternative to be evaluated for future researches.
- In order to improve fidelity of the dynamic model, actuator dynamics and bending stiffness of cables can be included in mathematical modeling phase. Since cables are uniform helical arrangement of wires, there actually exists a dissipated energy between them. As a future work, this effect also might be included within the model.
- As an alternative to the modeling method used in this thesis, equivalent discrete cable robot model might be obtained using the kinetic and potential energies of a continuous cable.

REFERENCES

[1] "IRB 5500-22 - Industrial Robots From ABB Robotics." [Online]. Available: https://new.abb.com/products/robotics/industrial-robots/irb-5500-22. [Accessed: 05-Mar-2018].

[2] "Download SCARA robot Linux 1.0." [Online]. Available: http://linux.softpedia.com/get/Science/SCARA-robot-100789.shtml. [Accessed: 05-Mar-2018].

[3] J. E. Gwinnett, "Amusement Device," 1789680, 1928.

[4] V. E. Gough and S. G. Whitehall, "Universal Tyre Test Machine," *FISITA Proc.*, pp. 117–137, 1962.

[5] D. Stewart, "A Platform with Six Degrees of Freedom," *Proc. Inst. Mech. Eng.*, vol. 180, no. 1, pp. 371–386, 1965.

[6] H. Wu, *Parallel Manipulators New Developments*. I-Tech Education and Publishing, 2008.

[7] S. Kawamura and K. Ito, "A new type of master robot for teleoperation using a radial wire drive system," *Proc. 1993 IEEE/RSJ Int. Conf. Intell. Robot. Syst. (IROS '93)*, vol. 1, no. C, pp. 55–60, 1993.

[8] J. J. German, K. W. Jablokow, and D. J. Cannon, "The cable array robot: theory and experiment," *Proc. 2001 ICRA. IEEE Int. Conf. Robot. Autom. (Cat. No.01CH37164)*, vol. 3, pp. 2804–2810, 2001.

[9] S. Kawamura, H. Kino, and C. Won, "High-speed manipulation by using parallel wire-driven robots," *Robotica*, vol. 18, no. September 2000, pp. 13–21, 2014.

[10] J. Albus, R. Bostelman, and N. Dagalakis, "The NIST Robocrane," *J. Res. Natl. Inst. Stand. Technol.*, vol. 97, no. 3, pp. 373–385, 1992.

[11] R. V. Bostelman, A. Jacoff, and R. Bunch, "Delivery of an Advanced Double-Hull Ship Welding System Using Robocra," in *Third International ICSC (International Computer Science Conventions) Symposia on Intelligent Industrial Automation and Soft Computing*, 1999.

[12] R. Bostelman, A. Jacoff, F. Proctor, T. Kramer, and A. Wavering, "Cable-Based Reconfigurable Machines for Large Scale Manufacturing," in *International Conference on New Technological Innovation for the 21st Century*, 2000.

[13] “Lunar Rover 3 | NIST.” [Online]. Available: https://www.nist.gov/el/intelligent-systems-division-73500/lunar-rover-3. [Accessed: 19-Mar-2018].

[14] E. Amatucci, R. Bostelman, N. Dagalakis, and T. Tsai, “Summary of Modeling and Simulation for NIST RoboCrane Applications,” in *Proc. 1997 Deneb International Simulation Conference and Technology Showcase*, 1997.

[15] Fraunhofer IPA, *Cable-Driven Parallel Robot for Automated Handling of Components in all Dimensions*. .

[16] D. Mayhew, B. Bachrach, W. Z. Rymer, and R. F. Beer, “Development of the MACARM - A novel cable robot for upper limb neurorehabilitation,” in *Proceedings of the 2005 IEEE 9th International Conference on Rehabilitation Robotics*, 2005, vol. 2005, pp. 299–302.

[17] G. Rosati, P. Gallina, S. Masiero, and A. Rossi, “Design of a new 5 d.o.f. wire-based robot for rehabilitation,” in *Proceedings of the 2005 IEEE 9th International Conference on Rehabilitation Robotics*, 2005, vol. 2005, pp. 430–433.

[18] R. Nan and D. Li, “The Five-Hundred Aperture Spherical Radio Telescope (FAST) Project,” in *Materials Science and Engineerins*, 2013, vol. 44, pp. 1–4.

[19] P. Dewdney, M. Nahon, and B. Veidt, “The large adaptive reflector: A giant radio telescope with an aero twist,” *Can. Aeronaut. Sp. J.*, vol. 48, no. 4, pp. 239–250, 2002.

[20] “SkyCam.” [Online]. Available: http://skycam.tv/. [Accessed: 20-Mar-2018].

[21] P. Bosscher, R. L. Williams, and M. Tummino, “A Concept for Rapidly-Deployable Cable Robot Search and Rescue Systems,” in *Volume 7: 29th Mechanisms and Robotics Conference, Parts A and B*, 2005, vol. 2005, pp. 589–598.

[22] E. Ottaviano, M. Ceccarelli, and M. De Ciantis, “A 4-4 cable-based parallel manipulator for an application in hospital environment,” in *15th Mediterranean Conference on Control and Automation*, 2007, pp. 3–8.

[23] R. L. W. Ii and J. Pagan, “Algae Harvesting from Large Outdoor Ponds Using a Novel Parallel Robot System,” *J. Comput. Sci. Appl.*, vol. 6, no. 1, pp. 38–42, 2018.

[24] J. Radojicic, D. Surdilovic, and J. Krüger, “Application challenges of large-scale wire robots in agricultural plants,” *IFAC Proceedings Volumes (IFAC-PapersOnline)*, vol. 1, no. PART 1, IFAC, pp. 77–82, 2013.

[25] D. Q. Nguyen and M. Gouttefarde, “Study of reconfigurable suspended cable-driven parallel robots for airplane maintenance,” in *IEEE International Conference on Intelligent Robots and Systems*, 2014, pp. 1682–1689.

[26] P. Lafourcade, M. Llibre, and C. Reboulet, “Design of a Parallel Wire-Driven Manipulator for Wind Tunnels,” in *Fundamental Issues and Future Research Directions for Parallel Mechanisms and Manipulators*, 2002, pp. 187–194.

[27] Y. Zheng, Q. Lin, and X. Liu, “A Wire-Driven Parallel Suspension System with 8 Wires (WDPSS-8) for Low-Speed Wind Tunnels,” *Robot Manip. Trends Dev.*, pp. 647–667, 2010.

[28] P. Bosscher, R. L. Williams, L. S. Bryson, and D. Castro-Lacouture, “Cable-suspended robotic contour crafting system,” *Autom. Constr.*, vol. 17, no. 1, pp. 45–55, 2007.

[29] M. H. Korayem, M. Bamdad, H. Tourajizadeh, H. Shafiee, R. M. Zehtab, and A. Iranpour, “Development of ICASBOT: A Cable-Suspended Robot’s with Six DOF,” *Arab. J. Sci. Eng.*, vol. 38, no. 5, pp. 1131–1149, 2013.

[30] J. Lamauru, M. Gouttefarde, M. Michelin, and O. Tempier, “Design and Control of a Redundant Suspended Cable-Driven Parallel Robots,” in *Latest Advances in Robot Kinematics*, 2012, pp. 237–244.

[31] M. A. Khosravi and H. D. Taghirad, “Dynamics Analysis and Control of Cable Driven Robots Considering Elasticity in Cables,” *Trans. Can. Soc. Mech. Eng.*, vol. 35, no. 4, pp. 543–557, 2011.

[32] J. Du, H. Bao, C. Cui, and D. Yang, “Dynamic Analysis of Cable-Driven Parallel Manipulators with Time-Varying Cable Lengths,” *Finite Elem. Anal. Des.*, vol. 48, no. 1, pp. 1392–1399, 2012.

[33] C. Lambert and M. Nahon, “An Aerostat Positioning System with Cable Control,” in *Proceedings of the 17th World Congress The International Federation of Automatic Control*, 2008, pp. 779–784.

[34] A. Lytle, F. Proctor, and K. Saidi, “Control of Cable Robots for Construction Applications,” in *Parallel Manipulators, towards New Applications*, no. April, 2008, pp. 1–21.

[35] B. Zi, Z. cai Zhu, and J. li Du, “Analysis and control of the cable-supporting system including actuator dynamics,” *Control Eng. Pract.*, vol. 19, no. 5, pp. 491–501, 2011.

[36] Q. J. Duan, J. L. Du, B. Y. Duan, and A. F. Tang, “Deployment/retrieval modeling of Cable-Driven Parallel Robot,” *Math. Probl. Eng.*, vol. 2010, 2010.

[37] A. Afshari and A. Meghdari, “New form of Jacobian matrix and equations of motion for a 6 d.o.f cable-driven parallel robot using constrained variables,” *Int. J. Adv. Robot. Syst.*, vol. 4, no. 1, pp. 63–68, 2007.

[38] M. Yamamoto, N. Yanai, and A. Mohri, “Trajectory control of incompletely restrained parallel-wire-suspended mechanism based on inverse dynamics,” *IEEE Trans. Robot.*, vol. 20, no. 5, pp. 840–850, 2004.

[39] S. R. Oh and S. K. Agrawal, “A reference governor-based controller for a cable robot under input constraints,” *IEEE Trans. Control Syst. Technol.*, vol. 13, no. 4, pp. 639–645, 2005.

[40] M. Filipovic, A. Djuric, and L. Kevac, “Influence of the Construction Type of a Cable-Suspended Parallel Robot on its Kinematic and Dynamic Model,” *Sci. Tech. Rev.*, vol. 63, no. 4, pp. 17–26, 2013.

[41] R. Babaghasabha, M. A. Khosravi, and H. D. Taghirad, “Adaptive robust control of fully-constrained cable driven parallel robots,” *Mechatronics*, vol. 25, pp. 27–36, 2015.

[42] H. Wei, Y. Qiu, and Y. Su, “Motion control strategy and stability analysis for high-speed cable-driven camera robots with cable inertia effects,” *Int. J. Adv. Robot. Syst.*, vol. 13, no. 5, pp. 1–14, 2016.

[43] S.-R. Oh, K. Mankala, S. K. Agrawal, and J. S. Albus, “A Dual-Stage Planar Cable Robot: Dynamic Modeling and Design of A Robust Controller with Positive Inputs,” *J. Mech. Des.*, vol. 127, no. 4, p. 612, 2005.

[44] A. Vafaei, M. A. Khosravi, and H. D. Taghirad, “Modeling and control of cable driven parallel manipulators with elastic cables: Singular perturbation theory,” in *ICIRA 2011*, 2011, pp. 455–464.

[45] Y. B. Bedoustani, P. Bigras, H. D. Taghirad, and I. A. Bonev, “Lagrangian dynamics of cable-driven parallel manipulators: A variable mass formulation,” *Trans. Can. Soc. Mech. Eng.*, vol. 35, no. 4, pp. 529–542, 2011.

[46] R. J. Caverly and J. R. Forbes, “Dynamic modeling and noncollocated control of a flexible planar cable-driven manipulator,” *IEEE Trans. Robot.*, vol. 30, no. 6, pp. 1386–1397, 2014.

[47] I. W. Stewart, *Advanced Classical Mechanics*. 2016.

[48] M. W. Spong, S. Hutchinson, and M. Vidyasagar, *Robot Modeling and Control*. Hoboken, NJ : John Wiley & Sons, 2006.

[49] J. Collard, J. Lamaury, and M. Gouttefarde, “Dynamics Modelling of Large Suspended Parallel Cable-Driven Robots,” in *Multibody Dynamics 2011, ECCOMAS Thematic conference*, 2011, pp. 1–13.

[50] G. Meunier, “Control of an Overactuated Cable-Driven Parallel Manipulator,” 2006.

[51] X. Zhao, “Statics and Dynamics Simulation of a Multi- Tethered Aerostat System,” 2004.

[52] H. Yuan, “Static and Dynamic Stiffness Analysis of Cable-Driven Parallel Robots,” 2015.

[53] Carl Stahl Sava Industries, “Design Guide for Cable Solutions ™.” p. 35, 2006.

[54] C. S. S. Industries, “Carl Stahl Technocables.” p. 51, 2017.

[55] B. Siciliano, L. Sciavicco, L. Villani, and G. Oriolo, *Robotics*. 2009.

[56] R. J. Schilling, *Fundamental of Robotics: Analysis and Control*. Prentice-Hall, Inc., 1990.

[57] J.Srinivas, R.V.Dukkipati, and K.Ramji, *Robotics Control and Programming*. Alpha Science International Ltd., 2009.

[58] A. Fortin-Côté, P. Cardou, and A. Campeau-Lecours, “Improving cable driven parallel robot accuracy through angular position sensors,” in *IEEE International Conference on Intelligent Robots and Systems*, 2016, pp. 4350–4355.

[59] The MathWorks Inc., *Curve Fitting Toolbox™: User’s Guide*. 2011.

[60] A. Messac, *Optimization in Practice with MATLAB®: For Engineering Students and Professionals*. Cambridge University Press, 2015.

[61] The MathWorks Inc., *Optimization Toolbox For Use With Matlab User’s Guide*, Version 2. 2002.

[62] R. Babaghasabha, M. Khosravi, and H. D. Taghirad, “Vision based PID control on a planar cable robot,” in *The 22nd Iranian Conference on Electrical Engineering*, 2014, pp. 1248–1253.

[63] T. Dallej, M. Gouttefarde, N. Andreff, M. Michelin, and P. Martinet, “Towards vision-based control of cable-driven parallel robots,” in *IEEE International Conference on Intelligent Robots and Systems*, 2011, pp. 2855–2860.

[64] T. Dallej *et al.*, “Vision-Based Modeling and Control of Large-Dimension Cable-Driven Parallel Robots,” in *2012 IEEE/RSJ International Conference on Intelligent Robots and Systems*, 2012.

[65] T. Dallej, N. Andreff, Y. Mezouar, and P. Martinet, “3D Pose Visual

Servoing Relieves Parallel Robot Control from Joint Sensing," in *IEEE International Conference on Intelligent Robots and Systems*, 2006, pp. 4291–4296.

[66] T. Dallej, N. Andreff, and P. Martinet, "Towards a Generic Image-Based Visual Servoing of Parallel Robots Using Legs Observation," in *12th IFToMM World Congress*, 2007.

[67] P. Martinet, N. Daucher, J. Gallice, and M. Dhome, "Robot Control using Monocular Pose Estimation," *Work. New Trends Image-Based Robot Servoing*, pp. 1–12, 1997.

[68] W. J. Wilson, C. C. W. Hulls, and G. S. Bell, "Relative end-effector control using cartesian position based visual servoing," in *IEEE Transactions on Robotics and Automation*, 1996, vol. 12, no. 5, pp. 684–696.

[69] L. E. Weiss, A. C. Sanderson, and C. P. Neuman, "Dynamic Sensor-Based Control of Robots with Visual Feedback," *IEEE J. Robot. Autom.*, vol. 3, no. 5, pp. 404–417, 1987.

[70] B. Zi, B. Y. Duan, J. L. Du, and H. Bao, "Dynamic modeling and active control of a cable-suspended parallel robot," *Mechatronics*, vol. 18, no. 1, pp. 1–12, 2008.

[71] X. Jin, D. I. Jun, A. Pott, S. Park, J. Park, and S. Y. Ko, "Four-cable-driven parallel robot," in *13th International Conference on Control, Automation and Systems (ICCAS 2013)*, 2013, pp. 879–883.

[72] S. Ohtomo and T. Murakami, "Estimation method for sway angle of payload with reaction force observer," in *International Workshop on Advanced Motion Control, AMC*, 2014, pp. 581–585.

[73] M. Peshkin, "Non-Contacting Sensors," US6668668 B1, 2003.

[74] B. H. Kim and T. Park, "Estimation of cable tension force using the frequency-based system identification method," *J. Sound Vib.*, vol. 304, pp. 660–676, 2007.